STATUS OF THESIS

Title of thesis	PREDICTIVE EQUATIONS FOR PERMEABILITY AND STRENGTH OF OILWELL CEMENT USING ELECTRICAL IMPEDANCE

I, SYAHRIR RIDHA

hereby allow my thesis to be placed at the Information Resource Center (IRC) of Universiti Teknologi PETRONAS (UTP) with the following conditions:

1. The thesis becomes the property of UTP
2. The IRC of UTP may make copies of the thesis for academic purposes only.
3. This thesis is classified as

☐ Confidential

☑ Non-confidential

If this thesis is confidential, please state the reason:

The contents of the thesis will remain confidential for _____ years.

Remarks on disclosure:

Signature of Author

Permanent address:
Komplek BTN Seuriget
Blok M No. 179, Kota Langsa, Aceh
Indonesia

Date : 18/02/2013

Endorsed by

Signature of Supervisor
Dr. Sonny Irawan

Dr. Sonny Irawan
Senior Lecturer
Geoscience & Petroleum Engineering Department
Universiti Teknologi PETRONAS
Bandar Seri Iskandar, 31750 Tronoh
Perak Darul Ridzuan, MALAYSIA

Date : 18/02/2013

UNIVERSITI TEKNOLOGI PETRONAS

PREDICTIVE EQUATIONS FOR PERMEABILITY AND STRENGTH OF OILWELL CEMENT USING ELECTRICAL IMPEDANCE

by

SYAHRIR RIDHA

The undersigned certify that they have read, and recommend to the Postgraduate Studies Programme for acceptance this thesis for the fulfilment of the requirements for the degree stated.

Signature: _____

Main Supervisor: Dr. Sonny Irawan

Signature: _____

Co-Supervisor: Assoc. Prof. Dr. Bambang Ariwahjoedi

Signature: _____

Head of Department: Assoc. Prof. Dr. Ismail Mohd Saaid

Assoc Prof Dr Ismail M Saaid
Head, Petroleum Engineering Department
Universiti Teknologi PETRONAS

Date: 19/2/2013

PREDICTIVE EQUATIONS FOR PERMEABILITY AND STRENGTH OF OILWELL CEMENT USING ELECTRICAL IMPEDANCE

by

SYAHRIR RIDHA

A Thesis

Submitted to the Postgraduate Studies Programme

as a Requirement for the Degree of

DOCTOR OF PHILOSOPHY

PETROLEUM ENGINEERING DEPARTMENT

UNIVERSITI TEKNOLOGI PETRONAS

BANDAR SERI ISKANDAR,

PERAK

FEBRUARY 2013

DECLARATION OF THESIS

Title of thesis	PREDICTIVE EQUATIONS FOR PERMEABILITY AND STRENGTH OF OILWELL CEMENT USING ELECTRICAL IMPEDANCE

I, SYAHRIR RIDHA

hereby declare that the thesis is based on my original work except for quotations and citations which have been duly acknowledged. I also declare that it has not been previously or concurrently submitted for any other degree at UTP or other institutions.

Signature of Author

Permanent address:
Komplek BTN Seuriget
Blok M No. 179, Kota Langsa, Aceh
Indonesia

Date : 18/02/2013

Witnessed by

Signature of Supervisor
Dr. Sonny Irawan

Dr. Sonny Irawan
Senior Lecturer
Geoscience & Petroleum Engineering Department
Universiti Teknologi PETRONAS
Bandar Seri Iskandar, 31750 Tronoh
Perak Darul Ridzuan, MALAYSIA

Date : 18/02/2013

DEDICATION

For my lovely wife Miftahul Jannah and my daughter and son
Mishkah Khalifati Ridha and Syahmi Fathan Ridha

ACKNOWLEDGEMENTS

Alhamdulillah, I express my praise and grateful to Allah SWT who gave me the strength and guide me in my life.

I would like to express my gratefulness towards my advisors, Dr Sonny Irawan and Associate Professor Dr. Bambang Ariwahjoedi, for their invaluable guidance, advice and friendship throughout my study. It was a precious change for doing my Ph.D program and research with great learning experience under their supervision.

Also, I would like to thank my examination committee, Professor Dr. Ir. Muhd Fadhil Nuruddin, Professor Dr. Mustafa Onur, and Professor Dr. Radzuan Junin for taking their time to review my thesis.

Many thanks to Professor Dr. Ir. Muhd Fadhil Nuruddin and Dr. Reza Ettehadi for their collaborative opportunities in providing times for sharing and discussion on cement research and technology. I especially thank Dr. Hilfan Khairy for his valuable assistance during the experimental procedure and its analysis of this study.

I also thank my "oilwell cementing" colleagues and technicians in Petroleum Engineering Department for their support, help and discussion, especially Mr. Irfan, Ms. Arina, Mr. Amin, Mr. Amirul 'BOB', Mr. Najib and Mr. Samsudin. For colorful discussion and sharing have been made, I thank my colleagues Mr. Askar, Mr. Julendra, Mr. Akmal, Mr. Maman, Mr. Aryo and Mr. Eko.

I sincerely thank Universiti Teknologi PETRONAS for the financial support during my study.

ABSTRACT

Oilwell cement plays an important role either to seal-off the casing or to isolate the formation layers from the fluids infiltration that might cause a wellbore damage. A cautious evaluation of cement after displacement is coming to be crucial to secure the long-term durability and integrity of wellbore. This work in turn is focused on the utilization of electrical properties for predicting the permeability and compressive strength of oilwell cement.

At present work, an electrical impedance measurement has been used to detect the conductivity evolution of oilwell cement during early hydration. It was then followed by an examination towards the potential existence of interface conductivity along with its effects on various water cement ratios, curing temperature, and also pressure. In analyzing the interface conductivity, the evaluation of the electrical responses in the form of conductivity dispersion characteristics has been done. Together with porosity data, conductivity data consisting of bulk and pore solution conductivity were examined to study several composite conductivity models to describe certain changes in the electrical conductivity of oilwell cement system.

Several empirical equations for predicting the permeability and compressive strength of oilwell cement based on its electrical properties response have been proposed. To validate the result, the proposed equations were experimentally compared to other cement samples with different water cement ratios and curing conditions. A comparison has also been made to the equation proposed by Katz-Thompson and Johnson's and also data from literatures. A good agreement between the proposed equation and measured data then shows that it is feasible to obtain the cement's strength and permeability in situ using bulk and pore solution conductivity. Permeability and compressive strength in mature stage, furthermore, can be predicted by the proposed equations.

ABSTRAK

Simen telaga minyak memainkan peranan yang penting sama ada untuk mengukuhkan selongsong atau untuk mengasingkan lapisan bawah tanah dari penyusupan air yang mungkin menyebabkan kerosakan telaga minyak. Permerhatian yang teliti adalah penting terhadap simen selepas dipam pada kedudukan yang di sasarkan untuk menjamin ketahanan jangka panjang dan integriti telaga minyak. Fokus kajian ini tertumpu kepada penggunaan arus elektrik dalam meramalkan kebolehtelapan dan kekuatan mampatan simen telaga minyak.

Berdasarkan kajian saat ini, ukuran elektrik impedans telah digunakan untuk mengesan evolusi kekonduksian simen ketika awal penghidratan. Kemudiannya diikuti dengan kajian ke atas potensi konduksi dengan kesan pada kepelbagaian nisbah simen terhadap air, suhu pengawetan dan tekanan. Dalam menganalisis konduksi permukaan, penilaian terhadap tindak balas elektrik dalam bentuk ciri-ciri penyebaran konduksi telah dijalankan. Bersama dengan data keliangan, data kekonduksian terdiri daripada campuran pukal dan liang dianalisis dengan mengkaji terhadap beberapa model komposit untuk menentukan sebarang perubahan di dalam kekonduksian elektrik bagi sistem simen telaga minyak.

Beberapa persamaan empirikal telah dicadangkan untuk meramal kebolehtelapan dan kekuatan mampatan simen telaga minyak berdasarkan kepada sifat elektrik. Bagi mengesahkan keputusan, persamaan yang dicadangkan telah diujikaji dengan membuat perbandingan dengan sampel simen lain dengan menggunakan kepelbagaian nisbah air terhadap simen dan juga keadaan pengawetan. Perbandingan juga telah dilakukan dengan menggunakan persamaan yang telah dicadangkan oleh Katz-Thompson dan Johnson dan juga data daripada kajian terdahulu. Daripada kajian yang dijalankan, dapat disimpulkan bahawa persamaan yang dicadangkan dan data yang diukur menunjukkan ia sesuai untuk menilai kekuatan dan kebolehtelapan simen dikedudukan tertentu menggunakan kekonduksian campuran pukal dan liang.

Tambahan pula, kebolehtelapan dan kekuatan mampatan di peringkat matang boleh diramalkan dengan menggunakan persamaan yang telah dicadangkan.

TABLE OF CONTENTS

LIST OF TABLES

LIST OF FIGURES

LIST OF ABBREVIATIONS

AC	Alternating Current
API	American Petroleum Institute
ASTM	American Standard Testing and Material
CBL	Cement Bond Log
CH	Calcium Hydroxide
CS	Calcium Sulfoaluminate
C-S-H	Calcium Silicate Hydrate
DC	Direct Current
DEM	Differential Effective Medium
EDL	Electrical Double Layer
EIS	Electrical Impedance Spectroscopy
GEM	Generalized Effective Medium
HPHT	High Pressure High Temperature
HS	Hashin Shtrikman
HSR	High Sulphate Resistant
MIP	Mercury Intrusion Porosimetry
PC	Personal Computer
TGA	Thermo Gravimetric Analysis
UCA	Ultrasonic Cement Analyzer
W/C	Water Cement Ratio
WOC	Wait-On-Cement
XRF	X-Ray Fluorescence
NIST	National Institute of Standards and Technology
VCCTL	Virtual Cement and Concrete Testing Laboratory

NOMENCLATURES

A	Cross section area of sample (m^2)
atm	Atmospheric condition
$A_{p\text{-}s}$	Area of pore-solid interface (m^2)
b	Empirical constant
C	Capacitance (farad)
d	Shape factor
d_c	Critical pore diameter of cement sample (μm)
$d_{c\text{-}exp}$	Diameter of cement particle expansion (μm)
$d_{p\text{-}red}$	Diameter of pore cement reduction (μm)
F	Formation factor
f	Frequency (hertz)
f_c	Cut-off frequency (hertz)
G	Geometry factor (m^{-1})
I	Current (ampere)
k	Permeability (μm^2)
l	Length of cement sample (m)
l_e	Effective path length (m)
m	Cementation factor
N_c	Number of cement particle
P	Pressure (psi)
P_c	Capillary pressure (psi)
R	Resistance (ohm)
R_b	Bulk Resistance (ohm)
R^2	Coefficient of determination
rpm	Revolutions per minute (rpm)
S	Compressive strength (psi)
S_o	Maximum strength at zero porosity (psi)

T	Temperature (°C)
T_{ref}	Reference temperature (°C)
V	Voltage (volts)
V_{exp}	Volume of the expanded cement particle (μm^3)
V_p	Pore volume of cement particle sample (fraction)
v	Ration of the volume of the expanded particle relative to that of the original cement value (v = 2.2)
W_c	Cement sample mass (g)
$Wt\%$	Weight percent
Z	Impedance (ohm)
Z'	Real impedance (ohm)
Z''	Imaginary impedance (ohm)
Z_o	Impedance amplitude (ohm)
α	Degree of hydration (fraction)
a	Empirical coefficient in Hammond & Robson equation (°C)
Λ	Microstructural parameter analogous to the surface to volume ratio (μm)
β	Connectivity
ε	Permittivity (farads/m)
ε_o	Permittivity of free space (8.85×10^{-12} farads/m)
σ	Electrical conductivity (siemens/m)
σ_b	Bulk conductivity (siemens/m)
σ_n	Normalized conductivity
σ_o	Pore solution conductivity (siemens/m)
σ_s	Interface conductivity (siemens/m)
θ	Phase angle
ϕ	Porosity (fraction)
ρ_c	Cement powder density (g/cm^3)
τ_f	Tortuosity factor
ω	Angular frequency (hertz)

CHAPTER 1

INTRODUCTION

This chapter begins with a general introduction of oilwell cement evaluation and its current development. The chapter continues with exploring the background, problems statements, objectives and contributions, and scopes of this study.

1.1 General

The application of cement system has been used through many fields including in oilwell cementing. In a wellbore, such cementing operations are performed to achieve a complete and permanent zonal isolation in which the cement sheath must prevent any fluid circulation (gas, oil, water) between different rocks layers. A good quality in cementing operation will confirm the long-term wellbore integrity of wells. Conversely, a failure of cementing during operation may lead to secondary cementing procedure which, as a consequence, might impose a huge expense in particular money in term of loss time, material and recovery.

Besides supporting the casing, preventing erosion in a cement job, in this case, by stopping the circulation of drilling fluids outside the casing comes to be very important. In this case, a surface of the casings must be cemented to seal off and protect water formations and to help support deeper casing strings. Cementing the intermediate strings is purposely to seal off several abnormal pressure formations, isolate incompetent formations, and shut off lost-circulation zones. Furthermore, production strings are cemented to prevent the migration of fluids in the annulus and also to ensure a zonal isolation. Cement also provides some corrosion protections to all the casing strings. Hence, an accurate selection in the methods of evaluation based on the objective to be reached, as a response, is a must.

One of the main challenges during cementing operation is to monitor the changes of cement's physical properties after displacement. These changes must be carefully monitored under an evaluation towards a cement job to ensure the integrity and durability of the well's life. This evaluation is aimed to check whether the cementing objectives have been reached after the job performance. The evaluation of the cement will be much more efficient if the objectives have clearly been defined.

Methods for cementing evaluation are initially performed either by testing the hydraulic isolation or by locating the top of the cement. These methods, however, are unable to detect the micro-annuli channeling between casing-cement and cement-formation. The developments of cementing evaluation logs by means of acoustic and ultrasonic properties have been intensively adopted in detecting the cement's physical properties. In fact, these techniques still have limitations to be applied in detecting the cement's inter-pores channeling due to its density based principles.

Regarding the cement's physical properties, there is an indication that several significant changes may still exist in the electrical properties of cement after the cement displacement. Its electrical properties, in this case, are dependent on its interconnected pore network filled with water containing mobile ions. Therefore, the continuous evolving network of pores governs the physical properties of displaced cement as well as detecting potential of micro-channeling, porosity, permeability, creep, and compressive strength. These interdependencies refer to a key to develop some representative predictive correlations for the permeability and compressive strength of well cement.

An investigation towards electrical response as an effect of water cement ratio changes, elevated curing pressure and temperature is required in order to have representative data for cementing evaluation. In turn, this study has been designed to deliver a laboratory investigation towards the electrical properties of oilwell cement by considering the effect of water cement ratios, elevated pressure and temperature. Here, an attention has been made to take into account the interface phenomenon and its magnitude contribution to the bulk conductivity. The main goal of this thesis is to develop a set of correlations for the prediction of permeability and compressive strength[1] of oilwell cement as a function of its electrical properties.

[1] the term strength will be used further for simplicity representing the compressive strength

1.2 Background of Research

Electrical properties becomes the important parameter in characterizing the cementitious materials as compared to several existing techniques that allow for investigating the evolution of the pore structure of cement-based materials [1, 2]. The development on the testing methodology has been improved with the advancement of electrical impedance spectroscopy that makes possible to study the microstructure evolution and those related to physical properties such as porosity and permeability [3–9]. An electrical method has several advantages over other the methods in terms of its noninvasive and nondestructive measurements and its capability in sampling the microstructure in-situ without any water removal, usually by heating, which recognizably can damage the cement microstructure permanently.

Archie [10] initially introduced a relationship between electrical attributes and some physical properties of reservoir rocks. The Archie's law describes an electrical behavior in sedimentary rock as a function of porosity, water content, cementation factor, and fluid conductivity. In the cement system, the electrical conduction via mobile ionic in common is transported through a continuous interconnected pore solution that contains several types of electrolytic ions. In addition, it has conductivity value ranging from 1 to 20 S/m compared to the matrix of cement system that has low conductivity that is approximately 10^{-9} S/m [6]. This phenomenon is interesting to be studied because it is related to the development of inter-connected pores, pore volume and bonding particles.

Furthermore, electrical properties are so sensitive to the complex factors that might create certain differences in the microstructure development of cement system such as in water cement ratios, curing conditions, chemical composition of cement and other factors which can change the hydration process. In that way, the microstructure changes such as pore volume and pores connectivity can be monitored by electrical information as a function of hydration time. These interrelationships, in essence, are the major interest in achieving a comprehensive understanding towards the evolution of the microstructure in place under reservoir conditions.

The application of electrical methods to the cementitious systems can be traced back to the early part of the 20^{th} century as noted by McCarter [1]. However, the progress was relatively slow until the early 80's where the testing methodology

significantly improved especially in the instrumentation through the development of sophisticated electrical impedance analyzers which are also the focus of this study.

Zhang *et al.* [7] used certain electrical and ultrasonic methods to interpret the hydration process of the cement-based materials, in this case by focusing the study on detecting the setting and hardening behaviors during the first 7 days of hydration process. Four stages of hydration process were identified by utilizing the critical points on resistivity and ultrasonic curves. To eliminate the contact effect generated by electrode-cement interface which might cause a polarization effect, the authors then employed a non-contacting resistivity measurement.

Neithalath *et al.* [8] investigated a relationship between an electrical conductivity and microstructural parameters of cement pastes and concretes containing several cement replacement materials. It was shown that the dependency of electrical conductivity to the pore volume reduction and the pore connectivity was significant. The authors explained that this interrelationship using GEM theory was a combination of an effective medium and several percolation theories. The characteristic exponent in the proposed equation, which was used as a fitting parameter, depended on the conducting phase geometry and connectivity.

Revil and Glover [11], on the other hand, proposed a model describing the surface conductivity. The model was based on the description of surface chemical reactions in which the processes of electrical diffuse layer were dedicated for the condition of diffuse layer thickness that were smaller than the local radius of mineral surface and its pore size. The authors in that case restricted the model to the case in which the electrical diffuse layer thickness was smaller compared to (a) the local radius of mineral surface, and (b) the pore size. The result of the model showed that the electrical surface conduction had both the dependency on electrolyte concentration and pH and the nonlinear relationship to the effective conductivity. In the cement system, Friedmann *et al.* [12], meanwhile, showed the results of electrical double layer phenomena occurred in the cement's gel pores rather than in capillary pores.

Most of the previous works were performed in the atmospheric conditions whereas, when dealing with oilwell cementing operation, the influence of elevated pressure and temperature should be taken into account. Furthermore, the interface conductivity and electrical dispersion characteristics were needed to be studied in

some detail as it may correlate to the physical properties of well cement - especially in the elevated conditions.

1.3 Problem Statement

An accurate identification and detection of the well integrity of cement after displacement is important to determine whether the cementing job has fulfilled its requirements. The involvement of certain major cementing evaluation tools are intended here to confirm that the cement has provided an adequate zonal isolation and ensured the good cement bonds either between the casing and cement or between the formation and cement. Failure to do so will affect on cementing operation and, as a result, a remedial cementing job, which is expensive and time-consuming, must be performed.

Consequently, an appropriate selection towards cement evaluation techniques is required to achieve the clear understanding of both physical and mechanical phenomena of a displaced cement system by still concerning the hydration times. The well known cementing evaluation tool is a cement bond log, which is used to confirm the good bonding quality either between the cement and the formation or between the cement and the casing. In this case, the tool works on an acoustic principle, transmits a signal or a vibration and receives that signal and records its arrival time. Both the arrival time and the amplitude of the vibration are used to determine bonding conditions. Although it has been widely used, some phenomena related to the inter-pores fluids channeling may not be accurately detected from its density based principle [13–15].

Furthermore, a channeling of the inter-pores fluids may occur in the early stages of cementing operation. It is tightly related to the slurry that develops insufficient strength to prevent fluids migration into the cement column. The effects are multistage then at which in the short term it may exhibit gas blowout and damage the wells and in the long term it may deteriorate cement integrity and durability. Additionally, the strength is deemed important because a certain minimum strength is required before drilling operation can be resumed. Hence, early detection of strength

and channeling becomes a top priority and may be detected and quantified by an electrical impedance method by an appropriate proposed correlation.

An electrical impedance technique has been rapidly developed and widely applied in composite material characterization in particular to cement-based system. Many attempts have been made to investigate the microstructure properties of cement system for certain purposes in construction such as building, road and bridge. [3, 4, 6–8]. However, its application into well cement still has less attention, especially during early hydration.

In an oilwell cementing application, there should be a good consideration to the effect of elevated pressure and temperature on electrical properties in that the temperature changes tends to accelerate the hydration mechanism and simultaneously the varying pressure will decreasing pores radius and connected pores. These interdependencies, therefore, should be carefully investigated to have the good representative data of both electrical impedance measurements and conductivity dispersion phenomena.

As such, the previous resulting correlations between electrical attributes and physical properties of cement material at atmospheric condition are not fully applicable for oilwell cement system at which elevated pressure and temperature are imposed. In response, some modified or new correlations must be introduced for better prediction of cement's physical properties. Furthermore, as cement hydration proceeds, the pore solution conductivity may not solely contribute to the overall conductivity due to the presence of interface conductivity - especially at the elevated pressures and temperatures. This condition may exist due to the effect of electrical double layer (EDL) on the interface of pore solution and solid grain.

EDL contributes dominantly in low water saturation degree, pore solution, and pore geometry. Therefore, as cement hydration proceeds with time, the conductivity measurement of the cement should incorporate the interface conductivity. The effect of EDL on electrical properties of cement depends on the ratio of interface surface thickness to the pore radius. If the pore radii are small, the double layer can touch each other and may prevent the motion of anion as well. The ion motion, in addition, is undisturbed if pore radii are large [16]. A clear understanding for this will answer

the magnitude of interface conductivity and its contribution to the effective conductivity of the well cement.

1.4 Objectives and Contributions of Research

This research attempts to correlate the electrical attributes of well cement to its physical properties evolution. The major objectives of this work are as follow.

1. To identify the conductivity dispersion phenomenon and quantify the magnitude of interface conductivity and its contribution to the bulk conductivity.
2. To establish the water cement ratios, curing temperature and pressure interrelationship and its effect to electrical conductivity.
3. To develop a set of correlations for the prediction of the permeability and strength of oilwell cement by means of its electrical properties.

In accordance with the objectives above, this work is expectedly intended to enrich the knowledge on the topic through the following main contributions.

1. The laboratory investigation of electrical conductivity of oilwell cement performed under elevated temperature and pressure at different water cement ratios provides more reliable predictive correlations.
2. The potential existence of interface conductivity as contributions of temperature, pressure and water content can be obtained by the aid of cement particle expansion model.
3. The investigation of a cement microstructural interrelationship to electrical properties may provide some correlations in extracting permeability and strength that might provide certain alternative ways for cementing evaluation.
4. The electrical impedance technique for oilwell cementing evaluation is a new alternative technique to monitor the cement microstructure evolution *in-situ.*

1.5 Scopes of Study

In the following are the scopes of study:

1. Cement class G HSR with water cement ratios of 0.25, 0.3, 0.4, 0.5, and 0.55 which is standard cement used in oilwell industries.
2. Electrical impedance measurements using CoreTestSystem Autolab in the ranges of frequency from 0.2 MHz to 1 Hz.
3. Cement hydration is conditioned for all measurements up to 24 hrs.
4. Curing conditions are set to achieve pressure of 3000 psi and temperature of 65°C that correspond to the depth of 5000 ft.
5. Cement pore solution extraction using Fann HPHT API filtration press and its conductivity measurement uses conductivity meter.
6. No additive in the cement formula with an assumption to have a good cementing job without any contamination by the drilling mud and fluids formation.
7. Cement's compressive strength, permeability, and porosity are measured by using ultrasonic cement analyzer, gas permeameter and mercury intrusion porosimetry, respectively.

CHAPTER 2

LITERATURE REVIEW

This chapter provides a discussion on an oilwell cementing operation started from primary cementing design, effect of elevated temperature and pressure, API cement classifications and potential failures in cementing job. This is then followed by a review on the process of cement hydration and the associated constituents in the system. The discussion is ended with a review of cementing evaluation operations. Still as a continuance of this chapter, a review about the background of electrical impedance spectroscopy along with its advantages and limitations over several conventional methods is presented as well. This chapter subsequently is finalized by introduction of the electrical impedance phenomenon and its implications to composite materials as well as some common features within impedance measurements related to its permeability and strength properties.

2.1 Oilwell Cementing

Cementing operation is an important process in wellbore applications and used thoroughly worldwide. It should date back in 1903 when Frank F. Hill [17] ceased the operation of down-hole water using 50 sacks of Portland cement in California. This became an accepted practice for other California fields wherever difficulties were encountered. In 1910, A.A. Perkins [17] developed a two-plug cementing method that later has become the foundation of the development of modern oilwell cementing methods.

In wellbore, cement commonly is used in drilling and completion operations by placing it in an annulus. This process is performed by first drilling the borehole to a desired depth, continued with the removal of drill pipe and running the casing into the well until reaching the bottom of the well. Before commencing the cementing

operation, the drilling fluid is used to remove the formation cutting remained in the wellbore. Then, the cement is pumped through the borehole and pushed upwards through the annulus. In this case, sufficient strength and bonding should be well developed to secure and support the casing and formation in the hole.

2.1.1 Primary Cementing

After the casing has been run into the hole, the first cementing operation takes place immediately in placing a cement sheath in the annulus between the casing and the formation. This operation is called primary cementing. Figure 2.1 illustrates a typical profile of an oilwell cementing.

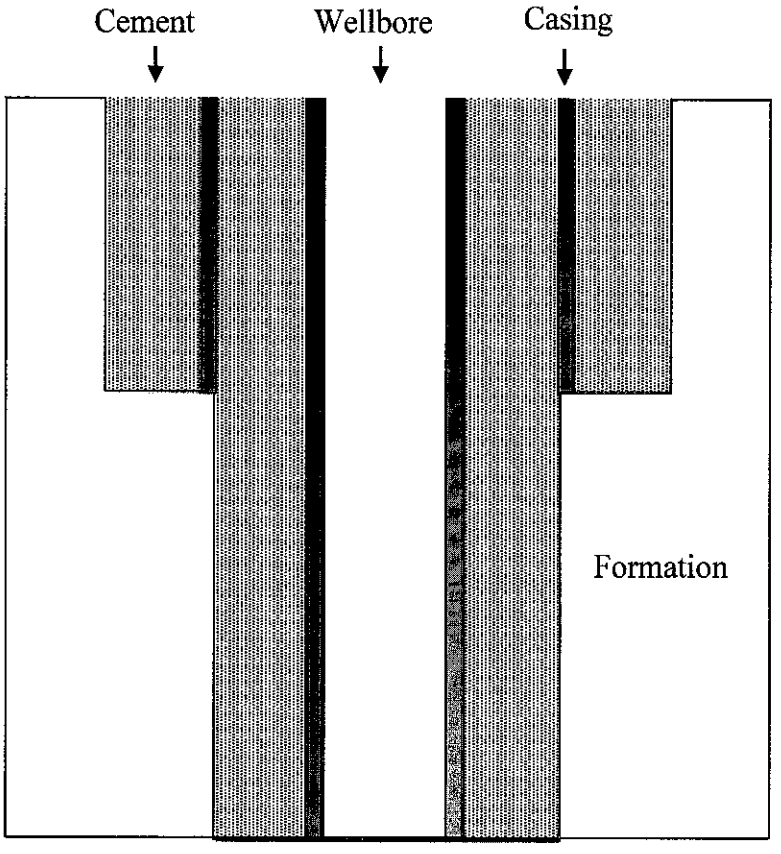

Figure 2.1 Illustration of typical cemented oilwell

The objective of the primary cementing is to provide a complete and permanent zonal isolation within the wellbore. This means that the cement sheath functionally must prevent any fluids circulation (gas, oil, water, etc) among different formation layers; specifically once the drilling fluid has been completely removed and replaced

by the cement slurry. In brief, the good mud removal and cement placement are very important to prevent a poor bonding quality which may cause gas channeling [18].

The other objectives of primary cementing are simultaneously to support and bond the casing to the formation and to protect the casing from corrosion. In response, the cementing operation must be designed to:

- restrict formation fluid to the wellbore,
- prevent these fluids to migrate among formation layers,
- ensure the control of well pressures encountered,
- prevent the contamination of freshwater, and
- withstand the casing.

Being failed to achieve these objectives may lead to reduce productivity. In the worst case, it may damage the well due to poor cementing condition. Burdylo and Birch [19] have identified several problems encountered in a poor primary cementing job:

- the well will never reach its full production potential,
- subsequent efforts to repair the cementing job may actually end up causing an irreparable damage to the formation,
- lost reserves,
- lower production rates,
- stimulation treatments may not be able to be confined to the producing formation,
- difficulty in confining secondary or tertiary fields to the pay zone,
- aquifer and reservoir damage from potential cross-flow,
- potential contamination of aquifers utilized as a resource.

Normally, once the primary cementing is failed to achieve its objectives, there will be a need to execute a remedial cementing operation. This is a basic operation that consists of two techniques, those are squeeze cementing and cement plugs [19]. It is performed by forcing cement slurry under pressure through holes or splits in the casing/wellbore annular space. Some challenges might occur such as in determining the appropriate position of cement failure or in assuring whether uniform filter cake has been formed. Therefore, representative evaluation tools, further discussed in Section 2.3, must be carefully conducted.

2.1.2 Effect of Curing Temperature and Pressure

Temperature and pressure in oilwell cementing operations are not similar to those in the general civil applications. The cement slurry during pumping may experience an elevated temperature (bottom hole circulating temperature) as high at 180°C. The pressure, meanwhile, may be at 22,000 psi consisting of hydrostatic load and pumping pressure, dependent on the geological formation and depth of the wells [20].

The effect of the elevated pressure and temperature on cement system, for some reasons, is manifold. Firstly, it may increase the hydration rate due to the accelerated consumption of Calcium Silicate (CS). Secondly, due to the acceleration of cement hydration, it may lead to enclosure of the cement grains by a product layer of low porosity, which will retard or prevent further hydration [20]. This has been confirmed in the latest research [21] on cement paste cured at 85°C exhibiting a less uniform microstructure due to a number of the clustered hydration products around the anhydrous grains. The role of this clustered hydration products acts as a barrier to continue the hydration and also to retard the diffusion process of the reagents. As a result, there will be no any ettringite (a hydrated calcium sulfoaluminate) appearing in the hydration products – not only leading the material product to be weaker in strength, but also making porosity and permeability higher compared to the similar water cement ratio and degree of hydration at identical curing periods.

The cement paste cured in temperature of about 70°C (or above) will modify the reaction of the aluminates and sulfate phases which can generate microcracking due to the delayed ettringite formation [20, 22]. It should be noted that the contribution of elevated temperature comes to be more significant than that of pressure to influence the hydration kinetic and physical properties of cement paste [20, 23]. The increases of temperature will accelerate the hydration rate as an effect of the heat increase liberated by the cement paste. This then makes the strength; grain surface area and gel water increase rapidly to its maximum values and then drop markedly. This drop is caused by the increase in the size of the particles of the reaction products [23]. Meanwhile, another author stated that this is related to the increased size of the crystals of the hydrated silicate [20].

On the other hand, the elevated pressure has less significant by which it causes slight increases in the hydration rate and surface area [22]. Undergone by mean of the

pressure, the elevated pressure during hydration process consolidates the structure of cement slurry and ceases the expansion of the entrained air in the slurry. Hence, the mixed cement particles and water, as the setting occurs, will experience a decrease in volume and also accelerate the rate of hydration.

2.1.3 American Petroleum Institute Classification

Because Portland cement was not applicable to be used in the wellbore conditions (elevated pressure and temperature); American Petroleum Institute (API) in response established the first committee to study cements in 1937. The first standard of recommended practice was published in 1952 and also has been periodically modified until present in which 8 classes of oilwell cement have already been resulted so far [17]. The classification itself was based on the depth, temperature, and pressure to which they experienced to. Additionally, they were listed in the API standards 10A Specification for cement and materials for well cementing dated April 2002 [24]. Tables 2.1 and 2.2 present the slurry requirement and strength specification for each class of API cements.

The descriptions of the API cement classifications are presented as follows:

Class A: Intended for use from surface to 6,000 feet when special properties are not required. It is similar to ASTM (American Society for Testing and Materials) Type I construction cement.

Class B: Intended for use from surface to 6,000 feet when conditions require a moderate or high sulfate-resistance. It is available in both moderate sulfate-resistant and high sulfate-resistant types. It is similar to ASTM C 150 (Type II).

Class C: Intended for use from surface to 6000 feet when conditions require high early strength. It is available in ordinary, moderate sulfate-resistant and high sulfate-resistant types. It is similar to ASTM C 150 (Type III).

Class D: Intended for use from 6000 to 10000 feet under the conditions of moderately high temperatures and pressures. It is available in moderate sulfate-resistant and high sulfate-resistant types.

Class E: Intended for use from 10000 to 14000 feet under conditions of high temperatures and pressures. It is available in moderate sulfate-resistant and high sulfate-resistant types.

Class F: Intended for use from 10000 to 14000 feet under conditions of extremely high temperatures and pressures. It is available in moderate sulfate-resistant and high sulfate-resistant types.

Class G and **H**: Intended for use as the basic well cement from surface to 8000 feet. These can be added with additives to overcome a wide range of depths and temperatures.

Table 2.1 Cement slurry requirement from various API cement classes [24]

Phase components	**Classes A and B (g)**	**Class C (g)**	**Classes D, E, F, H (g)**	**Class G (g)**
Mix water	355 ± 0,5	383 ± 0,5	327 ± 0,5	349 ± 0,5
Cement	772 ± 0.5	684 ± 0,5	860 ± 0,5	792 ± 0,5

Table 2.2 Compressive strength requirement of API cements classification [24]

Cement Class	**Curing temperature (°C)**	**Curing pressure (psi)**	**Minimum strength at 8 h ±15 min (psi)**	**Minimum strength at 24 h ±15 min (psi)**
A	38	14.7	250	1800
B	38	14.7	200	1500
C	38	14.7	300	2000
D	110	3000	500	2000
E	143	3000	500	2000
F	160	3000	500	1000
G	60	14.7	1500	no requirement
H	60	14.7	1500	no requirement

2.1.4 Potential Failures in Cementing Job

Failure in mechanisms in terms of time can be divided into two. The first failure is related to the occurrence during or after primary cementing and the second one is from days to months and years after cementing processes.

Watson *et al.* [18] stated that major problems occurred during or after cementing operation were the invasion of fluids through the cement matrix during waiting on cement (WOC). It might affect the high annular pressure at the surface, poor zonal isolation and blow-outs if not properly prevented. In the early hydration, they added, the gel strength development of the slurry was responsible for the migration process as it had changed from a liquid to solid. This changes in some literature are known as transition time as illustrated in Figure 2.2. According to Figure 2.2, it illustrates that when the hydrostatic pressure of the liquid phases matches the formation pore pressure, there is a risk of gas migration of formation fluid influx. A short critical hydration period limits migration of contaminants into the cement slurry [25].

Meanwhile Duguid [26] suggested that in common there were two possible paths of fluids to migrate in the wellbore. The first path was where fluids migrated through an annulus at the interface between the cement and the formation, and between the casing and the cement. The second one was through the pores of pathways of the well cement. Figure 2.3 illustrates these mechanisms.

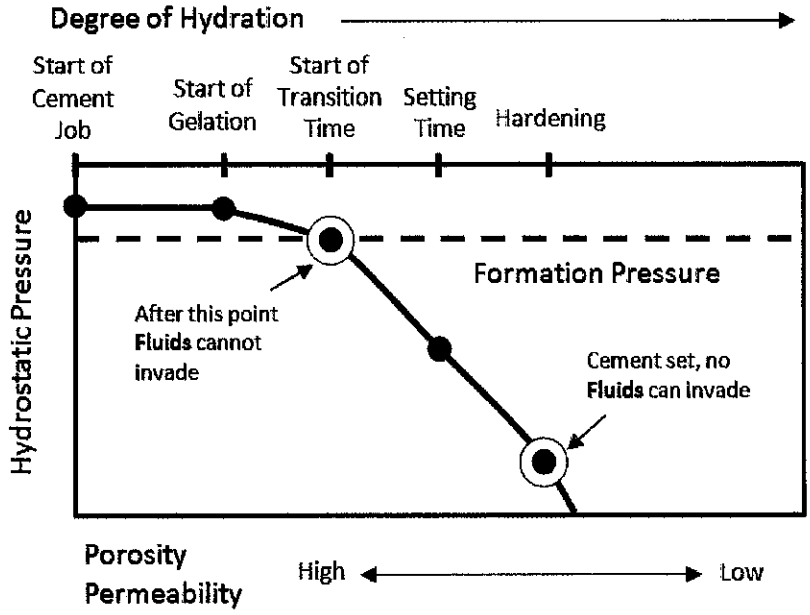

Figure 2.2 Hydration process of oilwell cement during hydration [25]

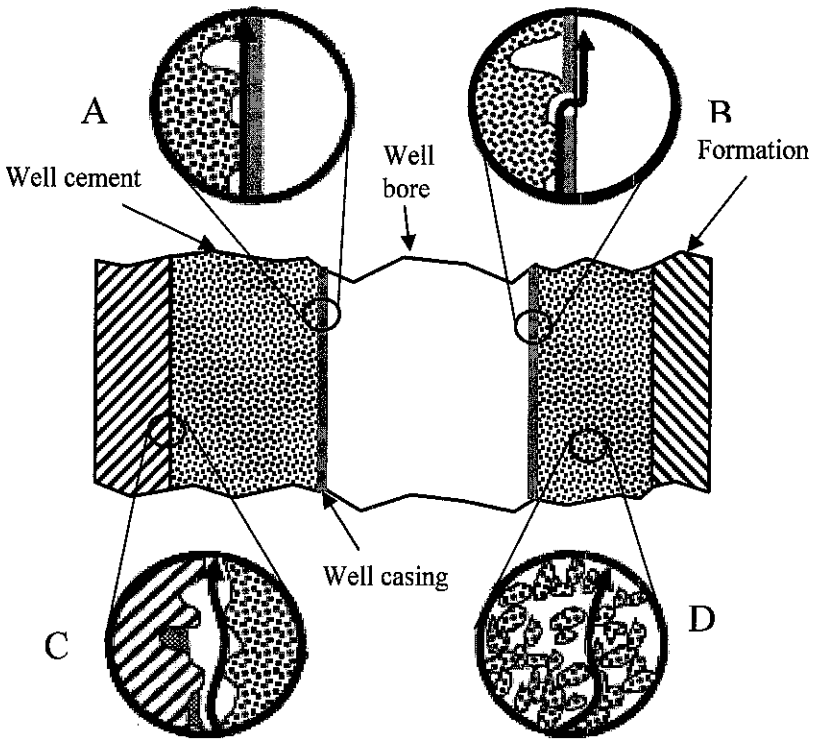

Figure 2.3 Illustration of fluids migration through (A) annulus at the interface between casing and cement, (B) damaged casing and migrating upward inside the well, (C) annulus at the interface between cement and formation, and (D) connected pores of the well cement [26]

It is found that the potential occurrence of fluids migration may be prevented by carefully designing the cement system that has met the designated requirement based on the well conditions. Among these requirements are accurate slurry density design, preventing excessive filtration loss, and free water, and short transition period of gel strength development. Moreover, proper mud removal and good casing cement bond should be well treated to support the aforementioned requirements.

Although it may be prevented, the actual conditions of cement after displacement must be evaluated in such a way that potential fluid migration can be detected. This not only can save extra expenses but also can make remedial cement job able to perform immediately. The well known detection tools for cementing evaluation are cement bond logs and acoustic log. They function well in detecting the bonding quality in the interface between cement-casing and cement-formation. However, they may not be able to detect and quantify the inter connected pore in the cement matrix due to its limitation of density based mechanism[13–15].

2.2 Hydration of Cement

Hydration of cement refers to a process in which the water-cement mixture is converted into the corresponding hydrates in the form of a stone-like material once the cement powders have been mixed with water. The chemical reaction taking place in cement hydration commonly is more complex than the simple conversions of cement powder into the solid materials. During a hydration process, both mechanical and physical properties change constantly along with the chemical reactions.

The major compounds in the cement clinker include tricalcium silicate ($3CaO \cdot SiO_2$), dicalcium silicate ($2CaO \cdot SiO_2$), tricalcium alumina ($3CaO \cdot Al_2O_3$), and tetracalcium aluminoferrite ($4CaO \cdot Al_2O_3 \cdot Fe_2O_3$). In cement chemistry terminology, these compounds are abbreviated as C_3S, C_2S, C_3A and C_4AF, respectively. Typically, the percentage composition of Portland cement consists of 50-70% C_3S, 15-35% C_2S, 5-10% C_3A, and 5-15% C_4AF [20]. These reactions along with hydration process may be represented in the form of degree of hydration which mainly depends on cement compositions and curing conditions. In turn, each compound has a specific contribution to the development of both physical and mechanical properties of cement system.

The degree of hydration (α) presents the ratio between the amount of cement that has reacted or has been dissolved at time t relative to the original amount of cement. It is a term that describes to what extent the hydration process has proceeded. Reports [6, 20] found that the strength could be related to the amount of the hydrated cement in the form of linear relationship. Meanwhile, it has also been confirmed [27] that strength of well cement has a linear relationship to hydration rate from Thermo Gravimetric Analysis (TGA) measurement from different water to cement ratios as shown in Figure 2.4.

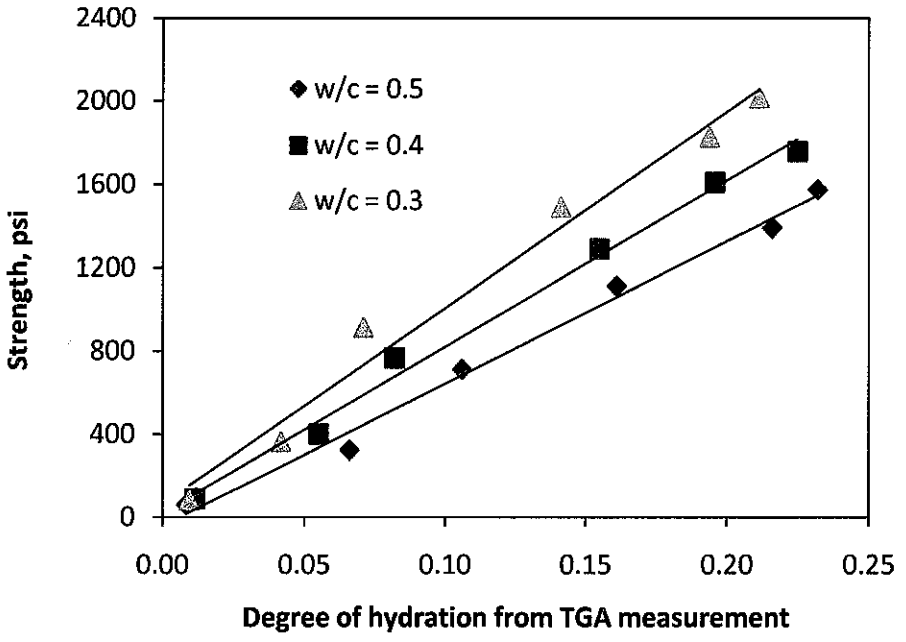

Figure 2.4 Linear relationships between compressive strength and degree of hydration at different water to cement ratios of Class G cement [27]

The strength and degree of hydration relationship simply related to the amount of strength achieves to that of the total (maximum) strength evolved for a 100% reacted sample. The degree of hydration as a function of time $\alpha_{(t)}$ here has been calculated through the Byfors equation [28]:

$$\alpha_{(t)} = \frac{S}{S_o} \tag{2.1}$$

where S is the cumulative strength evolved and S_o is the maximum theoretical strength of cement at complete hydration.

The number of S_o is dependent on water to cement ratios and obtained by correlating strength and porosity based on the Hasselman [29] model in the form of linear relationship as follows:

$$S = S_o - b\phi \tag{2.2}$$

where S is the strength, S_o is the strength at zero porosity, ϕ is porosity, and b is an empirical constant.

2.2.1 Calcium Silicate Hydrate (C-S-H)

In the hydration products calcium silicate hydrate is a major component occupying about 50 to 70% [20]. It is also the most important phase in determining the properties of the cement and significantly contributes to the strength development [6]. This phase is formed as the reaction of C_3S resulting in a particular variety of C-S-H, which is a generic name for any amorphous or poorly crystalline calcium silicate hydrate [20]. The dashes in "C-S-H" indicate that there is no any specific composition implied.

Although being poorly crystalline which is nearly amorphous and small particle with indefinite morphology and high surface area, C-S-H forms a continuous layer that bounds the original cement particles as one into a cohesive structure. The inter-layer bonding here is dependent on water to cement ratios, curing temperature, and additives.

Besides this dependent variable, the interlayer binding process is also affected by the ratio of CaO to SiO_2 (C/S ratio). Normally, the C/S ratio is approximately from 1.5 to 2.5 in height, depending on water cement ratios, present of admixtures and hydration temperature [20]. However, because of the variability in stoichiometry, the C-H-S interlayer may be buckled and does not fit together neatly. This, as a consequence, might form an irregular size and some shape of spaces between the sheets layer - known as the gel pores.

To comprehensively understand the physical and mechanical properties of C-S-H, which may represent the cement itself, it relies heavily on an interaction between the surface of the solid and water. The water in the C-S-H ranges from capillary water in the macro-pores to gel water in the micro-pores, in which both are normally electrically conductive. By this electrical conduction, it might be possible to describe and characterize the microstructure development using its electrical properties data.

The gel water is more dominant to keep the layers apart with a disjoining pressure. As a consequence, when this water is reduced due to the drying mechanism or even the partial drying of C-S-H, it can impart a permanent physical damage to a gel microstructure [20].

2.2.2 Calcium Hydroxide (CH)

Calcium hydroxide (portlandite) occupies about 10-35% of the volume of hydrated cement [20]. It forms from C_3S and to lesser extent C_2S. With its well-defined stoichiometry, calcium hydroxide then forms as crystals with a wide range of shapes and sizes, depending on the free space available for growing.

Apart from C-S-H, calcium hydroxide gives less contribution to the strength and permeability of the cement due to the total pore volume that has been reduced by converting some of the liquid water to be solid. Furthermore, as CH crystal is soluble, it then can leach out of the microstructure leaving large pore volume; generate a number of open channels for the entrance of aggressive fluids [20], increasing porosity, and permeability and also reduce strength making the cement more vulnerable to a chemical attack. However, calcium hydroxide, once dissolved into pore solution, may give a pH in excess of 13. In addition, the present of CH crystal can minimize the amount of shrinkage occurred in a dried cement [30].

2.2.3 Calcium Sulfoaluminates

Calcium sulfoaluminates (CS) occupies about 10-20% of the mature cement [30]. Similar to gypsum admixture, calcium sulfoaluminates, formed from the reaction of the aluminate, ferrite and sulfate phases with water, have less contribution to the engineering properties of cement. Sometimes, gypsum admixture is added to retard the premature setting due to a very fast reaction. The ettringite ($C_6AS_3H_{32}$) is formed as a result of C_3A (about 5-10%) and C_4AF (about 5-15%) [20] reaction with gypsum which then forms the needle-shaped prismatic crystals. In Portland cement, ettringite (due to being metastable) reacts with C_3A and transforms to the monosulfate hydrate (C_4ASH_{18}) in the form of hexagonal-plate crystal [20].

2.3 Cementing Evaluation Job

After the cement slurry has been displaced into wellbore, it is normally checked by using cementing evaluation tools. The main aim of using this tool is to check whether the objectives have been reached after displacing cement although the design and

execution in the cementing process have been well prepared. Therefore, a clear understanding of the objectives of the cement job becomes to be crucial if representative quality of cement evaluation jobs is needed to be employed. Otherwise, there will be no evaluation of cement job if the objectives are not clear. Some of the commonly techniques used in the cement evaluation job will be discussed in the next section.

2.3.1 Hydraulic Testing

Hydraulic testing, once primary cementing has been done, is used to assure an effective zonal isolation. It is strongly related to the hydraulic bonding which provides an adequate mechanical support to hold the pipe in place. Good hydraulic bonding blocks the migration of fluids in a cemented annulus and an evaluation mechanism therefore will be done by applying pressure at an interface between cement and casing. Dry and pressure testing become the two major techniques used to evaluate the degree of isolation provided by the cement job.

Dry testing is aimed to provide a good cement seal in wellbore particularly at the top of a liner [31] by ensuring that there is no change of downhole pressure due to a formation of fluids invasion during the opening of the downhole valve. While in pressure testing, additional pressure is exerted in the internal casing shoe which is larger than the expected pressure in the resuming drilling. A poor cement job is suspected when the casing shoe does not hold this pressure. However, these techniques may impair or induce the wellbore system due to the release of its high pressure.

2.3.2 Temperature and Noise Logging

Temperature testing works are based on the detection of the released temperature from the exothermic reaction during cement hydration. The increasing temperature, as a result, induces a deviation from the normal temperature gradient. It is used mainly in determining the top of cement and detecting the leaks and channeling in the interface between cement-casing and cement-formation. The test performance, furthermore, is determined by many factors such as annular thickness, heat conductivity of formation,

cement composition, additives, and long cement column by which these factor may bother the detection of temperature changing.

The noise log, meanwhile, is intended to detect noise caused by flowing gas, water, or oil behind the casing. From this tool, an indication of fluids flowing with its potential magnitude problem can be obtained. During performance, it is highly determined by the static noise measurement and, as consequence, it is found to be difficult to detect any flowing fluids in formation-cement or cement-casing if the tool moves continuously [31].

2.3.3 Acoustic Logging

Cementing evaluation using acoustic signal is the most widely used to locate the cement behind casing, that is by transmitting a signal or a vibration to the surrounding environment of well and by recording its amplitude and arrival time [15]. At this point, both the amplitude and arrival time are interpreted to ascertain the quality of bonding. A qualified bonding between cement-casing and cement-formation is reflected by a good acoustic coupling. However, because of the lack of reliable relationship between the acoustic signals and surrounding well isolation, this method requires a clearer understanding of the well, formation, and casing data and also the history of the previous neighbor wells.

The well known tool used based on the acoustic method is the cement bond log also known as CBL. It was initially developed in 1959 for induction and sonic logging based on the transit-time curve on open hole when it ran inside the casing [32]. This device subsequently started to improve in their configuration as well as in log response interpretation to minimize the attenuation made factors affecting the quality data measurement. In general, some factors that may affect the amplitude measurement of CBL include temperature and pressure, wellbore fluid properties, casing size and thickness, cement thickness, and rocks formation properties. In fact, this becomes a basis for any improvement in acoustic wave propagation between transmitter and receiver for the development of such tools in evaluating the cement-casing and the cement-formation bonding in wellbores.

However, there is still a limitation on acoustic log measurement - especially in the fast formation for not being able to provide an accurate data related to the bonding quality. The fast formation is a rock in which the shear velocity is faster than the compressional velocity of the fluid in the borehole. In addition, the sound velocity of the casing that is less than the fast formation, consequently resulting in an interfere from the formation arrival signal to the casing [31]. Furthermore, the high amplitude in acoustic log may result in deviation of data measurement in cemented section leading the precise determination towards channeling or microannulus to be difficult.

2.3.4 Electrical Logging

Electrical logging is a primary tool in formation evaluation to determine water saturation which is used as a basis for reserve calculations [10]. In application, this tool uses an electrical current penetrated through the interstitial water saturating the pore structure of the formation. The current, in this case, is supplied by the discharging electrodes to generate a static electric field. Meanwhile, the resulting electric potential is sampled at the measuring electrodes. The formation water is electrically conductive containing dissolved salts and dissociated into the positively charged cations and the negatively charged anions.

The logs could provide either resistivity or conductivity (inverse of resistivity) based measurement dependent on formation water, amount of water present and pore structure geometry. With the current development, electrical logging can be performed not only in open hole but also in the cased hole within wellbore [33]. The method for measuring electrical formation through casing is to apply the current into the casing and to measure the casing current between two segments. By measuring the tool voltages and currents, the formation current is derived using Ohm's law as described in Equation (2.3).

$$I = \frac{V}{R} \tag{2.3}$$

where I is formation current, V is voltage, R is resistance.

Most of the applications of these electrical logs are to characterize the formation of rocks including water saturation, porosity, and microstructure properties. However, with the advancement of cased hole electrical measurement, it also can measure the electrical properties of the wellbore profiles in a serial fashion as a function of the steel conductivity, cement conductivity, and formation conductivity as shown in Figure 2.5 [33]. Hence, the measured data of cement conductivity from electrical logs may be used to interpret its physical properties development as a function of hydration time.

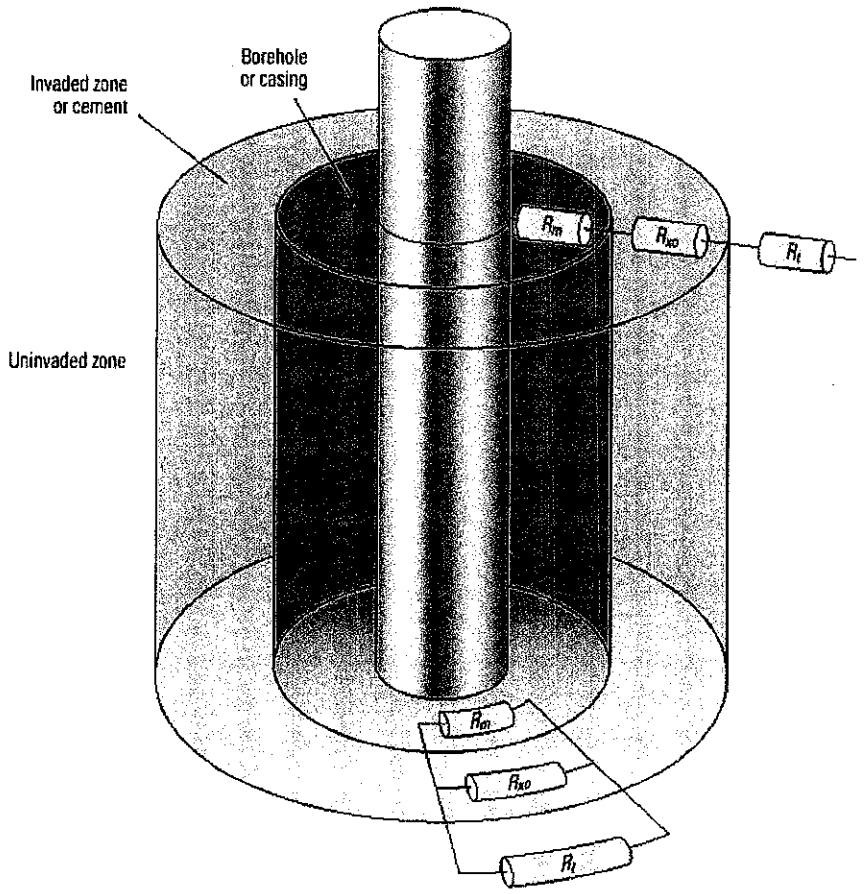

Figure 2.5 Cased hole resistivity current paths [33]

2.4 Electrical Impedance Spectroscopy (EIS)

EIS is a testing technique for measuring the electrical response of a material to an AC excitation. Although being relatively new in the cement and concrete science [8, 34], the applications of EIS have been used for several decades in the electrochemical field [2]. Gu *et al.* [35], for instance, have linked EIS parameters to the hydrated cement

paste properties such as ionic concentration of the pore solution and pore size distribution. Other investigations have used these parameters to characterize the microstructure properties of cement based materials [1, 2], and to monitor the evolution of some of its physical and mechanical properties later on, such as porosity, strength, and permeability commonly applied in the atmospheric condition [3–9].

The technique associated in the EIS measurement may overcome a major drawback in DC measurement such as electrical polarization as an effect of a displacement of bound charges in a dielectric when placed in an electric field. The electrical polarization occurs in an electrode-cement interface with a reaction initiating an excess of electrical field opposing the applied voltage needed to be well considered in a resistance calculation [2]. The conventional method in DC measurement to overcome electrical polarization is performed by applying high voltage values (usually in tens of volts) to generate heat which, as an effect, may alter the cement microstructure [36].

Through the recent development of the EIS technique such as a direct interface between machines to a PC, the data collection is made easy and flexible in the type of materials. Moreover, for being noninvasive and nondestructive, it enables the test to sample the microstructure *in-situ* without water removal, usually by heating, which is known to be possible to permanently damage the cement microstructure [2].

2.4.1 The Basic Concept of Electrical Impedance

Electrical impedance extends the resistance concept in AC circuit with the addition of a phase angle. It is a measure of the ability of material to resist (resistivity) or to flow (conductivity) electrical conduction through it. The technique is run by applying a small sinusoidal voltage to a material which exerts an induced current. As a result, this current will be out of phase with the voltage by an amount – also known as the phase angle (θ) (Figure 2.7). This phase shift is due to the presence of capacitive and inductive responses of the specimen. The measurement procedure involves a wide range of frequencies (MHz - mHz) that allows measurement to distinguish different electrical responses [35].

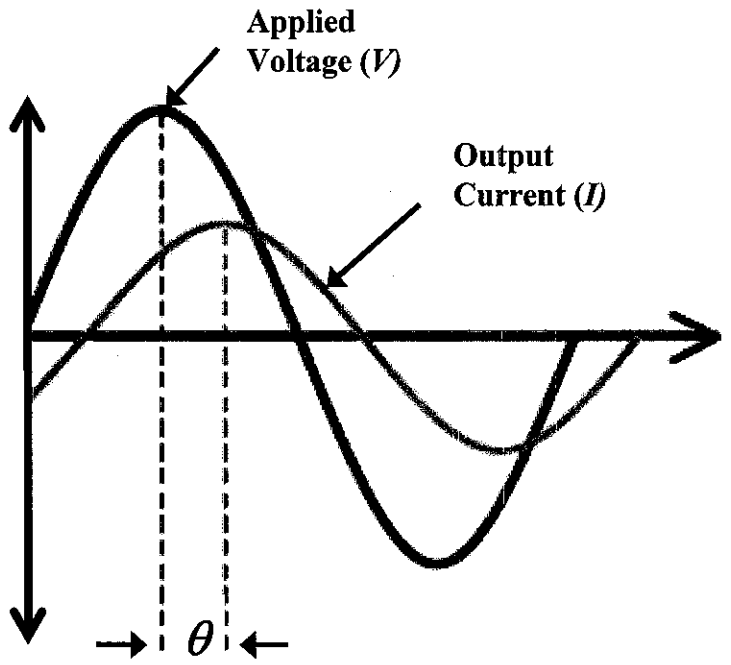

Figure 2.6 Schematic relationship between applied voltage, induced current and phase angle in EIS measurement [35]

The principle formulation of impedance calculation is according to the analog of Ohm's law as $V = I \cdot Z$, where V is the voltage, I is the current, and Z is the impedance. The impedance here refers to frequency dependence resulting in a set of real and imaginary impedances normally represented in vector in complex plane (Figure 2.7).

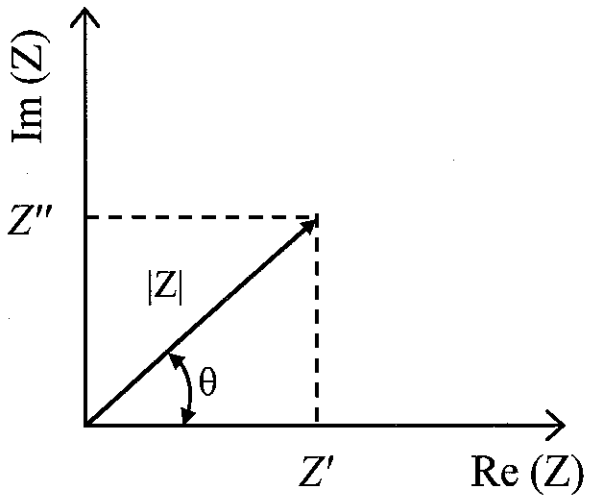

Figure 2.7 The impedance, Z, plotted on a complex plane in both rectangular and polar coordinates [35]

Figure 2.8 shows the result of impedance measurement in a Nyquist plot (a graph of Z' versus Z") for neat cement with w/c 0.4 at about 20 hrs of hydration. In the Nyquist plot, high frequency could be in a semi-circular form representing a material response, while low frequency exhibits polarization due to a contact between electrode and material. Furthermore, the bulk profile of the material obtained at the intersection of the two arcs where the imaginary impedance is practically zero becomes the most important parameter. Further analysis will be discussed in Chapter 4.

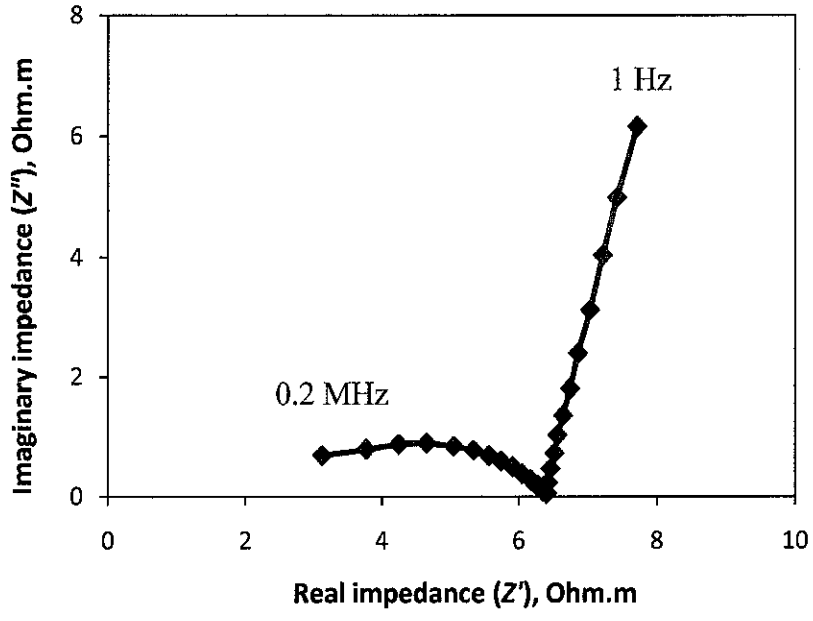

Figure 2.8 Typical Nyquist plot of Class G neat cement for w/c 0.4 at 20 hrs of hydration [37]

Once the impedance has been located in the complex plane, the voltage and current can be described in polar coordinates as stated in Equations (2.4 and 2.5) [38]:

$$V_{(t)} = V_o \exp(j\omega t) \tag{2.4}$$

$$I_{(t)} = I_o \exp(j\omega t - j\theta) \tag{2.5}$$

where t is time, V_o is voltage amplitude, I_o is current amplitude, $j = \sqrt{-1}$ (unitless), ω is angular frequency $(2\pi f)$, f is frequency, and θ is phase shift.

By submitting into Ohm law, $Z = V_{(t)}/I_{(t)}$, impedance in polar form would follow Euler expansion (Equation 2.6):

$$Z = Z_o \exp(j\theta) = Z_o cos\theta + jZ_o sin\,\theta \tag{2.6}$$

As such, impedance amplitude (Z_o) and phase shift (θ) can be related to the real and imaginary impedances as follows (Equations 2.7 and 2.8):

$$Z_o = \sqrt{(Z')^2 + (Z'')^2} \tag{2.7}$$

and,

$$\theta = tan^{-1}(Z''/Z') \tag{2.8}$$

Generally, the electrical response of a composite material is determined by the properties of raw phases, pore volume, connected pore, and geometry of the microstructure [4, 35]. In this case, the responses are represented in the form of the electrode, interface and the bulk material in the Nyquist plot. As a consequence, resistance (R) and capacitance (C) are exhibited based on the characteristics of relaxation time or time constant. Resistance is related to the resistivity (ρ) and capacitance is related to the dielectric constant (ε) through the relationships given in Equations (2.9 and 2.10):

$$R = \rho(l/A) \tag{2.9}$$

and,

$$C = \varepsilon\varepsilon_o A/l \tag{2.10}$$

where l is the length of the sample, A is the cross section area, and ε_o is permittivity of free space (8.85×10^{-12} F/m).

2.4.2 Electrical Impedance of Cement-Based Materials

The initial study using impedance technique was performed by McCarter *et al.* [40] on the Portland cement paste. A clear dependent was clearly shown for the frequency to the measured electrical profile which was reflected along hydration process. This then has triggered other investigators to apply such technique not only in investigating hydration mechanism [5, 9], microstructure characterization [2, 3, 41, 42], water content and pore structure assessment [43–45] but also in evaluating the physical properties performance [4, 8, 46–48]. Noted here, most of these studies were performed at atmospheric conditions and standard Portland cement.

Figure 2.9 depicts a typical impedance response in the form of Nyquist plot that mainly consists of low and high frequency arcs. The high frequency arc (low diameter) is associated with the bulk properties of the cement paste due to solid-liquid interface phenomena. It has a capacitance effect due to charge separation within the pore solution as illustrated in Figure 2.10. The low frequency arc (high diameter), on the other hand, is related to the interface of electrode-cement specimen which generates electrical polarization [36].

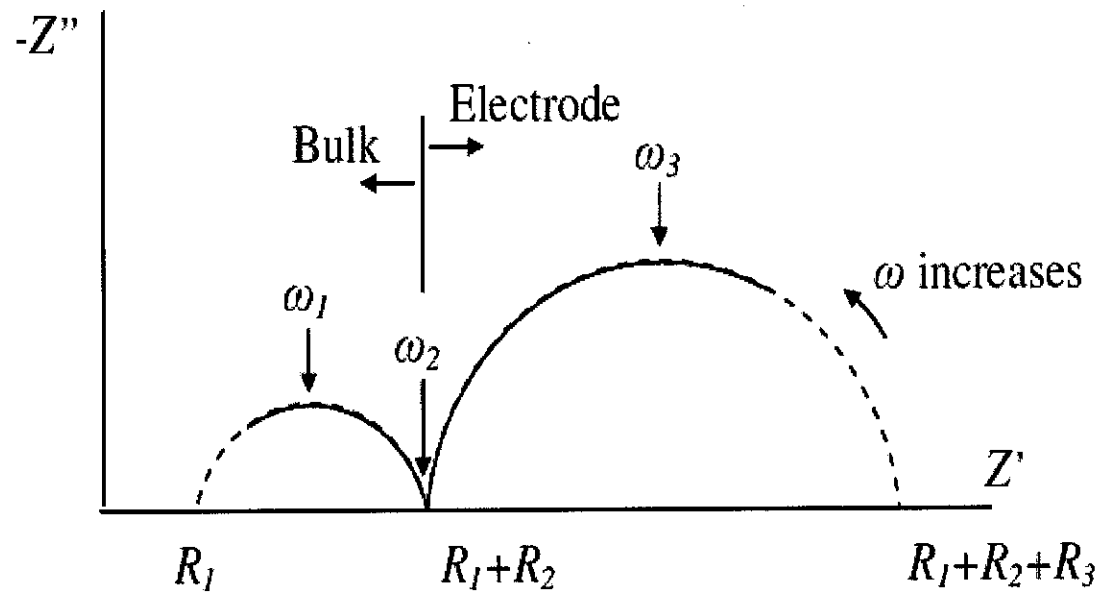

Figure 2.9 Schematic representation of a cement paste Nyquist plot obtained from EIS measurements [34]

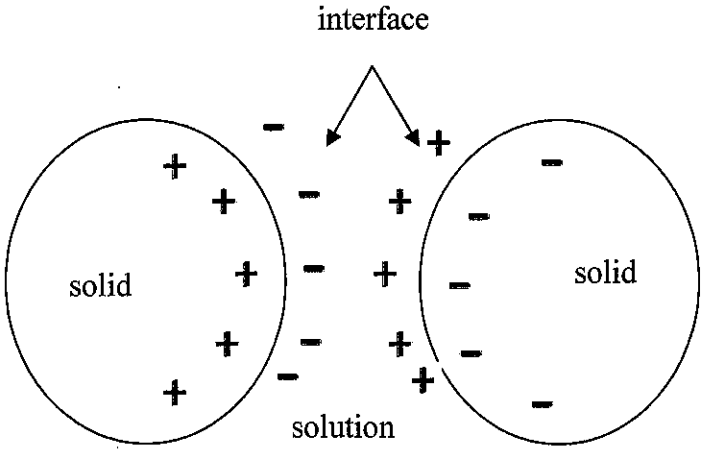

Figure 2.10 Illustration of the solid-liquid interface [35]

The intersection of two arcs in the Nyquist plot is found to describe the electrical resistance of the bulk specimen. This point usually refers to bulk resistance (R_b= R_1+R_2) which is observed to increase as cement hydration proceeds as an effect of connecting pore reduction and more tortuous [4]. The frequency at this point is called cut-off frequency and it dependent on the hydration rate, specimen compositions, and moisture content [40]. This indicates that a single AC frequency measurement may not be reliable in determining the bulk resistance as the cut-off frequency may vary to some orders of magnitude as function of hydration time, water cement ratios, and cement compositions [4].

Furthermore, a depression of bulk impedance between both arcs was observed (Figure 2.11) indicating a spread of relaxation times in the system and also a non-ideal capacitive nature of the system resulting in a distribution of time constant in the system. However, as hydration continues the bulk arcs tend to form complete semi-cycle as can be seen from Figure 2.11. Gu *et al.* [3] explained that the depression of the bulk arc was related to the pore size distribution and pore geometry at which wider pore size distribution could result in a higher depression. This depression angle was found to increase slightly with hydration ages.

This phenomenon can be described using a constant phase element (CPE) acting as a non-ideal capacitor with the impedance formulated as shown in Equation (2.11) [4]:

$$Z_{CPE} = \frac{1}{A(j\omega)^n} \tag{2.11}$$

where A is constant, ω is angular frequency, and n is a dimensionless parameter between 0 and 1. An n value of 1 indicates no depression, only one relaxation time for the system, *i.e.*, a perfect semicircle, and decreasing value of n increases relaxation time distribution in the system.

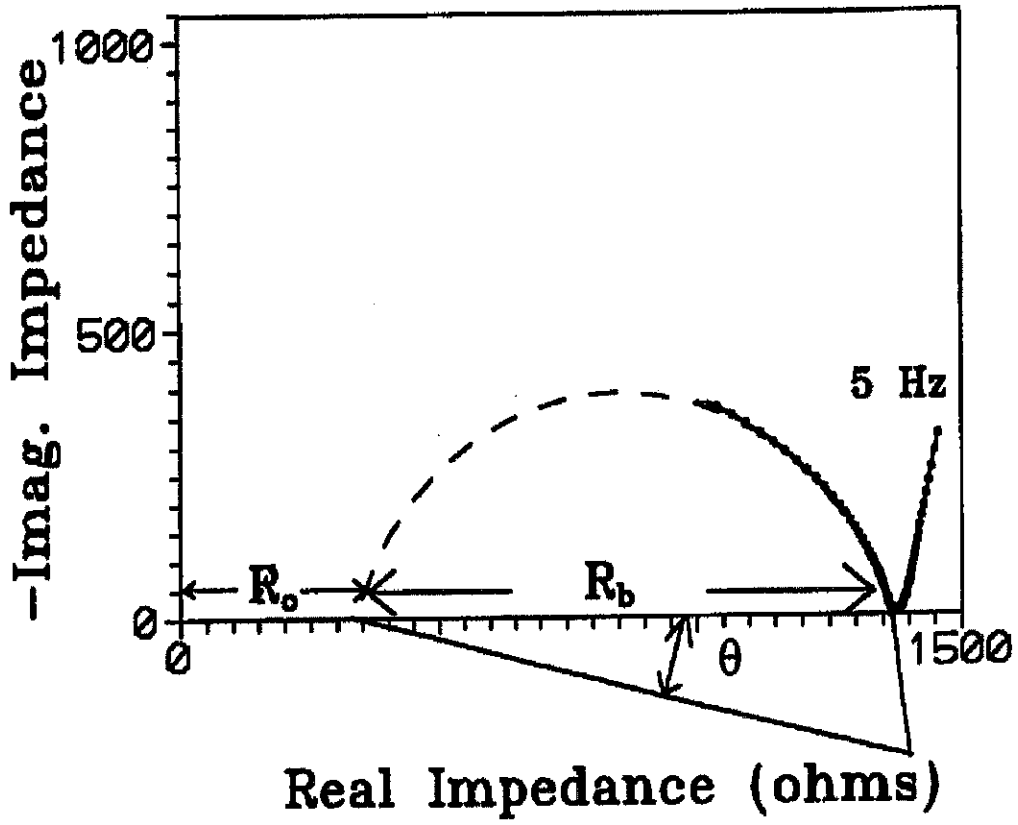

Figure 2.11 Schematic representation of a non-ideal capasitor (constant phase element) ilustrating the arc depression in the Nyquist plot of OPC cement at 12 days of hydration. The angle, θ, is defined as the angle between the real axis and the longest chord of the full semicircle [49].

As such, electrical conductivity (σ_b) is obtained from the bulk resistance (R_b) by taking into account the effect of geometry factor (G) as stated in the following Equation (2.12):

$$\sigma_b = \frac{G}{R_b} \tag{2.12}$$

The use of electrical conductivity seems to be trivially different from resistivity (just the inverse factor). However, conductivity for the physical point of view has a better pedigree as exemplified by Glover [50] in which the solution conductivity was defined by the density of charge carriers' n multiplied by their charge q and by their mobility β as stated below:

$$\sigma_o = n\,\beta\,q \tag{2.13}$$

Christensen *et al.* [4] concluded their impedance study by means of conductivity response in the cement pastes by which the electrical conductivity is increased with the amount of evaporable water in the paste. The conductivity is also increased with the concentration of mobile ions in the pore fluid, and is further influenced by the connectivity (or tortuosity) of the pore network. The connectivity is defined as the square of the ratio of the effective path length l_e in the pore to the shortest distance l in a porous medium as shown in Figure 2.12. It is a geometric parameter and accounted for the pore space geometry.

$$\tau_f = \left(\frac{l_e}{l}\right)^2 \tag{2.14}$$

where τ_f is tortuosity factor, l_e is effective path length in the pore, and l length of the shortest distance of the pore, respectively.

In wellbore application, temperature effect on an electrical conductivity measurement should be well considered. Arps [51] studied the effect of temperature on electrical resistivity of sodium chloride solution in the range of 0-156 °C and found that it followed a linear relationship between the temperature and the ratio of resistivity.

Hammond and Robson [52], meanwhile, found the same effect of increasing electrical conductivity along with temperature in various cement and concrete. Later on, McCarter [36] used impedance technique on Portland cement in the temperature range of 10-80°C. The result showed that both the real and the imaginary component of the complex impedance were temperature dependent and these interdependence can be related through the Arrhenius relationship in the range of 10-50°C.

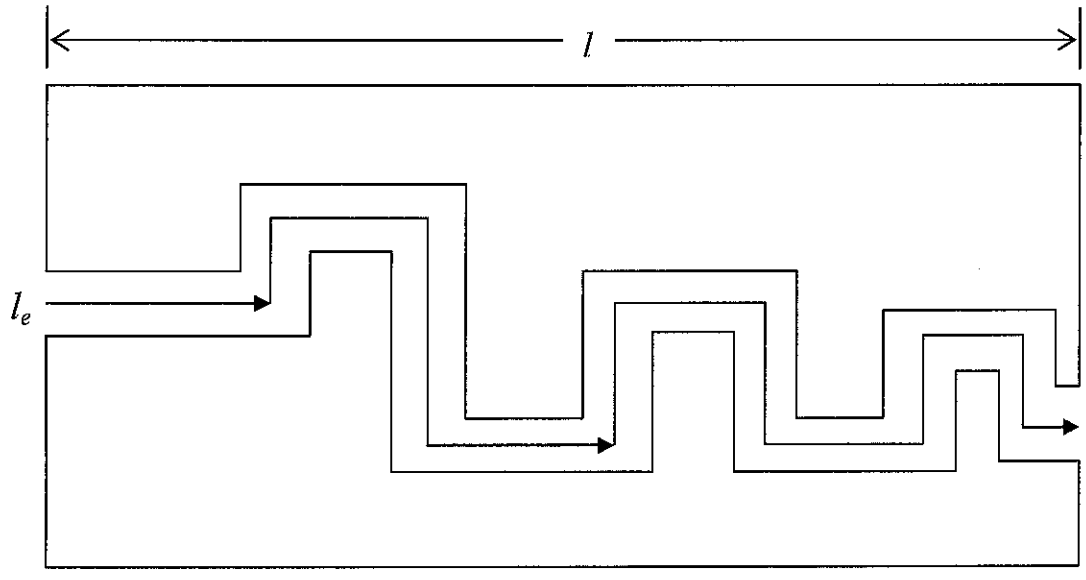

Figure 2.12 Schematic diagram of tortuosity concept [39]

2.5 Electrical Conductivity Properties and Relationship to Permeability and Strength of Composite Material

The electrical conductivity of a composite material containing a single conducting fluid phase depends upon the pore solution conductivities (σ_o) and pore volumes (ϕ). The bulk conductivity depends also upon the geometrical distributions of the matrix and the fluid, which control the connectivity of paths for current flow in the porous medium.

In composite material, the prediction of bulk conductivity is a non-trivial problem as a result of the complex distribution of solid and fluid phases each of which have different conductivities, volume fractions and connectivities. A large number of models have been published (refer to Section 2.5.2.2 for further discussion on the models) in the attempt to relate the electrical conductivity to its physical properties (i.e. permeability and strength). Some of them are valid only for particular composite material at normal conditions while many of them are fail to represent the cement system cured under elevated pressure and temperature. Hence, representative model that relates the electrical conductivity to permeability and strength of oilwell cement under elevated pressures and temperatures is required.

2.5.1 Conductivity Dispersion Characteristic

The dependent responses of conductivity on frequencies are called as conductivity dispersion. Electrical conductivity increases along with frequencies and in mixed cement (bulk conductivity) it is mainly controlled by properties of water. In most cases, the conductivity of its matrix is negligible, except if shaly materials are present which contribute to the bulk conductivity value. The contribution of pore solution to the bulk conductivity may occur in two ways, either by intrinsic electrolyte conductivity or by electrochemical interaction at the interface of fluid-solid matrix [16]. Bulk conductivity in this case is proportional to electrolyte conductivity for the first case, but in the letter, geometry of conductive path is controlling internal surface conductivity. It also should be noted here that an increase in a surface conductivity as a result of a decrease in water content will increase the magnitude of conductivity dispersion.

Panteny *et al.* [53] investigated the dependence of conductivity-frequency on the heterogeneous materials containing both conductive and dielectric (insulating) phases in a wide variety of materials, including ceramics, polymers and composites. They found that the bulk conductivity at low frequencies was frequency independent, but at higher frequencies the conductivity increased, following power-law behavior. However, Schon [54], in addition, mentioned that there was no dielectric material independence from frequency either in real or in imaginary part irrespective of low or high frequency. It was due to that, once the time varying electric field was applied through dielectric substance, the electric polarization may occur - depending on its frequencies. Electrical polarization was a phenomenon of relative displacement of the atoms or molecules.

The different types of electrical polarization are related to the different responses of resistance and capacitance of the product [36]. When the applying electric field is removed; the substance attempts to return to its initial state. The time needed for the system to return to its initial state is called as relaxation time and it may be different for the individual components in a cement system. This can be associated to the electrical response of individual components in the form of Nyquist plot. A different mechanism for electrical polarization can be developed that is electronic, atomic, dipole, interfacial, and double-layer polarization (Figure 2.13) [54].

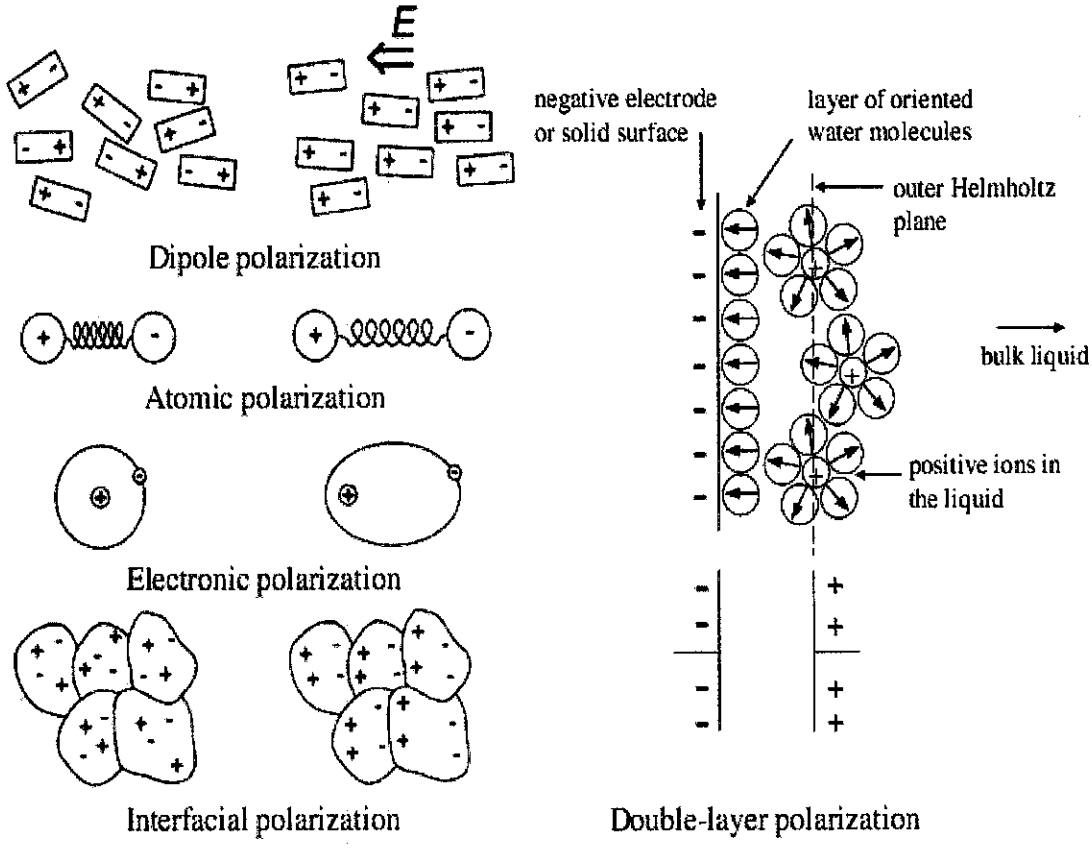

Figure 2.13 Mechanism of electrical polarization induced by the electrical excitation [54]

Electronic polarization arises from the displacement of electrons with respect to the nuclei with which they are associated upon application of an external electric field. It is occurred at frequency above 10^{13} Hz. Atomic polarization is intrinsic to the nature of the atom and is a consequence of an applied field. It is observed when the nucleus of the atom reorients in response to the electric field. Atomic polarization is usually small compared to electronic polarization in the ranges from 10^{9} to 10^{13} Hz. Dipole polarization originates from permanent and induces dipoles aligning to an electric field. Their orientation is disturbed by thermal noise that make dipole relaxation is heavily dependent on temperature. The frequency ranges for dipole polarization is about 10^{3} to 10^{9} Hz [54].

In conjunction with conductivity dispersion phenomena; pore solution, pore geometry and water content may generate an electrical double layer (EDL) that is formed on the interface of pore water and solid grain. The effect of EDL on electrical conductivity properties of cement material depends on the ratio of the thickness of

interface surface to pore radius [54]. Figure 2.14 illustrates the mechanism of the anion barriers due to change of pore radius. It is then suggested that the double layer can touch each other (barriers the anion) if the pore radii are small and the ion motion is undisturbed if the pore radii are large.

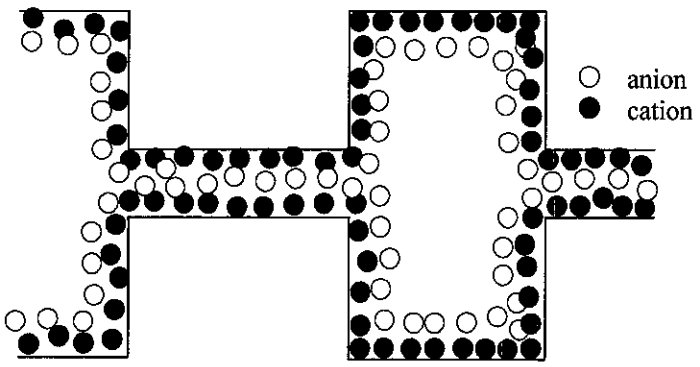

Figure 2.14 Mechanism of the anion barriers due to charge of pore radius [54]

The formation of an electrical double-layer adjacent to the solid surface is due to the effect of a net electric charge on the solid-pore void interface that attracts the counter ions from the solution. As a result, the pore solution has higher ionic concentration and electrical conductivity in the vicinity of solid surfaces. The interface excess conductivity is significant in some porous materials while it might be negligible in others, depending on the electric charge of solid surfaces. This value comes to be important to have a reliable interpretation of the overall conductivity data.

Johnson *et al.* [55] incorporated the surface conduction for the bulk conductivity (σ_b) of a porous material as below:

$$\sigma_b = \frac{1}{F}\left(\sigma_o + \sigma_s \frac{2}{\Lambda}\right) \tag{2.15}$$

where σ_s is the interface conductivity in siemens (S), F is formation factor, σ_o is pore solution conductivity (S/m) and term $2/\Lambda$ is a microstructural parameter analogous to the surface to volume ratio of the pores.

2.5.2 Electrical Properties of Cement System

Electrical properties of cement system depend on their curing conditions, water content, porosity, and interconnected pores. These responses also change as a function of hydration time, especially during early hydration. Any changes in the cement properties may reflect the electrical features of cement material. By that, the evolution of cement hydration process in terms of physical properties might be traced and predicted by means of its electrical attributes.

Cement material can be regarded as a composite material containing solid, liquid, and air phases. The solid phase mainly consists of calcium silicate hydrate and calcium hydroxide that have a conductivity of approximately 10^{-9} S/m. Meanwhile, air has a conductivity in the vicinity of 10^{-15} S/m [56]. By this, the solid and vapor phases practically are electrically insulating.

In liquid phase, Ca^{2+} and OH^- are the most important ions from an electrical conductivity point of view. Other significant ions that can be found in cement pore solution include Na^+, K^+, and SO_4^{-2}. Nevertheless, these ions are not able to be expected to have a constant conductivity during hydration processes since Ca^{2+} and SO_4^{-2} concentrations are gradually declined when hydration starts and Na^+, K^+, and OH^- concentrations increase slowly [57].

Since the solid and air conductivity are several orders of magnitude lower than that of pore solution conductivity, it may be considered that cement material consists of a single conductive component in which solid particles and air vapor are resistive. Here, the ratio of the bulk conductivity and pore solution conductivity is defined as normalized conductivity. As such, the electrical conductivity model is examined for certain samples that are fully saturated by water and only one phase, in this case, is to be considered to be conductive.

2.5.2.1 Temperature Correction

It is shown that electrical measurement is very sensitive to the change of ambient temperature. As such, a reasonable comparison between conductivity data obtained at the varying temperature can only be conducted after the temperature effect is corrected. The increase conductivity data is due to activated energy processes [58]

that enhance the mobility of ions and collide more vigorously in the pore solution. Therefore, correctness is a must purposively to compare the conductivity curve of well cement at different temperatures. Generally, the reference temperature to be corrected is at 25°C.

To determine and correct the effect of temperature variation on the conductivity of well cement, several methods have been proposed in the literatures. The approaches represent the theoretical and empirical-based equations. The theoretical one was introduced by Hammond and Robson [52] who have expressed the influence of temperature on conductivity on various cements and concretes using Arrhenius equation as stated in the following Equation (2.16):

$$\ln\left(\frac{\sigma(T)}{\sigma(T_{ref})}\right) = a\left(\frac{1}{T_{ref}} - \frac{1}{T}\right) \tag{2.16}$$

where T (°C) and T_{ref} (°C) are the absolute and reference temperature and a (°C) is an empirical coefficient. The authors suggested a = 2627 (°C) for concrete and a = 2027 (°C) for cement paste.

While the empirical-based equation was suggested by Arps [51] by which he generated the formula at temperature between 0 and 156°C based on the sodium chloride pore solution during logging process within wellbore as shown in Equation (2.17)

$$\sigma_{25} = \frac{46.5 \cdot \sigma_{(T)}}{21.5 + T} \tag{2.17}$$

where $\sigma_{(T)}$ is the conductivity at the designated temperature (S/m) and σ_{25} is the corrected conductivity at 25°C (S/m).

2.5.2.2 Conductivity Models for Composite Material

Many attempts have been made to model the microstructure properties of composite material by means of electrical conductivity. In response, both empirical and theoretical model have been employed to explain these phenomenon. Table 2.3 presents some of the commonly used models. In this table, σ_b represents the bulk

conductivity of composite material, σ_o represents pore solution conductivity and ϕ represents the pore volume fraction.

Parallel, also known as arithmetic, is a formula to estimate the normalized conductivity of a given phase conductivity and volume fractions [39]. However, this prediction usually tends to overestimate the conductivity of isotropic media since the model does not consider the microstructural geometry of the composite.

The Hashin-Shtrikman model [59], furthermore, provides an approach for estimating normalized conductivity using an upper and lower bound values. In this method, the phases are distributed in a number of parallel layers (beds with volume fractions and there are two values which limit the normalized conductivity). One parallel corresponds to a deformation perpendicular to the beds and the other one does to the beds. The upper bound is attained for a microstructure of spherical solid grains coated with a shell of water and fluids forms a percolating cluster, while the solid grains are isolated from each other [39]. For the lower bound, the solid phase forms the percolating cluster while the pores are isolated. As such, these bounds might be applicable to any types of particulate composites but not necessarily describing the behavior of layered materials.

Archie's law is an empirical relationship derived to estimate formation factor (inverse of normalized conductivity) for a saline solutions saturating clean porous sandstone [10]. This relation assumes that there is only one conductive phase (σ_o) to be distributed into an insulating matrix (σ_b). The cementation factor m in this case refers to an empirical parameter in the range of 1.5 to 4 based on the type of the sedimentary rocks. The larger the parameter is; the more tortuous the network will be.

Modified parallel law, principally as an extension of conventional parallel law, has been developed for a layered composite in which all conductive phases are percolated across the material [4]. However, an additional parameter (the so-called connectivity parameter) has been introduced in a modified model to take into account the tortuosity and constriction of the material.

Table 2.3 Summary of some commoner models for electrical conductivity in composite materials

Mixing models	**Simplified equation (One-path conductive)**	**Remarks** [39, 60]
Parallel Model	$\sigma_b = \sigma_0 \phi$	Parallel layer of constant arbitrary thickness with conductivity arranged axially to current flow
Modified Parallel Model	$\sigma_b = \sigma_0 \phi \beta$	Modified parallel model that incorporate in connectivity parameter
Archie's Law	$\sigma_b = \sigma_0 \phi^{\ m}$	Derived empirically, but provable analytically for particular cases
Hashin-Shtrikman (upper and lower bound)	$\sigma_b = \sigma_0 \frac{2\phi}{3-\phi}$	Derived from an effective medium consideration with the existence of upper and lower bound. These bounds are applicable to any types of particulate composites
Maxwell-Garneet Model	$\sigma_b = \sigma_0 \left[\frac{(d-1)\phi}{d-\phi} \right]$	Derived from effective medium theory. Valid for spherical particle
Differential Effective Medium (DEM)	$\sigma_b = \sigma_0 \phi^{\left(\frac{d}{d-1}\right)}$	Developed to model two-phase composites with inclusion mechanism
Self-Consistent (SC) Effective Medium	$\sigma_b = \sigma_0 \left(\frac{d\phi - 1}{d-1} \right)$	Providing a solution of the multi-particle random structures

Differential Effective Medium (DEM) theory is developed to model a dispersed particle in a system that always stays percolated. However, this model does not treat each constituent symmetrically. The notation d describes the spatial dimension of the system and usually d = 3 for a three dimensional composite [39]. Furthermore, Maxwell approximation is used to estimate the normalized conductivity by direct

substitution for small inclusion concentrations. The assumption in this model has been valid for spherical particle. However, Maxwell approximation has given some good estimates of normalized conductivity at non-dilute condition which the spheres have been well separated from each other [39].

Finally, the self-consistent model is described as a method to the solution of the multi-particle random structures. This model functions to simplify a complex picture of interaction among many particles and to reduce a multi particle problem to a problem for one particle [60]. Different from the Maxwell and DEM models, this model is not limited to particle matrix and acts on every particle in a random structure. The parameter *d* describes the spatial dimension of the composite.

To evaluate these models, the measured conductivity data were used in this study followed by comparing the results to the models. Here, porosity data were obtained using the MIP (as discussed in Chapter 3) and Power-Brownyard models [61]. In this hydration period, the electrical conductivity, porosity and microstructure parameter were changed as a function of time.

2.5.3 Relationship of Electrical Properties to Permeability and Strength

In oilfield, fluids migration through the cement column is considered as one of the most problems encountered during drilling operations in that it may damage the wellbore and also has a damaging effect to the environment. Factors that contribute to the gas migration might include fluid density, mud removal strategy, cement slurry design, and cement mechanical properties. Within these factors, the main controlling parameters allowing the fluids to migrate are permeability. Therefore, a low permeability is required for a good cement formulation. Burdylo *et al.* [19] stated that a rapid reduction in permeability after placement was a key design feature of a good cement. Permeability also may resist formation acid attack that may degrade cement quality.

On the other side, certain magnitude of cement strength is required to guarantee the integrity of wellbore. It will warrant the complete zonal isolation at which casing stands appropriately. For this purpose, early strength is deemed to be essential in ensuring structural support to the casing and mechanical isolation of downhole

intervals. Delay in strength development will cause a significant amount of lost time due to the need to wait-on-cement. In common, wait-on-cement is a time required for cement to achieve a minimum strength of about 500 psi [62]. Otherwise, drilling operations cannot proceed, and the rig must sit idle until the cement has been sufficiently hardened to continue.

Both permeability and strength of well cement, furthermore, depended on the elevated temperature and pressure. Usually cement strength is considered to increase with increasing temperature especially at the early stages of hydration. At the same time, the permeability decreases with increasing temperature. However, at the later stages, the strength of the cement decreases rapidly and permeability increases with high temperature [23] as an effect of cement's deterioration. As such, carefully monitoring the actual strength and permeability of well cement at certain interval period is necessary to prevent any wellbore failure.

In practice, these properties are tested on designing cement slurry formula. In response, a set of samples have been examined in the laboratory scale to meet the required objectives. However, once the cement has been displaced, the strength and permeability performance may not be similar with the results obtained from the routine lab. It is either due to the cement in wellbore that may mix with several formations of fluids/mud or due to the fluid loss problem which does not really represent the previous tested samples. Furthermore, an elevated temperature and pressure may degrade the cement quality in term of its strength and permeability.

For those conditions, cementing evaluation is then performed to confirm the success of cement job. However, the current applications are merely focused on the zonal isolation and detect the quality of bond between casing and cement and between casing and wellbore. It is executed by using the sonic and acoustic log measurements. Still, this technique has a limitation to be used in evaluating the permeability development due to its density based principle [13–15].

2.5.3.1 Permeability and Electrical Properties Relationship

A promising technique using an electrical impedance to evaluate microstructural properties of cement; including permeability, has been successfully applied [42, 43,

57, 62, 63]. The well known equations of Katz-Thompson [65] and Johnson's [55] have been most frequently discussed in literature in relating permeability to conductivity. These equations are successfully tested on the rock samples but may not be fully applicable to cement since having more rigid system [63, 65].

Katz and Thompson derived the following equation based on the percolation concepts relating the permeability of saturated random porous media to microstructural descriptors and conductivities:

$$k = \frac{1}{226}\left(\frac{\sigma_b}{\sigma_o}\right)(d_c)^2 \tag{2.18}$$

where k is hydraulic permeability (μm^2), σ_b/σ_o is normalized conductivity, and d_c is the critical pore diameter (μm).

Meanwhile, Johnson *et al.* [55] correlated the formation factor and the permeability of the porous medium with a production of the equation as follows:

$$k = \frac{1}{8}(\Lambda^2)\left(\frac{\sigma_b}{\sigma_o}\right) \tag{2.19}$$

where k is hydraulic permeability (μm^2), σ_b/σ_o is normalized conductivity, and Λ is a weighted pore volume-to-surface ratio (μm).

Several researchers have obtained a fair agreement between measured and calculated permeability using these equations [4, 47, 65], and also its application on cement pore structure [67]. However, since these samples are treated at mature stage and at ambient condition, a further study is required for sample during early hydration and under reservoir conditions. As a result, this thesis proposes an empirical equation based on the relation among the measured permeability data, pore radius and electrical responses of oilwell cement at elevated pressure up to 3000 psi and temperature up to 65°C during the first 24 hrs of hydration.

2.5.3.2 Strength and Electrical Properties Relationship

Typically, the wait-on-cement during a cementing operation could range from a few hours to several days - depending on the difficulty of the cement job. Prior to that, a

regular cement bond log may result in a pessimistic interpretation. Hence, an accurate evaluation and estimation on appropriate cement strength becomes considerably important to reduce cost expenditure - particularly at the early ages when the physical and mechanical properties of the well cement significantly change with times.

In literature, it is found that the influence of porosity on the strength of cement has already been well recorded into many models such as those of Balshin [68], Hasselman [29], Ryshkevitch [69] and Schiller [70]. These models have been applied using a measured porosity and relating it to its strength, this is rather impractical for the oilfield used. Therefore, a simpler correlation becomes necessary. An emerging electrical conductivity technique then is used as a tool to predict cement strength and conducted based on cement porosity along with the measured normalized conductivity. Considering the effect of elevated pressure and temperature, the suitability of the existing models between porosity and strength needs to be examined.

It is worth noting that the correlations between porosity and strength for several engineering materials have been intensively investigated [8, 29, 67–70]. However, its pertinence to the Class G oil well cement under elevated conditions needs to be carefully examined still.

Balshin [68] has suggested the following power law correlation for powder metal ceramic.

$$S = S_o(1 - \phi)^b \tag{2.20}$$

where S is strength, S_o is strength at zero porosity, ϕ is porosity, and b is empirical constant.

Meanwhile, Hasselman [29] proposed a linear relationship between strength and porosity for different refractory glass materials.

$$S = S_o - b\phi \tag{2.21}$$

where S is strength, S_o is strength at zero porosity, ϕ is porosity, and b is empirical constant.

Schiller [70] also suggested a logarithmic correlation between strength and porosity for gypsum paste or non-metallic brittle materials.

$$S = b \ln \frac{\phi_o}{\phi} \tag{2.22}$$

where S is strength, ϕ_o is porosity at zero strength, ϕ is porosity, and b is empirical constant.

Ryshkewitch [69] introduced an exponential equation for porous sintered alumina and zirconia in relating strength and porosity.

$$S = S_o e^{-b\phi} \tag{2.23}$$

where S is strength, S_o is strength at zero porosity, ϕ is porosity, and b is empirical constant.

To fit these models, an experimental study was made and used as a basis in predicting the strength using measured electrical conductivity for oilwell cement at an elevated pressure and temperature.

2.6 Summary of Review

The recent methods of sonic and ultrasonic cement log technique can only acquire informations regarding the bonding quality but the technique fails to obtain the inter-connected pores of a cement system [13–15]. Although the application of electrical impedance on cement system producing an interesting work, most of study in the literature did not directly relevant to oilwell cement condition. Some authors [57, 63] have produce some foundation in relating electrical impedance to some engineering properties such as porosity but they used a single frequency approach which is not appropriately reliable and, furthermore, the sample samples are treated at mature stages of hydration. As a result, the existing correlations that relate the electrical properties to cement system did not fully applicable for oilwell cement conditions.

CHAPTER 3

EXPERIMENTAL PROCEDURES AND METHODS

Chapter 3 describes the experimental program, apparatus, materials, and methods used in this study. In addition, it provides the comprehensive information about sample preparation, mixture proportions, and curing conditions. To support the discussion of this chapter, the electrical impedance measurement procedure is detailed. The last part of this chapter deals with the explanation about the method of pore solution extraction and its conductivity measurement together with the measurement of permeability, porosity, and strength.

3.1 Sample Preparation

In the sample preparation, five batches of cement slurry were mixed with tap water at water cement ratios (w/c) of 0.55, 0.5, 0.4, 0.3 and 0.25. In this case, some samples with w/c of 0.25 and 0.55 acted as a controller variable. In this study, API cement Class G High Sulphate Resistant (G-HSR) with the specific gravity of 3.2 g/cm^3 obtained from LaFarge Malaysia was used. Tables 3.1 and 3.2 present the composition of the cement measured by X-ray fluorescence analysis and the summary of the experimental measurement method, respectively.

Referring to the recommended practice of API 10A [24], the composition, subsequently, was mixed in a constant speed at 4,000 rpm for 30 minutes in which the cement powder was gently poured into the mixer that had been filled with water until well mixed. The mixing process was continued by increasing the speed of mixing up to 12,000 rpm for 35 minutes.

Having been prepared, the cement slurry was immediately placed into a 1-inch diameter x 1-inch length cylinder rubber jacket for the impedance measurement. Afterward, the sample was weighed using a digital balance in which the weight measurement was used as an input in the electrical conductivity measurement. Table 3.3 presents the scenarios of the measurements that illustrate the wellbore conditions during cementing operation starting at ambient condition to gradually achieve elevated temperature and pressure. For the strength measurement, the cement slurry was placed into the test cell of about 500 ml within UCA apparatus to be gently poured until the proper fill level was obtained using the slurry level gauge.

Table 3.1 Composition of Class G HSR cement

Raw Oxide	**Wt. %**	**Bogue Phases***	**Wt. %**
CaO	64.3	C_3S (tricalcium silicate)	62.5
SiO_2	21.2	C_2S (dicalcium silicate)	9.3
Al_2O_3	3.8	C_3A (tricalcium aluminate)	2
Fe_2O_3	4.76	C_4AF (tetracalcium aluminoferrite)	14.5
SO_3	2.61		
MgO	2.3		
K_2O	0.32		
Na_2O	0.46		

*Cement chemistry notation: C = CaO, S = SiO_2, A = Al_2O_3, F = Fe_2O_3

Table 3.2 Experimental measurement methods

Experimental	Measured parameters	Sample treatment	Measurement devices
Mixing	w/c of 0.55, 0.5, 0.4, 0.3, 0.25	Mixed at 4,000 rpm for 30 min & increase to 12,000 rpm for 35 min.	Constant Speed Mixer
Impedance measurement	• 0.2 MHz until 1 Hz • 25°C & 14.7 psi, 40°C & 1500 psi and 65°C & 3000 psi • Time varying	Measure at 30 min. intervals for first 5 hrs, 1 hr increment for up to 10 hrs and at 2 hrs interval up to 24 hrs of hydration	CoreTestSystem AutoLab
Pore solution extraction for conductivity measurement	• Time varying • w/c varying	Extracted at 1, 3, 5, 10, 16 and 24 hrs of hydration period	Fann 175 ml HPHT API Filter Press
Compressive strength	• 25°C & 14.7 psi, 40°C & 1500 psi and 65°C & 3000 psi • Time varying	Along 24 hrs of hydration (continuously)	Ultrasonic Cement Analyzer Model 200 from Cement Test Equipment
Porosity	• 25°C & 14.7 psi, 40°C & 1500 psi and 65°C & 3000 psi • Time varying	Measured at 5, 10, 16 and 24 hrs of hydration	A Pascal 240 and 440 high pressure Mercury Intrusion Porosimetry (MIP)
Permeability	• 25°C & 14.7 psi, 40°C & 1500 psi and 65°C & 3000 psi • Time varying	Measured at 5, 10, 16 and 24 hrs of hydration	Gas permeameter-coreval 30 (Vinci Technology)

On the other hand, for permeability measurement all the samples were cured to the same conditions as mentioned in Table 3.3. For samples at ambient condition, it was cured by placing them into a 1 x 1-inch cylinder rubber jacket. Other samples at elevated conditions were performed in the HPHT curing chamber containing a sample cell with a dimension of (1 x 1 x 1)-inch. Here, the curing duration was set around 5, 10, 16 and 24 hrs. Samples obtained from the curing chamber were then directly cored into the (1 x 1)-inch cylinder core plugs to fit the core holder of permeability measurement. A similar treatment of the samples was also performed for the porosity measurement using MIP method in which a cement sample of about 4-8 grams was used as the input measurement. To have representative data, the hydration process of cement samples was stopped using the solvent exchange procedure as mentioned by Zhang [72]. In overall, Figure 3.1 presents the general workflow of the research procedure.

Table 3.3 Measurement scenarios for conductivity measurement

Sample No.	**w/c**	**T (^{o}C)**	**P (psi)**
1	0.55	70	3000
2	0.5	25	14.7
3	0.5	40	1500
4	0.5	65	3000
5	0.4	25	14.7
6	0.4	40	1500
7	0.4	65	3000
8	0.3	25	14.7
9	0.3	40	1500
10	0.3	65	3000
11	0.25	70	3000

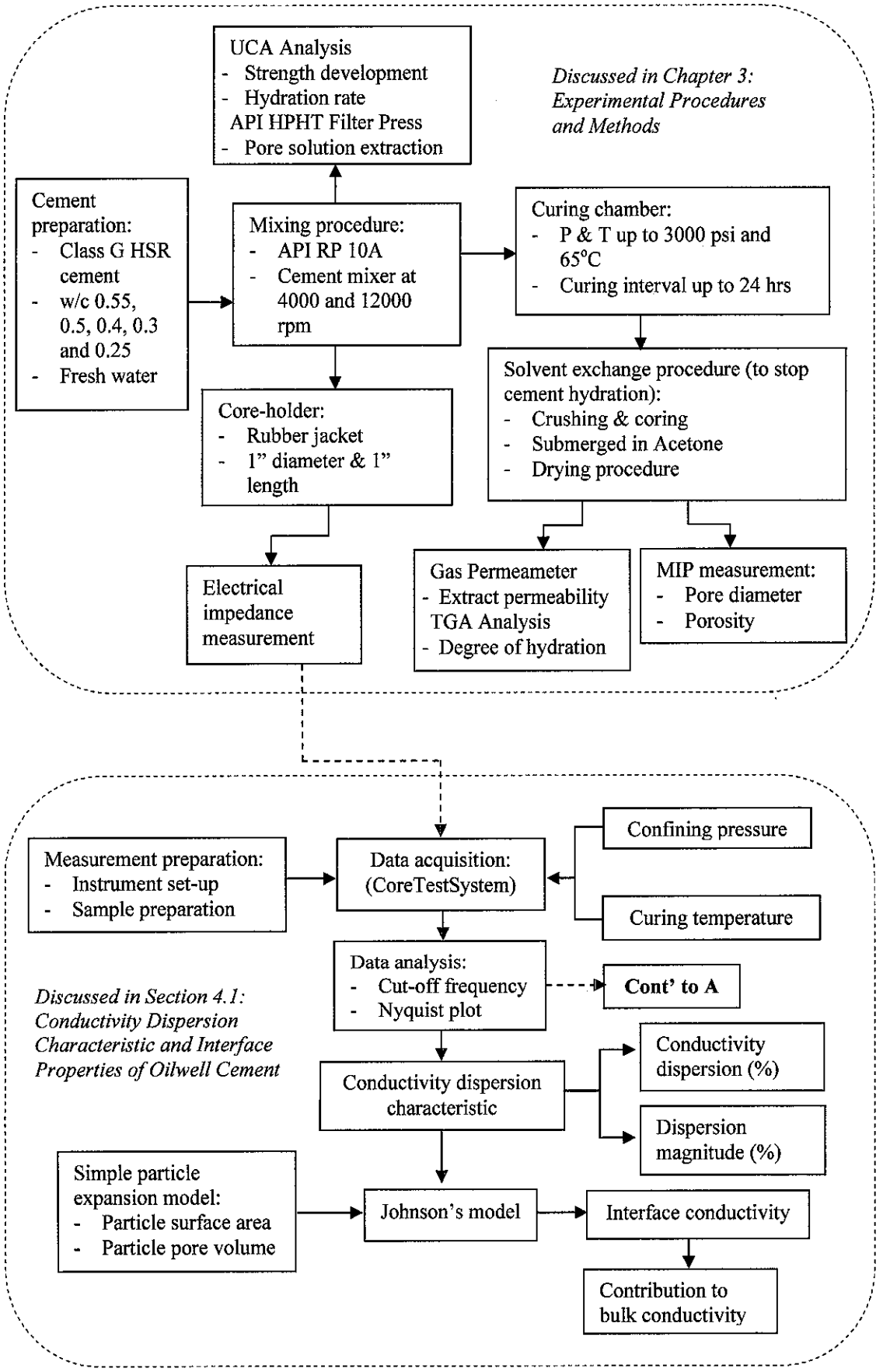

Figure 3.1 General workflow of the thesis

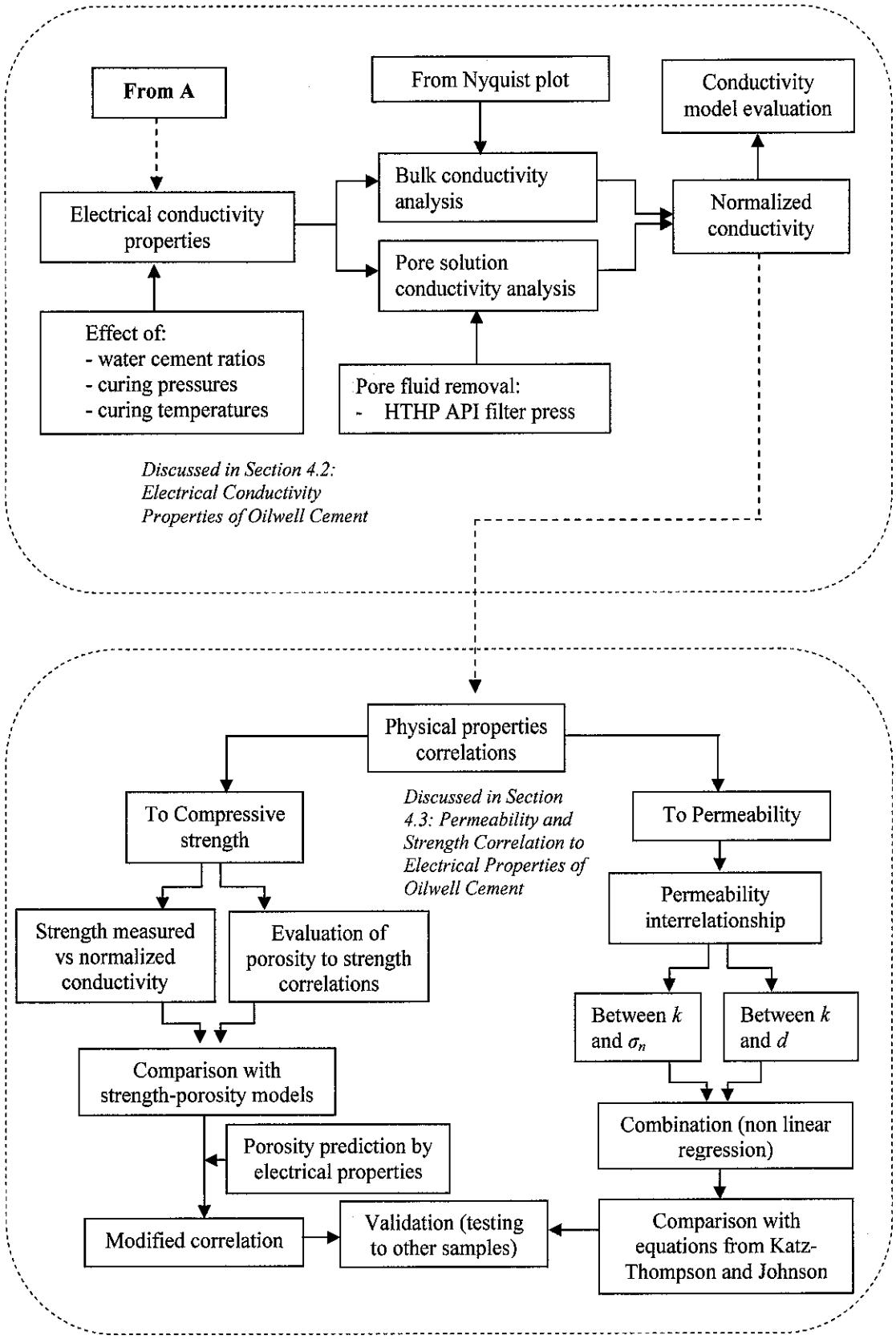

Figure 3.1 General workflow of the thesis (continuation)

3.2 Electrical Impedance Measurement

Electrical impedance information was obtained using CoreTestSystem AutoLab from New England Research [73]. Figure 3.2 depicts a schematic diagram of electrical impedance measurement. The instrument was allowed to perform both the two-electrode and the four-electrode impedance measurement as a function of temperature, pressure, and frequency.

The mixed cement samples were placed in accordance with the core-holder apparatus. Prior to installing the apparatus, the cement samples were firstly jacketed by a flexible rubber to avoid leakage or fluid loss. To measure electrical properties, the electrode was carefully aligned with each end of the sample. The standardized electrodes materials consisting of porous silver membrane filters produced by Osmonics Inc. were used here.

The execution of the electrical measurement using four electrode configurations was purposely to minimize the effect of electrode polarization [74]. For measuring four electrodes, the insulating pad (polyester felt), in turn, was placed on the voltage to recess the voltage contact at each end of cap and to mechanically isolate the contacts of those electrodes from the current electrode (Figure 3.3). This, as a result, could allow the voltage measurement to be made without any significant contamination from the electrochemical reactions affecting the current electrode.

Samples were inserted in a core-holder component consisting of two silver electrical contacts embedded in the face of each end cap (Figure 3.4). Here, the frequency of measurement, totally involving 25 data points of frequencies for each execution stored, was set from 0.2 MHz to 1 Hz in a logarithmic sweep. These measurements were performed repeatedly until the sample reached 24 hrs of hydration.

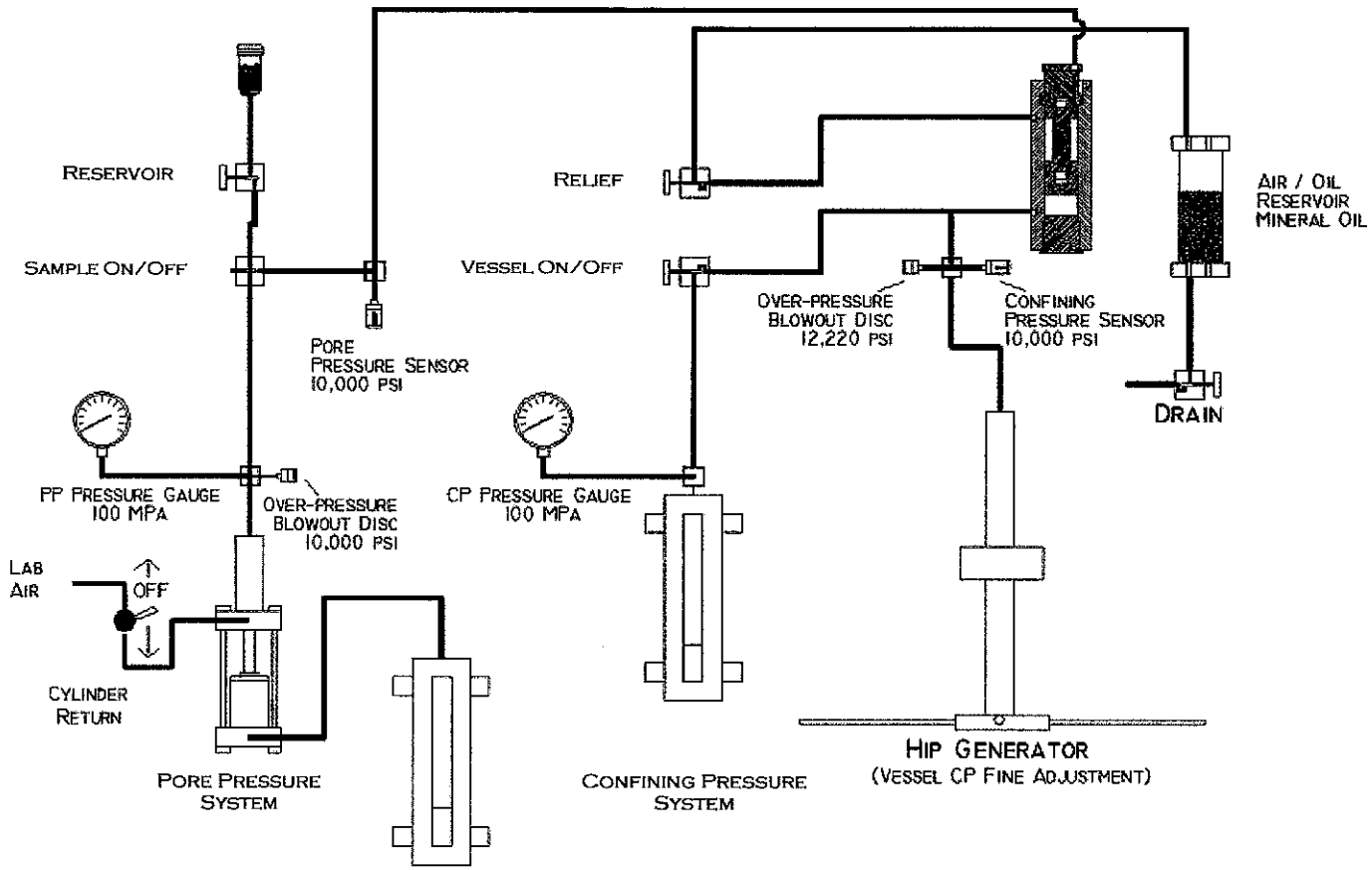

Figure 3.2 Electrical impedance measurement diagram [73]

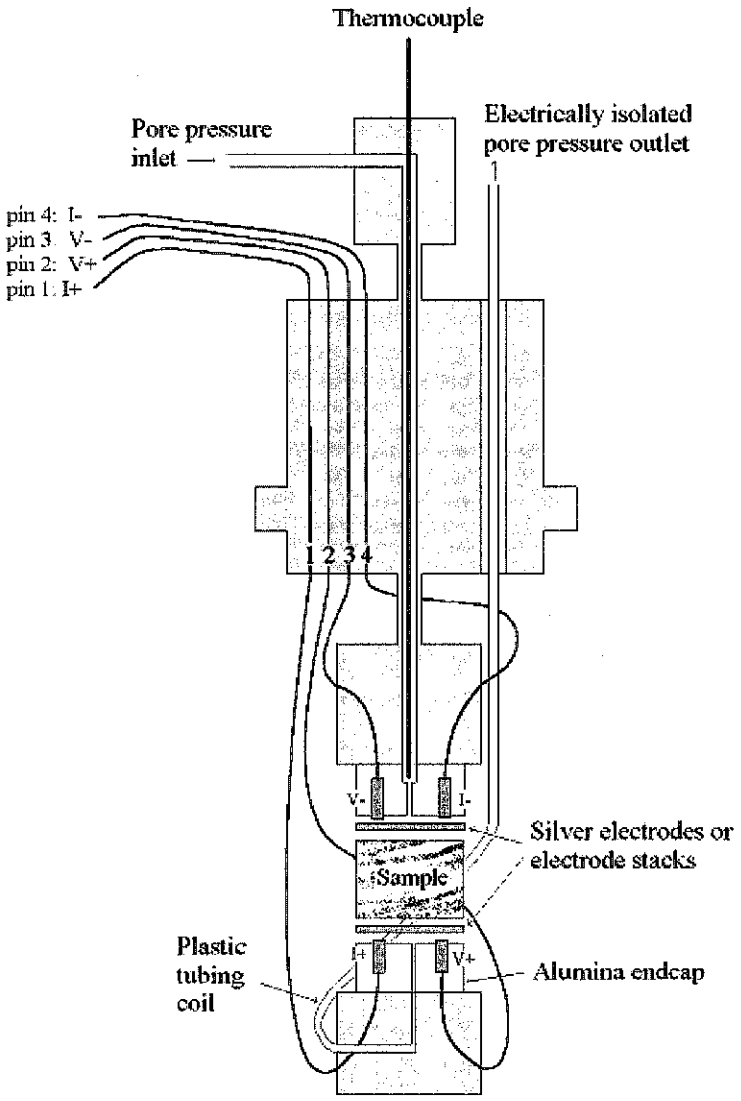

Figure 3.3 Schematic of Core Holder in the CoreTestSystem [73]

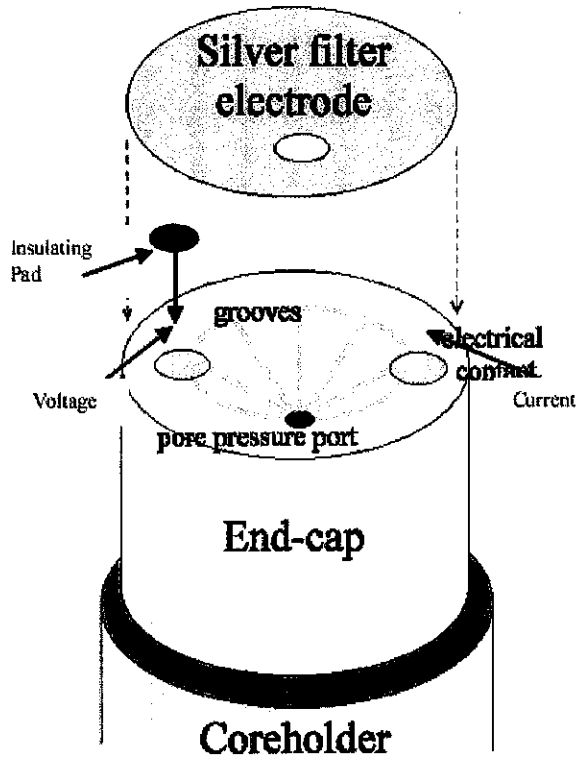

Figure 3.4 Set-up for a four electrode measurements. One silver filter is used on each side of the sample and makes direct contact with only the current contact [73]

The input files for the instrument included the length, diameter and density of the sample. Meanwhile, the measurement of electrical property of cement was made in a serial mode. Electrical impedance *(Z)* can be measured using a range of different frequencies for a better analysis of the electrical response of a material. Corresponding to the each frequency, a set of real and imaginary impedances was obtained (*i.e.,* impedance components were frequency dependent). These results could be described in terms of a Nyquist plot (a graph of Z' versus Z'').

The confining pressure of 3000 psi, on the other hand, was manually conditioned using a hydraulic pump. The output from the measurement system subsequently was recorded by the data acquisition system. The system temperature of about 65°C was then obtained by heating the oil chamber and recorded by an integrated thermocouple of the system. Measurements were gradually collected at several 30-minutes intervals for the first 5 hrs, followed by the one-hour increment for the next measurement up to 10 hrs and continued at the two-hour interval until reaching 24 hrs of hydration.

Temperature and pressure in the impedance measurement, in turn, were conditioned to increase as well as to represent wellbore conditions simultaneously. It

was started from an ambient condition; increased to 40°C & 1500 psi and ended by 65°C & 3000 psi that corresponded to a well depth of about 5000 ft. These conditions were then simulated as a function of water cement ratio.

For cement bulk conductivity (σ_b), it was calculated from the bulk resistivity (R_b) in the Nyquist plot at the cut-off frequency after having been normalized for geometry factor (G) according to the previous Equation (2.12).

At last, to adjust and enhance data quality, it was done by balancing Z-meter interfacing box with a reference resistor and by selecting the reference resistor that most closely matched to the effective (low frequency) resistance of the sample, respectively. This effectively balanced the voltage that was measured by the two amplifiers.

3.3 Pore Fluid Analysis

Pore fluid was obtained through an extraction of the cement sample at certain pressure using Fann 175 ml HPHT API Filter Press which could be pressurized to 1800 psig on the cell and 750 psig on the back pressure receiver. At this point, the maximum operating temperature was at 177°C. Pore fluid consisted of a filter paper connected to the orifice for fluid expulsion. Once removed, it was collected directly into a glass flask for the conductivity measurement. To obtain about 5 ml, the pore fluid was collected at several points of time period that were about 1, 3, 5, 10, 16, and 24 hrs of hydration period and then followed by sealing off the orifice using filter press. The pressure profile was generated by pumping Nitrogen (N_2) until reaching the desired pressure. At last, the conductivity measurement after fluid extraction was immediately performed using conductivity meter.

3.4 Compressive Strength

The development of compressive strength of all samples for the 24 hrs hydration was monitored using Ultrasonic Cement Analyzer (UCA) whose performance was based on the transmission characteristics of ultrasonic compressional wave through cement slurry. It was done by measuring the transit time by an analyzer and converting it to

an apparent compressive strength. The widespread use and acceptance of the UCA, as a result, has made it to be acceptable as a recommended practice for determining sonic strength in API RP 10 B [62]. This study, in turn, used the Model 200 UCA from Cement Test Equipment.

Soon after mixing, the sample was placed in the test cell until the proper fill level was obtained using the slurry level gauge. Extra water, afterward, was added until reaching the water filled line on the slurry level gauge. The measurement was performed for 24 hrs of hydration with the setting maximum pressure and temperature of 3000 psi and 65°C subjected to the same conditions as mentioned in Table 3.3. In addition, controlling samples of w/c 0.55 and 0.25 were prepared at 3000 psi and 70°C for its strength measurement up to 50 days of hydration.

3.5 Degree of Hydration

The degree of hydration was calculated using the Byfors equation [28] as mentioned in Equations (2.1) and (2.2). The values of maximum strengths calculated using the Hasselman correlation [29] as a function of water cement ratios are listed in Table 3.4 (refer to Section 4.3.6 for detailed discussions). A calculation result can be seen in Appendix A as well.

Table 3.4 Calculated maximum strengths at zero porosity using the Hasselman correlation for Class G cement

w/c	Max. Strength (psi)
0.5	5800
0.4	6090
0.3	6815

3.6 Mercury Intrusion Porosimetry (MIP) Measurement

MIP refers to a technique to measure the pore size distribution of a porous medium that is ranging from few nanometers to several hundred micrometers. It is also used to quantify the porosity by the same principle based on the capillary law governing

liquid penetration into the small pores as functions of surface and interfacial liquid tensions, pore-throat size and shape, and wetting properties of sample. This can be expressed in the form of Equation (3.1) by Washburn [75].

$$P_c = -\frac{2\gamma cos\theta}{r} \tag{3.1}$$

where P_c is capillary pressure (dynes/cm^2), γ is surface tension of Hg (489 dyne/cm), θ is contact angle between mercury and cement pore wall (typically 140° [64]), and r is radius of pore-throat aperture for a cylindrical pore (cm).

In this study, the hydration rates of slurry for samples after set were ceased before commencing MIP measurement, in this case by applying a solvent exchange procedure by replacing water inside the cement samples as suggested by Zhang [72]. Hydration was set to be ceased at 5, 10, 16 and 24 hrs for each sample. About 4-8 grams of cement sample were rinsed in an 80-ml acetone in the sealable container and shaken vigorously. The solvent was renewed regularly 2 to 3 times during the first 24 hrs and repeated about once per day for the rest two days. After soaking in acetone, the samples were dried up through the oven-drying method at 80°C for 24 hrs and followed by MIP measurement. To ensure data reproducibility three measurements were made for each sample condition, and the result was finally calculated by the mean analysis values. From the standard deviation analysis, the accuracy of the measurement for each sample conditions was about less than 4.5% with the standard value of ± 2.5%.

Pascal 240 and 440 high pressure porosimeters were used. Here, the pressurization system used a reversible pump continuously operated and making it possible for a perfect control in increasing or in decreasing the pressurization speed of about 54 and 108 psi/s. By doing so, the maximum pressure of 29,000 psi and 58,000 psi for Pascal 240 and 440 could be reached approximately in 9 minutes.

3.7 Permeability Measurement

Permeability measurements were performed on samples using gas permeameter-coreval 30 with the range of 10^{-5} - 10 μm^2 (Vinci Technology) based on an unsteady-state (transient) method. The pressure falling-off technique was applied on cores

placed in a core-holder under a hydrostatic confining pressure. The downstream end of the sample was conditioned to an atmospheric pressure whilst the upstream pressure used was at 200 psig. This method, a relatively fast technique compared to the steady-state method [76], made possible for the calculation of slip-corrected permeability and Klinkenberg slip factor [77] during the single transient test. Helium (He) was then passed through the core sample, and the pressure difference between the inlet and outlet was the main parameter to determine the permeability.

After mixing, cement slurry was directly placed into a curing chamber under elevated temperature and pressure. The curing duration was designed into several periods of around 5, 10, 16 and 24 hrs of hydration. After achieving some curing periods, the samples were directly cored into the 1 x 1-inch cylinder core plugs to fit the core-holder of permeability measurement device. The core plugs were then immersed in the acetone solution to stop the hydration process. About 100-150 g of cement plugs were rinsed in a 250-ml acetone in a sealable container and shaken vigorously as the same procedure for the MIP measurement in Section 3.6. After soaking in acetone, the samples were oven dried at 80°C for 24 hrs before conducting permeability measurement. Three measurements were also made for each sample conditions to ensure data reproducibility. The result was calculated by averaging these measurements. The accuracy of the measurement was tested using error analysis by standard deviation method. The percentage of error for each measurement at different sample conditions was found to be less than 6%.

CHAPTER 4

ELECTRICAL RESPONSES AND ITS CORRELATION TO PERMEABILITY AND STRENGTH OF OILWELL CEMENT

Chapter 4 presents and discusses about the results of impedance spectroscopy measurements in Class G oilwell cement. An interrelationship between frequency and electrical conductivity is dealt with in detail in the form of conductivity dispersion characteristics in which the conductivity dispersion and dispersion magnitude are evaluated. This chapter also explores the interface conductivity and its contribution to the bulk conductivity as an effect of electrical double layer. The simple particle expansion model is proposed as an aid to determine the interface conductivity. The next section of this chapter is designed to discuss about the analysis of parameters influencing the electrical conductivity of oilwell cement. Here, the effect of w/c, elevated pressure and temperature on electrical conductivity is discussed.- including the correctness of the direct effect of elevated temperature on conductivity measurement. Some models for conductivity changes with time are evaluated to correspond with the oilwell cement application as well. The last section in this chapter discusses about the development of empirical correlations to predict the permeability and strength of oilwell cement based on its electrical properties. For this purpose, two different approaches are employed. In the first approach, the correlations are carried out based on the cement physical properties measurement along with the measured normalized conductivity, and in the second one, the modified version of the existing correlations is proposed with respect to the cement's microstructure parameters.

4.1 Conductivity Dispersion Characteristics and Interface Properties

This section discusses in detail the interrelationship between frequency and electrical conductivity in the form of conductivity dispersion characteristics. It was made by taken into account the effect of water saturation, hydration time, and elevated temperature and pressure. Some microstructure parameters for the interface

conductivity determination additionally were calculated using a simple particle expansion model. The material parameters influencing the interface conductivity were identified and the magnitude of interface conductivity along with its contribution to the bulk conductivity was also quantified.

4.1.1 Impedance Spectroscopy of Oilwell Cement

Electrical impedance measurements have been generated as a function of hydration time as expressed in the Nyquist plot. Figure 4.1 presents a typical Nyquist plot at a different hydration time for w/c 0.5 (results of Nyquist plot can be seen in Appendix B). This measurement has included the geometry factor (l/A) of about 0.5 cm^{-1} in which l and A respectively equaled to 2.54 cm and 5.06 cm^2. The plot found that a two-arc behavior was continually formed at the later ages of hydration, indicating the formation of solid hydration products and reduction of pore-filled solution. These arcs were formed due to the different time constants (resistance-capacitance products) in the material as an effect of the different types of electrical polarization due to the electrical excitation. The high frequency arc (small arc) was due to the bulk processes and the low frequency (large arc) was due to the electrode interface effect.

A small curve of high frequency arc, *i.e.* 5 hrs, was due to cement in the form of suspension and no interfaces (solid-fluid) formed. At this point, the impedance performance was mostly contributed by a physical contact between the electrode and the sample which generated an electrical double layer and charge transfer phenomena. As the hydration continued, the bulk response on the impedance measurement gradually increased at the high frequency arc in the Nyquist plot.

In a high frequency region, one particular concern refers to a point at which imaginary impedance has the lowest or approximately zeros value. This point is called the bulk impedance with the frequency named cutoff frequency. The bulk impedance here is dependent on hydration period, water cement ratios and curing conditions. Figure 4.2 presents the dependence of w/c on impedance measurement - especially bulk impedance at several curing conditions. Furthermore, a similar trend was also observed for samples cured at different curing condition at which sample with low w/c a bigger value for bulk impedance had. As can be seen, the bulk impedance

shifted from w/c 0.4 to 0.3 was almost double that than of w/c 0.5 to 0.4. This was probably related to the quick reduction in pore solution at hydration time of 20 hrs.

Figure 4.3 shows the effect of curing temperature and pressure on electrical impedance. It can be noted that an increase of temperature and pressure has also increased the bulk impedance as an effect of accelerated hydration rate. Unlike w/c, the bulk impedance shifted due to curing temperature and pressure was relatively varied. These phenomena may be due the effect of w/c more dominant compared to that of curing temperature and pressure for which the bulk impedance shifted likely to form irregular pattern as a function of w/c.

From these Nyquist plots (Figures 4.2 and 4.3), the bulk impedance was observed to vary as a function of frequency. Thus, the use of multiple frequencies comes to be important to capture the correct bulk impedance otherwise the resulting data may not be reliable to be used in extracting physical properties.

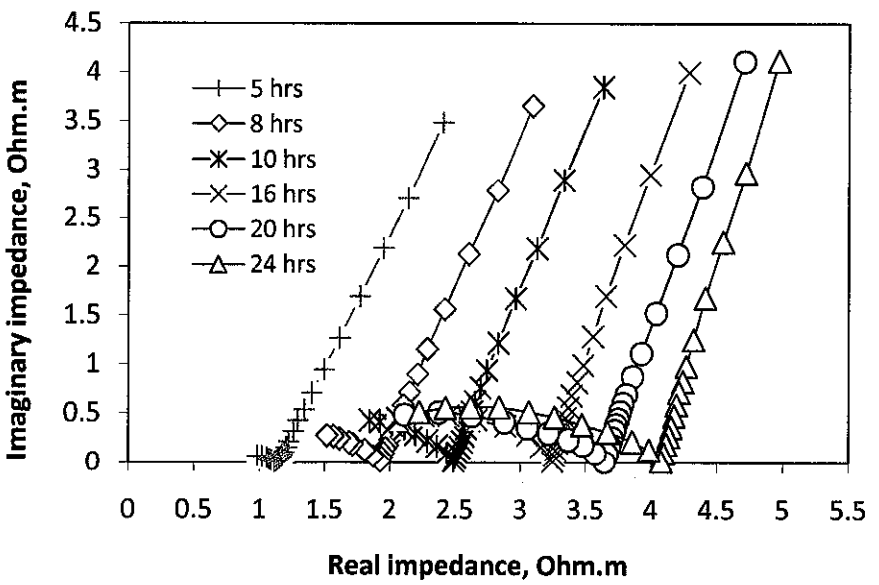

Figure 4.1 Typical Nyquist plot at different hydration time for Class G cement with w/c of 0.5 at atmospheric conditions

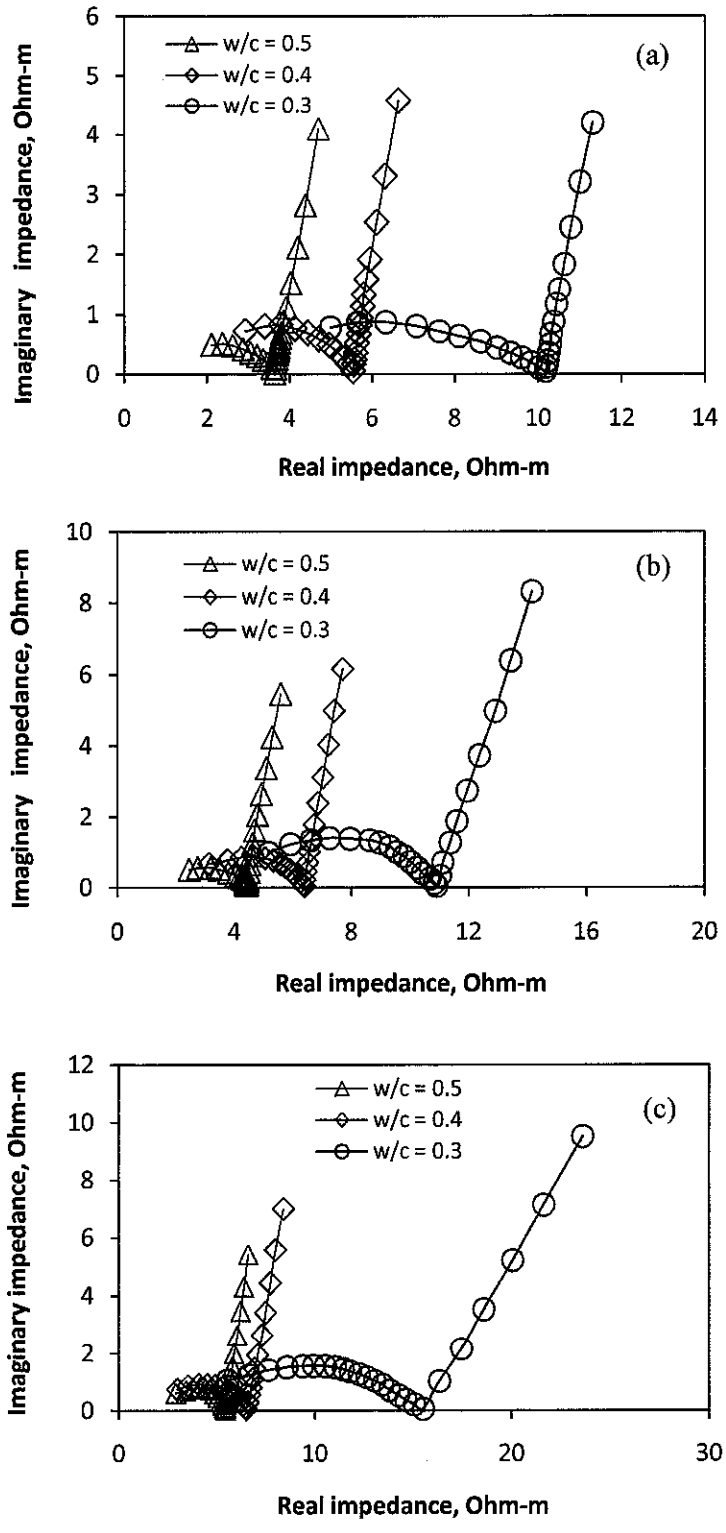

Figure 4.2 Nyquist plot of Class G cement at different water cement ratios (w/c) at 20 hrs of hydration time for (a) 25°C & 14.7 psi, (b) 40°C & 1500 psi, and (c) 65°C & 3000 psi

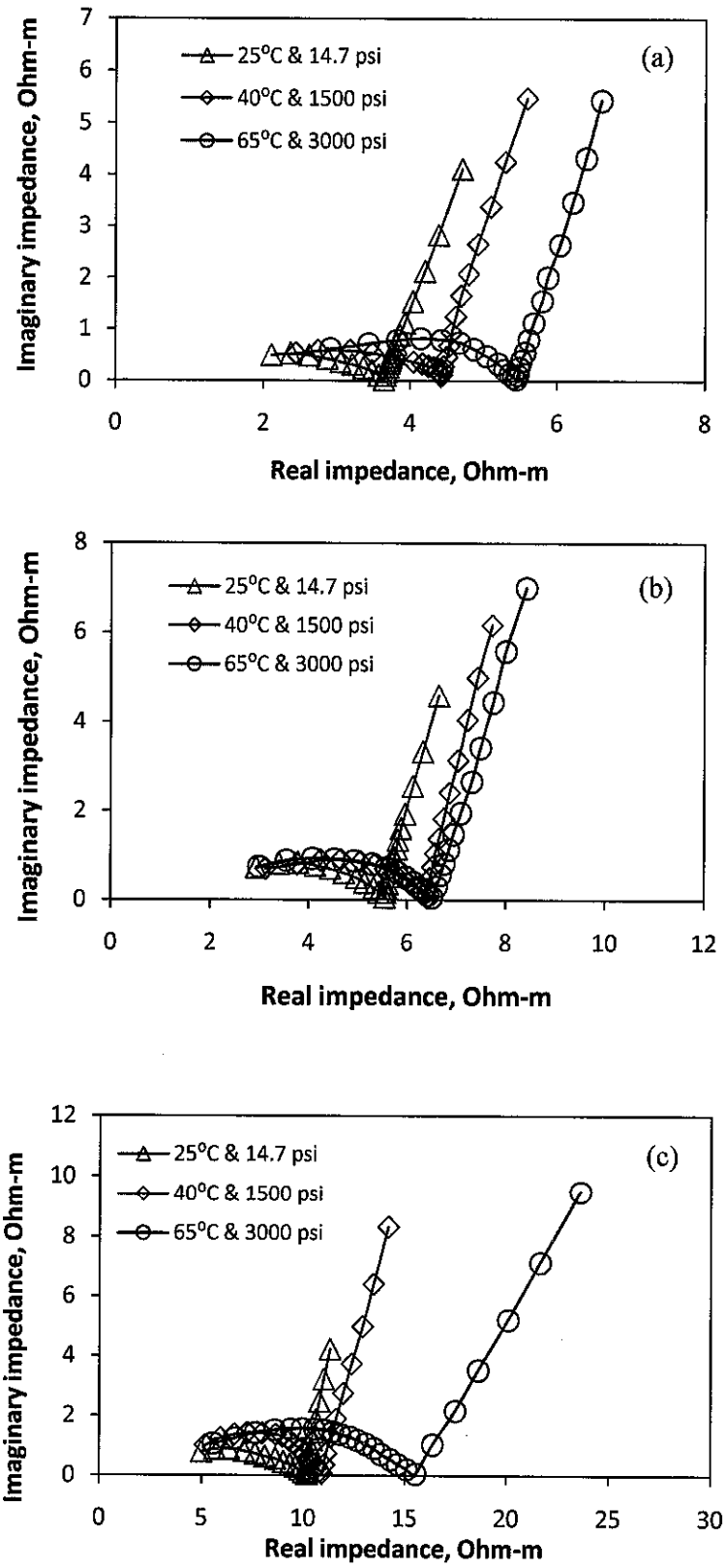

Figure 4.3 Nyquist plot of Class G cement at different curing condition at 20 hrs of hydration time for (a) w/c 0.5, (b) w/c 0.4, and (c) w/c 0.3

4.1.2 Conductivity Dispersion Characteristics

The change in electrical conductivity with frequency is called conductivity dispersion. It depends on the properties of the particles and the pore fluids. This characteristic may be used as an indication of the existence of electrical double layer that contributes to the electrical properties of the system. Electrical double layer here reflects the interface conductivity properties between pore fluid and particle depending on hydration time, water content, and pore size.

The dispersion characteristics of cement slurry during early hydration were conveyed in terms of conductivity dispersion and magnitude of conductivity dispersion. The first was applied into the cement system as a function between frequencies and electrical conductivity - while the letter was only focused on the cement system at above cut-off frequency. The magnitude of conductivity dispersion, furthermore, was explained through the comparison of the conductivity at maximum point and cutoff frequency within the available frequency ranges $(\sigma_{max} - \sigma_{cf})/\sigma_{max}$ [78]. Here, the cut-off frequency was selected at the intersection of the electrode and bulk arcs.

Figure 4.4 presents typical conductivity dispersion. As the frequency of the impedance measurement increased, so did the electrical conductivity of cement system. It shows that conductivity dispersion exhibited a significant trend at points below cut-off frequency (5690 Hz) as an effect of electrode-system contact. In addition, it indicates that the water filled pore at this system dominated conductivity measurement.

In the following sections, a systematic study was carried out to investigate certain dispersion characteristics of oilwell cement during early hydration with regard to the hydration time, water cement ratio, and elevated temperature and pressure. This investigation was made to indicate the presence of interface conductivity as a function of these parameters.

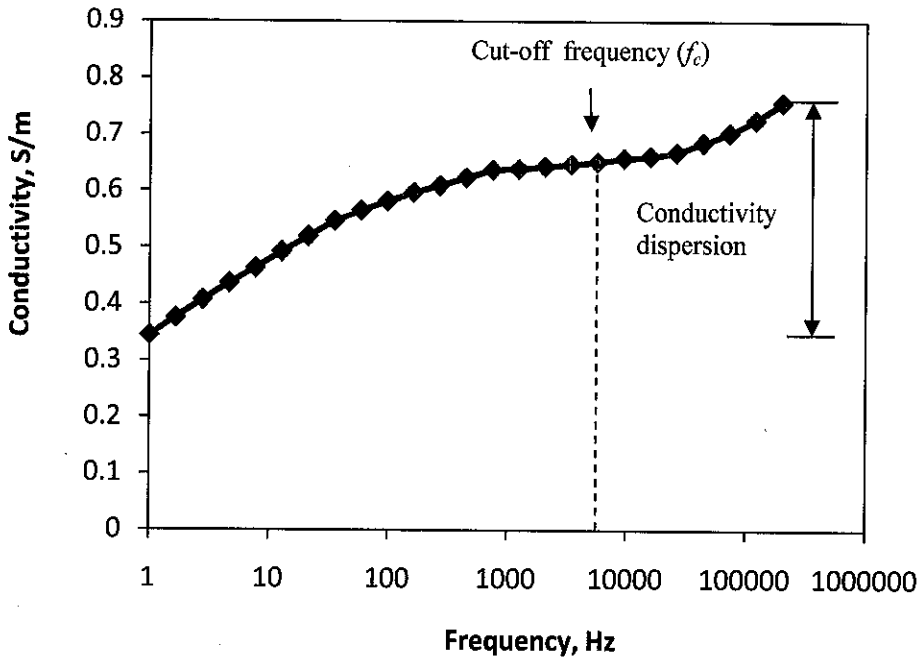

Figure 4.4 Conductivity dispersion of Class G cement at 5 hrs of hydration time with w/c 0.5 cured under 40°C & 1500 psi

4.1.2.1 Effect of Water Cement Ratios on Conductivity Dispersion

Being contrast with cement matrix that was considered to be negligible, water cement ratios, playing an important role in determining the conductivity dispersion characteristic, were mainly controlled by water properties. As cement was mixed with water, hydration process existed by steadily consuming the initial water until hydration was completed. As a result, initial water saturation of cement after mixing could be reduced accordingly as a function of hydration time.

By mechanism, the contribution of w/c as a pore solution to the cement conductivity might occur in two ways. Firstly, it might occur by their intrinsic electrolysis by which cement conductivity was proportional to electrolyte conductivity. Secondly, it might happen by the process of electrochemical interaction at the interface of fluid-solid system. In this condition, the inter-connected pore of conductive path is controlling interface conductivity.

Figure 4.5 shows the contribution of w/c on conductivity dispersion characteristics at (a) 5 hrs of hydration time and (b) 20 hrs of hydration time. Conductivity dispersion not only increased with frequency as expected but also had an

increasing profile as water content reduced. This gave a clue that the cement with fully or high water content will be less affected to the conductivity dispersion.

In the very early hydration (Figure 4.5a) it was shown that the effect of different w/c on dispersion characteristic was relatively small compared to the similar effect at the later hydration time (Figure 4.5b). In 5 hrs of hydration time, the conductivity dispersion was almost similar for each w/c due to the less physical change exhibited in cement hydration (dominated by volumetric conductivity). In the later period, cement already had formed a hardened phase and restricted the current through water and, as a result, it was now controlled by both water and inter-connected pores. As an effect of these the discrepancies between w/c to conductivity dispersion were more pronounced.

Above cut-off frequency (dominated by bulk response), the conductivity dispersion was higher at the later stages. It can be seen that for 20 hrs of hydration the conductivity dispersion was higher at w/c 0.3 followed by 0.4 and 0.5. This indicates that the pores volume at higher w/c was still covered by water that contributed to the domination of volumetric conductivity more than surface conductivity. Because of the dispersion and the surface conductivity had a similar analogy to the capacitor, the bigger the inter-connected pores, the easier the dispersion vanished. In other words, a small w/c tended to have a surface conductivity for a similar hydration period. This also can be seen in the magnitude of conductivity dispersion (Figure 4.6) in which the magnitude increased as w/c decrease indicating that surface conductivity potentially existed at lower w/c at the later stages.

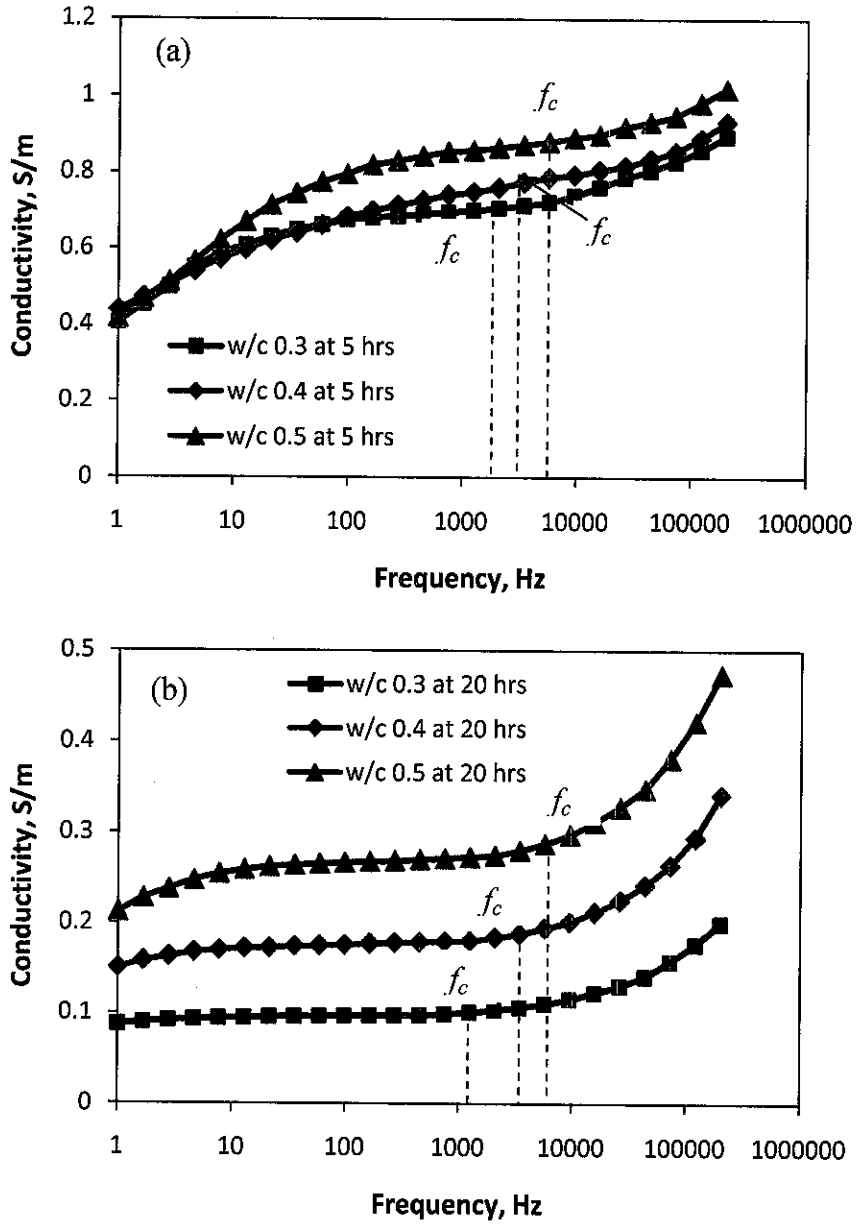

Figure 4.5 Conductivity dispersion curve as an effect of water cement ratios at atmospheric condition for (a) 5 hrs of hydration time and (b) 20 hrs of hydration time

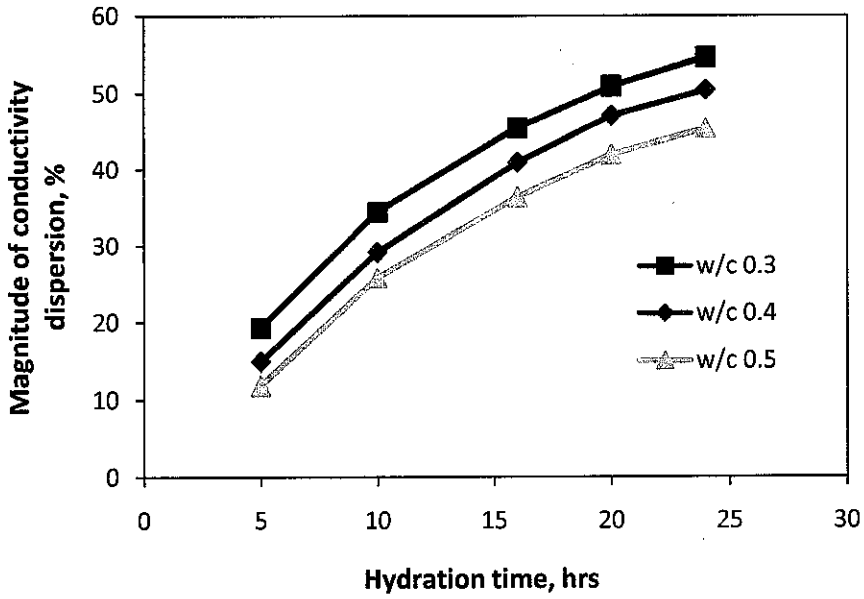

Figure 4.6 Magnitude of conductivity dispersion as a function of water cement ratios at ambient condition

4.1.2.2 Pressure and Temperature Effect on Conductivity Dispersion

Figures 4.7a-f show the effect of pressure and temperature on conductivity dispersion. It can be seen here that these contributions were dominant at the very early stages of hydration - especially below cut-off frequency (Figures 4.7a,c,e). This might be as an effect of the enhanced mobility of ions in the pore solution once the temperature was increased. Hence, there was a need to be corrected to compare conductivity curve at different temperature profile. The procedure of the temperature correction was delivered in Section 4.2.2. Meanwhile, the effect of pressure at these stages was less significant because its conduction path was mainly controlled by volumetric water. The effect of pressure to the electrical current was very small and might be negligible as noted by Khairy *et al.* [16].

The conductivity dispersion characteristics as an effect of curing temperature and pressure were observed at the later stage of hydration (Figures 4.7b, d, f) at the point above cut-off frequency. The discrepancies between different P and T were not as high as those in the early hydration as the system at these points had already been controlled by the bulk conductivity instead of electrode contact effect. It can be seen that as temperature and pressure increased together with the decreasing w/c, the conductivity dispersion also slightly increased in the form of magnitude dispersion.

This increase occurred as a result of hydration acceleration which affected the formation of cement particle network and its initial water consumption. Hence, volumetric conduction steadily vanished as hydration continued and at the same time it was replaced by the interface conductivity between water and grain system. The cut-off frequency at different w/c for each curing condition and hydration time is given in Table 4.1.

Table 4.1 Cut-off frequency at different w/c and curing conditions for 5 hrs and 20 hrs of hydration time

Curing Conditions	**w/c**	**Cut-off Frequency (f_c), Hz**	
		5 hrs	**20 hrs**
25°C & 14.7 psi	0.3	5690	447
	0.4	9460	1240
	0.5	15700	2060
40°C & 1500 psi	0.3	5690	97
	0.4	5690	269
	0.5	9460	744
65°C & 3000 psi	0.3	2060	21
	0.4	5690	269
	0.5	9460	447

In other words, when the water fully filled the pore space, the conductivity dispersion effect was to be relatively small. This reflects that bulk fluid volumetric controlled the path of the electrical current. The dispersion curve reflected the water-coating grain by which as conductivity dispersion increased (magnitude increase), the interface of water-coating grain potentially controlled the current path.

Based on the observation, the effect of temperature and pressure on the cement samples at similar hydration time might change the cut-off frequency. This was important since the value of bulk conductivity depended on this frequency. The trend indicates that as pressure and temperature increased, the cut-off frequency tended to decrease. This also indicates that a half-circle curve was clearly shown in the Nyquist

plot in elevated curing conditions compared to that of normal for the similar hydration time.

These effects were also indicated in the form of magnitude of conductivity dispersion (Figure 4.8). The magnitude increased as temperature and pressure increased in the form of linear profile as function of hydration time. As expected, the high magnitude of conductivity dispersion occurred at the lower w/c at maximum curing temperature and pressure. So, the existence of interface conductivity potentially took place in this condition.

As a result, it was suggested that conductivity dispersion was influenced by inter-connected pore and saturation degree. This dispersion occurred at the interface or at the boundary between grain and pore fluid. The bigger pore radius caused smaller conductivity dispersion.

Due to the potential existence of the interface conductivity from the previous discussion, it was important to determine the magnitude of interface conductivity and to find out its contribution to the bulk conductivity. This will be discussed in Section 4.1.3.

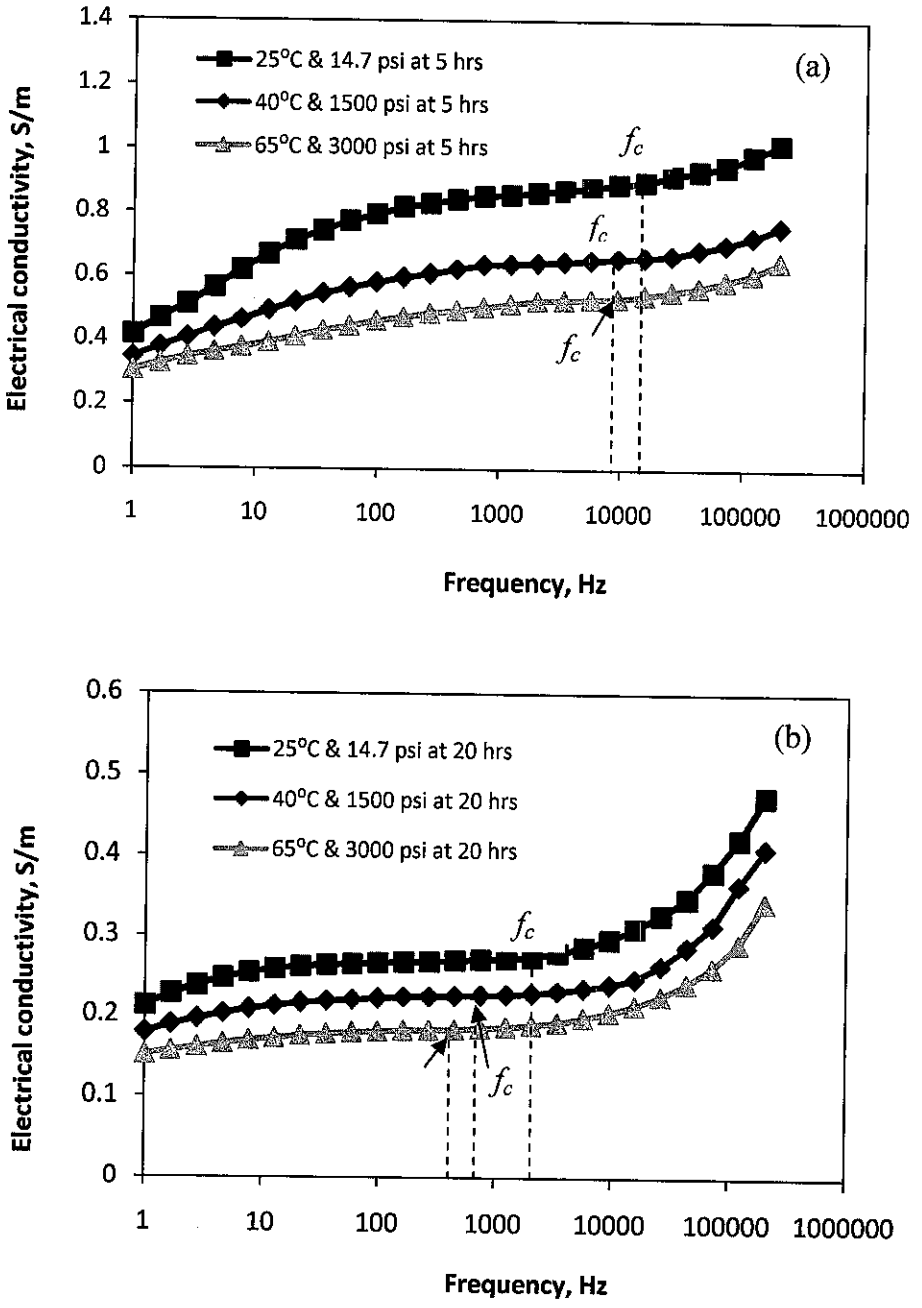

Figure 4.7a-b Conductivity dispersion curve as an effect of different curing conditions at w/c 0.5 for (a) 5 hrs of hydration time and (b) 20 hrs of hydration time

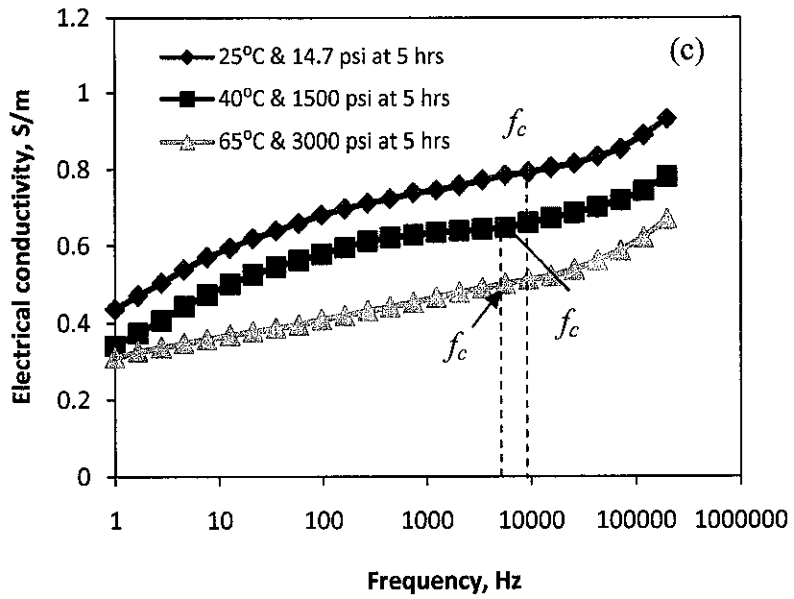

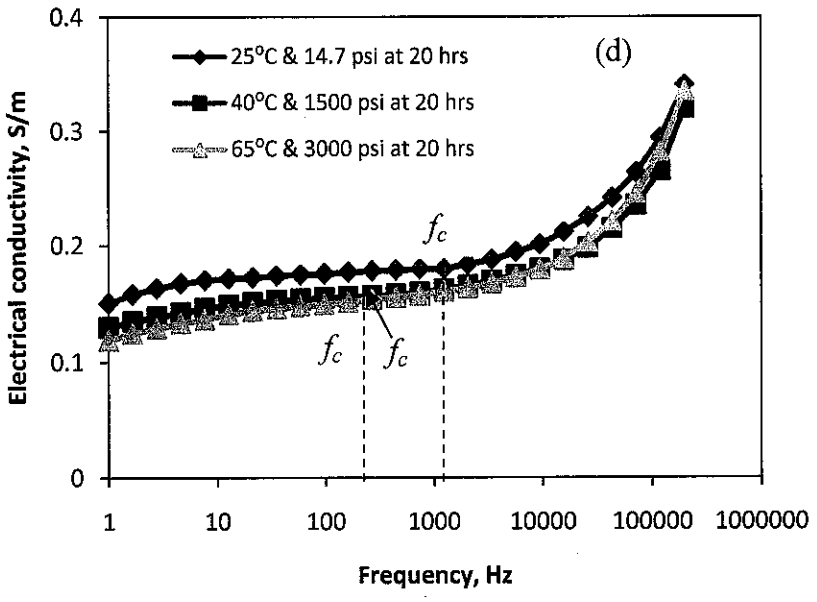

Figure 4.7c-d Conductivity dispersion curve as an effect of different curing conditions at w/c 0.4 for (c) 5 hrs of hydration time and (d) 20 hrs of hydration time

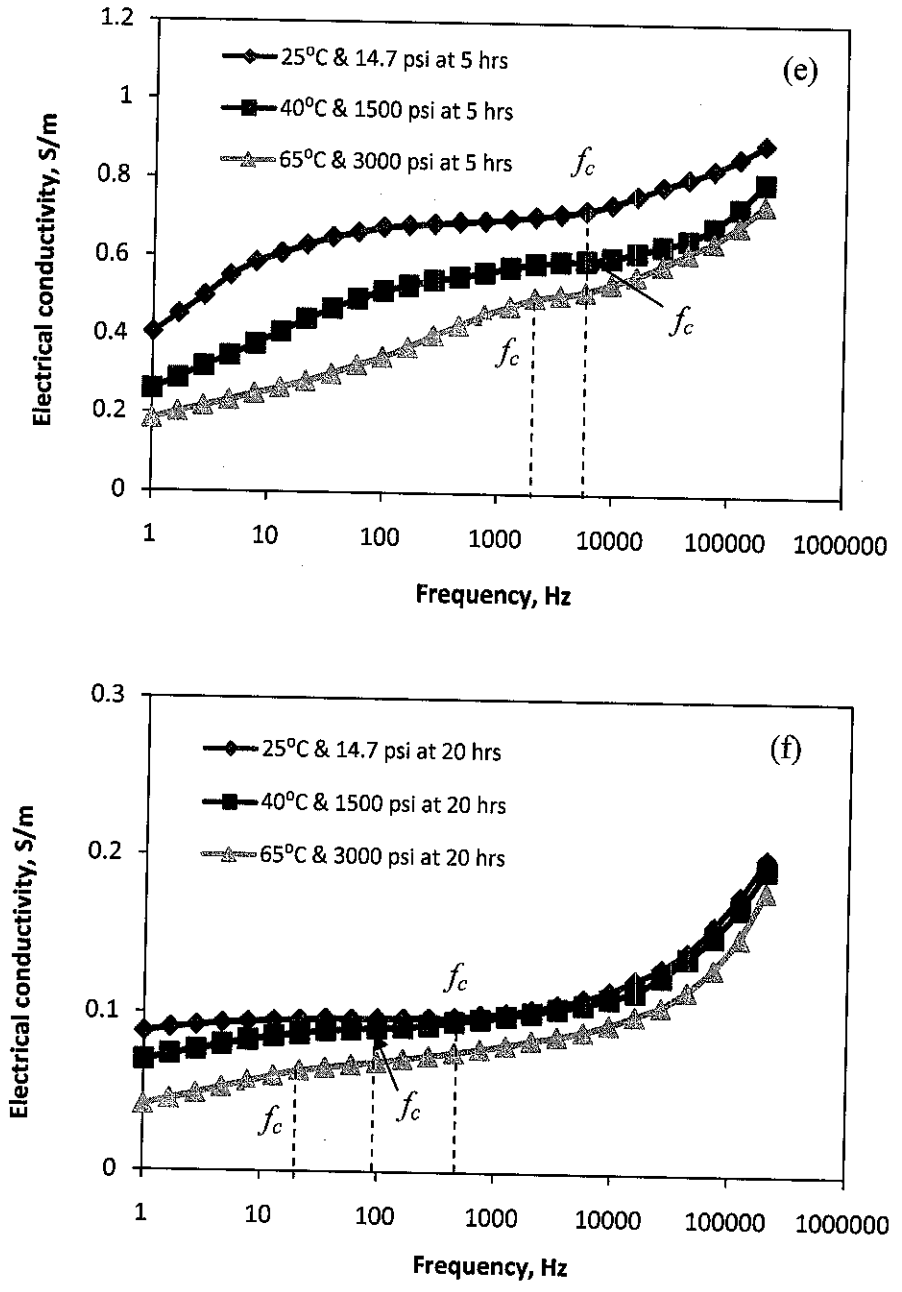

Figure 4.7e-f Conductivity dispersion curve as an effect of different curing conditions at w/c 0.3 for (e) 5 hrs of hydration time and (f) 20 hrs of hydration time

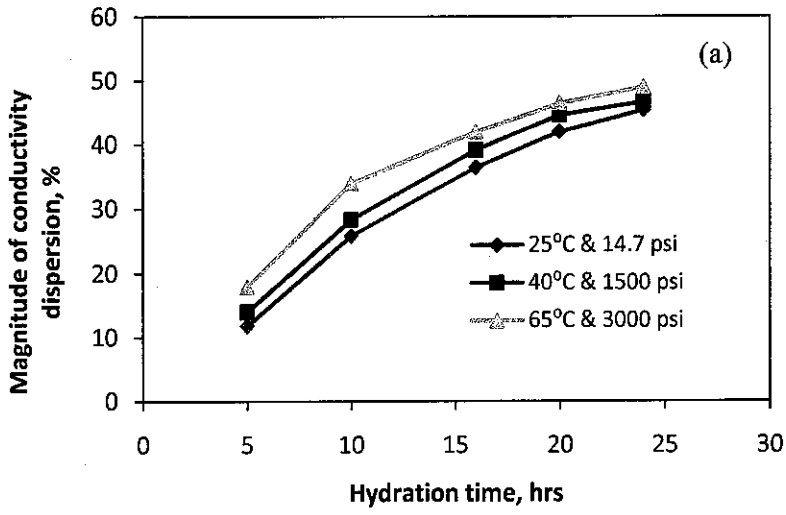

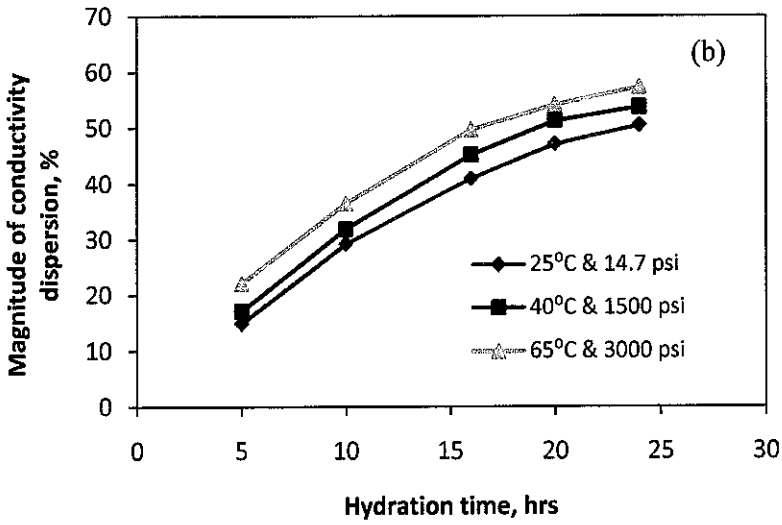

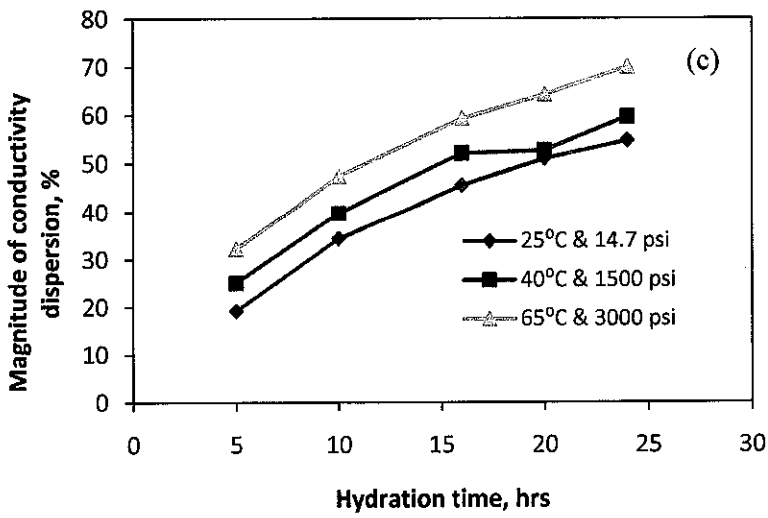

Figure 4.8 Magnitude of conductivity dispersion at water cement ratios of (a) 0.5, (b) 0.4 and (c) 0.3 as a function of curing temperature and pressure at different hydration time

4.1.3 Interface Conductivity Properties

If excess conductivity occurs at the interface between solid-pore solutions, it will contribute to both the higher ionic concentration of pore solution and the bulk electrical conductivity. As such, to ensure that cement physical properties can be reliably estimated using electrical attributes; there must be an evaluation on the magnitude of interface conductivity and its influence on the bulk conductivity.

Further, the effect of water cement ratios and curing pressure and temperature on interface conductivity profile was also considered in this study. Because of interface conductivity was directly related to the microstructural parameters (surface to volume ratio of the pores), a simple particle expansion model is proposed to simulate the growth of cement particles and to calculate the development of its pore size as a function of hydration time.

4.1.3.1 Simple Particle Expansion Model

The basic concept of simple particle expansion model is by assuming that the cement particle could be represented as a regular cubic lattice in the form of spherical particle that had the equal radius and growth. The pore size here could be estimated to be a diameter of the pores between the edge to edge distances as a function of degree of hydration. As cement hydrated, the cement particles expand and its pore volume contract as a function of time (Figure 4.9). By this, the degree of hydration, pore volume fraction and the average particle size were the only information required. The degree of hydration was calculated using Byfors correlation [28] (see Section 3.5) while pore volume fraction was measured using MIP procedure started from 5 hrs to 24 hrs of hydration time. For porosity below 5 hrs as a function of time $\phi_{(t)}$, it was calculated using Power-Brownyard model [61] as a function of hydration rate and water cement ratio with the following Equation (4.2).

$$\phi_{(t)} = 1 - \frac{\left(1 + \left(1.3 \cdot \alpha_{(t)}\right)\right)}{\left(1 + \left(\rho_c \cdot w/c\right)\right)} \tag{4.2}$$

where $\alpha_{(t)}$ is hydration rate as a function of time, ρ_c is cement powder density ($\mathrm{g/cm^3}$), and w/c is water to cement ratio.

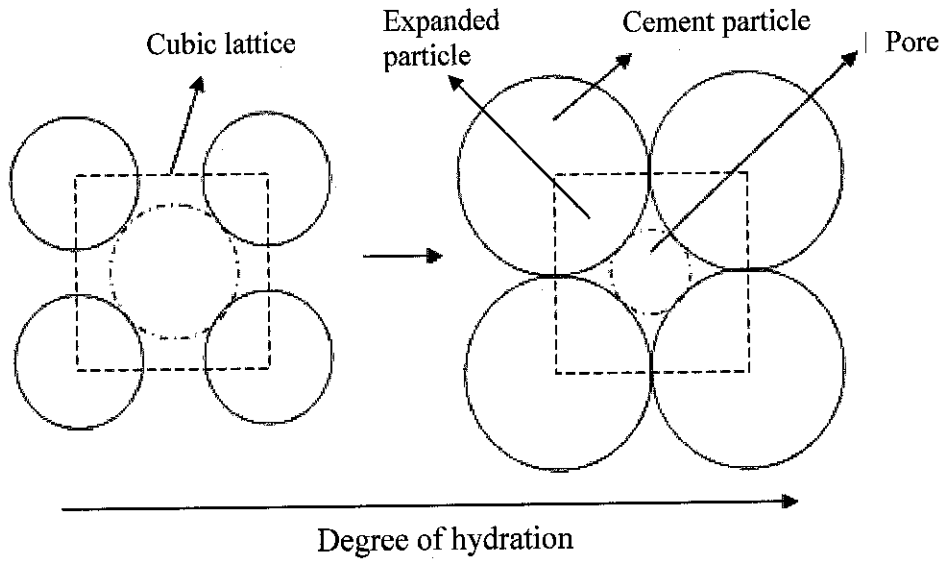

Figure 4.9 Shematic diagram of cement particle expansion mechanism in a cubic lattice as a function of hydration time

The cement particle volume can be expressed as follow (Equation 4.3):

$$v_c = \frac{4}{3}\pi {r_c}^3 \tag{4.3}$$

where v_c and r_c are cement particle volume (μm^3) and cement radius (μm), respectively.

The volume of the expanded particle $V_{exp(t)}$ (μm^3) corresponded to the degree of hydration at certain time followed Equation (4.4) [20],

$$V_{exp(t)} = v_c . \alpha_{(t)} . (v - 1) \tag{4.4}$$

where $\alpha_{(t)}$ is degree of hydration, v is the ratio of the volume of the expanded particle relative to that of the original cement value, $v = 2.2$ [61].

Due to the reaction products (v), the volume of the expanded particle was dependent on the curing temperature. Its values then decreased as curing temperature increased. Van Breugel [79] has derived a mathematical expression below for v-factor as a function of curing temperature as shown in Equation (4.5).

$$v(T) = 2.2\exp[-28 \cdot 10^{-6} * T^2] \tag{4.5}$$

where T is curing temperature (°C).

The volume of the expanded particles with time $V_{\exp(t)}$ (μm^3) as a function of particles diameter, contains both the expanded particle at certain hydration time $d_{c-\exp(t)}$ and the initial particle diameter r_c, is given below (Equation 4.6):

$$V_{\exp(t)} = \frac{4\pi}{3}\left(\left(r_{c-exp}\right)^3 - (r_c)^3\right) \tag{4.6}$$

Then, by using $d_{c-\exp(t)} = 2 \cdot r_{c-exp}$, the diameter of cement particle expansion $d_{c-\exp(t)}$ (μm) as a function of hydration time can be derived as follows (Equation 4.7):

$$d_{c-\exp(t)} = 2 \cdot \left[\left(\frac{3 \cdot V_{\exp(t)}}{4\pi}\right) + (r_c)^3\right]^{1/3} \tag{4.7}$$

Since the diameter of cement particle increased, its pore volume (porosity) might be decreased. This analogue can be used to calculate the diameter of pore cement reduction as a function of hydration time $d_{p(t)}$ (μm) with respect to the degree of hydration as stated in Equation (4.8):

$$d_{p-red(t)} = \frac{\phi_{p(t)} \cdot d_{c-\exp(t)}}{\phi_{c(t)}} \tag{4.8}$$

where $\phi_{p(t)}$ and $\phi_{c(t)}$ are pore volume and cement particle volume within cement system at specific hydration time.

Using these values (diameter of cement particle and diameter of pore cement) at specific hydration time, the pore-solid interface area $A_{p-s(t)}$ (μm^2) and the pore volume of cement particle samples of $V_{p(t)}$ (μm^3) might be calculated. By assuming the pore–solid interfaces remain covered by moisture, the surface area (Equation 4.9) and pore volume (Equation 4.10) followed:

$$A_{p-s\,(t)} = \pi \cdot d_{c-\exp(t)}{}^{2} \tag{4.9}$$

and,

$$V_{p(t)} = \frac{1}{6} \cdot \pi \cdot d_{p-red(t)}{}^{3} \tag{4.10}$$

where $d_{c-\exp(t)}$ and $d_{p-red(t)}$ are the diameter of cement particle expansion and the diameter of pore cement reduction as a function of hydration time, respectively.

It is then found that the average particle size of Class G cement was 10 μm ranging from 5 to 20 μm. Initially, using Equation 4.2, the cement grain occupied about 44% of the total volume when mixed to water at w/c 0.4. The pore size diameter would be around 12.7 μm as the pore volume consisted of about 56%. Furthermore, it is found that by applying equations 4.3 - 4.8, when hydration reached 5 hrs, the pore size diameter became about 12.1 μm. At this time, the degree of hydration was 0.043 with pore volume of about 54%. Table 4.2a-c depicts some results of diameter particle expansion and pore diameter reduction at different curing conditions and volume of w/c.

Figure 4.10 shows the reduction of cement pore diameter as a function of time. Here, the pore diameter decreased as w/c decreased for a similar hydration period. The effects of temperature and pressure on pore diameter are straight forward by which the pore diameter decreased as temperature and pressure increased due to the acceleration of hydration rate. These results give a reasonably fair trend to the data from MIP measurement using inflection point method (Figure 4.11). A steady rate expansion in the model calculation was due to the simplified assumption used and also directly due to the function of hydration rate which was considered only for physical properties instead of both this and chemical reactions. However, it has provided an indication of the possibility in using such a model for tracking the pore diameter development when the cement was in an unset form.

Table 4.2a Pore diameter reduction and particle diameter expansion calculation using the simple particle expansion model at different w/c for 25°C and 14.7 psi

w/c	Time (hrs)	Hydration Rate	Pore Volume	Particle Volume	v	V_{exp} (μm^3)	$d_{c\text{-}exp}$ (μm)	$d_{p\text{-}red}$ (μm)
0.5	1	0.0018	0.6130	0.3870	2.2	1.1591	10.0074	15.8540
	5	0.0217	0.6038	0.3962	2.2	13.6276	10.0861	15.3693
	10	0.1228	0.5566	0.4434	2.2	77.1262	10.4689	13.1416
	16	0.1918	0.5244	0.4756	2.2	120.4503	10.7149	11.8149
	20	0.2396	0.5021	0.4979	2.2	150.4687	10.8789	10.9711
	24	0.2711	0.4874	0.5126	2.2	170.2664	10.9844	10.4445
0.4	1	0.0018	0.5589	0.4411	2.2	1.0611	10.0068	12.6781
	5	0.0269	0.5456	0.4544	2.2	15.4813	10.0977	12.1221
	10	0.1391	0.4859	0.5141	2.2	80.0724	10.4860	9.9100
	16	0.2119	0.4472	0.5528	2.2	121.9875	10.7234	8.6733
	20	0.2645	0.4192	0.5808	2.2	152.2637	10.8885	7.8583
	24	0.2889	0.4062	0.5938	2.2	166.3316	10.9636	7.4993
0.3	1	0.0013	0.4875	0.5125	2.2	0.7248	10.0046	9.5147
	5	0.0207	0.4754	0.5246	2.2	11.9083	10.0753	9.1317
	10	0.1342	0.4053	0.5947	2.2	77.2403	10.4696	7.1338
	16	0.2186	0.3530	0.6470	2.2	125.8333	10.7447	5.8635
	20	0.2723	0.3198	0.6802	2.2	156.7674	10.9127	5.1311
	24	0.3061	0.2989	0.7011	2.2	176.2289	11.0158	4.6966

Table 4.2b Pore diameter reduction and particle diameter expansion calculation using the simple particle expansion model at different w/c for 40°C and 1500 psi

w/c	Time (hrs)	Hydration Rate	Pore Volume	Particle Volume	v	V_{exp} (μm^3)	$d_{c\text{-}exp}$ (μm)	$d_{p\text{-}red}$ (μm)
0.5	1	0.0023	0.6128	0.3872	2.1036	1.3537	10.0086	15.8405
	5	0.0370	0.5966	0.4034	2.1036	21.3697	10.1343	14.9902
	10	0.1794	0.5302	0.4698	2.1036	103.6176	10.6207	11.9859
	16	0.2789	0.4838	0.5162	2.1036	161.0810	10.9357	10.2483
	20	0.3350	0.4576	0.5424	2.1036	193.4993	11.1057	9.3689
	24	0.3539	0.4488	0.5512	2.1036	204.4195	11.1618	9.0869
0.4	1	0.0024	0.5586	0.4414	2.1036	1.3837	10.0088	12.6656
	5	0.0527	0.5318	0.4682	2.1036	30.4421	10.1903	11.5757
	10	0.1986	0.4542	0.5458	2.1036	114.7313	10.6831	8.8903
	16	0.2780	0.4120	0.5880	2.1036	160.5447	10.9329	7.6609
	20	0.3343	0.3821	0.6179	2.1036	193.0585	11.1034	6.8654
	24	0.3744	0.3607	0.6393	2.1036	216.2577	11.2220	6.3319
0.3	1	0.0023	0.4868	0.5132	2.1036	1.3479	10.0086	9.4932
	5	0.0529	0.4555	0.5445	2.1036	30.5660	10.1910	8.5253
	10	0.2004	0.3643	0.6357	2.1036	115.7632	10.6888	6.1248
	16	0.2797	0.3152	0.6848	2.1036	161.5708	10.9383	5.0353
	20	0.3404	0.2777	0.7223	2.1036	196.6180	11.1218	4.2759
	24	0.3786	0.2541	0.7459	2.1036	218.6799	11.2343	3.8266

Table 4.2c Pore diameter reduction and particle diameter expansion calculation using the simple particle expansion model at different w/c for 65°C and 3000 psi

w/c	Time (hrs)	Hydration Rate	Pore Volume	Particle Volume	v	V_{exp} (μm^3)	$d_{c\text{-}exp}$ (μm)	$d_{p\text{-}red}$ (μm)
0.5	1	0.0048	0.6116	0.3884	1.9545	2.4189	10.0154	15.7736
	5	0.0483	0.5914	0.4086	1.9545	24.1343	10.1514	14.6905
	10	0.2149	0.5136	0.4864	1.9545	107.3475	10.6417	11.2386
	16	0.3007	0.4736	0.5264	1.9545	150.2031	10.8775	9.7869
	20	0.3694	0.4415	0.5585	1.9545	184.5419	11.0593	8.7439
	24	0.4073	0.4238	0.5762	1.9545	203.4865	11.1571	8.2077
0.4	1	0.0050	0.5572	0.4428	1.9545	2.4859	10.0158	12.6041
	5	0.0596	0.5281	0.4719	1.9545	29.7959	10.1863	11.4010
	10	0.2286	0.4383	0.5617	1.9545	114.2060	10.6801	8.3324
	16	0.3195	0.3899	0.6101	1.9545	159.6094	10.9279	6.9842
	20	0.3935	0.3506	0.6494	1.9545	196.5438	11.1214	6.0040
	24	0.4499	0.3206	0.6794	1.9545	224.7406	11.2648	5.3149
0.3	1	0.0050	0.4851	0.5149	1.9545	2.5019	10.0159	9.4374
	5	0.0821	0.4374	0.5626	1.9545	41.0348	10.2548	7.9736
	10	0.2322	0.3446	0.6554	1.9545	115.9939	10.6901	5.6213
	16	0.3289	0.2848	0.7152	1.9545	164.3110	10.9529	4.3617
	20	0.4015	0.2399	0.7601	1.9545	200.5442	11.1420	3.5175
	24	0.4598	0.2039	0.7961	1.9545	229.6569	11.2894	2.8916

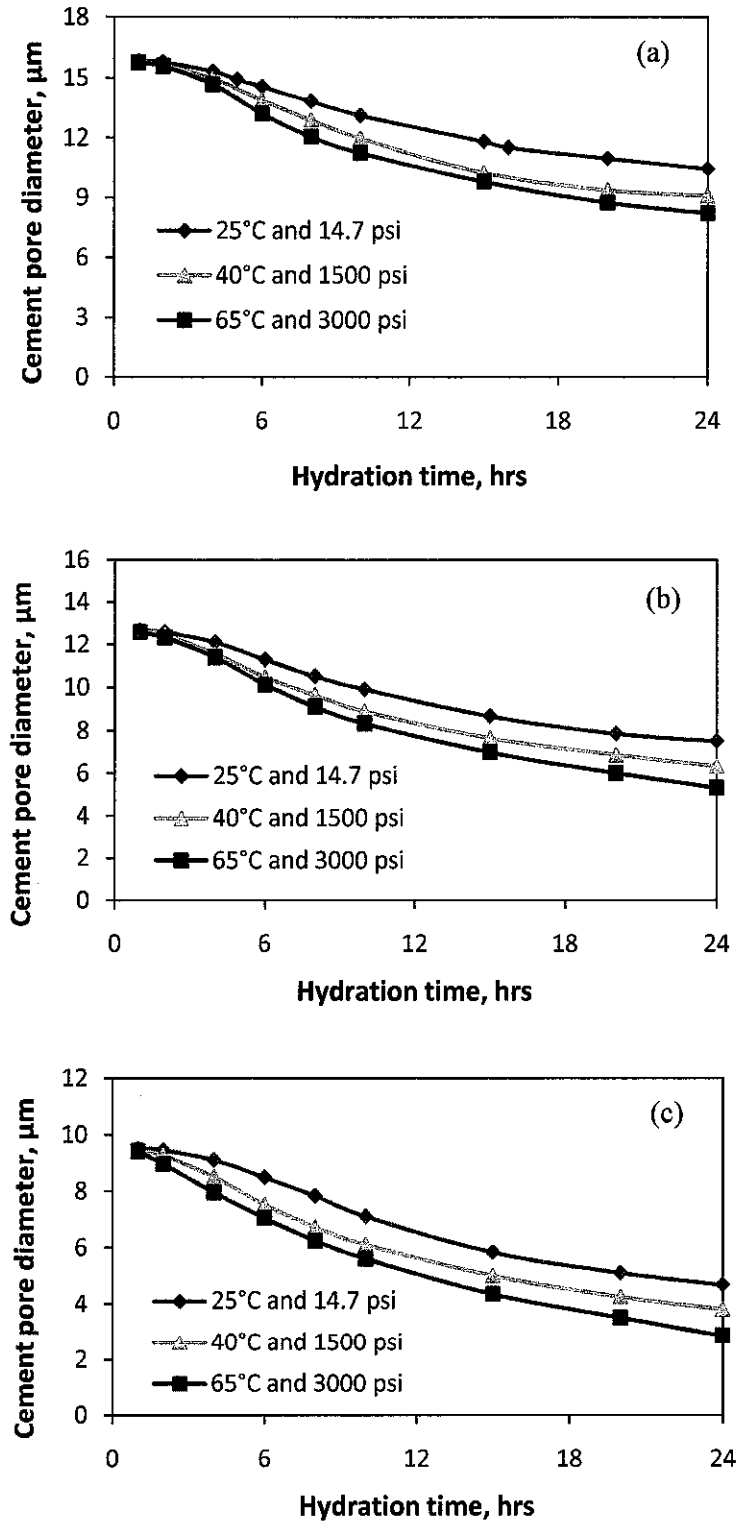

Figure 4.10 Pore diameter reduction of Class G cement calculated using the simple particle expansion model at different temperature and pressure for (a) w/c 0.5, (b) w/c 0.4, and (c) w/c 0.3

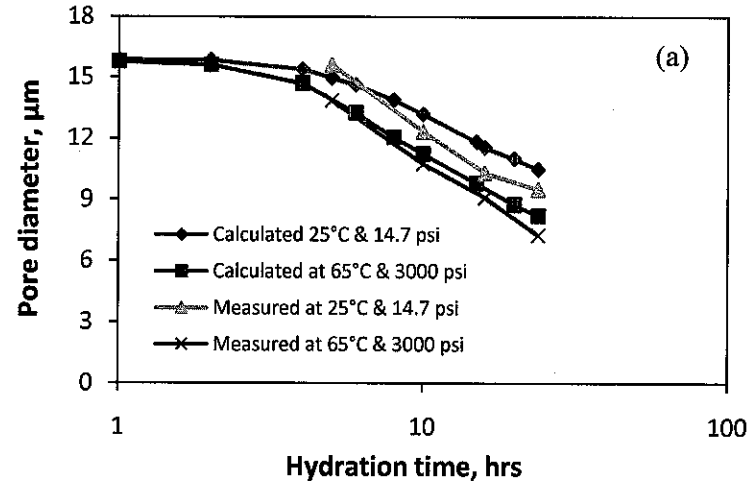

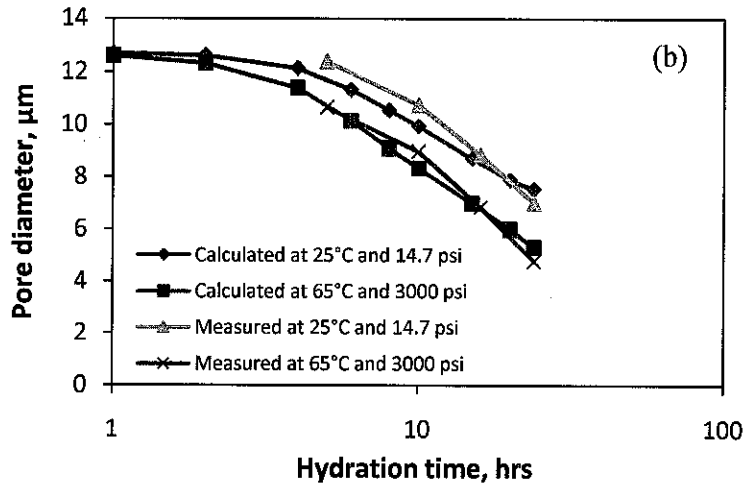

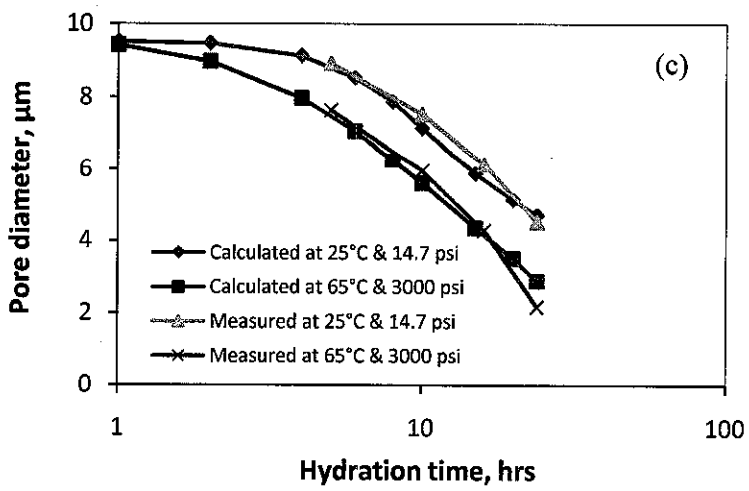

Figure 4.11 Comparison of measured and calculated of pore diameter reduction of Class G cement at different temperature and pressure for (a) w/c 0.5, (b) w/c 0.4, and (c) w/c 0.3

4.1.3.2 Interface Conductivity Calculation and Its Contribution on Bulk Conductivity

For a given cement sample that had a mass (W_c) about 1 g, the volume of cement sample (V_c) would be $V_c = W_c/\rho_c$, where ρ_c represents the density of the cement (g/cm^3). The number of cement particles N_c in sample mass (W_c) afterward was found by dividing the cement volume V_c by the volume of single particle v_c.

As such, the total surface area (Equation 4.11) and total pore volume (Equation 4.12) of all particles are followed:

$$A_{p-s(tot)} = N_c \cdot A_{p-s(t)} \tag{4.11}$$

and

$$V_{p(tot)} = N_c \cdot V_{p(t)} \tag{4.12}$$

The total surface area $A_{p-s(tot)}$ and the total volume $V_{p(tot)}$ of the pores calculated from a simple particle expansion model might represent the microstructure parameter approximation $2/\Lambda \approx (A_{p-s(tot)}/V_{p(tot)})$. By this information together with the normalized conductivity, the interface conductivity (σ_s) of cement samples was calculated using Johnson model as stated in Equation (2.15).

Tables 4.3a-c present a report of the calculated interface conductivity at different w/c and curing temperature and pressure. These values have included the effect of geometry factor of the cement sample for which the result may come to be reasonably comparable to the bulk conductivity. Based on the observation, the interface conductivity increased along the hydration process, indicating that the more volumetric water loses the more significant interface conduction took place. This also corresponded to the decreasing of normalized conductivity; hence the term $\sigma_s * 2/\Lambda$ was dependent on the moisture content as reflected by the expanded particle within the hydration process. Hence, it could be assumed that the pore-solid interface areas remained covered by moisture and the interface conductivity of pore-solid interface, as a consequence, was not influenced by the microstructural properties of the material as suggested by Revil *et al.*[11]. However, water saturation contributed to the excess

of charged ions in the EDL as reflected by an increasing of interface conductivity. Degree of salinity concentration had a similar role as previously shown by Khairy [16].

The contribution of interface conductivity (σ_s) on the bulk conductivity (σ_b) was achieved by dividing the size of σ_s to the values of σ_b at each hydration time in the percentage manner. From the results shown in Figure 4.12, it is found that the contribution of interface conductivity on the bulk conductivity is relatively very small of about factor -6 in order of magnitude. The contribution of interface conductivity, in this case, seemed to increase as w/c decreased and hydration time proceeded. An increase of the interface conductivity contribution was also found as curing temperature and pressure increased, although its influence was not as much as w/c for similar hydration period. The rule of elevated temperature and pressure accelerated the hydration time of cement system and also might reduce the amount of water in comparing to the normal curing condition. This then implies that the saturation of water content within cement system had a significant contribution to the values of interface conductivity and its contribution to the bulk conductivity.

Table 4.3a Result from the calculation of interface conductivity at 25°C & 14.7 psi

w/c	Time (hrs)	Bulk Conductivity (S/m)	Normalized Conductivity	$A_{p-s(tot)}$ (m^2/g)	$V_{p(tot)}$ (m^3/g)	Interface Conductance (S)	Interface Conductivity (S/m)
0.5	1	1.271	0.4395	0.4747	1.2543E-06	2.10621E-11	1.6519E-09
	5	1.101	0.1636	0.4358	1.1162E-06	2.75488E-11	2.16066E-09
	10	0.402	0.0435	0.2849	6.23996E-07	4.165E-11	3.26661E-09
	16	0.321	0.0304	0.2148	4.22931E-07	5.13797E-11	4.02971E-09
	20	0.274	0.0243	0.1769	3.23551E-07	6.43359E-11	5.04586E-09
	24	0.245	0.0202	0.1558	2.71191E-07	6.9356E-11	5.43959E-09
0.4	1	1.2663	0.3992	0.3036	6.41534E-07	2.30621E-11	1.80876E-09
	5	1.0476	0.1227	0.2701	5.45778E-07	3.14488E-11	2.46653E-09
	10	0.3156	0.0300	0.1612	2.66275E-07	4.547E-11	3.56621E-09
	16	0.2236	0.0195	0.1155	1.66915E-07	5.22497E-11	4.09795E-09
	20	0.1802	0.0146	0.0905	1.18583E-07	6.73449E-11	5.28186E-09
	24	0.1343	0.0099	0.0808	1.0096E-07	7.39356E-11	5.79877E-09
0.3	1	1.2620	0.3979	0.1711	2.71347E-07	2.52621E-11	1.9813E-09
	5	1.0059	0.1178	0.1543	2.34868E-07	3.43788E-11	2.69633E-09
	10	0.2207	0.0210	0.0839	9.97969E-08	4.21982E-11	3.3096E-09
	16	0.1381	0.0120	0.0525	5.12667E-08	5.32497E-11	4.17638E-09
	20	0.0981	0.0079	0.0383	3.27925E-08	6.93449E-11	5.43872E-09
	24	0.0876	0.0065	0.0312	2.44482E-08	7.59356E-11	5.95563E-09

Table 4.3b Result from the calculation of interface conductivity at 40°C & 1500 psi

w/c	Time (hrs)	Bulk Conductivity (S/m)	Normalized Conductivity	$A_{p\text{-}s(tot)}$ (m^2/g)	$V_{p(tot)}$ (m^3/g)	Interface Conductance (S)	Interface Conductivity (S/m)
0.5	1	1.1855	0.4098	0.4737	1.25062E-06	2.30621E-11	1.80876E-09
	5	0.8533	0.1268	0.4086	1.0209E-06	2.95488E-11	2.31752E-09
	10	0.3084	0.0334	0.2270	4.53415E-07	4.34998E-11	3.41169E-09
	16	0.2612	0.0247	0.1520	2.59629E-07	5.52797E-11	4.33559E-09
	20	0.2261	0.0200	0.1213	1.89396E-07	6.94634E-11	5.44801E-09
	24	0.2151	0.0177	0.1124	1.70211E-07	7.62736E-11	5.98214E-09
0.4	1	1.1795	0.3718	0.3028	6.39244E-07	2.54721E-11	1.99777E-09
	5	0.8633	0.1011	0.2397	4.62407E-07	3.53788E-11	2.77476E-09
	10	0.2884	0.0274	0.1227	1.81805E-07	4.93698E-11	3.87207E-09
	16	0.2062	0.0180	0.0850	1.08539E-07	5.95397E-11	4.6697E-09
	20	0.1561	0.0126	0.0652	7.45717E-08	7.46449E-11	5.8544E-09
	24	0.1351	0.0100	0.0537	5.66659E-08	8.14236E-11	6.38605E-09
0.3	1	1.1695	0.3687	0.1701	2.6919E-07	2.57841E-11	2.02224E-09
	5	0.8364	0.0980	0.1300	1.84678E-07	3.63344E-11	2.84971E-09
	10	0.1784	0.0169	0.0581	5.93502E-08	4.28982E-11	3.3645E-09
	16	0.1112	0.0097	0.0367	3.07729E-08	5.53975E-11	4.34482E-09
	20	0.0916	0.0074	0.0252	1.79272E-08	7.64899E-11	5.9991E-09
	24	0.0717	0.0053	0.0195	1.24667E-08	8.42356E-11	6.6066E-09

Table 4.3c Result from the calculation of interface conductivity at 65°C & 3000 psi

w/c	Time (hrs)	Bulk Conductivity (S/m)	Normalized Conductivity	$A_{p\text{-}s(tot)}$ (m^2/g)	$V_{p(tot)}$ (m^3/g)	Interface Conductance (S)	Interface Conductivity (S/m)
0.5	1	1.116	0.3858	0.4688	1.23233E-06	2.47205E-11	1.93883E-09
	5	0.7177	0.1066	0.3905	9.56021E-07	3.37884E-11	2.65003E-09
	10	0.2441	0.0264	0.1984	3.7157E-07	4.79282E-11	3.75901E-09
	16	0.2141	0.0203	0.1409	2.29772E-07	6.29745E-11	4.93909E-09
	20	0.1837	0.0163	0.1070	1.55913E-07	7.26336E-11	5.69665E-09
	24	0.1682	0.0138	0.0918	1.25591E-07	8.1356E-11	6.38075E-09
0.4	1	1.076	0.3392	0.2993	6.28661E-07	2.82651E-11	2.21683E-09
	5	0.6677	0.0782	0.2328	4.423E-07	3.94388E-11	3.09319E-09
	10	0.2441	0.0232	0.1079	1.49803E-07	5.42898E-11	4.25795E-09
	16	0.1841	0.0160	0.0707	8.23527E-08	6.49745E-11	5.09595E-09
	20	0.1637	0.0132	0.0496	4.96336E-08	8.52449E-11	6.68576E-09
	24	0.1282	0.0095	0.0374	3.31324E-08	9.35356E-11	7.336E-09
0.3	1	1.0560	0.3329	0.1678	2.63895E-07	2.72605E-11	2.13804E-09
	5	0.6437	0.0754	0.1116	1.48293E-07	4.15344E-11	3.25755E-09
	10	0.1441	0.0137	0.0490	4.58682E-08	5.18982E-11	4.07037E-09
	16	0.0866	0.0075	0.0274	1.99215E-08	6.53975E-11	5.12912E-09
	20	0.0644	0.0052	0.0169	9.92588E-09	8.3849E-11	6.57628E-09
	24	0.0468	0.0035	0.0110	5.3008E-09	9.83236E-11	7.71152E-09

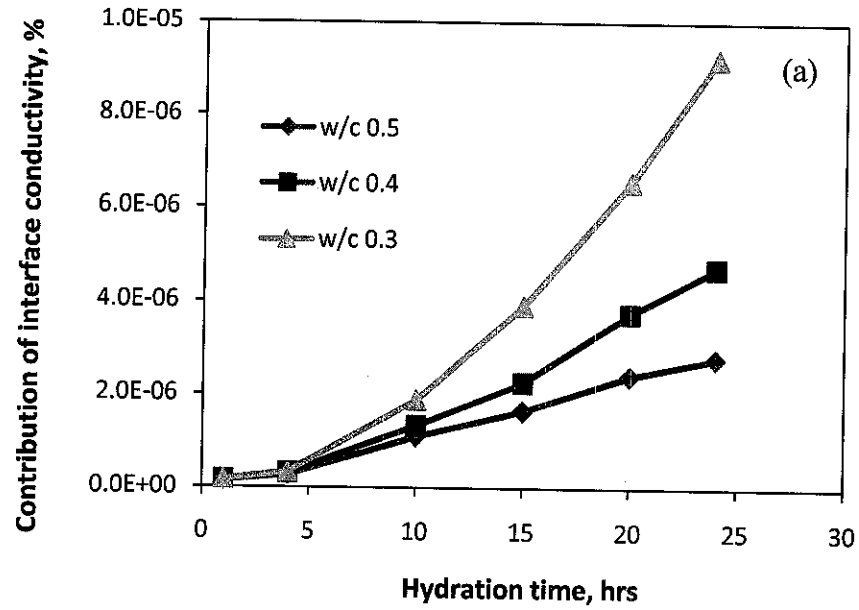

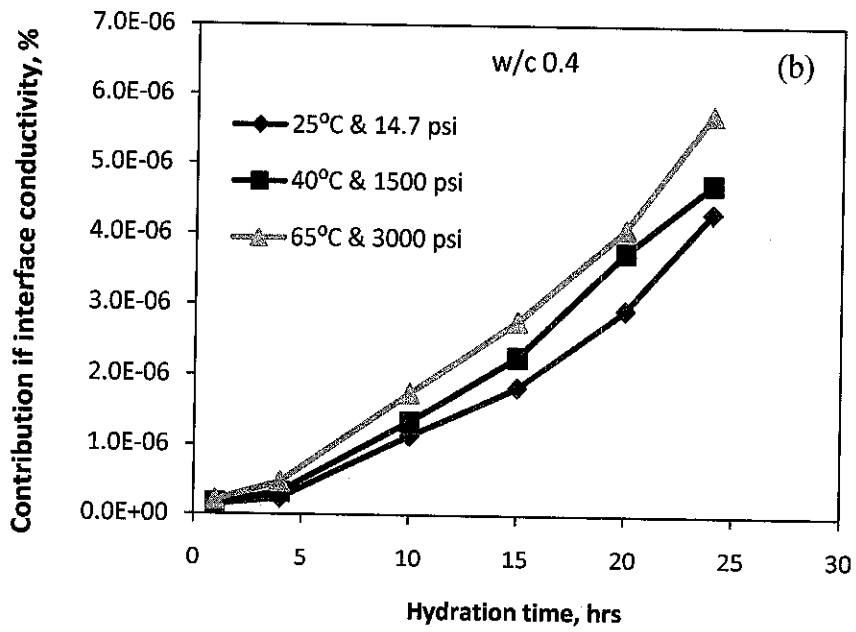

Figure 4.12 Contribution of interface conductivity on the bulk conductivity at (a) different w/c at ambient condition, and (b) different curing temperature and pressure

4.1.4 Summary

The conductivity dispersion characteristic was delivered in the form of magnitude of conductivity dispersion. It was found that the water saturation played a significant contribution to the conductivity dispersion characteristic during early hydration by means of decreasing water saturation that affected the increasing of conductivity dispersion. Curing temperature and pressure furthermore were appeared to provide a gradual increase of conductivity dispersion that, in this case, was by accelerating the hydration process. The smaller w/c tended to have interface conductivity as indicated in the increases of magnitude of conductivity dispersion. However, in a 24 hrs hydration process both w/c and curing temperature and pressure contributed to a relatively small effect on the conductivity dispersion since the bulk fluid volumetric at this period mainly controlled the path of the electrical current.

The magnitude of interface conductivity as a function of w/c and curing temperature and pressure was calculated using Johnson equation. Some difficulties in measuring microstructure parameter within Johnson equation were overcome by applying a simple particle expansion model. It was observed that the value of interface conductivity for 24 hrs of hydration was very small of about factor -9 in orders of magnitude. It then increased along with the hydration process and curing temperature and pressure, which indicated that the more volumetric water loses, the more significant interface conduction takes place.

It was also found that the contribution of interface conductivity on the bulk conductivity was relatively very small of about factor -6 in orders of magnitude. The contribution of interface conductivity seemed to increase as w/c decreased and hydration time proceeded. When the volumetric fluids dominated most of the pore spaces, the electrical double layer vanished which was reflected in the smallest values of interface conductivity during very early hydration period. This implies that the saturation of water content within cement system has a significant contribution to the values of interface conductivity and its contribution to the bulk conductivity.

4.2 Electrical Conductivity Properties of Oilwell cement

The next subsection of this section is designed to discuss about the analysis of parameters influencing the electrical conductivity of oilwell cement. Here, the effect of w/c, elevated pressure and temperature on electrical conductivity is discussed, including the correctness of the direct effect of elevated temperature on conductivity measurement. Some models for conductivity changes with time are evaluated to correspond with the oilwell cement application as well.

4.2.1 Bulk and Pore Solution Conductivity

A slight increase in bulk conductivity was observed at the beginning of hydration for all water cement ratio (Figure 4.13). This, as observed, was caused by the dissolution of ions of cement into the mixing water. However, as the hydration of cement progressed, the bulk conductivity decreased due to a combination of physical effects; one was the reducing volume fraction of solution and the other was the increasing tortuosity of pore connecting path.

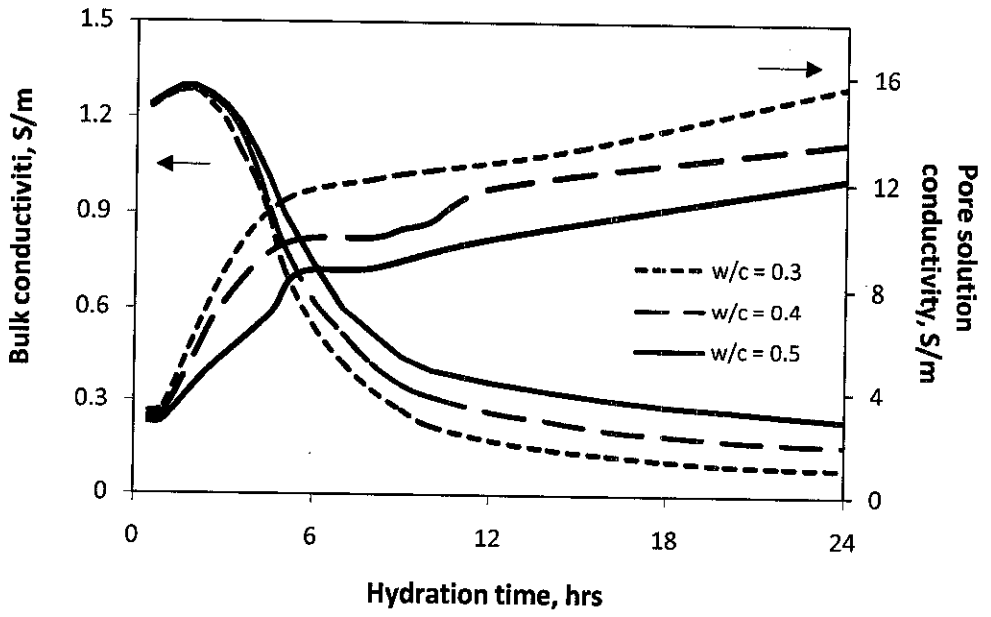

Figure 4.13 Bulk and pore solution conductivity at ambient conditions as a function of hydration time

In a similar period, an increasing trend was observed for pore solution conductivity which was attributed to the effect of ions movement in domination of Ca^{2+}, OH^-, Na^+, K^+, and SO_4^{2-} [57]. In the literature, the values [43, 80] vary between

0.6 and 15 S/m, but the pore solution conductivity reported in this study was relatively high, possibly due to the used of tap water instead of distilled water for cement mixing. The former, on the other hand, was electrically more conductive due to the existence of a number of additional active ions, such as Cl^-, Cu^{2+} and F^-. In fact, the pore solution conductivity value was difficult to obtain experimentally and by then it can be predicted based on the concentrations of species ions variety in the pore solution of the well cement as a function of time. Method of pore solution conductivity calculation was given in Appendix C.

Furthermore, the bulk conductivity profile may explain the hydration process. This hydration process itself, as shown in Figure 4.14, could be divided into 5 different periods: pre-induction, induction, acceleration, deceleration, and diffusion.

In pre-induction period, after cement mixed with water, the ions of water alone contributed significantly to the values of bulk conductivity. As hydration proceeded, the ions in the cement dissolved into the water and formed an electrolytic solution. These free mobile ions within cement [5], such as potassium (K^+), sodium (Na^+), calcium (Ca^+), hydroxyl (OH^-), and sulfate (SO_4^{2-}) served an increase in the electrical conductivity of the solution at about 1.5 hrs of hydration. From this point to about 3.5 hrs of hydration, there were no much changes in the electrical conductivity (approximately only 0.08 S/m), indicating that the reaction was relatively inactive. The reasons remained unclear on either the reaction controlled by nucleation and growth phenomena or controlled by the formation of a protective layer around the cement grains. This period was called dorman period.

Further, the acceleration period was marked by a decrease of electrical conductivity, indicating a rapid change in microstructure properties. At this period, the hydration reaction started to form the crystallization of solid calcium hydroxide and the deposition of C-S-H gel in pores. The formation of C-S-H, due to reaction dominated by C_3S, resulted in a percolation of the cement matrix which led to form a rigid structure. This period represented the setting time of cement hydration. After setting to about 8 hrs, the conductivity reduced at a temporarily slow rate due to the solid grains that became highly connected and the availability of water became lower leading to deceleration of hydration. Above this point of about 17 hrs, the reaction was mainly controlled by a diffusion mechanism. The very small decrease of

conductivity described a slowdown in the chemical reaction rate due to ion-diffusion process with the thickness of the hydrates on the cement grain surface that was formed.

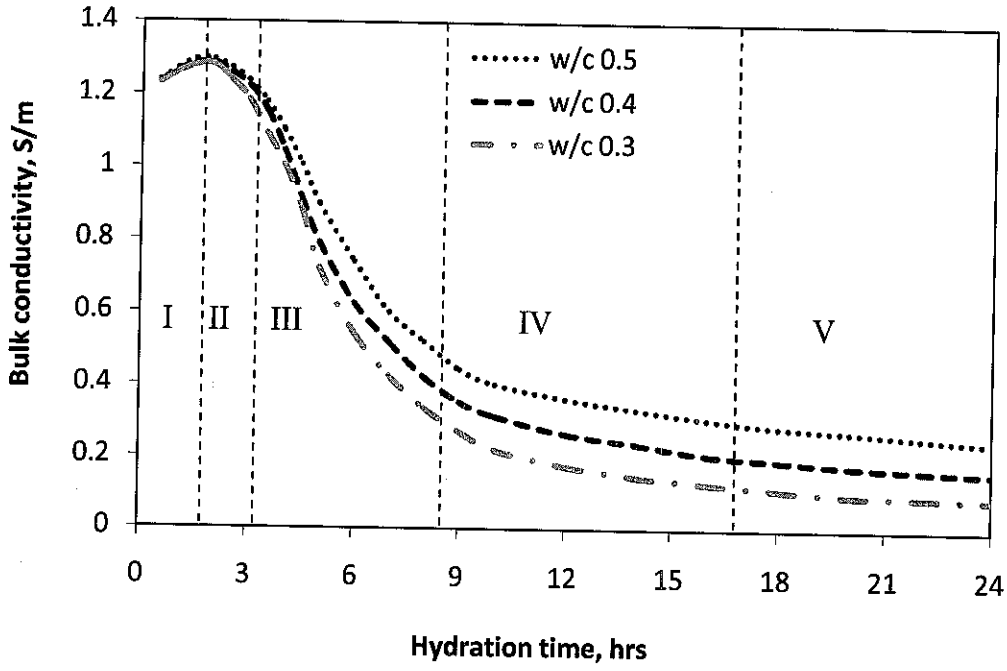

Figure 4.14 Development of electrical conductivity as a function of hydration time at different w/c

4.2.2 Temperature Correction

For cementing system, the effect of curing temperature on conductivity measurement is doubles either contributing to the hydration acceleration or overestimating the conductivity reading for the direct effect of temperature on conductivity measurement. The latter effect might come out with an equivalent temperature correction in order to have a physically representative meaning by means of the microstructural changes.

The comparison between the conductivity curve obtained under constant temperature and the curve obtained under varying temperature is given in Figure 4.15. It can be seen that the conductivity fluctuates with varying temperature, showing the temperature influence on the conductivity. The constant temperature was maintained at 25°C. The varying temperature was ranging from 25 to 30°C and from 25 to 65°C as shown in Figures 4.15 (a) and (b), respectively.

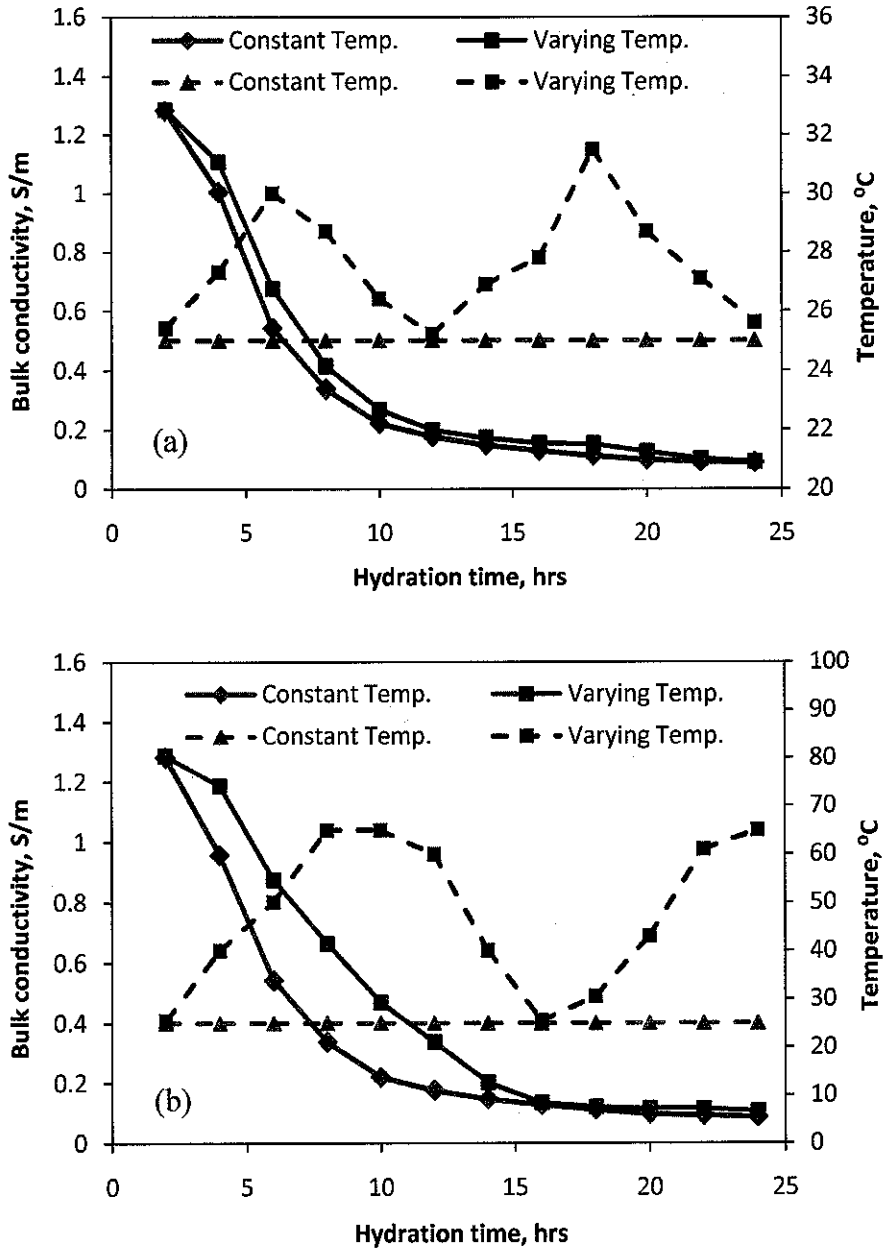

Figure 4.15 Comparison between the conductivity curve obtained under constant temperature and the curve obtained under varying temperature for w/c 0.3 (solid lines are conductivity values and dashed lines are temperature profile) for temperature ranging from (a) 25 to 30°C and (b) 25 to 65°C

Figure 4.16 shows the comparison of the curve of conductivity vs. hydration time with temperature influence corrected by Hammond [52] and Arps [51] equations and the conductivity vs. hydration time curve measured in a constant temperature. For simplicity, only the results of the specimen with w/c 0.3 are shown. The results seem to appear nearly identical which, in turn, validates that both equations are effective in correcting the temperature influence on the conductivity of oilwell cement. However,

both methods deviate slightly once varying temperature is increased as shown in Figure 4.16 (b). The Hammond method locates just below the Arps method and, however, both methods are very close to the tested data.

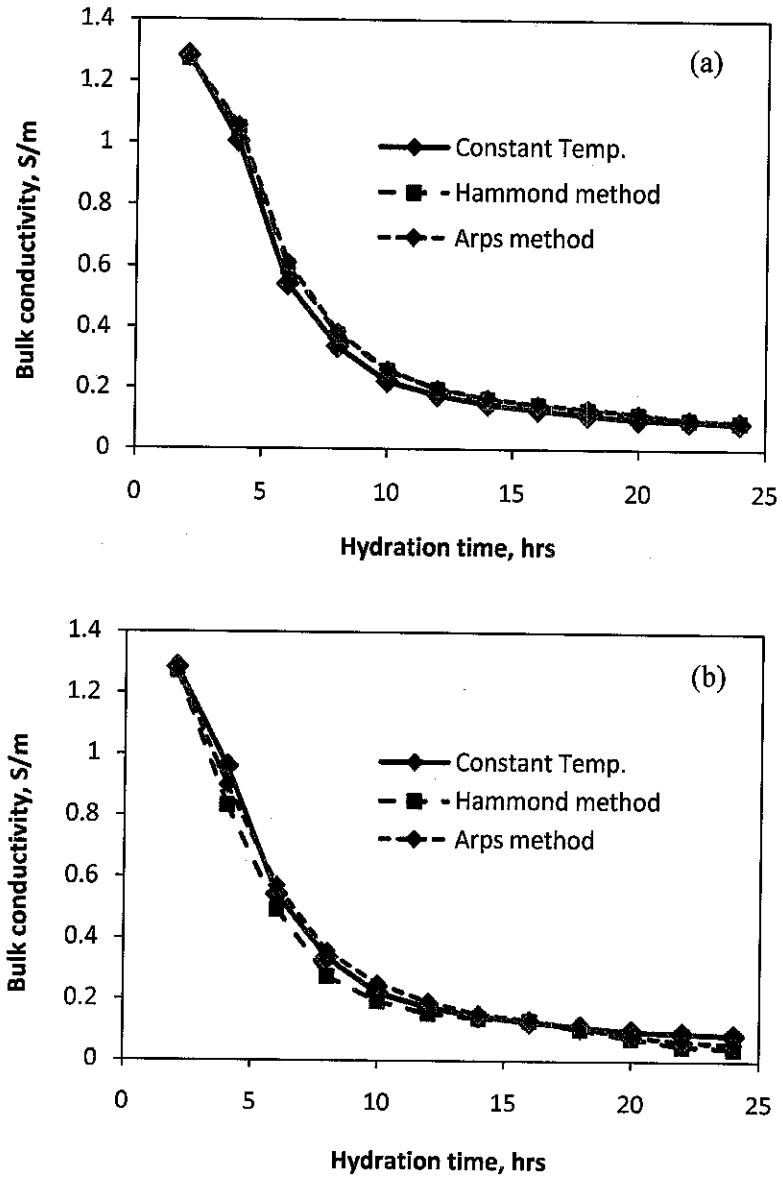

Figure 4.16 Comparison of the conductivity curves corrected by Hammond equation and Arps equation and the conductivity tested with constant temperature for w/c 0.3 for temperature ranging from (a) 25 to 30°C and (b) 25 to 65°C

The deviation can be described in the sensitivity analysis as can be seen in Figure 4.17. The sensitivity analysis was made by comparing the changing of conductivities $(\sigma_T/\sigma_{T(ref)})$ to that of temperature changing $(T - T_{ref})$. The effect of temperature change on the conductivity is obvious. The relationship between temperature and conductivity calculated by the Hammond and Arps equations shows good agreement

in a temperature range of ±25°C. These two methods show an obvious deviation in the varying temperature larger that ±50°C from reference point of view. When the temperature is much larger that the reference temperature, the Hammond method shows a remarkable increase. The Arps method, comparatively, shows a linear increase. It should be noted that when temperature is much smaller, even below 0°C, the Hammond method moves very slightly. Comparatively, a linear increase still occurs for Arps method. By that, it should be point out that when temperature is below 0°C, the Arps equation will give the meaningless result. However, both methods fit until the temperature reaching 25°C and above this value the methods deviate accordingly.

Based on the results, however, compared with the Arps method, the Hammond method is more convenient in temperature correction. Hence, the conductivity for all samples at different curing temperature followed this method.

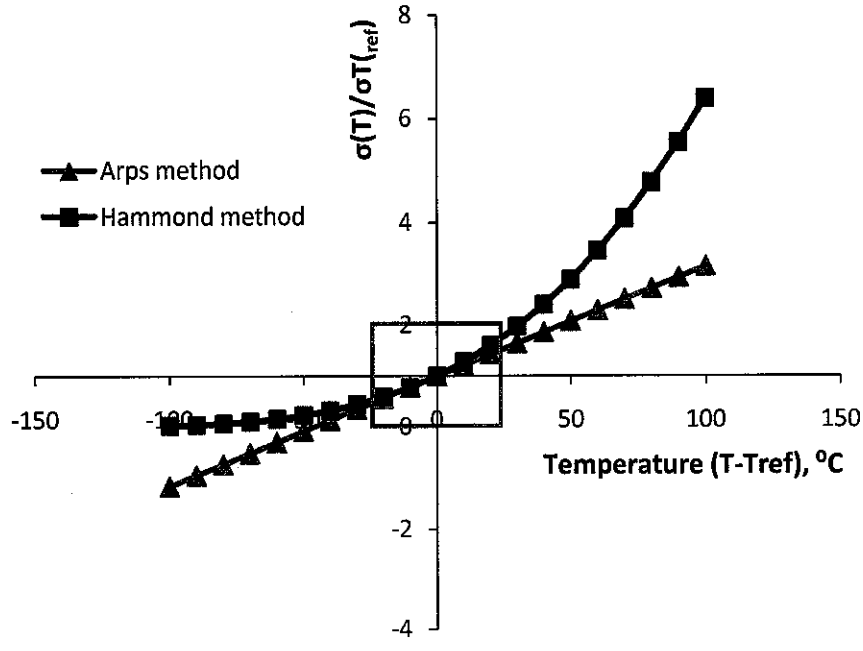

Figure 4.17 Comparison of conductivity variation with temperature change calculated by the Hammond and Arps equations.

Figure 4.18 presents the typical profile of the bulk conductivity at the elevated temperature and pressure of w/c 0.5 (refer to Appendix D for details). Bulk conductivity decreased as temperature and pressure increased mainly due to the acceleration of hydration process - in particular within 10 hrs of hydration. In this

period, pre-induction, induction and acceleration periods occurred with the free ions within a considerably very active pore solution.

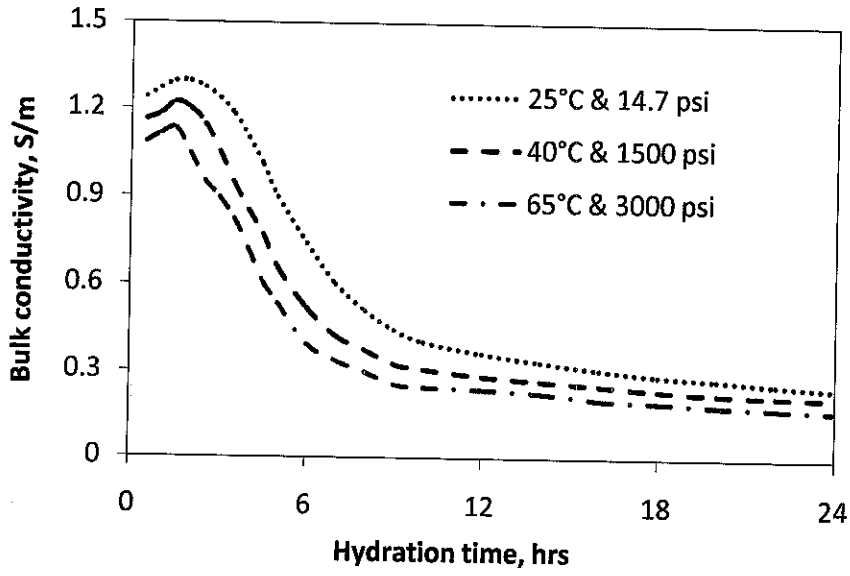

Figure 4.18 Conductivity profile after temperature correction at w/c 0.5

Due to these influence on hydration process, it indicates that different conductivity responses may be generated at similar hydration periods for sample cured at different curing temperature and pressure. Meanwhile, the effect of elevated pressure on electrical conductivity was less significant compared to that of elevated temperature as shown in Figure 4.19. For a given 10 hrs of hydration, the conductivity from 14.7 to 3000 psi was shifted about 0.0375 S/m compared to that of about 0.1357 S/m for conductivity from 25 to 65°C. It was because the pressure has small contribution for cement to accelerate hydration process. Appendix E gave the plot of individual contribution of elevated temperature and elevated pressure on bulk conductivity measurement.

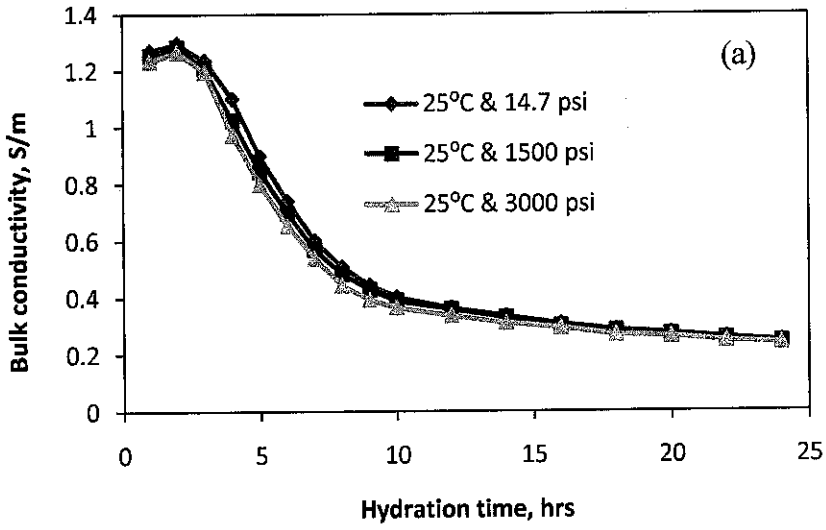

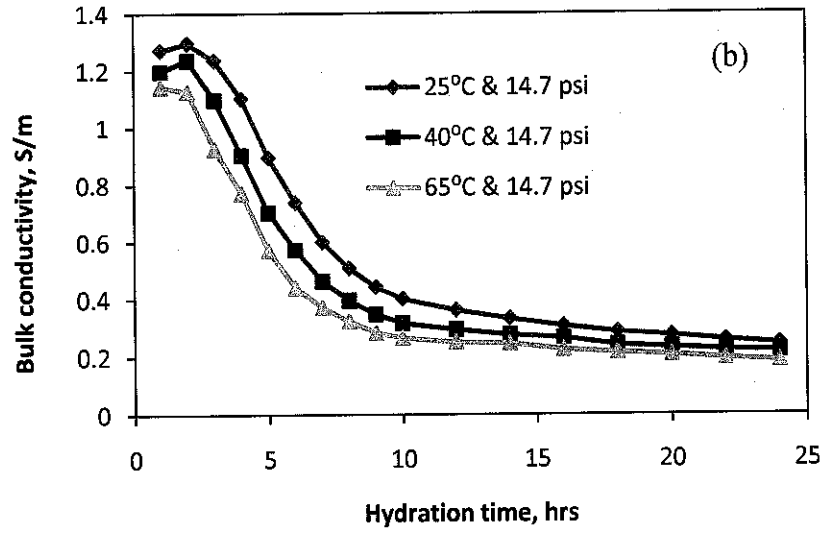

Figure 4.19 Effect of (a) varying pressure and constant temperature and (b) varying temperature and constant pressure on electrical conductivity measurement at oilwell cement of w/c 0.5

4.2.3 Effect of Water Cement Ratios on Electrical Conductivity

The effect of water cement ratio tended to increase the values of bulk conductivity linearly as shown Figure 4.20. It was suggested that the contribution of water cement ratio on electrical conductivity rose simultaneously as hydration degree continued to proceed. In the very early hydration of about 2 hrs, the conductivity values were less affected at varying w/c. In fact, conductivity drops significantly during very early hydration irrespective of water cement ratio. As hydration continues to proceed; the contribution of varying w/c increases accordingly as can be seen in Figure 4.21.

As can be seen in Figure 4.21, the conductivity profile as an effect of w/c was the other way around compared to the effect of different curing temperature and pressure at which the former case the conductivity has greater difference at very early hydration. This is true because during very early hydration the cement system is still dominated by the pore solution and as a result the bulk conductivity readings were less variation at different w/c. In contrast once elevated temperature and pressure were imposed, the hydration was accelerated and pore solution consumed which bring the conductivity to be varied at different pressure and temperature. Approximately after 6 hrs of hydration the different in conductivity between the w/c 0.4 and 0.3 was far greater that the difference in conductivity between the w/c 0.5 and 0.4 at elevated pressure and temperature. The rate of decrease after 6 hrs of hydration at elevated pressure and temperature decreases from w/c 0.5 to 0.4 to 0.3, and was virtually negligible for the w/c 0.5 to 0.4.

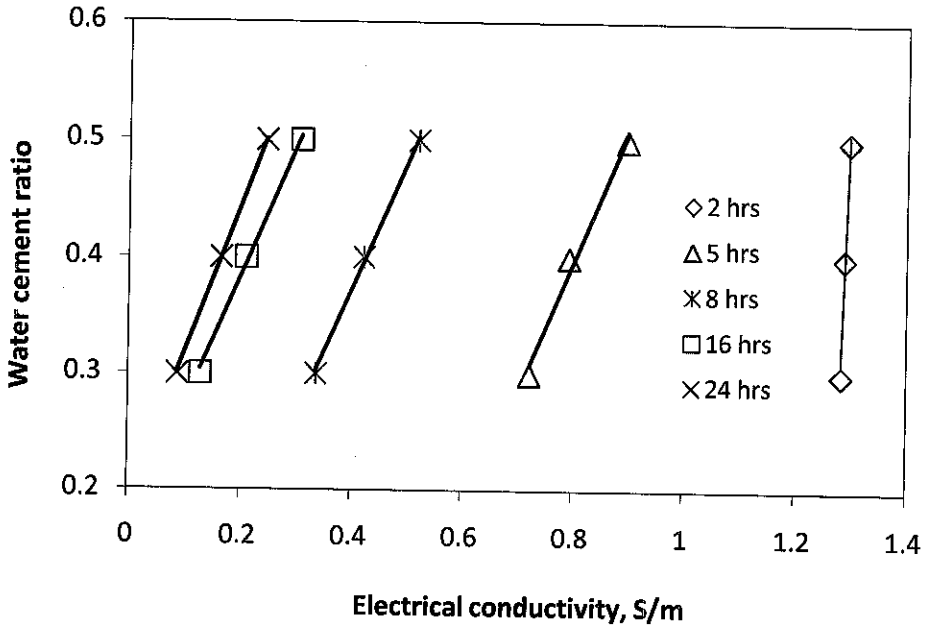

Figure 4.20 Relationship between water cement ratios and bulk conductivity at early stages of hydration

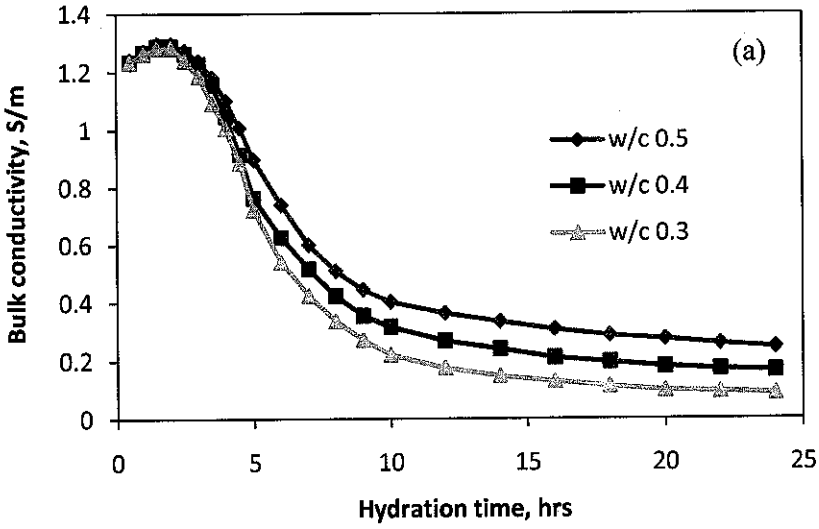

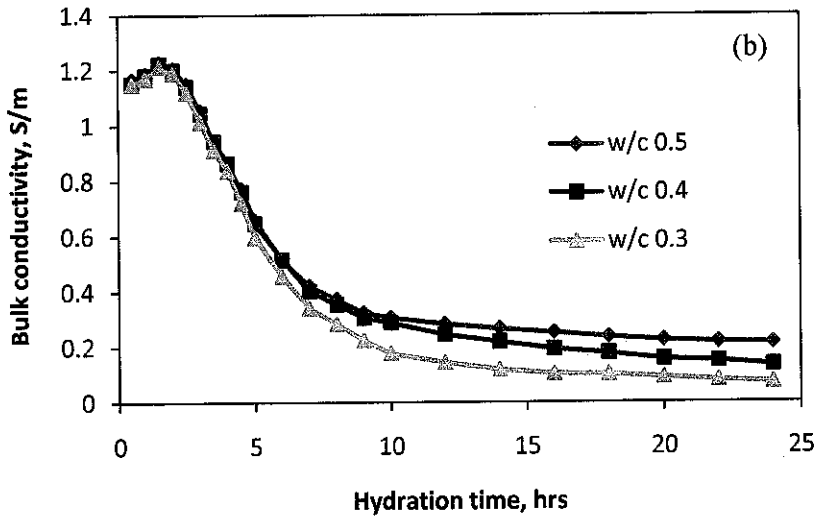

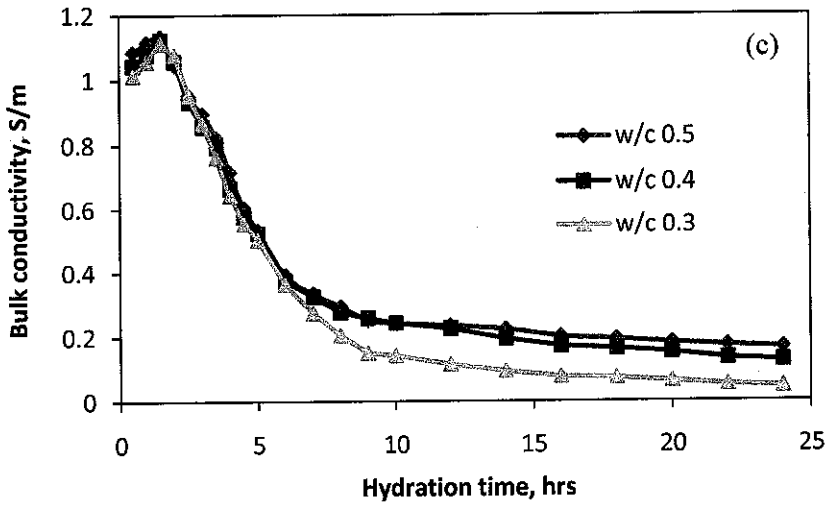

Figure 4.21 Effect of different w/c on conductivity measurement at (a) 25°C & 14.7 psi, (b) 40°C & 1500 psi and (c) 65°C & 3000 psi

Since the electrical conductivity relates to water cement ratio content, the electrical responses can be used to determine the water cement ratio at fluid state until hardened state. In this conduction, a normalized conductivity (discussed in section 4.2.4) with its dimensionless unit was plotted with water cement ratio as shown in Figure 4.22. This relationship is given by the following form of equation, $y = Ax \pm B$, which was then might be used to calculate the water cement ratio at certain hydration time for a given cement samples. The difference of the equations at different hydration time was increased with time for varied water cement ratios. The water cement ratio can be determined at very early hydration and it gives the right perspective with accuracy and rapid evaluation, though they seem to be unique according to the sample composition, curing period, and sample treatment.

At hydration time (t) = 2 hrs, $R^2 = 0.98$

$$\frac{w}{c} = 2.733\sigma_{n(2)} - 0.274$$

At hydration time (t) = 5 hrs, $R^2 = 0.97$

$$\frac{w}{c} = 3.736\sigma_{n(5)} + 0.073$$

At hydration time (t) = 8 hrs, $R^2 = 0.998$

$$\frac{w}{c} = 6.316\sigma_{n(8)} + 0.126$$

At hydration time (t) = 16 hrs, $R^2 = 0.986$

$$\frac{w}{c} = 10.26\sigma_{n(16)} + 0.210$$

At hydration time (t) = 24 hrs, $R^2 = 0.994$

$$\frac{w}{c} = 13.64\sigma_{n(24)} + 0.228$$

where σ_n is normalized conductivity and R^2 is the coefficient of determination.

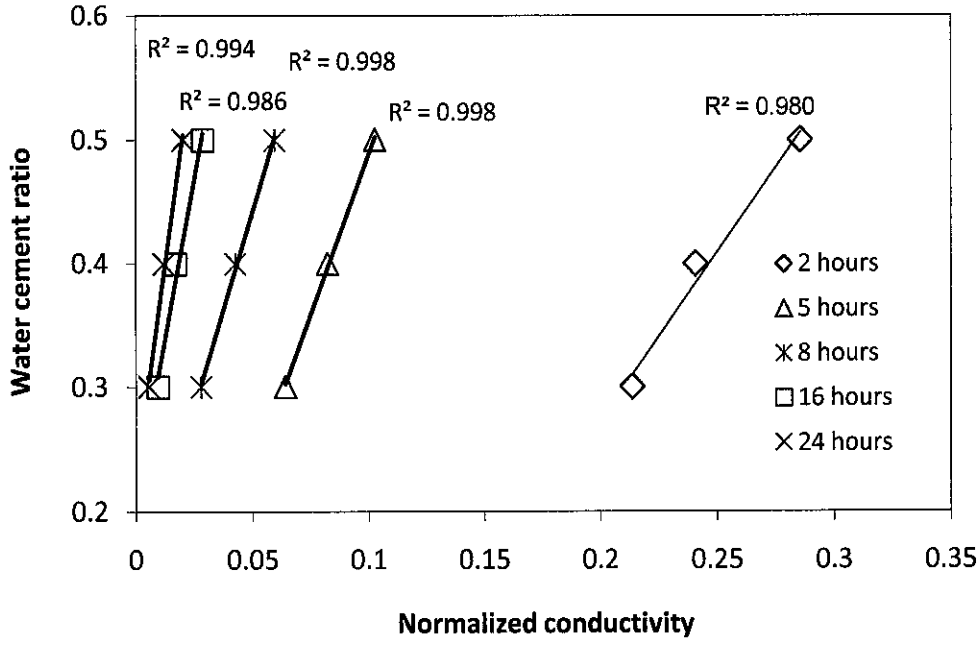

Figure 4.22 Relationship between water cement ratios and normalized conductivity at early stages of hydration

4.2.4 Normalized Conductivity

Since the bulk conductivity (σ_b) decreases and pore solution conductivity (σ_o) inversely increases with hydration time, it was deemed important to apply a normalized conductivity for better describing a physical phenomenon within the electrical responses. Normalized conductivity is defined as a comparison between bulk conductivity and pore solution conductivity (σ_b/σ_o) and is also often referred as the inverse of the material's "formation factor" (F; unit less) [60]:

$$\frac{\sigma_b}{\sigma_o} = \frac{1}{F} \tag{4.13}$$

In reservoir rocks, the formation factor was related to the formation resistivity, lithology and texture, pore solution resistivity, porosity, salinity, density, saturation, cementation, cations-exchange capacity, and clay content. These properties may also be related to the normalized conductivity in the cement system especially during early hydration due to its rapid changed of hydration process.

One of the important points to mention is that the normalization was required when comparing fresh and saltwater slurries because the bulk conductivity of the latter is two to three times higher than that of the former. The profile of the normalized conductivity as a function of hydration at different w/c can be seen in Figure 4.23 showing that cement with low w/c, as expected, exhibits the lowest normalized conductivity owing to a faster hydration process which narrows the inter-connected pore for current pathway.

It also has a similar effect once exposed at the elevated curing temperature and pressure at which the increasing temperature and pressure tended to decrease the values of normalized conductivity (Figure 4.24). However, for a given temperature and pressure, the contribution of w/c from 0.5 to 0.3 had more pronounce in term of its discrepancies. For instance, the gap of normalized conductivity at normal condition between w/c 0.3 and 0.5 is 0.03161, while the discrepancy between 25°C & 14.7 psi and 65°C & 3000 psi for w/c 0.3 is 0.01081 and for w/c 0.5 is 0.0256.

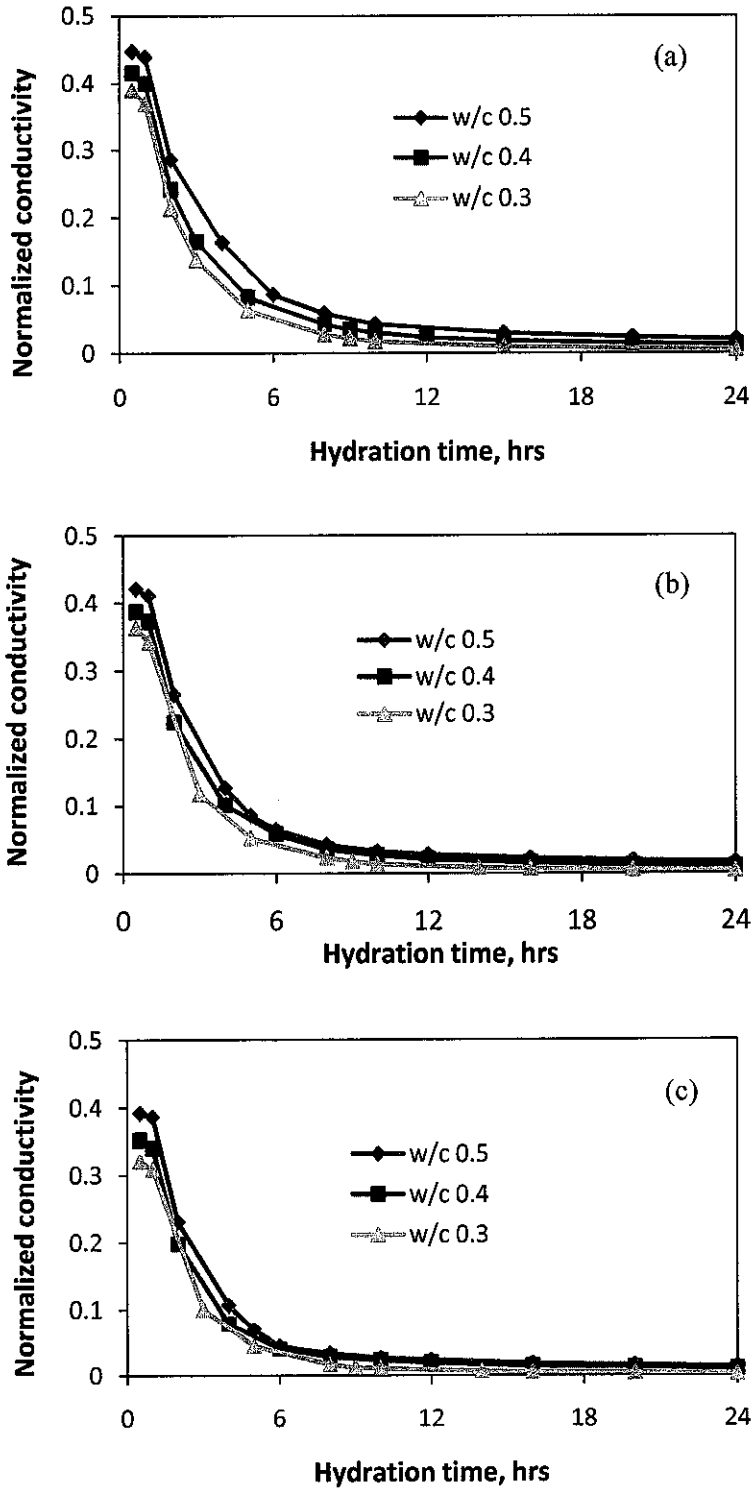

Figure 4.23 Normalized conductivity versus hydration time for different water cement ratios at (a) 25°C & 14.7 psi, (b) 40°C & 1500 psi, and (c) 65°C & 3000 psi

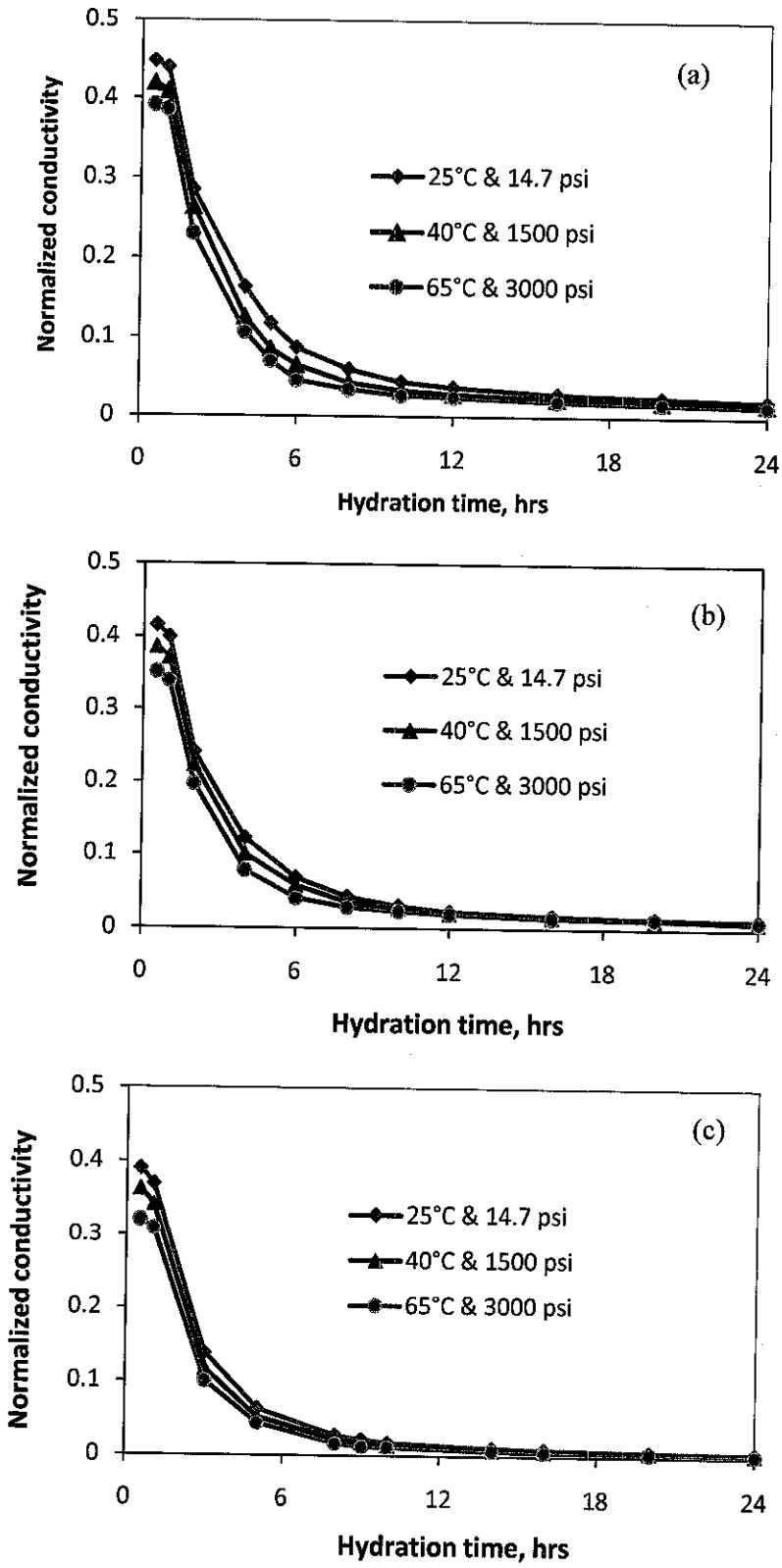

Figure 4.24 Normalized conductivity versus hydration time at different temperature and pressure for (a) w/c 0.5, (b) w/c 0.4, and (c) w/c 0.3

4.2.5 Evaluation of Electrical Conductivity Model

For the purposes of applying conductivity models, the Class G cement was approximated as two phase components; cements and pore solution conductivity at which the latter was considered to be electrically conductive. A comparison was made between an experimental measurement and models that described the material's normalized conductivity based on the porosity information and microstructural parameter for some models. Porosity values were generated from MIP measurements. Results of normalized conductivity versus porosity at atmospheric conditions for different w/c are shown in Figure 4.25a and the complete data of measured porosity are presented in Table 4.4.

Most of models tended to excessively predict the normalized conductivity except for Archie, Modified parallel and Self-consistency model which were intersectional to the experimental measurement at higher porosity of above 0.57. Parallel, Hashin-Shtrikman upper-bound (HS_{ub}), Maxwell and Differential Effective Medium (DEM) model seemed to have a poor prediction result. The first two models did not consider the contribution of microstructural parameter and only relied on porosity numbers. Furthermore, HS_{ub} model has been developed for the macroscopically isotropic materials and was not directly applicable for a layered composites material. Although DEM and Maxwell model included d parameter, but their use was not appropriate for materials in which the inclusions formed large clusters as suggested by Torquato [39].

It was observed that only Archie's, modified parallel, and self consistency models could provide a qualitative prediction of electrical conductivity behavior. In fact, as the cement hydrated, the connectivity became narrower and more tortuous resulting in a microstructural parameter change at age. Accounting for these changes, a fitting procedure was performed on the models to the experimental measurements of electrical conductivity both at atmospheric condition (Figure 4.26) and at elevated temperature and pressure (Figure 4.27). It was expected that as hydration continued to proceed; a monotonic increase or decrease of the liquid phase distribution parameters (β, m, or d) would be exhibited.

A similar appearance was also observed for Archie, modified parallel and self consistency at elevated pressure and temperature, but a rapid change occurred in porosity during the first 3 hrs as an effect of hydration acceleration (Figure 4.25b).

This corresponded to the time of initial set where the cement changed from a fluid suspension to a rigid solid. It was followed by a fairly smooth decrease of normalized conductivity with decreasing porosity.

Among these equations only self consistency that was not able to physically represent the microstructure distribution as it did not change consistently. Furthermore, of the simple models, these were only Archie's and modified parallel law that included a variable term describing the connectivity of the conducting phase.

In the meantime, only the cementation factor in Archies law had a physical meaning and a theoretical foundation since it could be derived by applying a continuum percolation theory to fractal porous media [81]. Glover [50] suggested the following formulation to describe a very reasonable physical meaning for the cementation factor.

$$m = \frac{d}{d\chi}\left(\frac{dG}{d\phi}\right) \tag{4.14}$$

where $d/d\chi$ is the rate of change of the connectivity, dG is rate of change of connectedness (normalized conductivity), and $d\phi$ is rate of change of porosity.

The cementation factor (m) was supposed to increase along with hydration process considering the pore structure that became rigid and tortuous. However, the downturn of m values starting at porosity of about 0.48 was suspected due to the used of capillary porosity instead of total porosity which included the gel porosity. The capillary porosity represents the volume of the capillary pores (> 0.03 μm) and it depends mainly on both cement-water ratio of the mix and the degree of hydration. The gel porosity represents the gel pores (< 0.03 μm) [82]. As hydration progresses, the amount and distribution of porosity between capillary and gel pores will change. Initially all the pores are capillary pores. As hydration precedes the capillary pore volume is reduced because the capillary space becomes filled with hydration products, and the gel porosity increases.

Results of other researchers, on the other hand, have shown that the downturn of m values started at porosity of about 0.35 [4] and 0.25 [34] once total porosity were applied. Capillary porosity might underestimate the total porosity especially at the later stages of hydration at which gel porosity has been developed. However, the use

of total porosity might cause both capillary and gel porosity lumped together and, thus, values of *m* were measured of the characteristics of both scales of porosity.

In supporting the physical meaning with its changing of connectivity, porosity and connectedness, the experimental results between normalized conductivity and porosity, as shown in Figure 4.25, showed a correspondence to Archie's model in the form of power law equation. The complete profiles of conductivity responses to porosity for various composite models applied to Class G cement system at different w/c and curing conditions are provided in Appendix F.

Table 4.4 Measured porosity of Class G cement at various w/c and curing conditions

Temperature and Pressure	**Hydration time (hrs)**	**Porosity (w/c = 0.5)**	**Porosity (w/c = 0.4)**	**Porosity (w/c = 0.3)**
25°C & 14.7 psi	5	0.592	0.565	0.468
	10	0.556	0.514	0.416
	16	0.485	0.437	0.363
	24	0.455	0.401	0.321
40°C & 1500 psi	5	0.579	0.545	0.442
	10	0.507	0.472	0.383
	16	0.432	0.422	0.331
	24	0.412	0.372	0.291
65°C & 3000 psi	5	0.562	0.532	0.424
	10	0.481	0.452	0.365
	16	0.412	0.383	0.322
	24	0.377	0.334	0.272

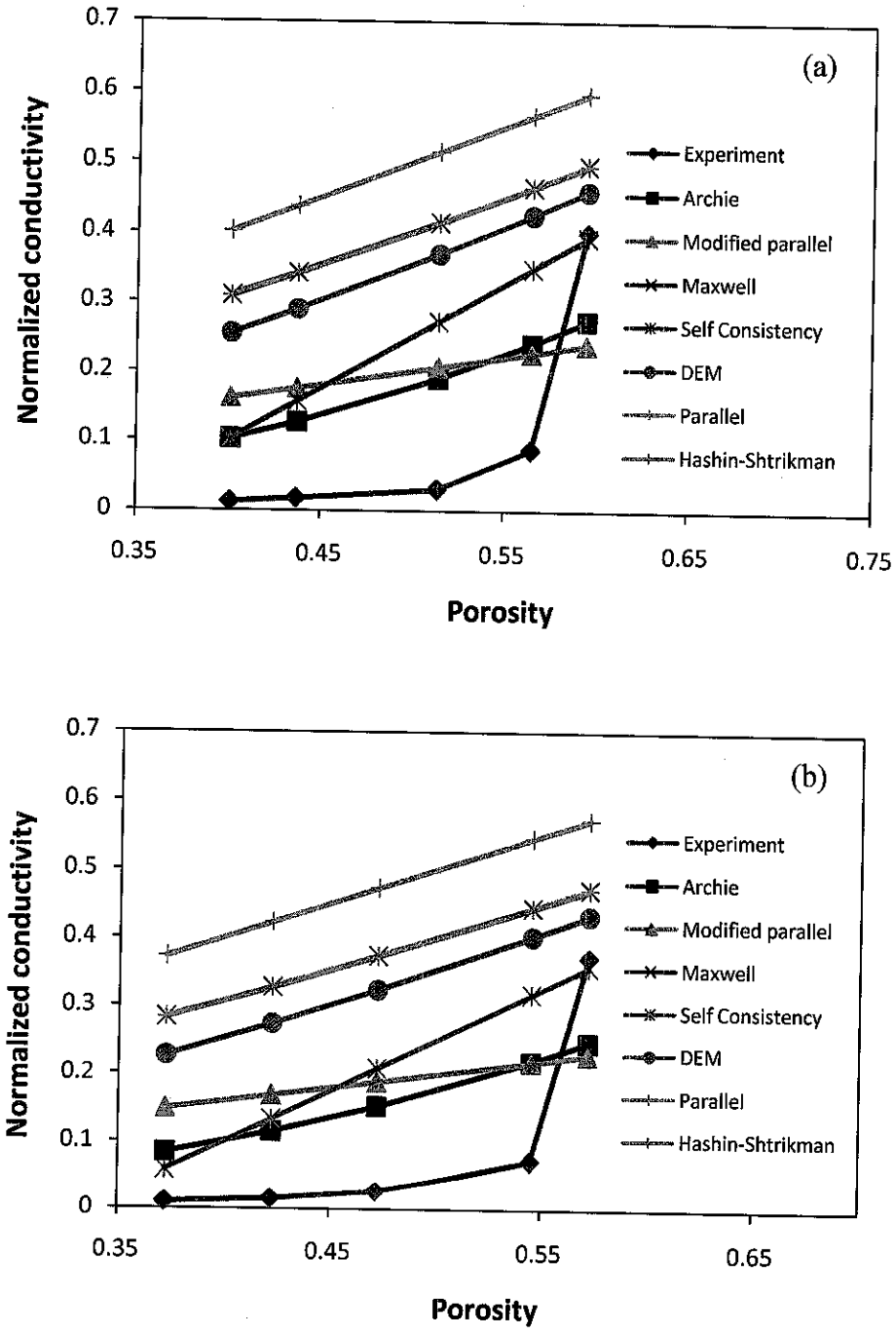

Figure 4.25 Typical result of normalized conductivity versus porosity for class G cement of w/c 0.4 at (a) 25°C & 14.7 psi and (b) 65°C & 3000 psi showing comparisons with prediction from various conductivity models

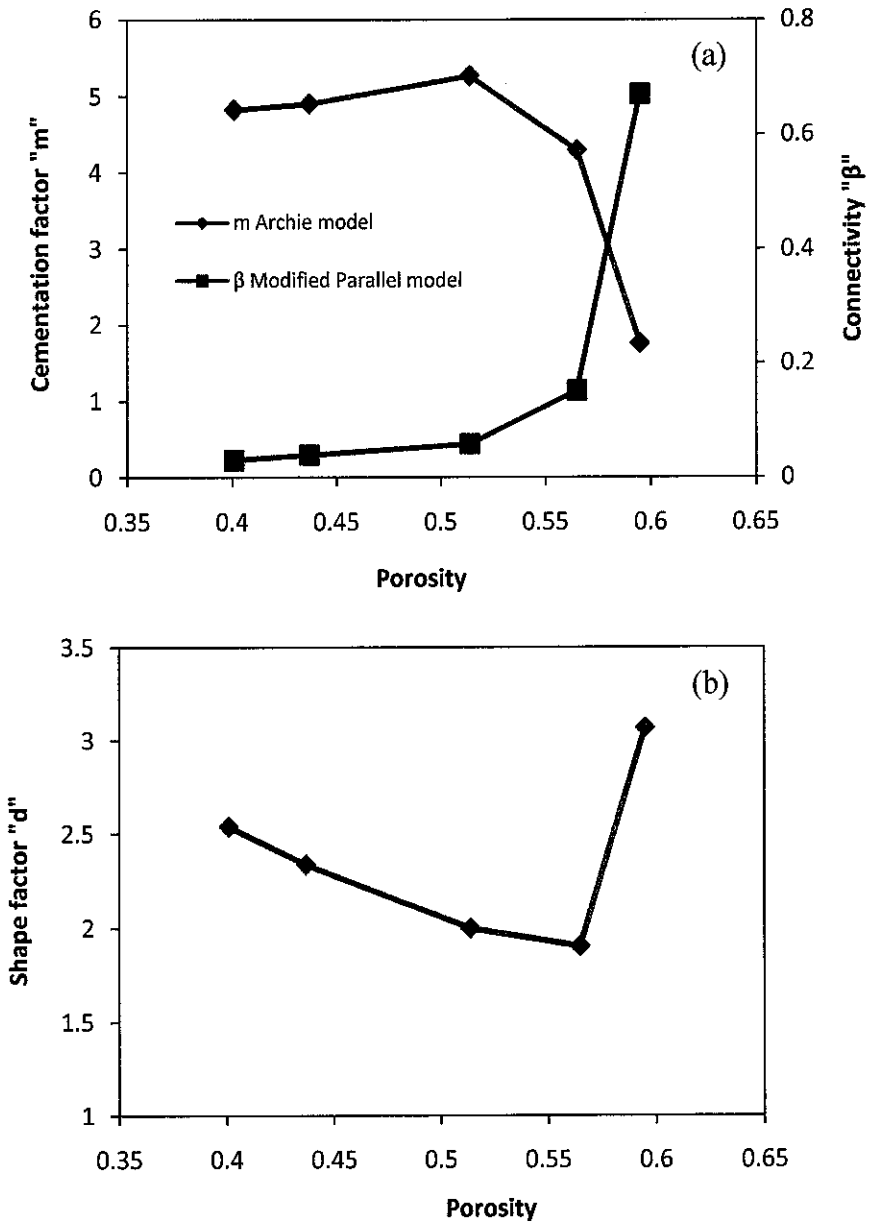

Figure 4.26 Typical result of microsructure parameters distribution from fitting procedure between conductivity models and experimental measurements for Class G cement of w/c 0.4 at atmospheric condition; (a) Archie's law and modified parallel, (b) self consistency model

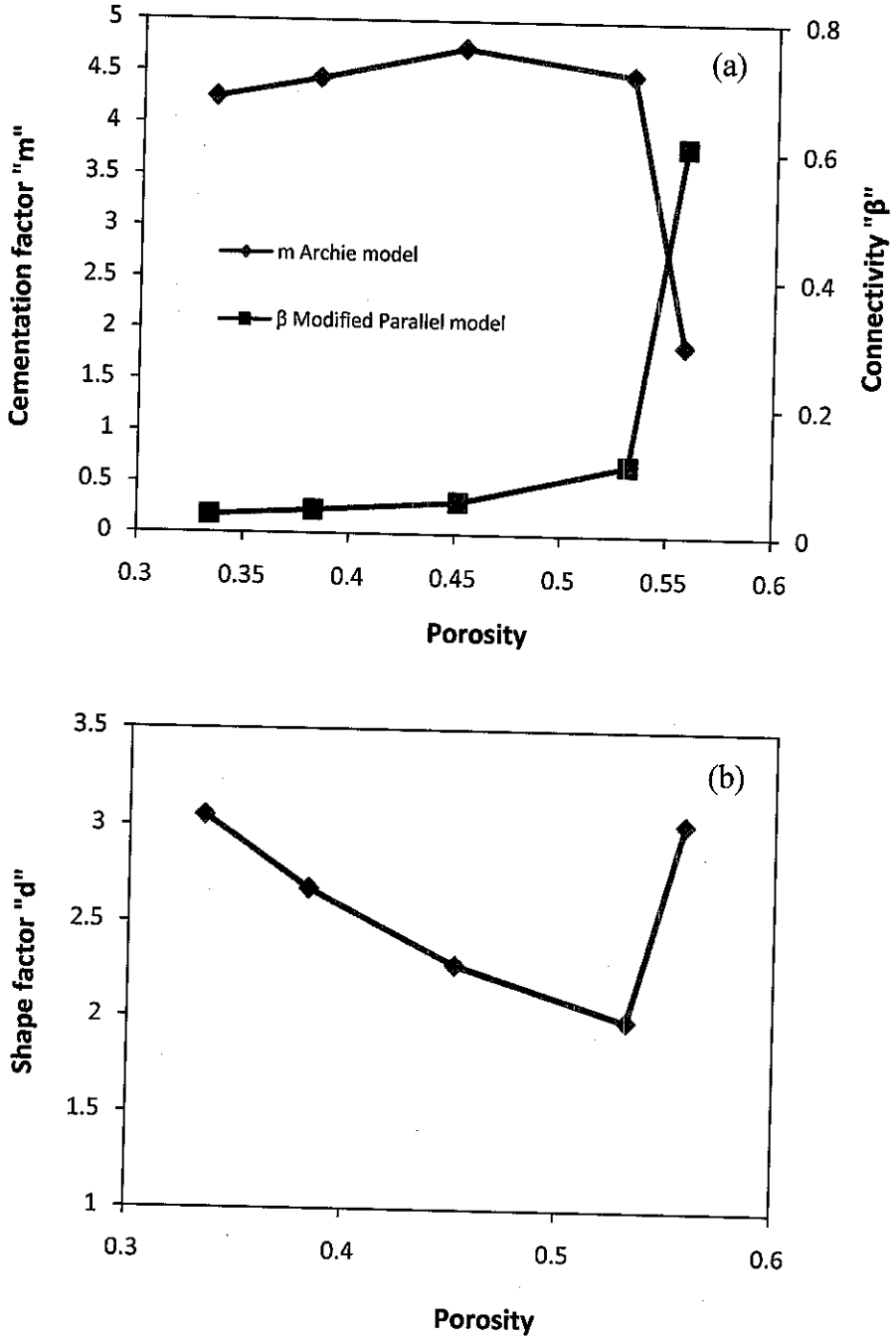

Figure 4.27 Typical result of microsructure parameters distribution from fitting procedure between conductivity models and experimental measurements for Class G cement of w/c 0.4 at 65°C & 3000 psi; (a) Archie's law and modified parallel, (b) self consistency model

4.2.6 Summary

It is found that the contribution of water cement ratio from 0.5, 0.4 and 0.3 on conductivity responses was bigger than that of curing temperature and pressure between 25°C & 14.7 psi and 65°C & 3000 psi. A direct effect of elevated temperature on electrical conductivity measurement was corrected using Hammond method. The relationship of electrical conductivity and w/c followed a linear trend and then prediction equation for w/c might be generated at specific hydration period for cement before and after being hardened.

The relationship between normalized conductivity and porosity of Class G cement under elevated conditions, furthermore, followed the power laws in the form of Archie's law. Although the modified parallel model and self consistency model were able to provide a qualitative prediction of electrical conductivity behavior, these models might not physically represent the cement hydration phenomenon. The cementation exponent in Archie's law was shown to reflect the changing in cement's connected pores. This might be used to predict porosity of well cement *in-situ* with electrical properties as the only one information needed. For the future study, it is recommended to evaluate these models for cement samples that contain additives.

4.3 Permeability and Strength Correlation to Electrical Properties

The applicability of some composite models on Class G cement has previously been discussed. The model proposed by Archie's represented the measured data obtained in this study and indicated that the Archie's equation could be used to predict or to monitor the values of porosity of well cement in-placed by means of its normalized conductivity. However, for oilfield use, permeability and strength are more important than porosity in term of wellbore durability. The strength is deemed important because a certain minimum strength is required before drilling operation can be resumed. Conversely, a poor controlling permeability may cause formation fluids, either gas or water that migrate to the surface.

In this section, the electrical responses of cement system were used to develop a set of correlations for permeability and strength prediction as a function of hydration time. At this, the influence of water cement ratios and elevated temperature and

pressure were taken into account. The contribution of some microstructure properties such as porosity and pore diameter were discussed as well. The result finally was compared to other cement samples and data from literatures for the validation of this study.

4.3.1 Permeability and Electrical Properties Relationship

The measured permeability for all samples at some specific curing conditions was presented in Table 4.5. It can be seen that permeability decreases as hydration proceeds. Once the elevated curing temperature and pressure were applied, a rapid decrease of permeability is observed by comparing it at normal condition for similar hydration periods and water cement ratio. This is done due to the accelerated hydration experienced by the cement mixture as temperature increases, and at the same time the pore size is reduced due to the applied elevated pressure. However, the elevated pressure may affect the change of hydration rate, but not altering the hydration of the product. A similar trend of permeability reduction is also observed when water to cement ratio decreases; this was because of the limited pore connection generated in the mixtures with small w/c ratio.

The results of measured permeability data were found to be relatively comparable to the outcome of typical Class G cement during transition period with larger values as generated in this study, that is about an order of magnitude compared to that of in literature [83]. This was possibly due to the effect of oven-drying treatment that altered the pore structure of cement samples contributing to the increase of inter-connecting pores.

The comparisons of permeability to normalized conductivity of individual curing sample in addition have provided a reasonable agreement. Some typical results can be seen in Figure 4.28. In this case, all samples followed power law model with the least square error (R^2) of approximately 0.952. A similar performance was also observed for a variety of porous materials [39]. However, as the physical properties of cement were changing over time, its conductivity responses in the form of normalization might be used for monitoring any changes in permeability during cement hydration as a function of time.

Table 4.5 Measured permeability of Class G cement at various curing conditions

Temperature and Pressure	Hydration time (hrs)	Permeability, μm^2 (w/c=0.5)	Permeability, μm^2 (w/c=0.4)	Permeability, μm^2 (w/c=0.3)
	5	0.06356	0.03474	0.01155
25°C & 14.7	10	0.02297	0.01074	0.0026
psi	16	0.0076	0.0022	0.00041
	24	0.00314	0.00097	0.00018
	5	0.0407	0.0251	0.00918
40°C & 1500	10	0.0149	0.0071	0.00188
psi	16	0.0057	0.00143	0.00033
	24	0.0028	0.0007	0.00007
	5	0.02319	0.01494	0.0057
65°C & 30000	10	0.00693	0.00337	0.0013
psi	16	0.00154	0.00128	0.00009
	24	0.00096	0.0002	0.00002

Since the aim was to generate a representative single correlation based on these data, all the permeability data were then plotted on the same graph. The resulting plot tended to be identical with the individual plot in the form of power law as presented in Figure 4.29a. The least square error (R^2) showed a number of about 0.909. The correlation obtained from the regression analysis has the following form of Equation (4.15).

$$k = 11.06\left(\frac{\sigma_b}{\sigma_o}\right)^{2.16} \tag{4.15}$$

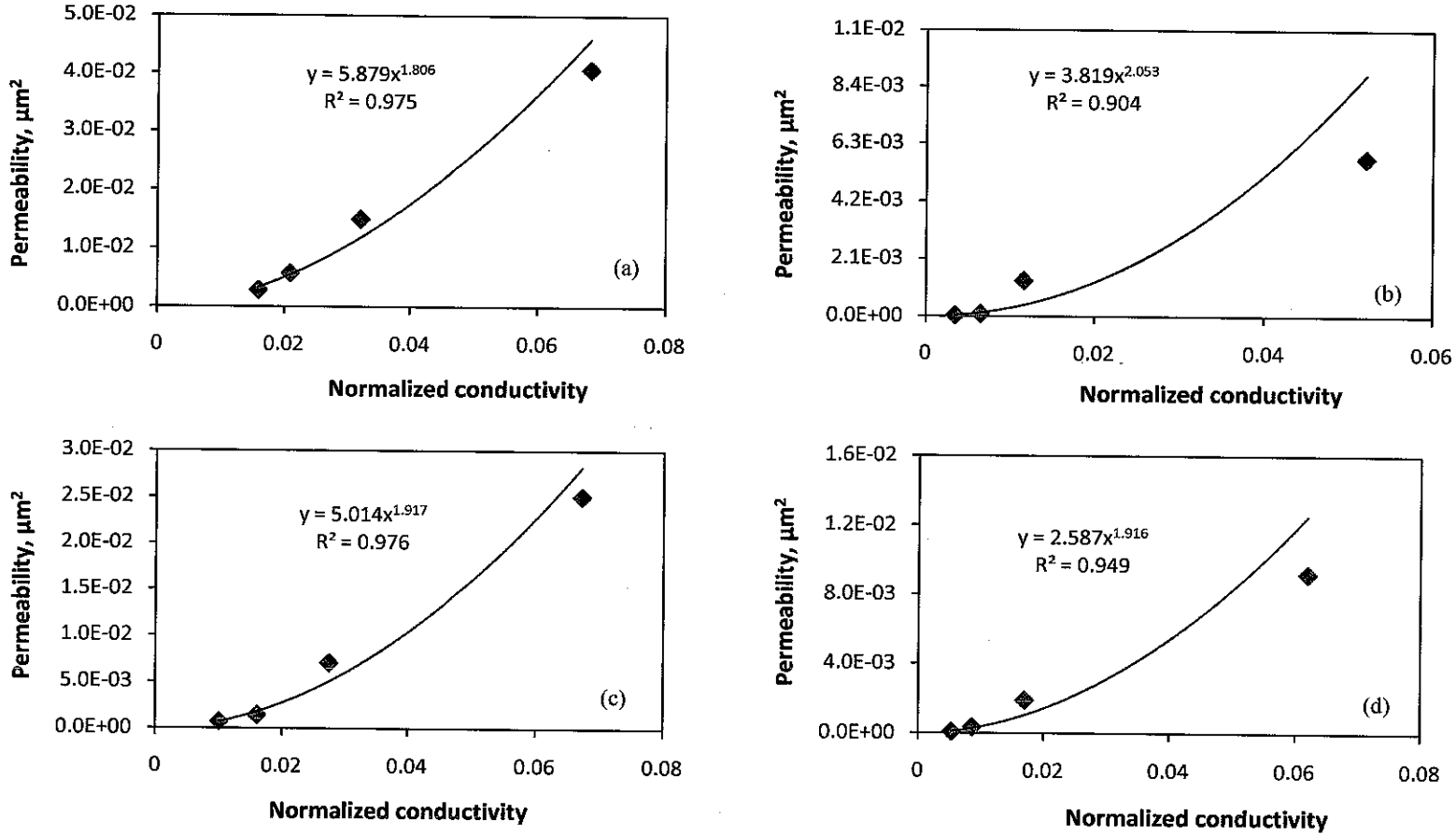

Figure 4.28 Relationship of measured permeability and normalized conductivity (a) w/c 0.5 at 40°C & 1500 psi, (b) w/c 0.3 at 65°C & 3000 psi, (c) w/c 0.4 at 40°C & 1500 psi, and (d) w/c 0.3 40°C & 1500 psi

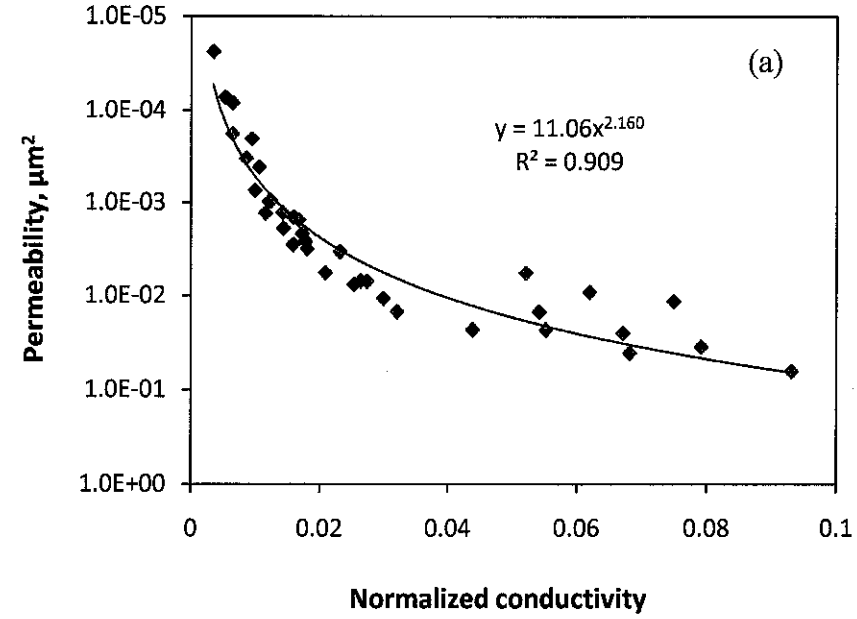

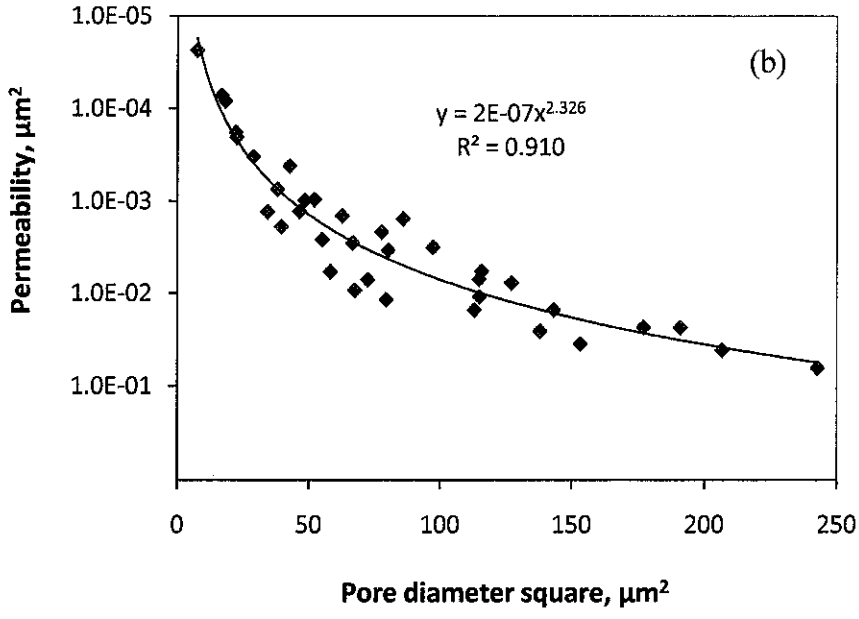

Figure 4.29 Relationship of (a) measured permeability and normalized conductivity, and (b) measured permeability and pore diameter

It has been suggested that the microstructural parameter in the form of characteristic length was sensitive to the permeability profile. The permeability depended mainly on the connected pores and pore length scale at which the former represented normalized conductivity, and the latter corresponded to characteristic length. The length scale could be generated from Mercury Intrusion Porosimetry (MIP) experiment that corresponded to the pore diameter at the inflection point on a

cumulative volume versus pressure diagram [63]. However, in this study the pore length of cement sample was calculated using a simple particle expansion model which is easy, fast and comparably accurate [84]. This model simulated cement as a regular cubic lattice in the form of a spherical particle that had the same radius and growth, and then the pore size was estimated to be a diameter of the pore between the edge to edge distances (see Section 4.1.3.1). The resulting relationship between normalized conductivity and pore length scale using regression analysis complied to power law with the least square error (R^2) of about 0.910 as can be seen in Figure 4.29b with the following correlation (Equation 4.16):

$$k = 2 * 10^{-7}(d_c^2)^{2.326} \tag{4.16}$$

4.3.2 Empirical Equation for Permeability Prediction

To have a comprehensive correlation for permeability prediction that represented the pore diameter and normalized conductivity, a multiple non-linear regression analysis was performed by nominating permeability as the independent variable, whilst normalized conductivity and pore diameter as the dependent variable. A non-linear plot was shown in Figure 4.30 and the following Equation (4.17) was obtained after the regression analysis:

$$k = \frac{1}{828}(\sigma_b/\sigma_0)^{1.15}(d_c^2)^{1.25} \tag{4.17}$$

The natural log symbols for each axis in Figure 4.30 were meant to provide an ease in calculating a non-linear form by taking the natural log of the data, performing the multiple linear regressions on the logged data, and then transforming the resulting equation into the non-linear form by taking the natural exponential of both sides. The resulting Equation (4.17) is similar to that of proposed by Katz-Thompson equation with different constant values.

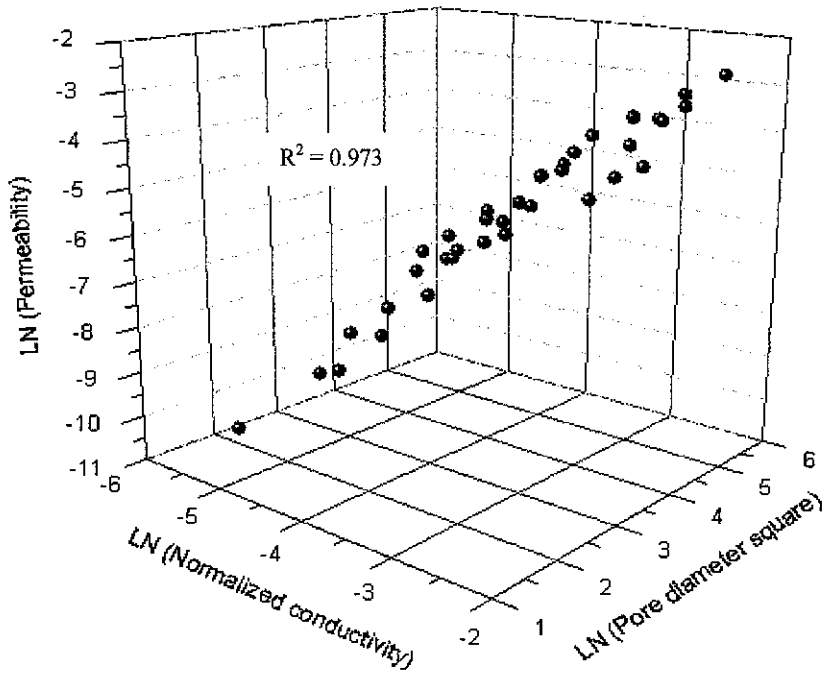

Figure 4.30 Relationship of measured permeability to normalized conductivity and pore diameter square at elevated pressure and temperature

Different from the Katz-Thompson constant that was based on theoretical considerations by assuming local cylindrical pore geometry, the constant values in equation (4.17) were empirically generated to provide the best fit to the experimental data. It was arguable that an oven-drying procedure would alter the pore structure [82] and, therefore, its constant values in the Katz-Thompson equation did not reflect the true value of critical pore diameter. Moreover, the constant values in the Katz-Thompson equation were simulated based on the reservoir rocks at which it relatively has rigid structures, while in the cement system, especially during early hydration, the structures are changed simultaneously as a function of time. As such, its constant values in the Katz-Thompson were less likely to be accurate for cement system.

An interesting result from this regression was that it had a better value of least square error (R^2) of about 0.973 compared to that of single dependent variable. A similar appearance was also observed for other sample conditions with w/c 0.25 at 70°C & 3000 psi and w/c 0.55 at 70°C & 3000 psi. The plot between permeability to normalized conductivity and pore diameter had a least square error (R^2) of about 0.948, higher than those between permeability and normalized conductivity of about 0.894 and between permeability and pore diameter of about 0.874. This may indicate

that a poor permeability result will be generated if only the contribution of normalized conductivity is considered, and vice versa for pore diameter.

4.3.3 Comparison with Different Measured Data

A reasonably good comparison of permeability values between measured and calculated data of new cement conditions with w/c 0.25 at 70°C & 3000 psi and w/c 0.55 at 70°C & 3000 psi was observed as shown in Figure 4.31. The proposed equation (Equation 4.17) has less than 30% level of error which is better compared to that of the Katz-Thompson equation with level of errors more than 75%.

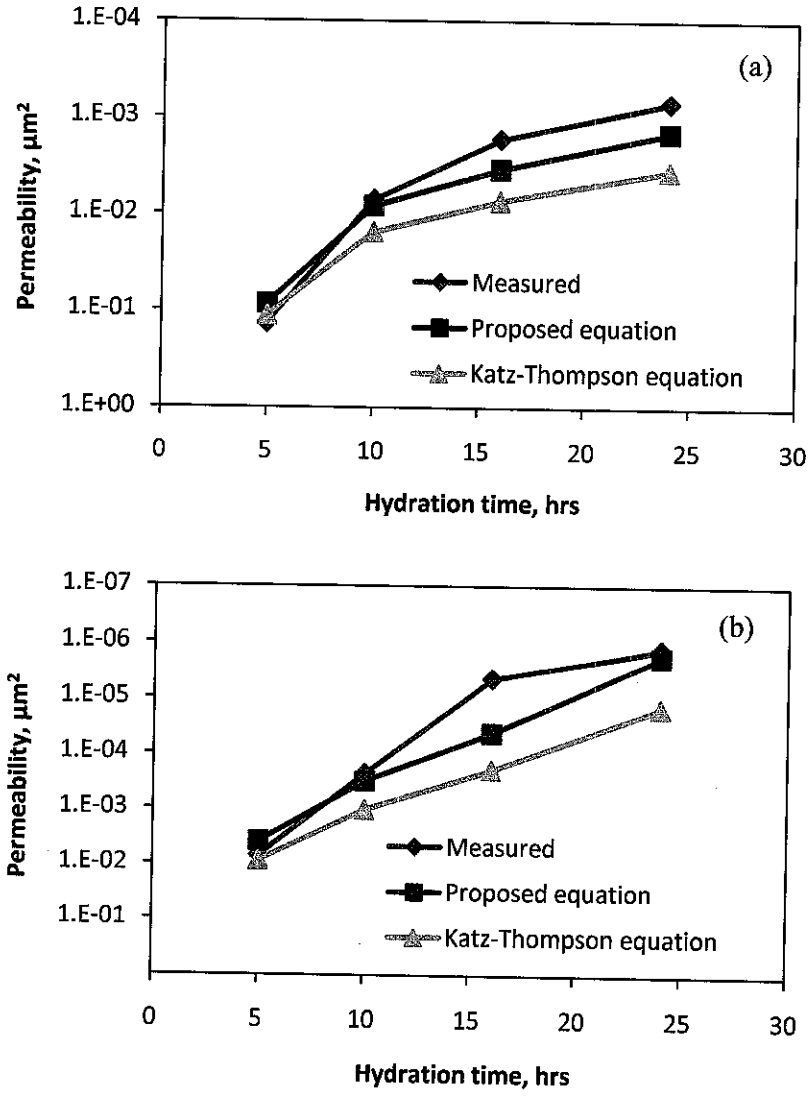

Note: The R^2 of (a) 0.995 and (b) 0.989

Figure 4.31 Comparison of measured permeability to the one calculated from the proposed equation and Katz-Thompson equation on new cement samples (a) w/c 0.55 at 70°C & 3000 psi and (b) w/c 0.25 at 70°C & 3000 psi

Furthermore, although this equation was empirically generated within 24 hrs of hydration period, its applicability can be extended to a longer hydration periods. To confirm this, the measured permeability (k) data of neat cement from Nyame and Illston [85] and impedance measurement (σ_b and σ_o) and pore diameter (d_c) with similar samples treatment from Christensen [64] were used. These data were obtained within 3, 7, 14 and 28 days of hydration time as presented in Table 4.6. Results of the calculated permeability using the proposed Equation (4.17) and the Katz-Thompson can be seen in Figure 4.32. A better agreement between experimental permeability and Equation (4.17) was observed of about below factor 1 discrepancies compared to that of Katz-Thompson equation. The level of error produced from Equation (4.17) was relatively small of about less than 155% compared to that of the Katz-Thompson equation that has more than 720% level of error. However, the general applicability of this approach on cement at mature stages and cement that contained additives should be further studied.

Table 4.6 Measured data of cement obtained from Nyame & Illston [85] and Christensen [64]

w/c	Hydration time (days)	σ_b (S/m) [64]	σ_o (S/m) [64]	d_c (μm) [64]	k (μm2) [85]
0.47	3	0.131	6.58	1	2.55E-05
	7	0.111	5.53	0.38	3.06E-07
	14	0.101	5.01	0.16	4.60E-08
	28	0.0902	4.16	0.078	7.15E-09
0.71	3	0.265	2.19	2.2	1.02E-03
	7	0.198	1.93	0.8	3.17E-05
	14	0.157	1.45	0.3	3.06E-06
	28	0.148	1.71	0.2	2.04E-07

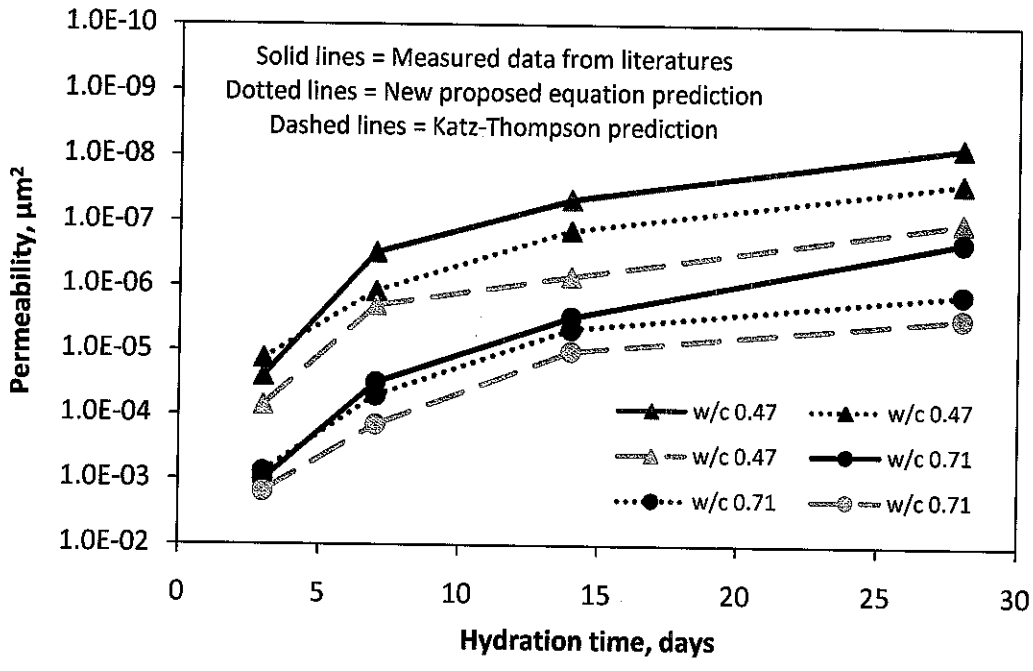

Figure 4.32 Comparison of permeability as a function of hydration time with permeability data obtained from Nyame and Illston [85] and normalized conductivity and pore diameter data obtained from Christensen [64].

4.3.4 Comparison to the Johnson Equation

With the measured normalized conductivity and estimated length scale, Johnson equation was then applied to calculate the permeability of cement system. The length scale was calculated using a simple particle expansion model (see Section 4.1.3.1). The values of Λ was expected to change over time as cement sample was further hydrated. Table 4.7 presents the values of Λ as a function of hydration time and curing condition.

Figure 4.33 in addition provides some results of the comparison among the measured permeability, proposed Equation (4.17), and the calculated one using Johnson equation. The agreement was good anyway; yet in most cases the calculated values underestimated the measured ones by a factor less than one by which its value seemed to increase as cement further hardened. The proposed equation provides better values of predictive permeability compare to that of the Johnson equation. It was due to the assumption used in the length scale calculation that cement particles were treated as spherical grains. In fact, it was not always true and the discrepancies from the measured data were then suspected due to the deviation from sphericity.

Table 4.7 Calculated length scale of cement sample using simple particle expansion model at various w/c and curing conditions

Curing conditions	Time (hrs)	Length scale, Λ (μm)		
		w/c 0.5	w/c 0.4	w/c 0.3
25°C & 14.7 psi	1	2.642	2.113	1.586
	5	2.496	1.952	1.470
	10	2.190	1.652	1.189
	16	1.935	1.418	0.931
	24	1.741	1.250	0.783
40°C & 1500 psi	1	2.640	2.111	1.582
	5	2.41	1.839	1.340
	10	1.998	1.482	1.021
	16	1.672	1.236	0.819
	24	1.514	1.055	0.638
65°C & 3000 psi	1	2.629	2.101	1.573
	5	2.326	1.795	1.253
	10	1.873	1.389	0.937
	16	1.583	1.146	0.694
	24	1.368	0.886	0.482

An interesting point to discuss was the selected constant number of 1/8 in the Johnson model. This constant value was theoretically generated by Johnson *et al.* [55] in a tube-like porous media. Another modeling study performed by Bernabé [86] found that the constant numbers in Johnson's model (Equation 2.19) were varied between 1/8 and 1/12, depending on the porous medium assumption, *i.e.*, tubes, cracks or mixes. It was observed that decreasing number of constant value to 1/12 resulted in a better comparison to the measured permeability data. The modified version was also applicable for various w/c and curing temperature and pressure as shown in Figure 4.34. The improvement of calculated permeability after constant modification was not significant - only less than factor one. However, for samples at lower temperature and pressure, the effect was beneficial that put the calculated and measured permeability relatively closer. Furthermore, still, the proposed equation has better values compared to that of modified version of the Johnson equation.

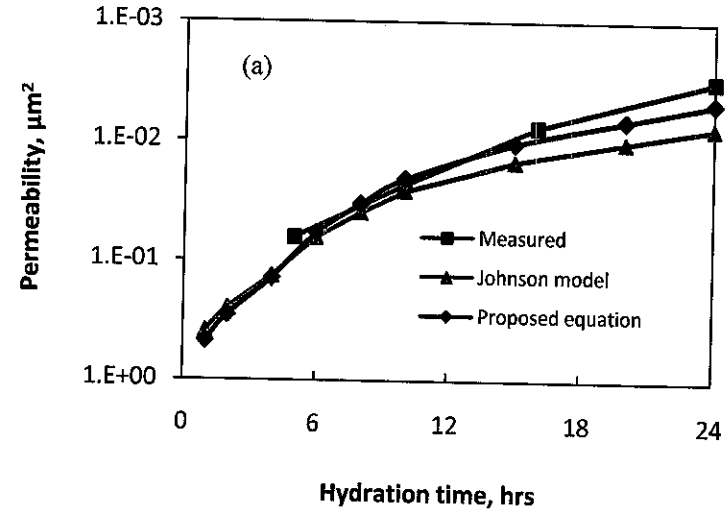

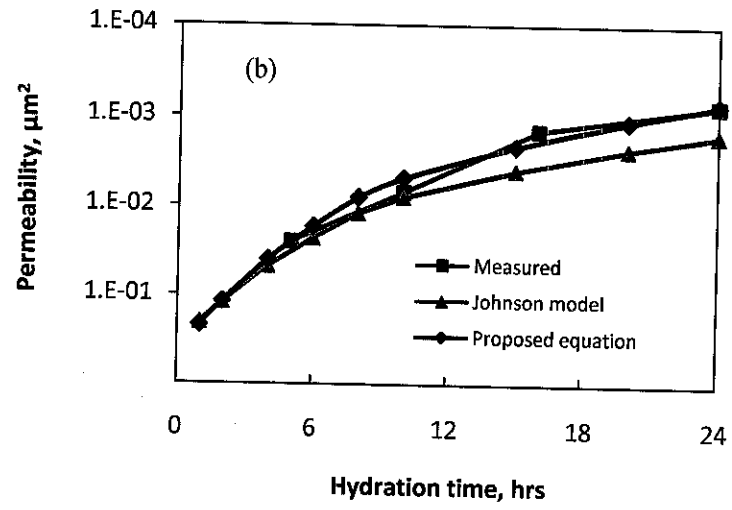

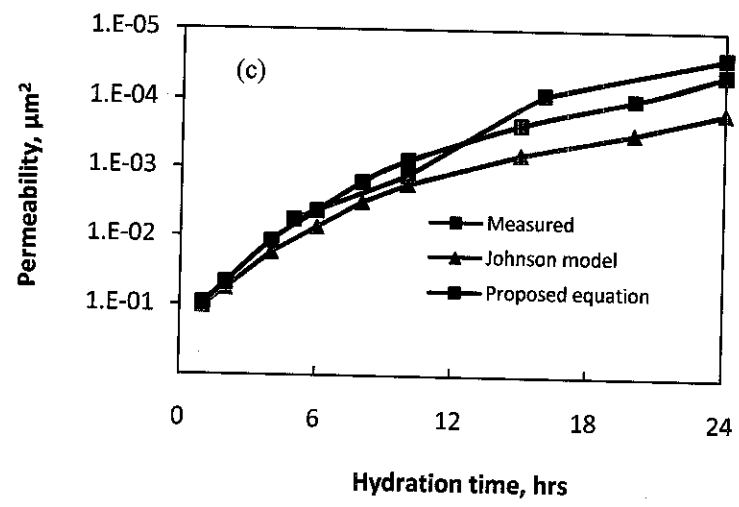

Figure 4.33 Comparison of the Johnson's model and measured data for cement sample with (a) w/c 0.5 at 25°C & 14.7 psi, (b) w/c 0.4 at 40°C & 1500 psi, and (c) w/c 0.3 at 65°C & 3000 psi

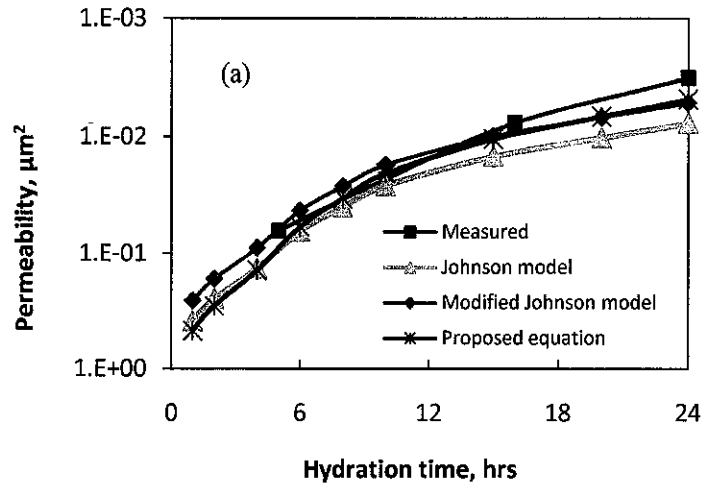

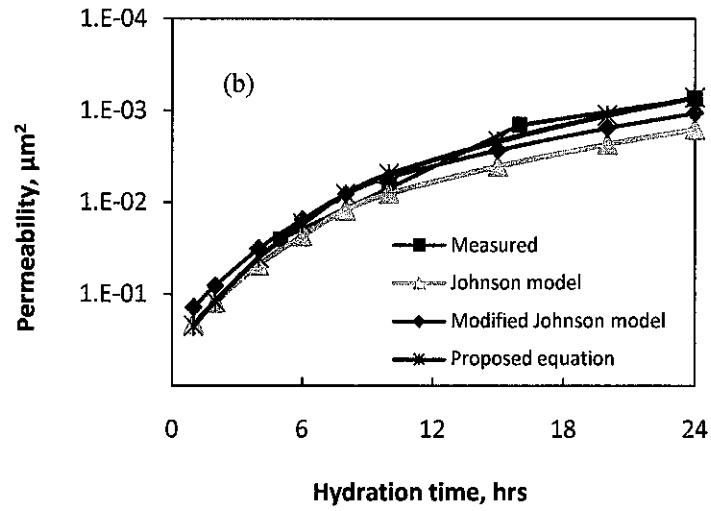

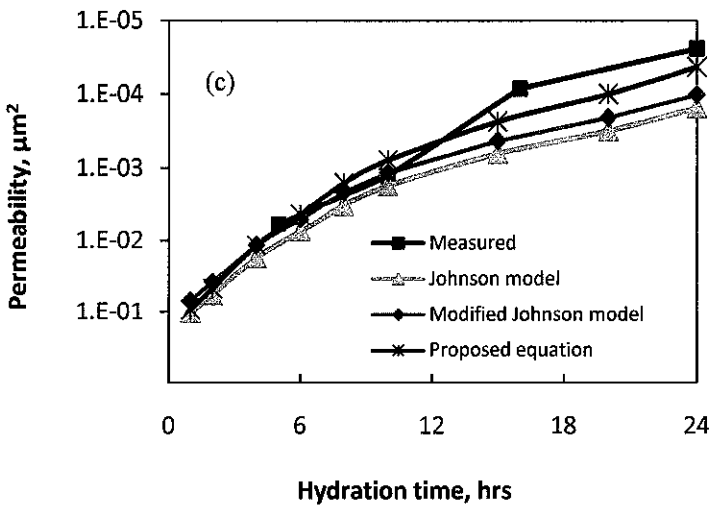

Figure 4.34 Comparison of the Johnson's model, modified Johnson's model, proposed equation, and measured data for cement sample with (a) w/c 0.5 at 25°C & 14.7 psi, (b) w/c 0.4 at 40°C & 1500 psi, and (c) w/c 0.3 at 65°C & 3000 psi

4.3.5 Comparison to the Katz-Thompson Equation

The typical comparison of Katz-Thompson equation and equation (4.17) can be seen in Figure 4.35. For samples at later stages of above 10 hrs of hydration, it was observed that the Katz-Thompson equation gave less accurate results compared to the results given by the new proposed equation. This could be due to much more complicated pore structure found in cement compared to that of porous rocks. In addition, the pore space of cement was subject to change as an effect of curing hydration conditions and oven-drying treatment. By that, these conditions might be improved once it used the empirical constant values in equation (4.17) and, later on, the better prediction of permeability in cement system can be obtained.

Figure 4.36 presents a very similar comparison between models proposed by Johnson and Katz-Thompson (complete comparisons were presented in Appendix G). This came to be interesting since the Katz-Thompson model was derived from very different physics compared to that in Johnson model. From this finding, it may be implied that value of $\Lambda \approx d_c$; in other words, Λ was a good estimator of the pore throat radius of a porous medium. Furthermore, a very similar result from these two models could be explained due to the manner in which fluid that flowed through individual pores at a local scale passed from the viscous flow to the inertial one. This phenomenon may be linked to the frequency behavior of hydraulic flow and streaming potential caused by the viscous-inertial transition as described by Walker *et al.*[87].

It is found out that the characteristic length of Johnson model, as can be seen in Figure 4.37, was relatively less affected by curing temperature and pressure as well as w/c. At this point, the contribution of curing temperature and pressure of 65°C & 3000 psi at 24 hrs on d_c was about 2.4 μm, while contribution on Λ was only 0.4 μm. A similar contribution also occurred for w/c from 0.3 to 0.5 at 24 hrs by which contribution on d_c was about 5.2 μm and on Λ was only 0.87 μm. It was probably due to Λ value was not physically observable length and relatively independent upon curing conditions and w/c. By that, both length scales might not be very identical in term of its values.

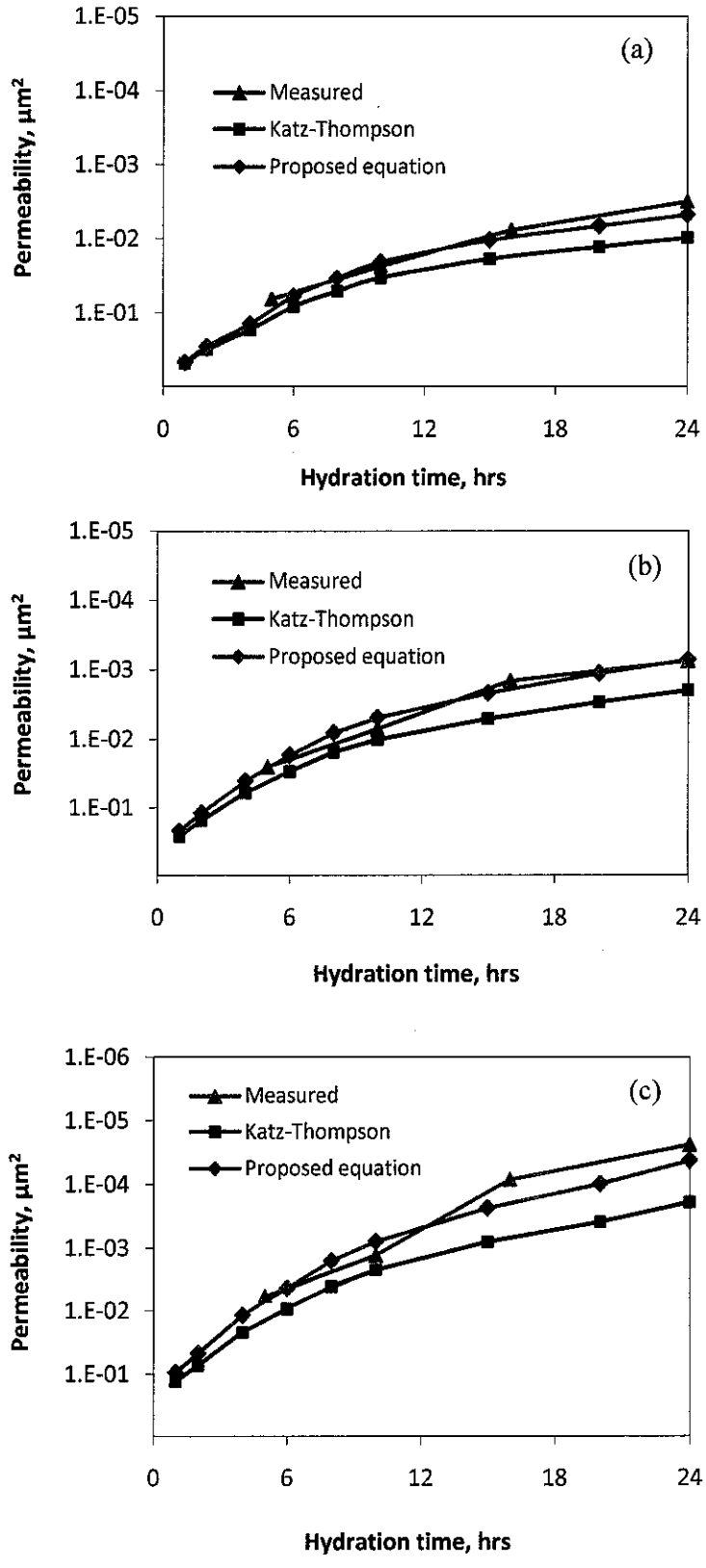

Figure 4.35 Comparison of the Katz-Thompson model, proposed equation and measured data for cement sample with (a) w/c 0.5 at 25°C & 14.7 psi, (b) w/c 0.4 at 40°C & 1500 psi, and (c) w/c 0.3 at 65°C & 3000 psi

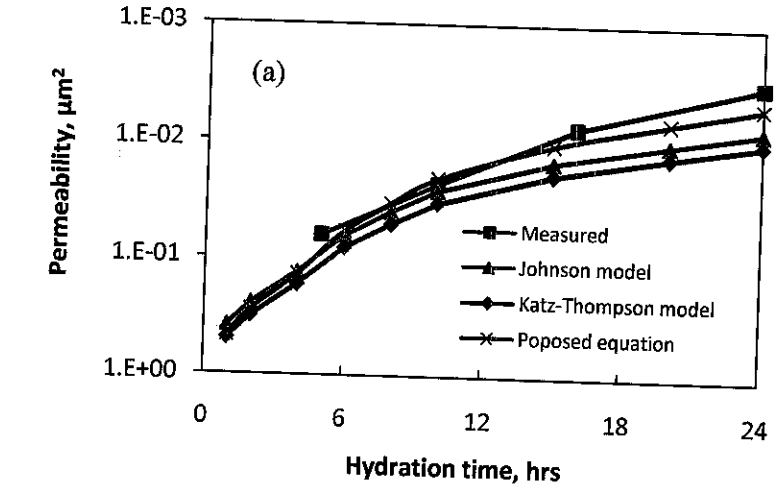

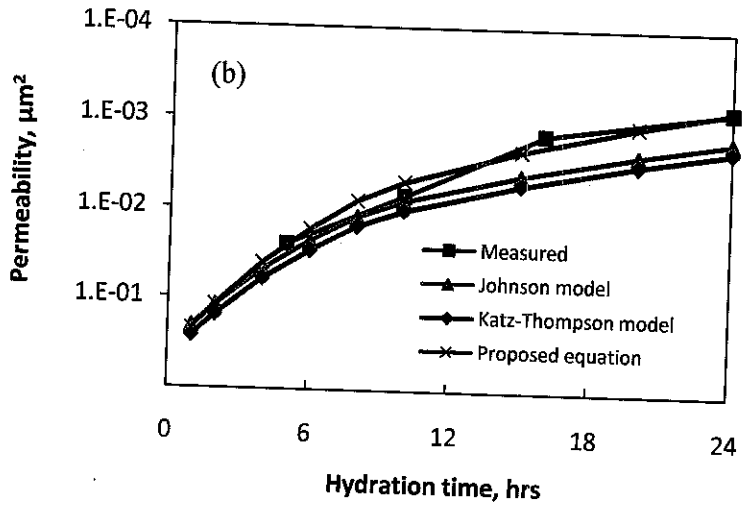

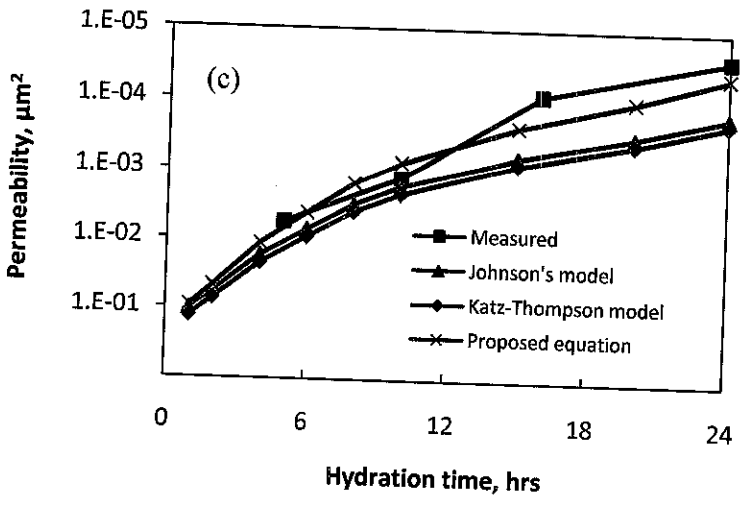

Figure 4.36 Comparison of the Johnson model, Katz-Thompson model, measured data and proposed equation for cement sample with (a) w/c 0.5 at 25°C & 14.7 psi, (b) w/c 0.4 at 40°C & 1500 psi, and (c) w/c 0.3 at 65°C & 3000 psi

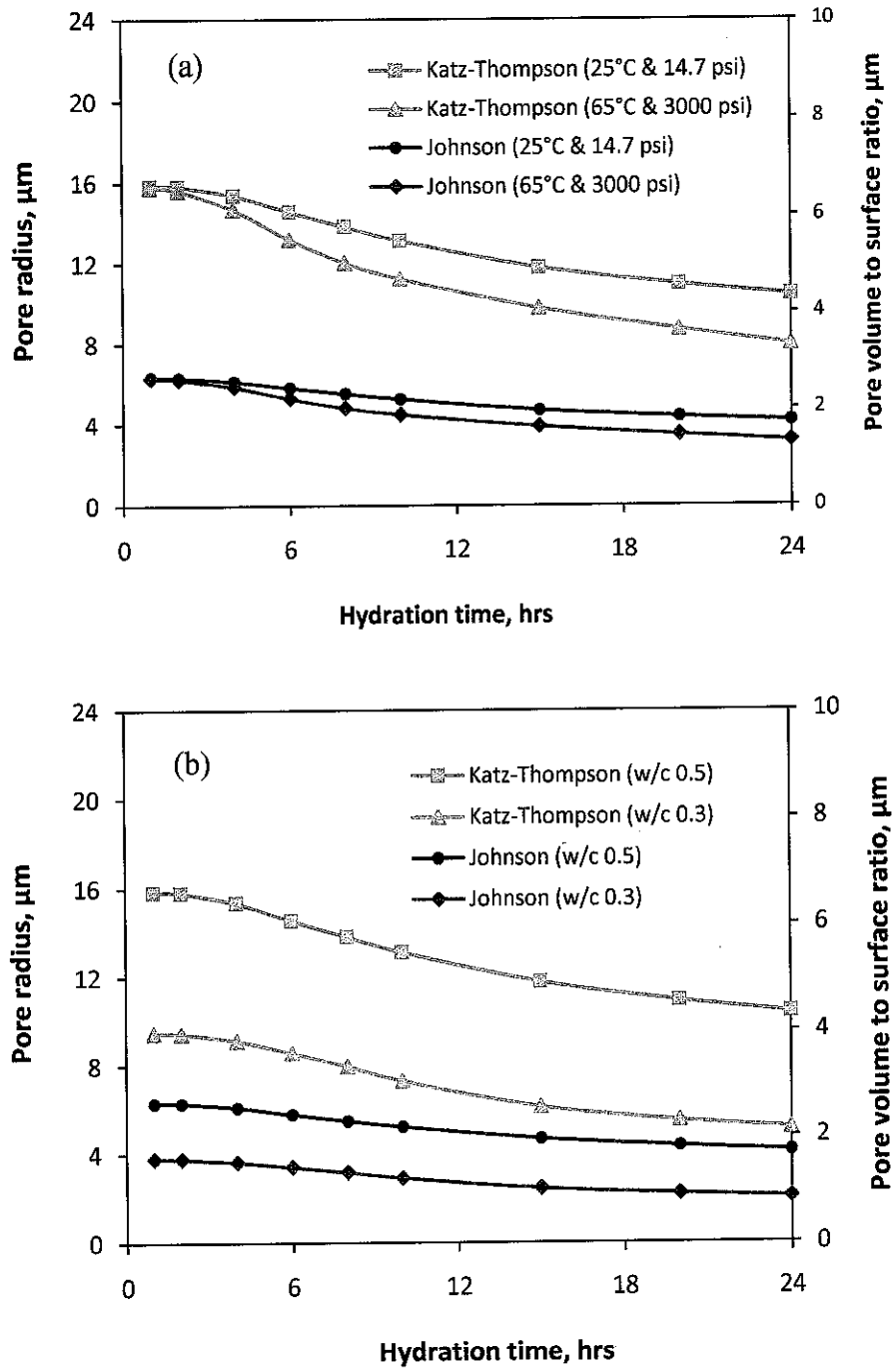

Figure 4.37 Microstructural parameter development employed in the Katz-Thompson and Johnson equation as a function of hydration time with respect to (a) different curing conditions and (b) water cement ratios

4.3.6 Relationship between Compressive Strength and Electrical Properties

It has been shown in section 4.2.5 that Archie's law can be used for predicting porosity of well cement by means of its electrical properties (further discussion will be given in Section 4.3.6.2). Furthermore, porosity has a strong correlation to strength by which the reverse side of the porosity decrease is growth of crystals and, thus, strength build-up. This study used both porosity-strength correlation and strength-electrical properties relationship to produce predictive equations of oilwell cement.

4.3.6.1 Porosity-Strength Model Evaluation

To evaluate the porosity-strength relationship, it was performed by correlating both a measured porosity to a compressive strength of oilwell cement at different curing conditions and water to cement ratio. Data of measured strength using UCA device are shown in Table 4.8 and detailed results in the graphical form are displayed in Appendix H. The relationship shows that a linear function has been produced between porosity and strength as shown in Figure 4.38. The result of linear equations follows to the equation proposed by Hasselman [29] (Equation 2.21), respectively.

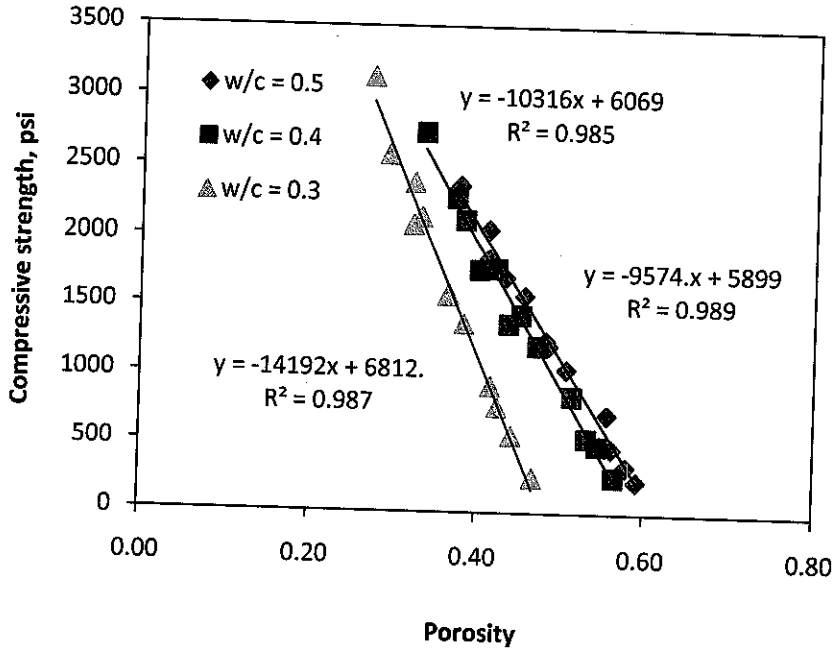

Figure 4.38 Experimental data on porosity-strength linear relationship for Class G neat cement at different w/c ratios

From Figure 4.38, it can be seen that the fitted linear curve has yielded the equations $S = S_o - b\phi$ for which the values of S_o and b for w/c 0.5, 0.4 and 0.3: $S = 5899 - 9574(\phi)$ with an R^2 value of 0.989, $S = 6069 - 10316(\phi)$, with an R^2 value of 0.985, and $S = 6812 - 14192(\phi)$, with an R^2 of 0.987. It is also noticed that the value of empirical parameters for maximum strength, S_o, was relatively similar irrespective of w/c ratios and reflected an intrinsic property of the hydration products. However, the maximum strength constant tended to increase as water cement ratios increased. The values were in the range of 5899 to 6812 psi with an average approximation is 6355 psi. It is mentioned that value in literature was about 5800 psi [57]. The difference might be due to the various cement samples used and also sample curing conditions. The value of the empirical constant b was in the range between 9574 and 14192, which increases as w/c ratios decreases. The values of constant parameters can be seen in Table 4.9.

Table 4.8 Measured strength of Class G cement at various curing conditions using UCA analysis

Temperature and Pressure	**Hydration time (hrs)**	**Strength, psi (w/c=0.5)**	**Strength, psi (w/c=0.4)**	**Strength, psi (w/c=0.3)**
	5	217	262	252
25°C & 14.7	10	712	847	914
psi	16	1179	1366	1570
	24	1572	1759	2086
	5	371	487	551
40°C & 1500	10	1040	1210	1366
psi	16	1703	1771	1997
	24	2052	2280	2580
	5	469	542	763
65°C & 3000	10	1246	1392	1582
psi	16	1841	2036	2341
	24	2449	2740	3133

Table 4.9 Constant parameters obtained from linear fitted of Hasselman equation

Water cement ratio (w/c)	**Maximum strength, psi (S_o)**	**Empirical parameter, psi (b)**
0.5	5899	9574
0.4	6069	10316
0.3	6812	14192

The above constant parameters (Table 4.9) could be elaborated in the form of equations as a function of w/c using a linear regression analysis in which the result of the equations then might be used in determining the constant parameter for sample at different water cement ratio as follows.

$$b = 20597 - 23090(^{w}/_{c}) \tag{4.18}$$

$$S_o = 8086 - 4565(^{w}/_{c}) \tag{4.19}$$

The porosity-strength relationship from these results was taken as a basis for predicting the strength from measured normalized conductivity (σ_n), at this point, using the porosity-electrical conductivity relations. As a result, having been measured, the normalized conductivity on the Class G cement by using the well known Archie's law could be related to the porosity.

Figure 4.39a shows the shift of the data between strength and porosity observed as a function of w/c. It was moved to lower porosities for smaller w/c ratios. The initial measurements of porosities at 5 hrs for w/c ratios 0.5, 0.4, and 0.3 were 58%, 54% and 44%, respectively. In turn, the lower initial porosity of the cement was responsible for the shift of the data. These profiles then showed a similar appearance in cement with an additional admixture such as fly ash, silica fume and slag [8].

Another shift also existed on porosity and strength due to pressure and temperature changes at w/c 0.4 (Figure 4.39b). For a given hydration period, cement

strength increased and porosity decreased as pressure and temperature increased. However, porosity subsequently shifted due to the changes of pressure and temperature was considered smaller compared to the effect of water to cement ratios. This occurred since the initial water mixing dominantly contributed to form void spaces and significantly appeared at the early stages of hydration. At mature stages, the effect of elevated pressure and temperature were prevalent in controlling the values of porosities. In turn, the shift of strength values was pronoun due to elevated temperature and pressure.

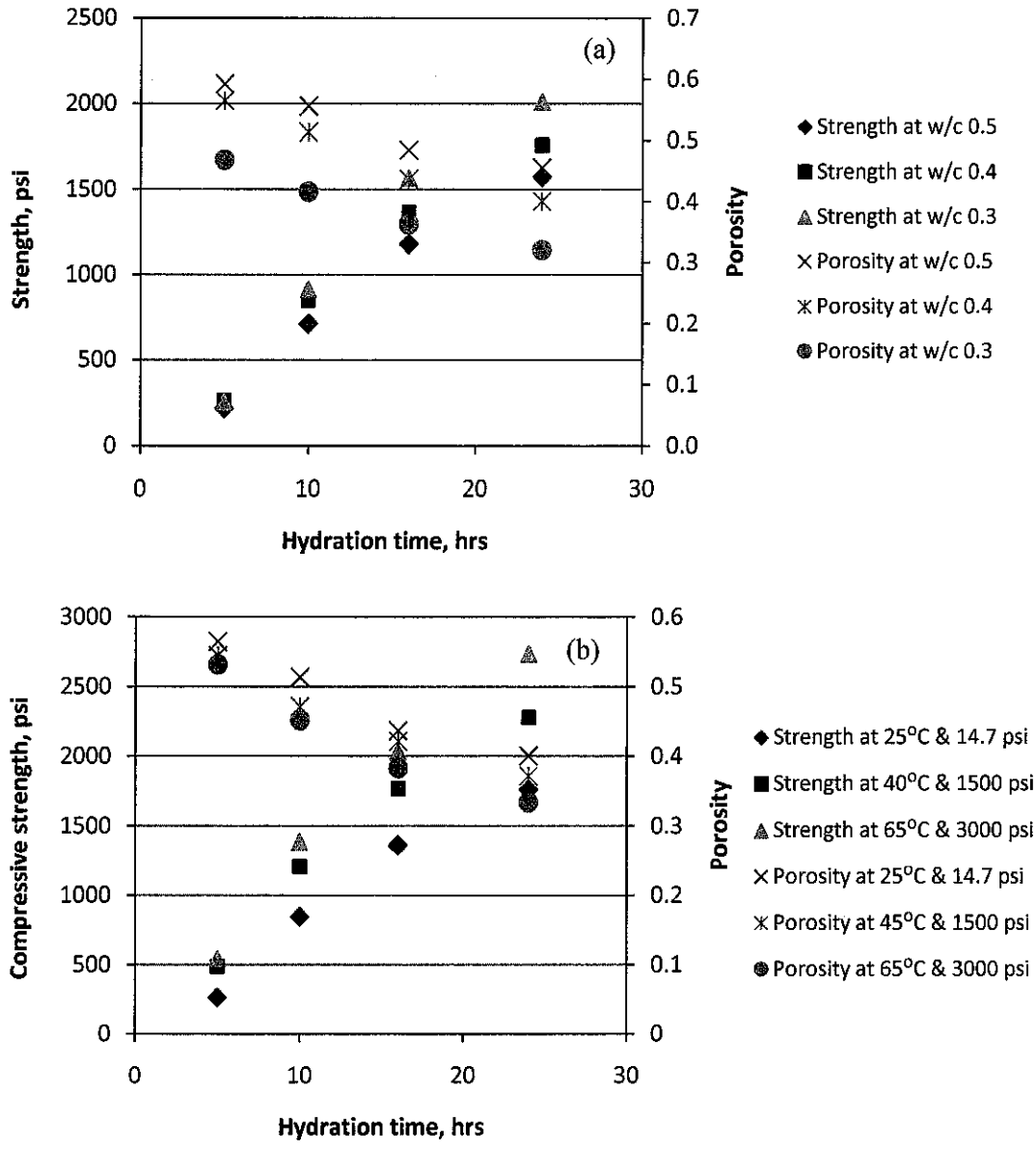

Figure 4.39 Shifted of the porosity and strength data as a function of (a) w/c and (b) curing pressure and temperature as a function of hydration time for w/c 0.4

4.3.6.2 Archie's Porosity Assessment

Archie's law has become a standard method for relating the conductivity of a clean reservoir rock to its porosity. In this study, it has been shown that Archie's equation can be used to estimate porosity of oilwell cement. The general form of Archie's law can be stated as Equation (4.20) follows [10]:

$$\sigma_b = \sigma_o \phi^m \tag{4.20}$$

where σ_b is the bulk conductivity, σ_o is the pore solution conductivity, ϕ is the porosity and m is the cementation factor.

It was shown that Archie's law included a variable term describing the connectivity of the conducting phase (cementation factor). Ewing and Hunt [81] stated that Archie's law has a theoretical foundation as it can be derived by applying continuum percolation theory to fractal porous media. Furthermore, a reasonable physical phenomenon at the elevated temperature could be explained by Archie's model by the cementation exponent profile (refer to Section 4.2.5).

Figure 4.40 shows the experimental results between normalized conductivity and porosity corresponding to Archie's model in the form of power law. The cementation factors in the equations were found to be varied referring to water cement ratio and curing conditions. The larger it was, the more tortuous the network would be. As the cement further hydrated, the connectivity became narrower and more tortuous as indicated by the microstructural parameter change with age. Accounting for these changes, a fitting procedure was performed on the models to the experimental measurements of electrical conductivity.

The downturn of the m factor was observed - especially at elevated curing condition after cement was set. This was an artifact of the data approaching the percolation limit. The limit number proposed by Bentz [88] was $\phi_c = 0.18$ based on simulation. This turn point was early experienced at elevated curing conditions as an effect of hydration acceleration.

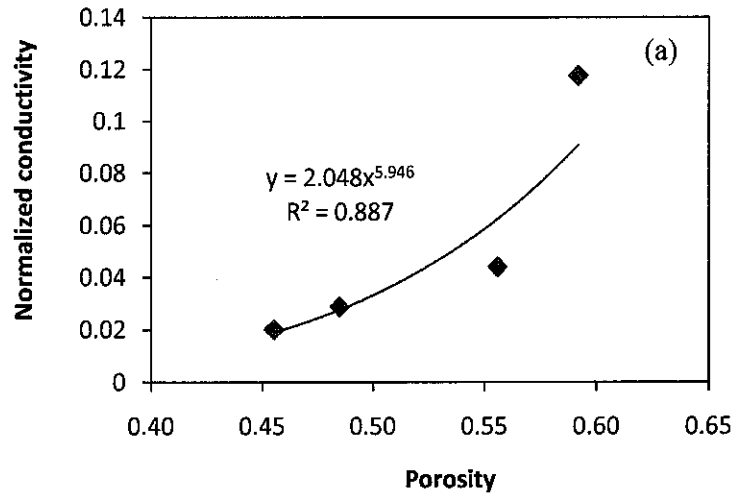

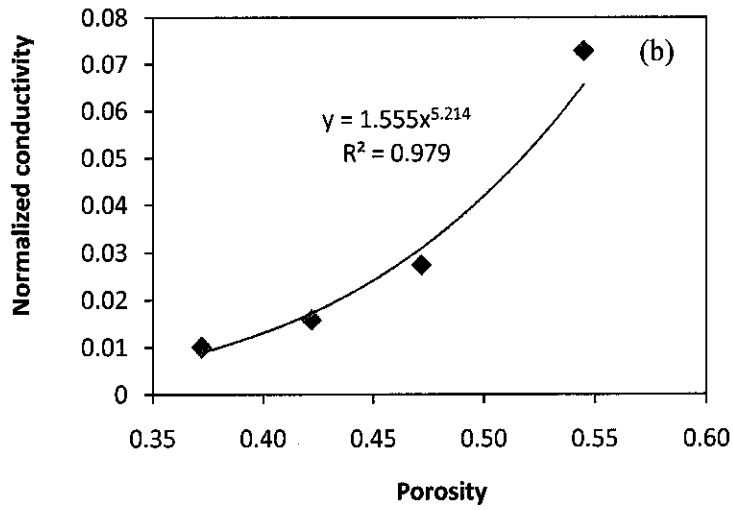

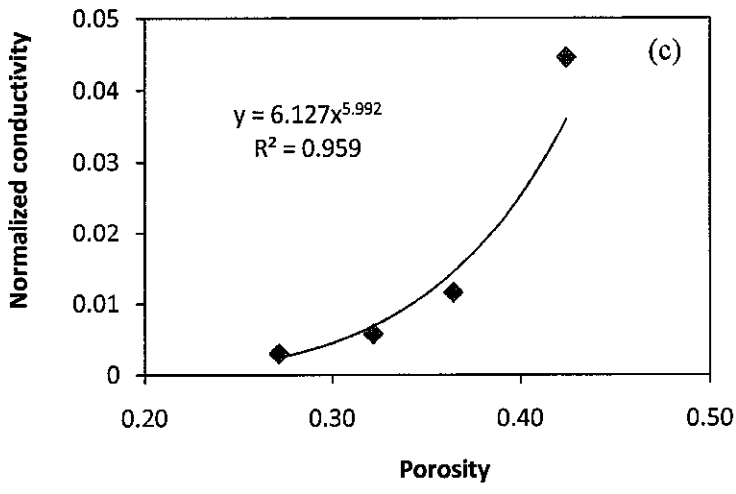

Figure 4.40 Typical result of normalized conductivity versus porosity for neat Class G cement wit (a) w/c 0.5 at 25°C & 14.7 psi, (b) w/c 0.4 at 40°C & 1500 psi, and (c) w/c 0.3 at 65°C & 3000 psi

Figure 4.41 presents the comparisons of measured and calculated porosity. The Archie's equation over predicted the porosity at the early ages for all w/c. The relatively low over prediction occurred at the high w/c due to the chosen cementation factor that might have caused this behavior. The phenomena of over prediction seemed to appear due to the dominant effect of pore solution conductivity compared to that of porosity. On the other hand, as hydration product started to form and an opening pore dilute, the predictions seemed to agree well with the experimental values at the later ages. These values were used as an input for the strength estimation applied in the Hasselman model.

The relationship shows the indication of the linear least square of about 0.92 for w/c 0.3, 0.915 for w/c 0.4 and 0.89 for w/c 0.5 about the achievement of the good quality of estimated data. The m values for each w/c were regressed and averaged to different curing conditions due to its effect on cementation factor to be relatively less significant than that of w/c. These values are stated as follow, m for w/c 0.5 = 3.8, w/c 0.4 = 4.3, and w/c 0.3 = 5.8. Thus, it can be observed that when w/c increased, the m values decreased due to pore structure less tortuous in higher w/c.

However, for strength prediction the cementation factors used in the porosity calculation were fitted from measured data at a specific curing hydration time. By this, each curing condition, for certain w/c, hydration time, and temperature and pressure, had its own m value. Concerning with these contributions, these values were averaged as a function of w/c. The fitting procedure might represent the m values during hydration process at specific time duration for the different initial values. As presented in Table 4.10, the cementation fitting result and its averaging were at 4.7 for w/c 0.5, 4.6 for w/c 0.4 and 4.3 for w/c 0.3.

Different from the regression analysis, the m fitted values seemed to increase as w/c increased. This occurrence was because the cementation values during fitting procedure had taken into account the hydration periods at which certain numbers were lower at the latter stages of hydration – probably caused by the double effects. Firstly, the use of capillary porosity instead of total porosity may underestimate the m values as previously discussed and secondly, the elevated temperature may alter and damage the pore structure, thus making the cementation factor decreased.

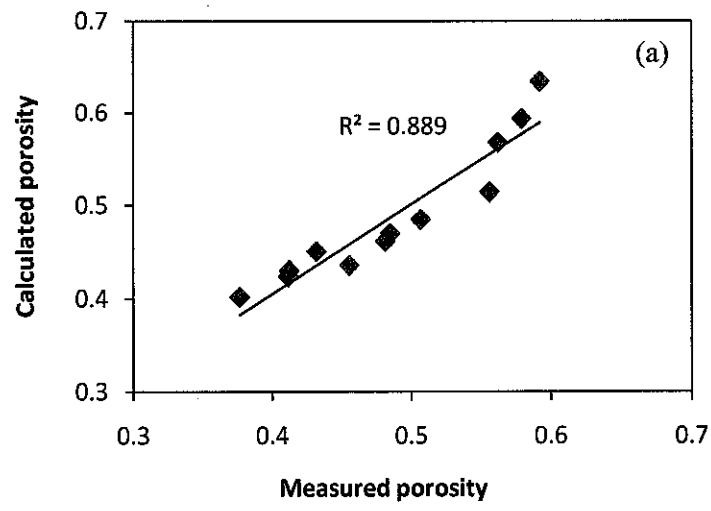

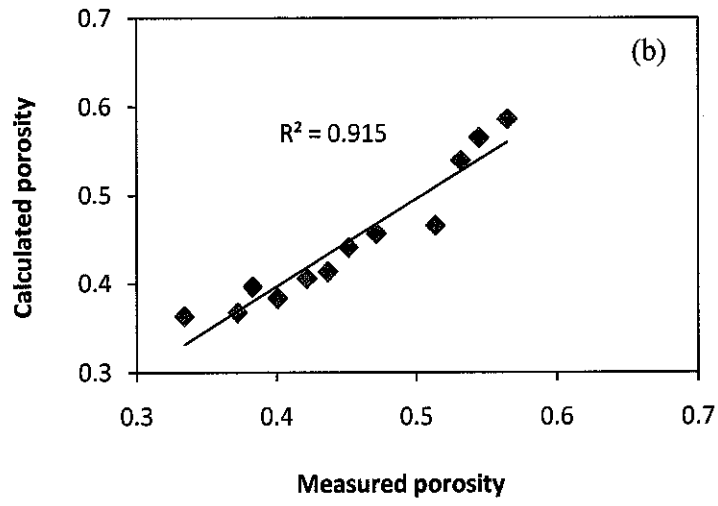

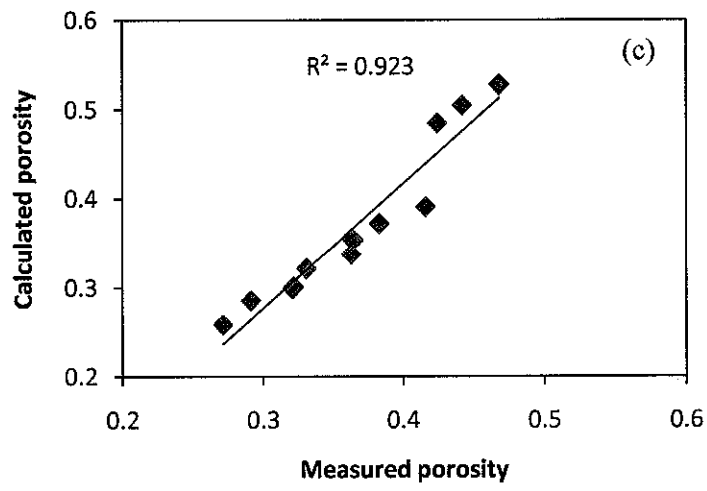

Figure 4.41 Comparison of measured porosity and porosity predicted from Archie's equation of (a) w/c 0.5, (b) w/c 0.4 and (c) w/c 0.3

The cementation constant could be expressed in terms of the material parameter as function of w/c using regression analysis. Equation relating w/c to the cementation factor and following Power law with least square error (R^2) of about 0.95 could be described as follows (Equation 4.21).

$$m = 5.33(^{w}/_{c})^{0.177} \tag{4.21}$$

Equation (4.21) provided a convenience way to estimate cementation factor as a function of w/c.

Table 4.10 Cementation factor generated from fitting procedures and averaged

Temperature & Pressure	Hydration time (hrs)	w/c 0.5		w/c 0.4		w/c 0.3	
		m **fitted**	***m*** **averaged**	***m*** **fitted**	***m*** **averaged**	***m*** **fitted**	***m*** **averaged**
25°C & 14.7 psi	5	4.1	4.7	4.3	4.6	3.6	4.3
	10	5.3		5.3		4.6	
	16	4.9		4.9		4.6	
	24	4.9		4.8		4.5	
40°C & 1500 psi	5	4.5		4.3		3.6	
	10	5		4.8		4.4	
	16	4.5		4.8		4.4	
	24	4.5		4.7		4.3	
65°C & 3000 psi	5	4.6		4.5		3.6	
	10	5		4.7		4.4	
	16	4.5		4.4		4.5	
	24	4.4		4.3		4.4	

4.3.7 Empirical Equation for Strength Prediction

From the values of porosities predicted using Archie equation as described in the previous sections 4.3.6.2, the strengths of Class G cement could be predicted using Hasselman equation. The combination of these equations may produce the following modified model (Equation 4.22):

$$S = S_o - b\left(\frac{\sigma_b}{\sigma_0}\right)^{1/m} \tag{4.22}$$

where S is strength, S_o is strength at zero porosity, b is empirical constant, σ_b is bulk conductivity, σ_o is pore solution conductivity, and m is cementation factor.

Figure 4.42 shows the predicted strengths and the measured ones of the oilwell cement as a function of hydration time. The strength predicted using modified Hasselman equation showed a good agreement between the experimental data and predicted one with level of error below 30%. It was satisfactory for all water cement ratio with coefficient of determination (R^2) for each w/c was 0.92 for 0.5, 0.95 for 0.4 and 0.90 for 0.3. The values of the constants and cementation factors used in the Hasselman equation might be the reason for the slight discrepancy for each w/c ratios. However, it may give the shortest way in estimating the strength development of well cement by using its electrical properties data. Figure 4.43 shows the comparison of experimentally measured strength and predictably strength using the modified Hasselman equation for all samples. The least square error (R^2) of about 0.89 here indicates that a relatively good correlation has been obtained.

Equation (4.22), subsequently, was applied for the strength prediction of cement at different mixing and curing condition and samples with w/c 0.25 and w/c 0.55 were conditioned at 70°C & 3000 psi. The measured strength and prediction using equation (4.22) are exhibited in Figure 4.44. The values of constant parameter (S_o, b and m) were calculated using equation (4.18, 4.19 and 4.21) with a result showing a good agreement between the predicted and measured strengths with the level of error about below 20%.

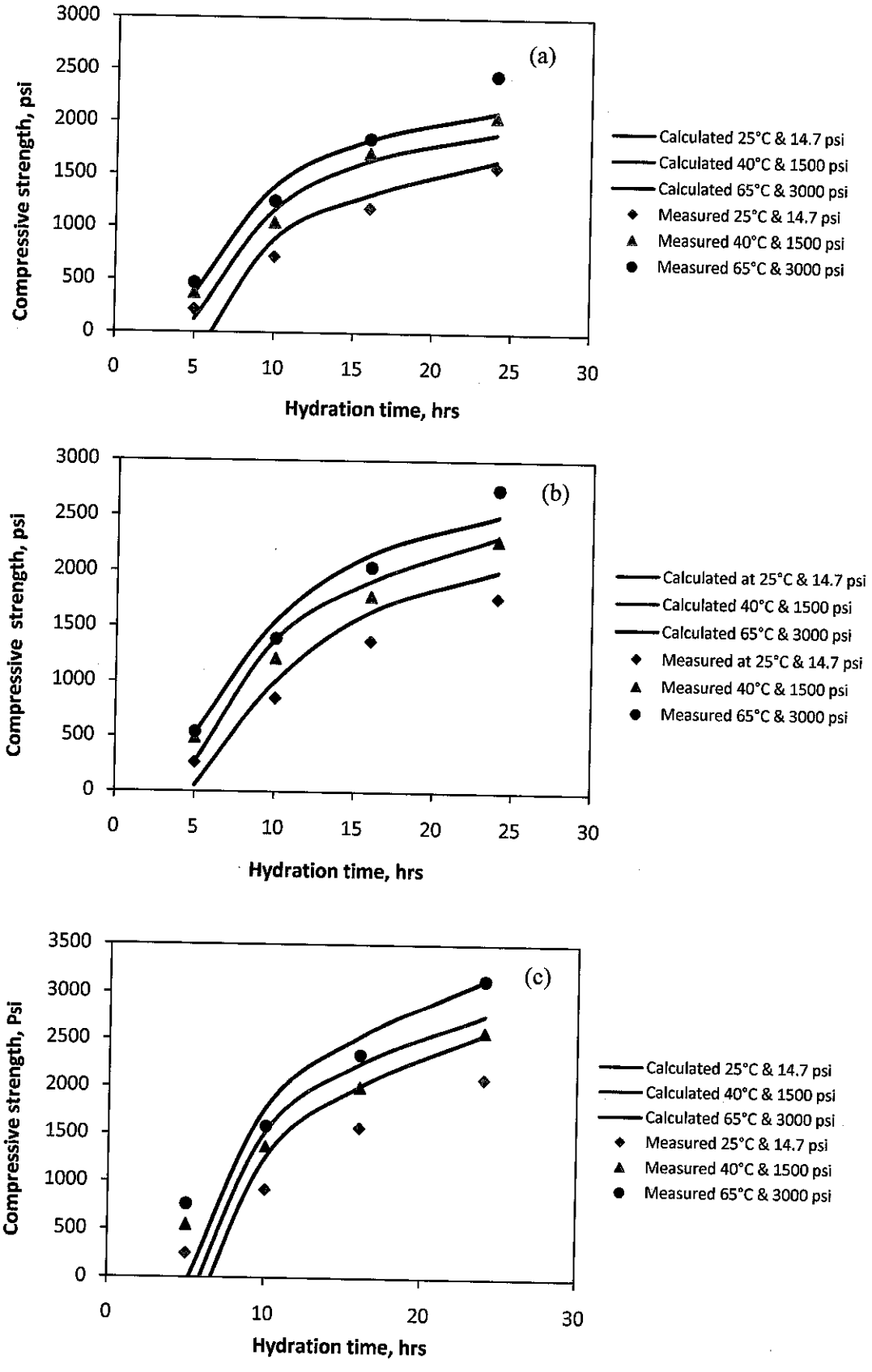

Figure 4.42 Comparison of strength predicted from modified Hasselman equation and measured strength under different curing conditions (a) w/c 0.5, (b) w/c 0.4 and (c) w/c 0.3

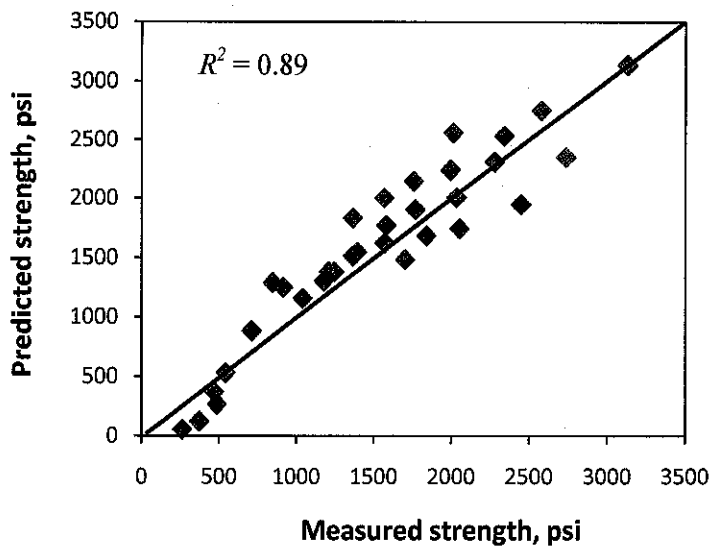

Figure 4.43 Comparison of experimentally measured strength and strength predicted using modified Hasselman equation for all specimens

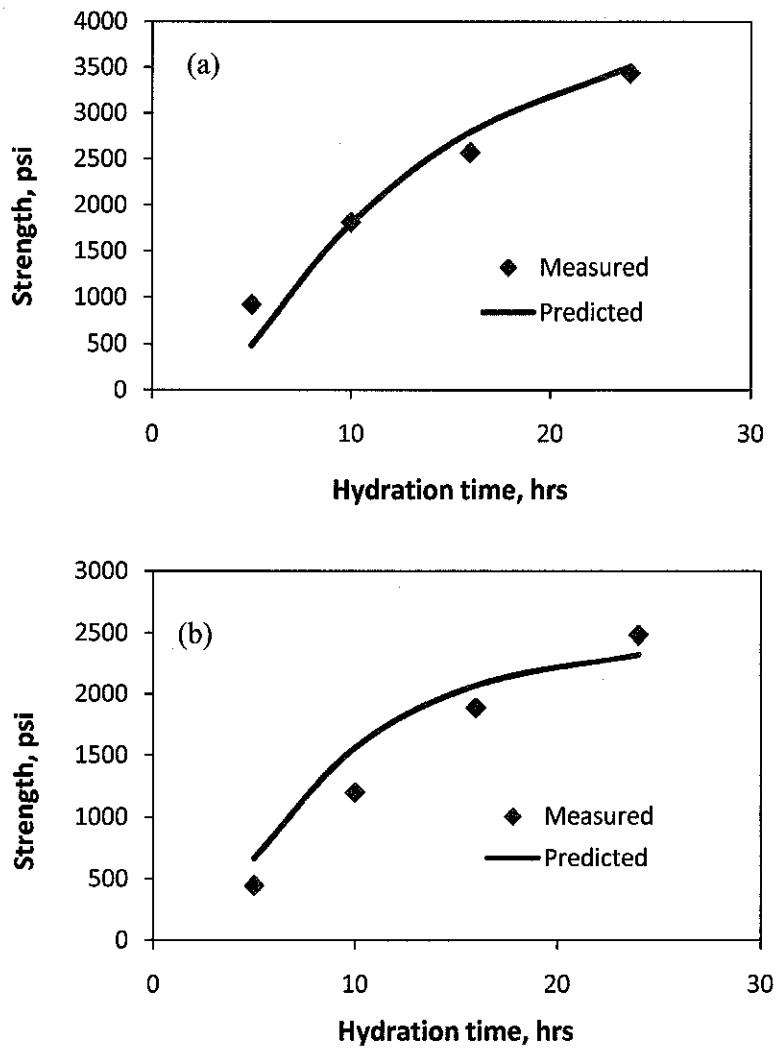

Note: Prediction for both cement sample, average $R^2 = 0.971$

Figure 4.44 Comparison of measured and predicted strength using modified Hasselman equation at 70°C & 3000 psi for w/c (a) 0.25 and (b) 0.55

Moreover, Equation (4.22) was also performed for these samples conditions with hydration period up to 50 days. The result of measured and predicted strength was given in Figure 4.45. It can be seen that with 1 day electrical conductivity measurement, the error in estimating 50 days strength was less than 31% and the error in estimating 15 days was less than 15%. The predicted strength above 15 days of hydration time seems to under-estimate the measured value. It was suspected due to the selection of constant cementation factor instead of changing simultaneously as an effect of hydration mechanism and curing condition. It can be said that the measured resistivity data for 1 day can be used to predict the strength development up to 15 days with acceptable accuracy.

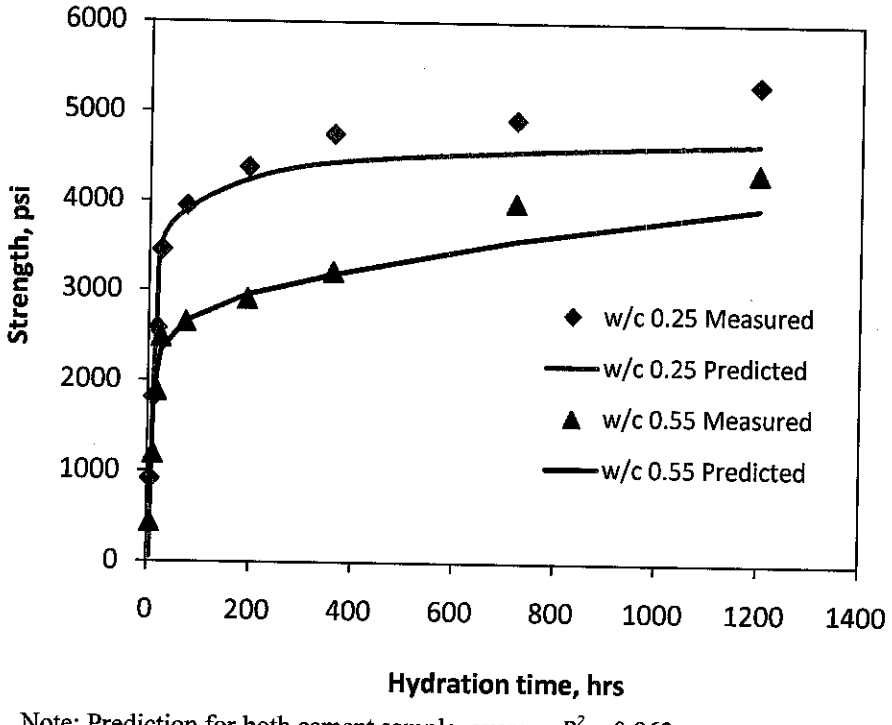

Note: Prediction for both cement sample, average $R^2 = 0.963$

Figure 4.45 Measured and predicted strength of Class G cement sample at 70°C & 3000 psi up to 50 days of hydration

4.3.8 Generalized Equation

A generalized equation may be generated to directly relate the normalized conductivity to strength of oilwell cement. Figure 4.46 shows a relationship between normalized conductivity and measured strength for Class G cement. This relationship corresponded to power law with least square error (R^2) of about 0.831. The correlation

seemed to be unique according to the sample composition and treatment. The generalized form for strength prediction is shown in Equation (4.23):

$$S = 69.96\left(\frac{\sigma_b}{\sigma_o}\right)^{-0.72} \tag{4.23}$$

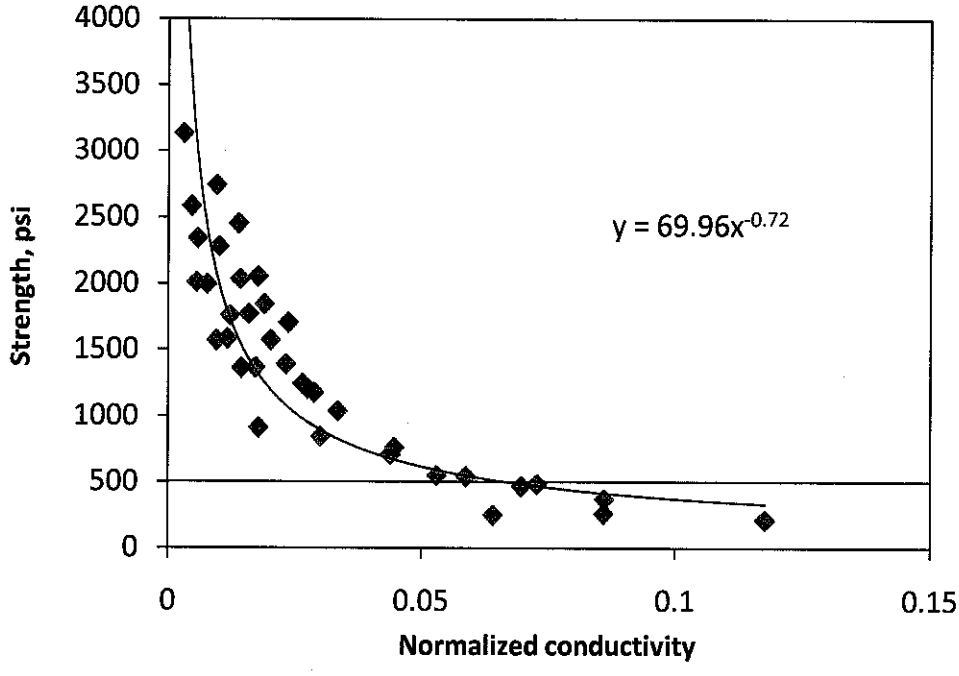

Figure 4.46 Generalized relationships between strength and normalized conductivity for Class G oilwell cement

A better prediction was achieved once the influence of w/c on strength prediction was considered (Figure 4.47). The relatively good R^2 at higher w/c indicated that the resulted generalized equation seemed to be more effective for cement at high w/c, probably be due to a very high value of solution conductivity at lower w/c. Hence, it may sometime cause the over prediction of cement strength.

However, Equation (4.23) has poor prediction results once it is tested on other cement sample for w/c 0.55 and 0.25 at 70°C & 3000 psi as shown in Figure 4.48 with the level of error was above 27% compared to that of below 20% for Equation (4.22). The predicted strength deviates accordingly with over predict for low w/c and under predict for high w/c. This is due to the effect parametric bound that limits its applicability once it is used outside the range of w/c 0.5, 0.4, and 0.3.

An interesting point to be noted here is that these curves (Figures 4.46 & 4.47) may provide an indication of the strengths of the cement at certain interval number

such as 500 psi for well that could be drilled-out when the electrical conductivity was the only available parameter. A normalized conductivity number of about 0.06 from the entire sample was obtained representing the cement strength of 500 psi.

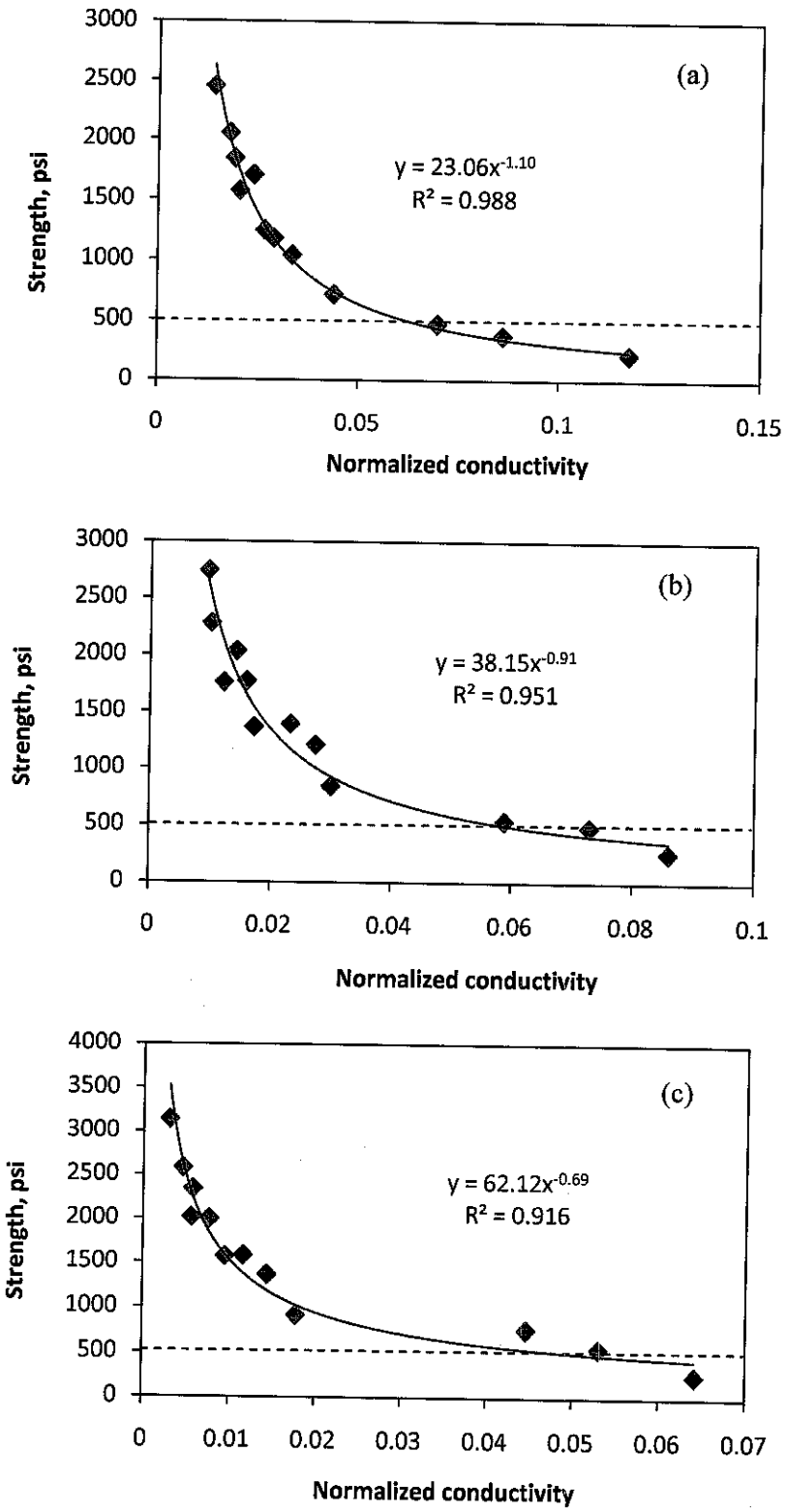

Figure 4.47 Measured strength with normalized conductivity for Class G cement under elevated curing conditions of (a) w/c 0.5, (b) w/c 0.4 and (c) w/c 0.3

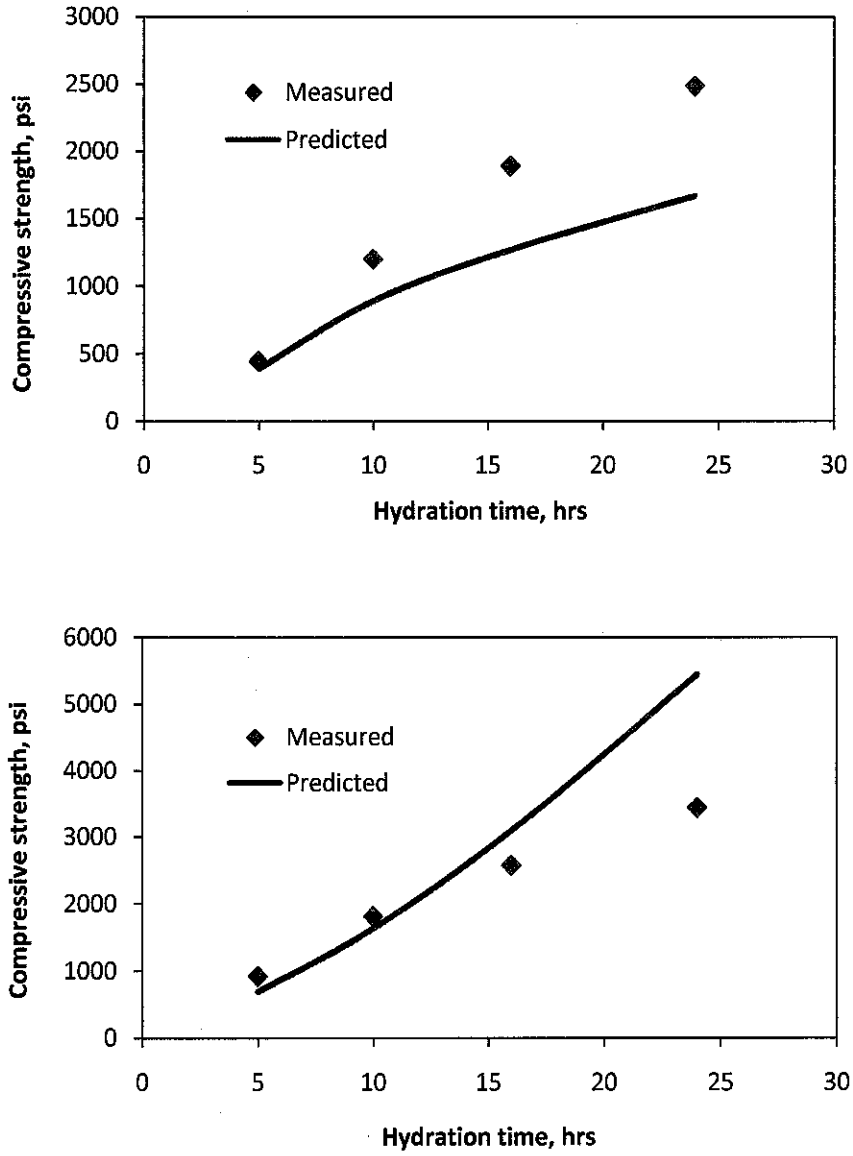

Figure 4.48 Comparison of measured and calculated compressive strength of new cement sample using generalized equation for (a) w/c 0.55 and (b) w/c 0.25 at 70°C & 3000 psi

4.3.9 Summary

Pore diameter and electrical properties in the form of normalized conductivity were two important parameters in calculating permeability of cement sample. Once these parameters were plotted, the resulted empirical formula followed the Katz-Thompson equation with different constant values. The constant values here might reflect the hydration process and alteration process of pore structure due to oven-drying

intervention at about 80°C. Although this new equation was generated in periods up to 24 hrs of hydration, it could provide a better prediction of permeability until 28 days of hydration time using literature data compared to that of the Katz-Thompson equation. Furthermore, permeability prediction using Johnson's model seemed to have a very similar result to that of Katz-Thompson, although its characteristic length scale was differently generated. The decreasing constant number of Johnson's model to 1/12 might result a better comparison with the measured permeability data. Meanwhile, the result from a constant modification in Johnson's model had less accuracy compared to the equation as proposed in this study. As such, this approach can be used to simultaneously identify the potential leakage or migration of fluids once the cement has been displaced in the wellbore.

A good correlation was observed between porosity and strength in the form of power law. It was then used as a basis for strengths prediction using electrical properties measurements. The porosity values for strength prediction were calculated using Archie's equation based on its electrical properties. The employment of electrical properties on Power law correlation resulted in the modified version of Hasselman equation. The correlation between measured strength and strength predicted using modified Hasselman equation was found to be satisfied. The predictive equation was also applicable for the new cement sample conditions up to 50 days of hydration period. A generalized relation between effective electrical conductivity and predicted strength was additionally established; though the use of this relationship needed to be limited to a parametric range chosen in this study. A normalized conductivity number of about 0.06 from the entire sample was obtained representing cement strength of 500 psi. This, after all, provided an indication of the strength of well cement *in-situ* when the electrical conductivity was the only parameter to be measured. Hence, the wait-on-time of cement can be estimated to assure the resumption of the drilling operation.

CHAPTER 5

CONCLUSIONS AND RECOMMENDATIONS FOR FUTURE WORK

This chapter is to provide several general conclusions from the experimental observations and its analysis in this research study. Several suggestions for the future works are presented and also become the last part of this chapter.

5.1 Conclusions

- The variation of cut-off frequency with hydration time reflects that single frequency measurement comes to be not applicable to obtain representative data of electrical conductivity.
- Elevated curing temperature and pressure are found to be able to increase the conductivity dispersion. In turn together with low w/c can increase the magnitude of conductivity dispersion which contributes to form interface conductivity.
- The proposed simple particle expansion model has overcome some difficulties in measuring microstructure parameters related to the interface conductivity phenomena. The value of the interface conductivity is relatively very small of about factor -9 in order of magnitude.
- The cementation exponent in Archie's law shows a reflection to the changing in cement's connected pores. This may be used to predict porosity of well cement in-place with electrical properties that are the only information needed.
- The proposed permeability predictive equation has followed the Katz-Thompson equation with different constant values. Then, a good comparison has been obtained using the proposed correlation between the predicted and measured permeability compared to that of the Katz-Thompson equation.

- Permeability prediction using Johnson's model seems to have a very similar result to that of Katz-Thompson, although its characteristic length scale has been differently generated. Decreasing constant number of Johnson's model may result in a better comparison with the measured permeability data.
- Power law correlation has been observed between porosity and strength corresponding to the Hasselman model. Once the porosity values have been obtained using Archie equation, the correlation then produces a modified version of Hasselman equation. The comparison to measured data is found to be satisfied.
- A normalized conductivity number of about 0.06 has been obtained from generalized strength-conductivity correlation representing cement strength of 500 psi. It provides an indication of the strength of well cement in-place when the electrical conductivity becomes the only parameter to be measured.

5.2 Future Work

Several potential studies for furthers investigation are identified as follows:

1. This research has shown the usefulness of electrical properties on characterizing the strength and permeability of well cement. It is then suggested that studies in future be carried out on the freezing condition below $0^{o}C$ with a broader frequency range since the oilfield reservoir is also found in that conditions.
2. Permeability and strength predictions have been successfully shown in this study. However, further studies need to be conducted for cement that contains additives with ultra high temperature and pressure.
3. Further study is also needed for strength and permeability predictions of oilwell cement with the presence of interface conductivity.
4. Using X-ray analysis to investigate the physical justification of the constant values in the proposed predictive equations.
5. Applying the permeability and strength predictive equations to the foam cement and green cement.

REFERENCES

[1] W. J. McCarter, "Electrical monitoring and characterisation of cement-based systems," *Cement and Concrete Composites*, vol. 24, no. 5, pp. 413–414, 2002.

[2] W. J. McCarter, G. Starrs, T. M. Chrisp, and J. Blewett, "Characterization and monitoring of cement-based systems using intrinsic electrical property measurements," *Cement and Concrete Research*, vol. 33, no. 2, pp. 197–206, 2003.

[3] P. Gu, Z. Xu, P. Xie, and J. J. Beaudoin, "Application of A.C. impedance techniques in studies of porous cementitious materials, (I). Influence of solid phase and pore solution on high frequency reristance," *Cement and Concrete Research*, vol. 23, no. 3, pp. 531–540, 1993.

[4] B. J. Christensen, R. T. Coverdale, A. Rudolf, S. J. Ford, E. J. Garboczi, H. M. Jennings, and T. Mason, "Impedance spectroscopy of hydrating cement-based materials: Measurement, interpretation, and application," *Journal of the American Ceramic Society*, vol. 77, no. 11, pp. 2789–2802, 1994.

[5] Z. Li, X. Wei, and W. Li, "Preliminary interpretation of portland cement hydration process using resistivity measurements," *ACI MaterialsJournal*, vol. 100, no. 3, pp. 253–257, 2003.

[6] S. Mindess, J. F. Young, and D. Darwin, *Concrete*, 2nd Edition., vol. 40, no. 10. Prentice Hall Englewood Cliffs, NJ, 2003.

[7] J. Zhang, L. Qin, and Z. Li, "Hydration monitoring of cement-based materials with resistivity and ultrasonic methods," *Materials and Structures*, vol. 42, no. 1, pp. 15–24, Mar. 2009.

[8] N. Neithalath, J. Persun, and R. K. Manchiryal, "Electrical conductivity based microstructure and strength prediction of plain and modified concretes," *International Journal of Advances in Engineering Sciences and Applied Mathematics*, vol. 2, no. 3, pp. 83–94, Feb. 2011.

[9] Y. Liao, X. Wei, and G. Li, "Early hydration of calcium sulfoaluminate cement through electrical resistivity measurement and microstructure investigations," *Construction and Building Materials*, vol. 25, no. 4, pp. 1572–1579, Apr. 2011.

[10] G. E. Archie, "The electrical resistivity log as an aid in determining some reservoir characteristics.pdf," *Pet. Trans. Americ. Inst. Mineral. Met*, vol. 146, pp. 54–62, 1942.

[11] A. Revil and P. W. J. Glover, "Theory of ionic-surface electrical conduction in porous media," *Phys. Rev. B*, vol. 55, no. 3, pp. 1757–1773, 1997.

[12] H. Friedmann, O. Amiri, and A. Ait-Mokhtar, "Physical modeling of the electrical double layer effects on multispecies ions transport in cement-based materials," *Cement and Concrete Research*, vol. 38, no. 12, pp. 1394–1400, Dec. 2008.

[13] D. Mavroudis, "Downhole environmental risks associated with drilling and well completion practices in the cooper/eromanga basins," *Department of Primary Industries and Resources South Australia*, Report Book 00009, March 2001.

[14] D. Vo-thanh, "Effects of fluid viscosity on shear-wave attenuation partially saturated sandstone in," *Geophysics*, vol. 56, no. 8, pp. 1252–1258, 1991.

[15] T. C. Sheives, L. N. Tello, V. E. Makir, T. E. Standley, and T. J. Blankinship, "A comparison of new ultrasonic cement and casing evaluation logs with standard cement bond logs," *Society of Petroleum Engineers*, no. 15436, 1986.

[16] H. Khairy and Z. T. Zahir, "Interfacial, pore geometry and saturation effect on complex resistivity of shaly sandstone: dispersion and laboratory investigation," *Geosciences Journal*, vol. 15, no. 4, pp. 395–415, 2011.

[17] D. K. Smith, *Cementing,* Society of Petroleum Engineers, Monograph Volume 4, 1990.

[18] L. T. Watson and S. Bachu, "Evaluation of the potential for gas and CO2 leakage along wellbore," *Society of Petroleum Engineers*, no. 106817, 2009.

[19] L. Burdylo and G. Birch, "Primary cementing techniques," in *Well Cementing*, E. B. Nelson, Ed. New York: Elsevier, 1990.

[20] H. F. W. Taylor, *Cement Chemistry*, 2nd Edition. Thomas Telford, London, Oct. 1997.

[21] I. Elkhadiri, M. Palacios, and F. Puertas, "Effect of curing temperature on cement hydration," *Journal of Ceramic-Silikaty*, vol. 53, no. 2, pp. 65–75, 2009.

[22] G. W. Scherer, G. P. Funkhouser, and S. Peethamparan, "Effect of pressure on early hydration of class H and white cement," *Cement and Concrete Research*, vol. 40, no. 6, pp. 845–850, Jun. 2010.

[23] N. C. Ludwig, "Portland cements and their application in the oil industry," *American Petroleum Institute*, vol. 53, pp. 183–209, 1953.

[24] "Recommendation 10A for cements specifications and materials for well cementing," *American Petroleum Institute*, 23rd Edition, 2002.

[25] A. Salehpour, "Cementing casing in deepwater a balencing act," *Offshore Magazine*, vol. 68, no. 10, 2008.

[26] A. Duguid, "The effect of carbonic acid on well cements as identified through lab and field studies," *Society of Petroleum Engineers*, no. 119504, 2008.

[27] S. Ridha, S. Irawan, and B. Ariwahjoedi, "Strength prediction of Class G oilwell cement during early ages by electrical impedance," *Submitted to Journal of Petroleum Exploration and Production Technology*, 2012.

[28] J. Byfors, *Plain concrete at early ages*. Stockholm: Swedish Cement and Concrete Research Institute, 1980.

[29] D. P. H. Hasselman and R. M. Fulrath, "Effect of small fraction of spherical porosity on elastic moduli of glass," *Journal of the American Ceramic Society*, vol. 47, no. 1, pp. 52–53, 1964.

[30] C. M. Hansson, "Concrete: The advanced material of the 21st century," *Metallurgical and Materials Transactions B*, vol. 26, no. 3, pp. 417–437, 1995.

[31] J. Jutten and S. L. Morriss, "Cement job evaluation," in *Well Cementing*, E. B. Nelson, Ed. New York: Elsevier, 1990.

[32] M. P. Tixier, R. P. Alger, and D. R. Tanguy, "New developments in induction and sonic logging," *Society of Petroleum Engineers*, no. 1300-G, 1960.

[33] D. May, S. Jacobsen, B. Reynolds, J. Rushing, and L. Swager, "Identifying and correcting for high-resistivity cement effects for cased-hole resistivity-log analysis," *Society of Petroleum Engineers*, no. 100340, Sep. 2006.

[34] F. Rajabipour and J. Weiss, "Electrical conductivity of drying cement paste," *Materials and Structures*, vol. 40, no. 10, pp. 1143–1160, 2007.

[35] P. Gu, P. Xie, Y. Fu, and J. J. Beaudoin, "Microstructural characterization of cementitious materials: Conductivity and impedance methods," *Materials Science of. Concrete IV, The American Ceramic Society*, pp. 201–262, 1995.

[36] W. J. McCarter, "Effects of temperature on conduction and polarization in portland cement mortar," *Journal of the American Ceramic Society*, vol. 78, no. 2, pp. 411–415, 2005.

[37] S. Ridha, S. Irawan, B. Ariwahjoedi, and M. Jasamai, "Conductivity dispersion characteristic of oilwell cement slurry during early hydration," *International Journal of Engineering & Technology*, vol. 10, no. 6, pp. 129–132, 2010.

[38] F. Rajabipor, "Insitu electrical sensing and material health monitoring in concrete structures," *PhD Thesis*, Purdue University, 2006.

[39] S. Torquato, *Random heterogeneous materials: Microstructure and macroscopic properties*. New York: Springer–Verlag, 2002.

[40] W. J. McCarter, S. Garvin, and N. Bouzid, "Impedance measurements on cement paste," *Journal of Materials Science Letters*, vol. 7, no. 10, pp. 1056–1057, 1988.

[41] E. J. Garboczi and D. P. Bentz, "Modelling of the microstructure and transport properties of concrete," *Construction and Building Materials*, vol. 10, no. 5, pp. 293–300, 1996.

[42] J. Zhang and Z. Li, "Application of GEM equation in microstructure characterization of cement-based materials," *Journal of Materials in Civil Engineering*, vol. 21, no. 11, pp. 648–656, 2009.

[43] W. J. McCarter and P. Puyrigaud, "Water content assessment of fresh concrete," in *Proc. of the Institution of Civil Engineers—Structures and Buildings*, 1995, pp. 417–425.

[44] K. A. Snyder, C. Ferraris, N. S. Martys, and E. J. Garboczi, "Using impedance spectroscopy to assess the viability of the rapid chloride test for determining concrete conductivity," *Journal of Research of the National Institute of Standards and Technology*, vol. 105, no. 4, 2000.

[45] N. Neithalath, J. Weiss, and J. Olek, "Characterizing enhanced porosity concrete using electrical impedance to predict acoustic and hydraulic performance," *Cement and Concrete Research*, vol. 36, no. 11, pp. 2074–2085, 2006.

[46] P. J. Tumidajski, A. S. Schumacher, S. Perron, P. Gu, and J. J. Beaudoin, "On the relationship between porosity and electrical resistivity in cementitious systems," *Cement and Concrete Research*, vol. 26, no. 4, pp. 539–544, 1996.

[47] P. J. Tumidajski and B. Lin, "On the validity of the katz-thompson equation for permeabilities in concrete," *Cement and Concrete Composites*, vol. 28, no. 5, pp. 643–647, 1998.

[48] W. J. McCarter, G. Starrs, and T. M. Chrisp, "Electrical conductivity, diffusion, and permeability of portland cement-based mortars," *Cement and Concrete Research*, vol. 30, no. 9, pp. 1395–1400, 2000.

[49] B. J. Christensen, "Microstructure studies of hydrating of Portland cement-based materials using impedance spectroscopy," *PhD Thesis*, Northwestern University, 1993.

[50] P. W. J. Glover, "What is the cementation exponent? A new interpretation," *The Leading Edge, SEG*, 2009.

[51] J. J. Arps, "The effect of temperature on the density and electrical resistivity of sodium chloride solutions," *Petroleum Transactions, AIME*, vol. 198, pp. 327–330, 1953.

[52] E. Hammond and T. D. Robson, "Comparison of electrical properties of various cements and concretes," *The Engineer*, vol. 199, pp. 78–80, Oct. 1955.

[53] S. Panteny, R. Stevens, and C. R. Bowen, "The frequency dependent permittivity and AC conductivity of random electrical networks," *Ferroelectrics*, vol. 319, no. 1, pp. 199–208, Jul. 2005.

[54] J. H. Schon, "Electrical properties of rocks," in *Physical properties of rocks: Fundamentals and principles of petrophysics*, Pergamon, Netherland, 1998.

[55] D. L. Johnson, J. Koplik, and L. M. Schwartz, "New pore-size parameter characterizing transport in porous media," *Physical Review Letters*, vol. 57, no. 20, pp. 2564–2567, 1986.

[56] K. L. Aplin, "Aspirated capacitor measurements of air conductivity and ion mobility spectra," *Review of Scientific Instruments*, vol. 76, no. 10, p. 104501, 2005.

[57] K. R. Backe, O. B. Lile, S. K. Lyomov, and N. U. Science, "Characterizing curing cement slurries by electrical conductivity," *Society of Petroleum Engineers*, no. 74694, 2001.

[58] S. Arrhenius, "On the reaction rate of the inversion of non-refined sugar upon souring," *Z Phys Chem*, vol. 4, pp. 226–248, 1889.

[59] Z. Hashin and S. Shtrikman, "A variational approach to the theory of effective magnetic permeability of multiphase materials," *Journal of Applied Physics*, vol. 33, no. 10, pp. 3125–3131, 1962.

[60] P. W. J. Glover, M. J. Hole, and J. Pous, "A modified Archie's law for two conducting phases," *Earth and Planetary Science Letters*, vol. 180, no. 3–4, pp. 369–383, 2000.

[61] T. C. Powers and T. L. Brownyard, "Studies of the physical properties of hardened portland cement paste," *Journal of American Concrete Institute*, vol. 43, no. 9, pp. 101–132, 1946.

[62] "Recommended practice 10B-2 for testing well cements," *American Petroleum Institute*, 1st Edition, 2005.

[63] B. Nettelblad, B. Ahlen, G. A. Niklasson, and R. M. Holt, "Approximate determination of surface conductivity in porous media," *Journal of Physics D: Applied Physics*, vol. 28, no. 10, pp. 2037–2045, 1995.

[64] B. J. Christensen, T. O. Mason, and H. M. Jennings, "Comparison of measured and calculated permeabilities for hardened cement pastes," *Cement and Concrete Research*, vol. 26, no. 9, pp. 1325–1334, 1996.

[65] A. J. Katz and A. H. Thompson, "Prediction of rock electrical conductivity from mercury injection measurements," *Journal of Geophysical Research*, vol. 92, no. B1, pp. 599–607, 1987.

[66] A. S. El-Dieb and R. D. Hooton, "Evaluation of the Katz-Thompson model for estimating the water permeability of cement-based materials from mercury intrusion porosimetry data," *Cement and Concrete Research*, vol. 24, no. 3, pp. 443–455, 1994.

[67] M. S. Sumanasooriya and N. Neithalath, "Pore structure features of pervious concretes proportioned for desired porosities and their performance prediction," *Cement and Concrete Composites*, vol. 33, no. 8, pp. 778–787, 2011.

[68] M. Y. Balshin, "Relation of mechanical properties of powder metals and their porosity and the ultimate properties of porous metal-ceramic materials," *Doklady Akadimi Science*, vol. 67, no. 5, pp. 831–834, 1949.

[69] E. Ryshkewitch, "Compression strength of porous sintered alumina and zirconia," *Journal of the American Ceramic Society*, vol. 36, no. 2, pp. 65–68, 1953.

[70] K. K. Schiller, "Strength of porous materials," *Cement and Concrete Research*, vol. 1, no. 4, pp. 419–422, 1971.

[71] L. Li and M. Aubertin, "A general relationships between porosity and uniaxial strength of engineering materials," *Canadian Journal of Civil Engineering*, vol. 30, no. 4, pp. 644–658, 2003.

[72] J. Zhang, "Microstructure study of cementitious materials using resistivity measurement," *PhD Thesis*, The Hong Kong University of Science and Technology, 2008.

[73] *Autolab-500 manual book.* New England Research Inc, 2007.

[74] S. J. Ford, T. O. Mason, B. J. Christensen, R. T. Coverdale, H. M. Jennings, and E. J. Garboczi, "Electrode configurations and impedance spectra of cement pastes," *Journal of Materials Science*, vol. 30, no. 5, pp. 1217–1224, 1995.

[75] E. W. Washburn, "The dynamics of capillary flow," *Physical Review*, vol. 17, no. 3, pp. 273–283, 1921.

[76] "Recommended practice 40 for core analysis," *American Petroleum Institute*, 2nd Edition, 1998.

[77] L. J. Klinkenberg, "The permeability of porous media to liquids and gases," *American Petroleum Institute, Drilling and Productions Practices*, pp. 200–213, 1941.

[78] M. Mehran, "Low frequency conductivity dispersion in clay-water-electrolyte systems," *Clays and Clay Minerals*, vol. 25, pp. 39–48, 1977.

[79] K. van Breugel, "Numerical simulation of hydration and microstructural development in hardening cement-based materials (I) Theory," *Cement and Concrete Research*, vol. 25, no. 2, pp. 319–331, 1995.

[80] J. D. Shane, T. O. Mason, H. M. Jennings, E. J. Garboczi, and D. P. Bentz, "Effect of the interfacial transition zone on the conductivity of Portland Cement Mortars.pdf," *Journal of the American Ceramic Society*, vol. 83, no. 5, pp. 1137–1144, 2000.

[81] R. P. Ewing and A. G. Hunt, "Dependence of the electrical conductivity on saturation in real porous media," *Vadose Zone Journal*, vol. 5, no. 2, pp. 731–741, 2006.

[82] C. Galle, "Effect of drying on cement-based materials pore structure as identified by mercury intrusion porosimetry: A comparative study between oven- , vacuum- , and freeze-drying," *Cement and Concrete Research*, vol. 31, no. 10, pp. 1467–1477, 2001.

[83] S. Appleby and A. Wilson, "Permeability and suction in setting cement," *Chemical Engineering Science*, vol. 51, no. 2, pp. 251–267, 1996.

[84] S. Ridha, S. Irawan, and B. Ariwahjoedi, "Microstructure parameter estimation in permeability calculation of well cement during early hydration by a simple particle expansion model," in *2nd National Postgraduate Conference*, 2011, pp. 1–5.

[85] B. K. Nyame and J. M. Illston, "Relationships between permeability and pore structure of hardened cement paste," *Magazine of Concrete Research*, vol. 33, no. 116, pp. 139–146, 1981.

[86] Y. Bernabe, "The transport properties of networks of cracks and pores," *Journal of Geophysical Research*, vol. 100, no. B3, pp. 4231–4241, 1995.

[87] E. Walker and P. W. J. Glover, "Permeability models of porous media: Characteristic length scales , scaling constants and time-dependent electrokinetic coupling," *Geophysics*, vol. 75, no. 6, pp. 235–246, 2010.

[88] F. Lin, C. Meyer, "Hydration kinetics modeling of Portland cement considering the effects of curing temperature and applied pressure," *Cement and Concrete Research*, vol. 39, no. 4, pp. 255–265, 2009.

[89] D. P. Bentz, C. J. Haecker, X. P. Feng, and P. E. Stutzman, "Prediction of cement physical properties by virtual testing," in *Fifth International VDZ Congress*, 2003, pp. 53–63.

APPENDIX A

DEGREE OF HYDRATION CALCULATION

Appendix A provides calculations of degree of hydration using Byfors equation [28] (Equation 2.1) that related to the amount of strength achieved to that of the total (maximum) strength at completed hydration. The maximum strength was obtained by assuming that a complete hydration occurred at zero porosity. Figures A.1 to A.4 present the calculated degree of hydration at different curing conditions and at different water cement ratios (w/c). The results show that the calculated degree of hydration increases as a function of hydration time.

The effect of w/c on the degree of hydration during 24 hrs of hydration for all curing conditions is almost similar by which the values at w/c 0.3 is slightly higher than that of w/c 0.4 and the value at w/c 0.4 is slightly higher than that of w/c 0.5. A relatively similar value of degree of hydration during early of hydration is due to the availability of pore water that makes cement further hydrated and, furthermore, initial hydrate network is permeable enough to ensure free flow of water to the unreacted cement particles. However, experimental results have shown that a higher water cement ratio leads to a higher hydration rate after the middle period of hydration of about above 48 hrs of hydration [88].

On the other hand, the effect of elevated temperature on the degree of hydration is clear at which it increases as temperatures increases. In this case, the increasing is due to two factors, first, the degree of hydration increases with the increase in temperature. Second, the density of hydration products at higher temperature is higher, which slows down the permeation of free water through the hydration products [88]. Meanwhile, elevated pressure increases the degree of hydration of oilwell cement, but has only a negligible effect on the pore structure of hydration products when different cement pastes at similar degrees of hydration are compared.

The finding of is important since it implies that the density of the hydration products is not considerably affected by the applied hydrostatic pressure, at least not up to 1000 psi, which is the pressure they used [88].

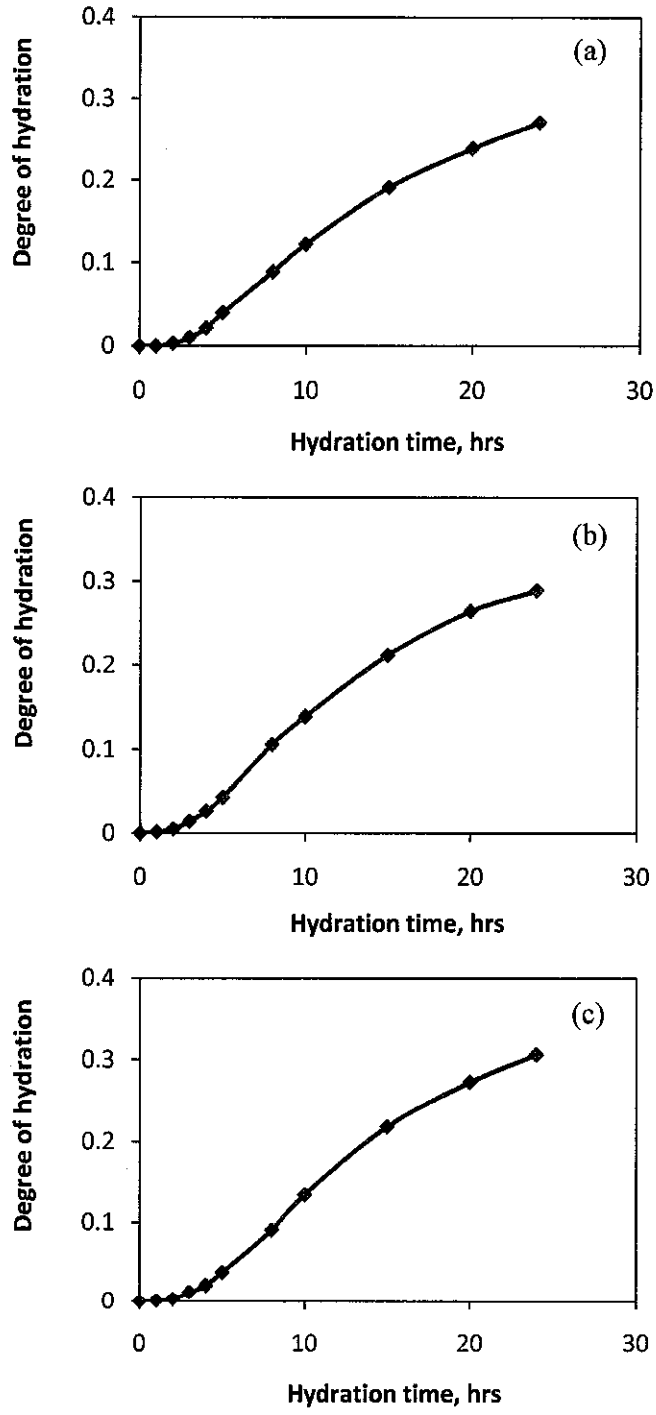

Figure A.1 Degree of hydration calculation of oilwell cement at 25°C & 14.7 psi for w/c at (a) 0.5, (b) 0.4 and (c) 0.3

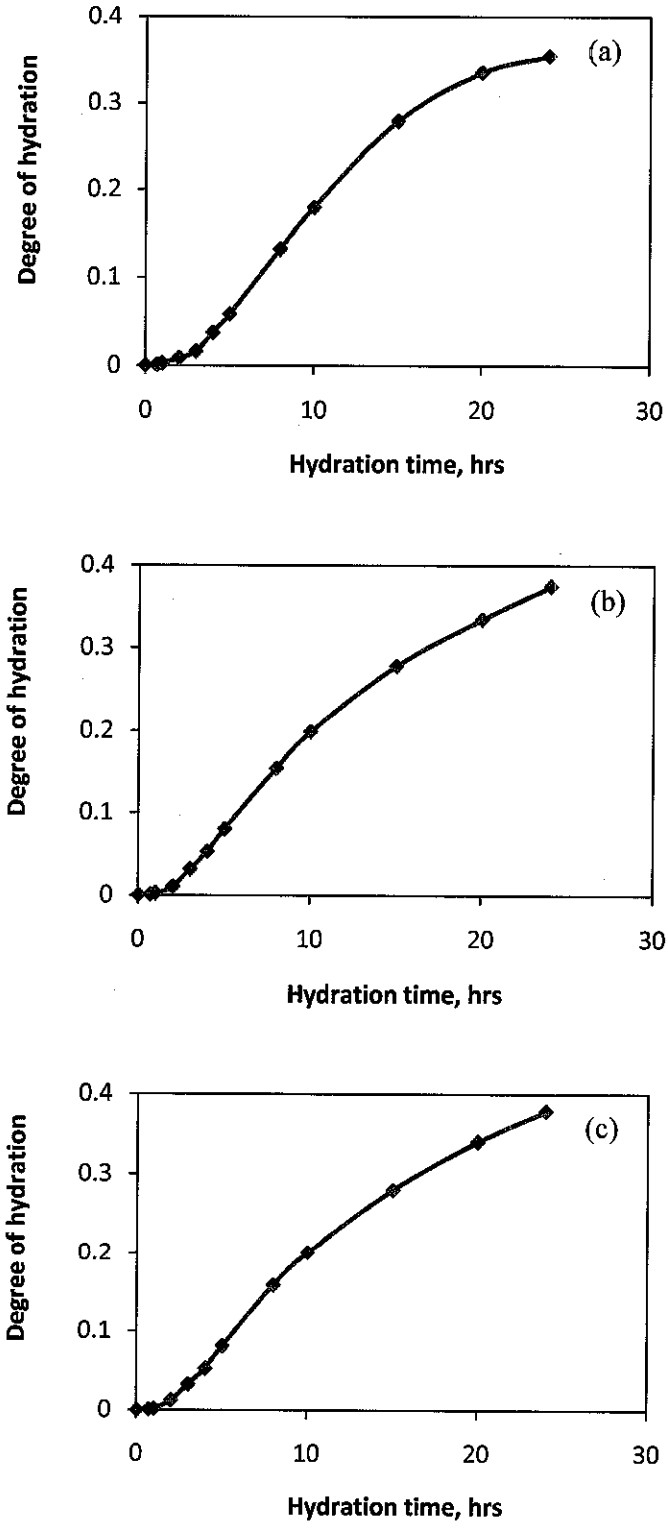

Figure A.2 Degree of hydration calculation of oilwell cement at 40°C & 1500 psi for w/c at (a) 0.5, (b) 0.4 and (c) 0.3

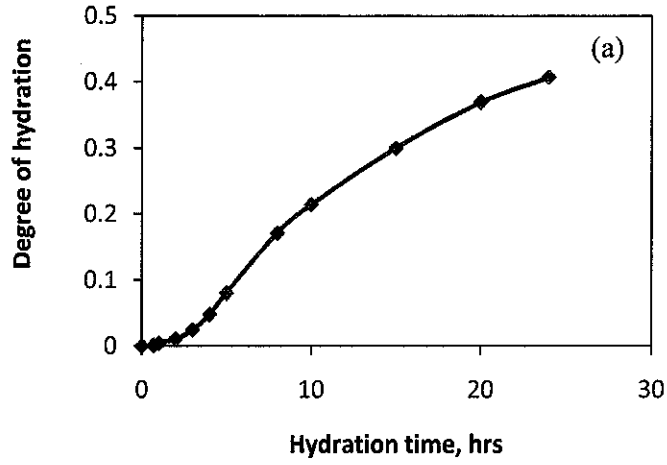

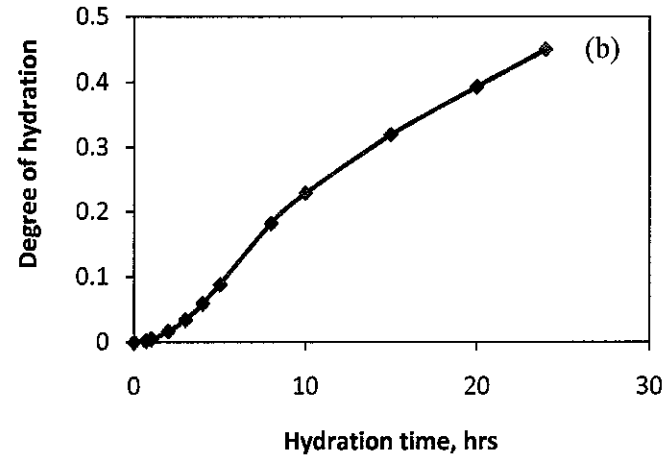

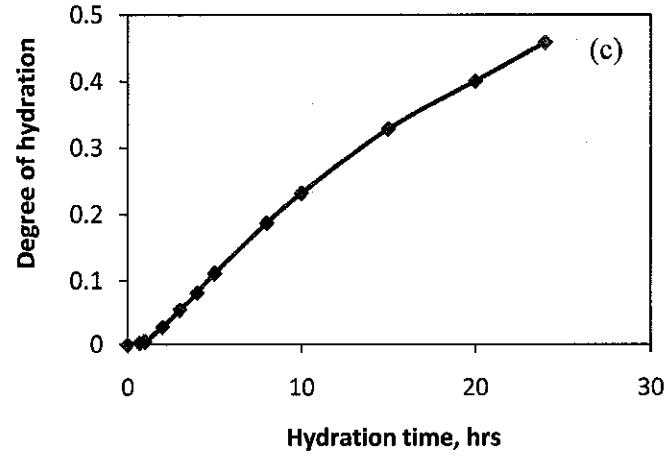

Figure A.3 Degree of hydration calculation of oilwell cement at 65°C & 3000 psi for w/c at (a) 0.5, (b) 0.4 and (c) 0.3

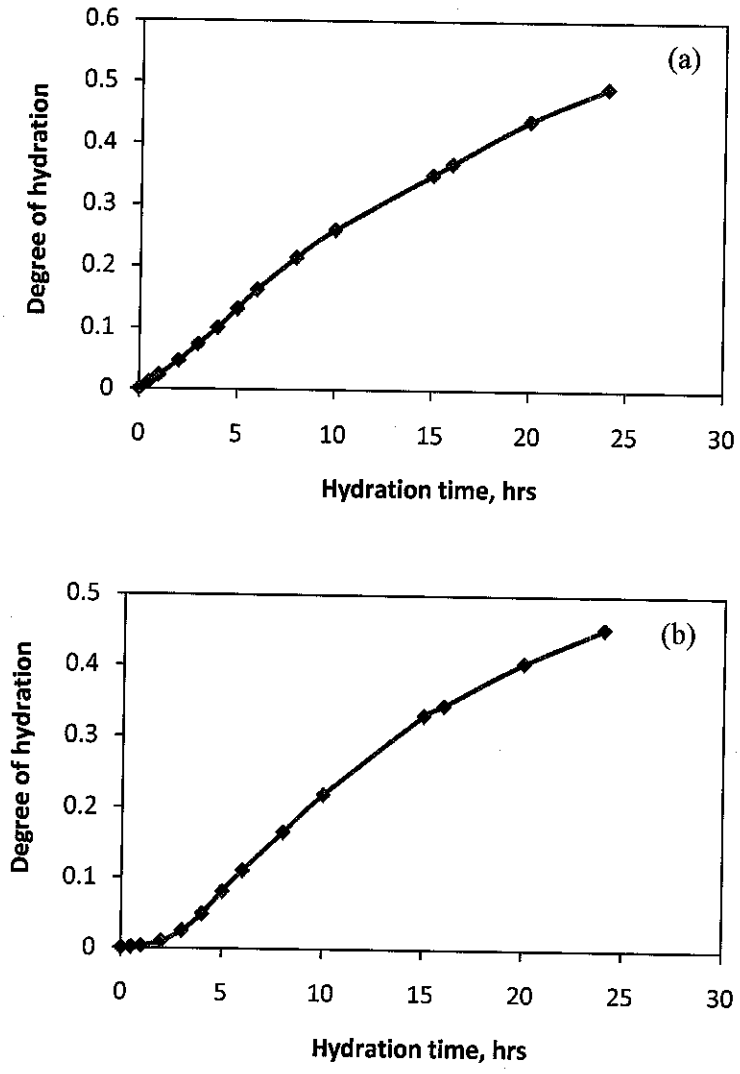

Figure A.4 Degree of hydration calculation of oilwell cement at 70°C & 3000 psi for w/c at (a) 0.25 and (b) 0.55

APPENDIX B

PLOT OF REAL AND IMAGINARY RESISTIVITY

(NYQUIST PLOT)

This appendix presents the results of the Nyquist plot consisting real and imaginary resistivity. The plot found that a two-arc behavior was continually formed especially at the later stages of hydration, indicating the formation of solid hydration products and reduction of pore-filled solution. These arcs are formed due to the different time constants (resistance-capacitance products) in the material as an effect of the different types of electrical polarization due to the electrical excitation. The high frequency arc (small arc) is due to the bulk processes and the low frequency (large arc) is due to the electrode interface effect. In a high frequency region, one particular concern refers to a point at which imaginary impedance has the lowest or approximately zeros value. This point is called the bulk impedance with the frequency named cutoff frequency. The bulk impedance here is dependent on hydration period, water cement ratios and curing conditions.

As can be seen from Figures B.1 to B.4, the bulk resistivity (located at the smallest value of imaginary resistivity) is changing as a function of hydration time. It tends to increase with increasing hydration time. High w/c has lower values of bulk resistivity compared to the small w/c at similar hydration time. This phenomenon occurred due to at higher w/c the pore solution contributes more for conduction process which makes small values of resistivity. Effect of elevated temperatures and pressures on the bulk resistivity is dominant by increasing its values especially at the later stages of hydration.

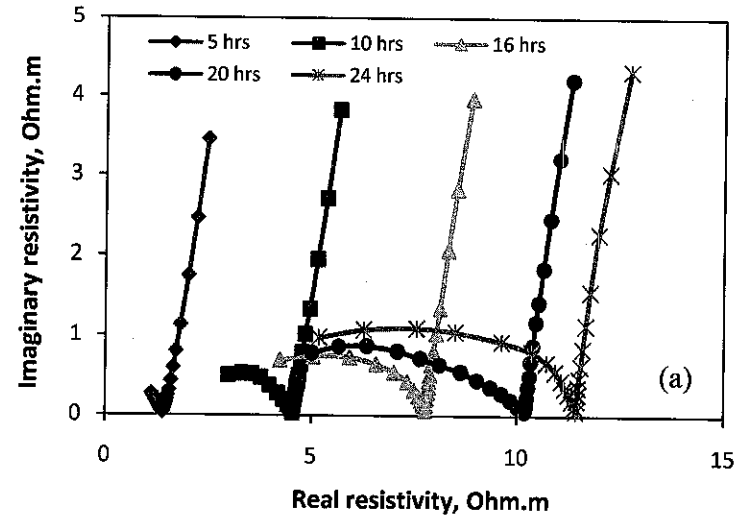

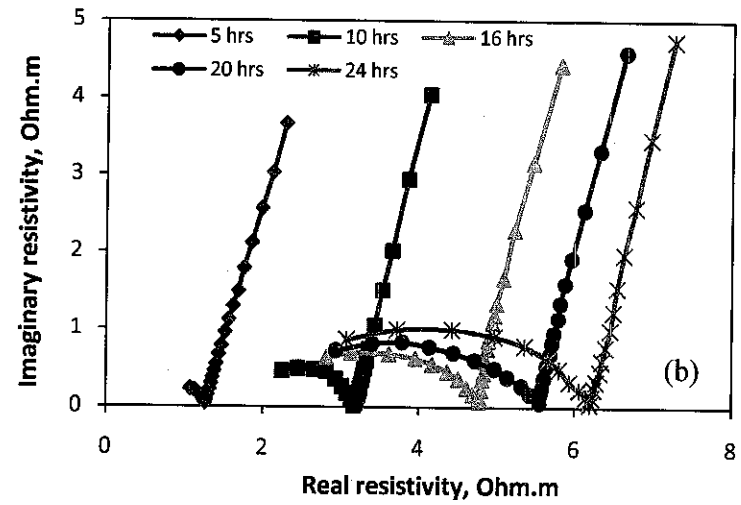

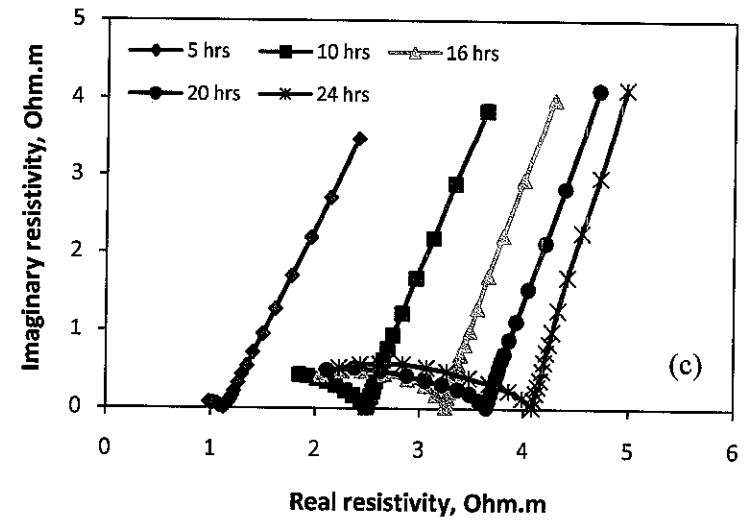

Figure B.1 Plot of real and imaginary resistivity at 25°C & 14.7 psi for w/c at (a) 0.3, (b) 0.4 and (c) 0.5

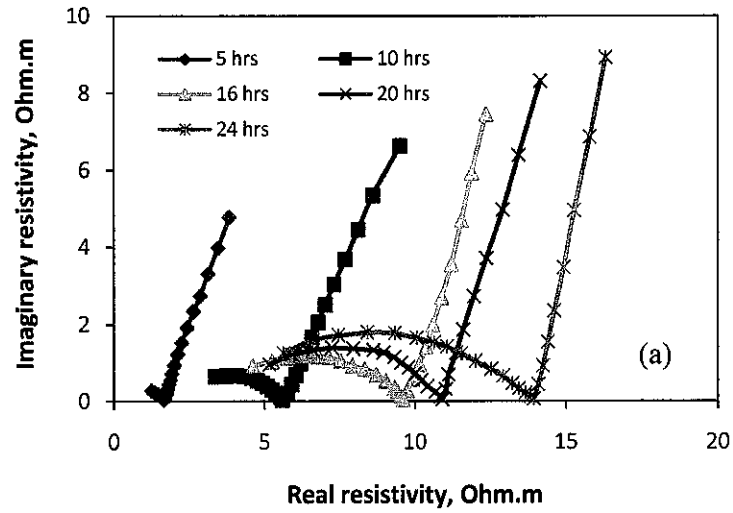

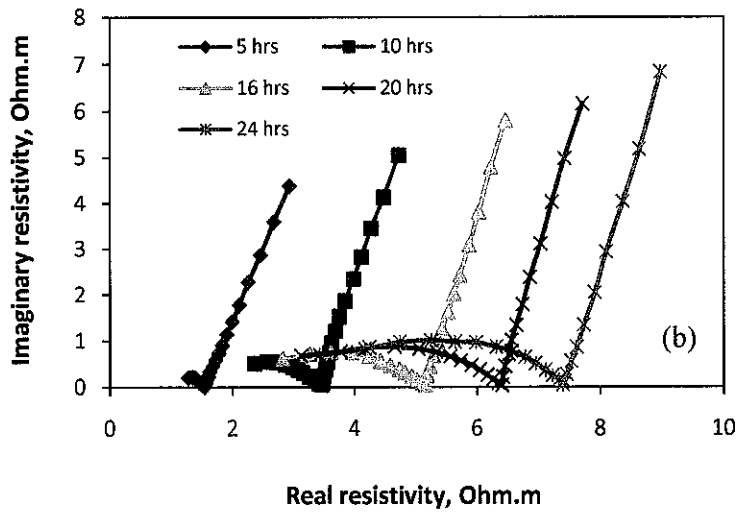

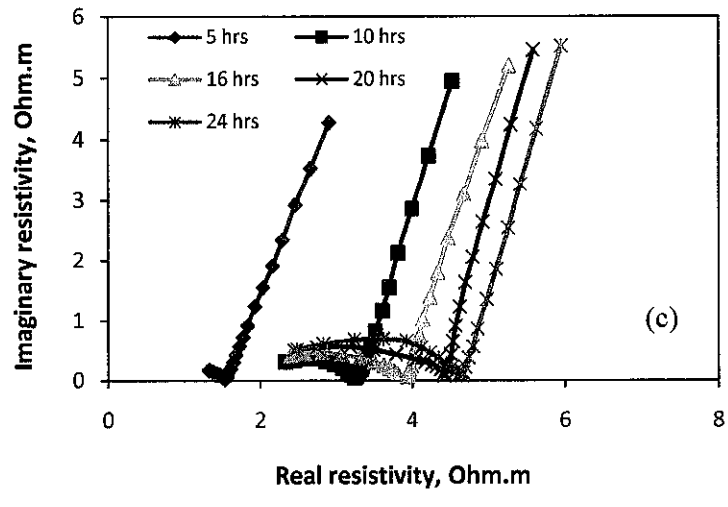

Figure B.2 Plot of real and imaginary resistivity at 40°C & 1500 psi for w/c at (a) 0.3, (b) 0.4 and (c) 0.5

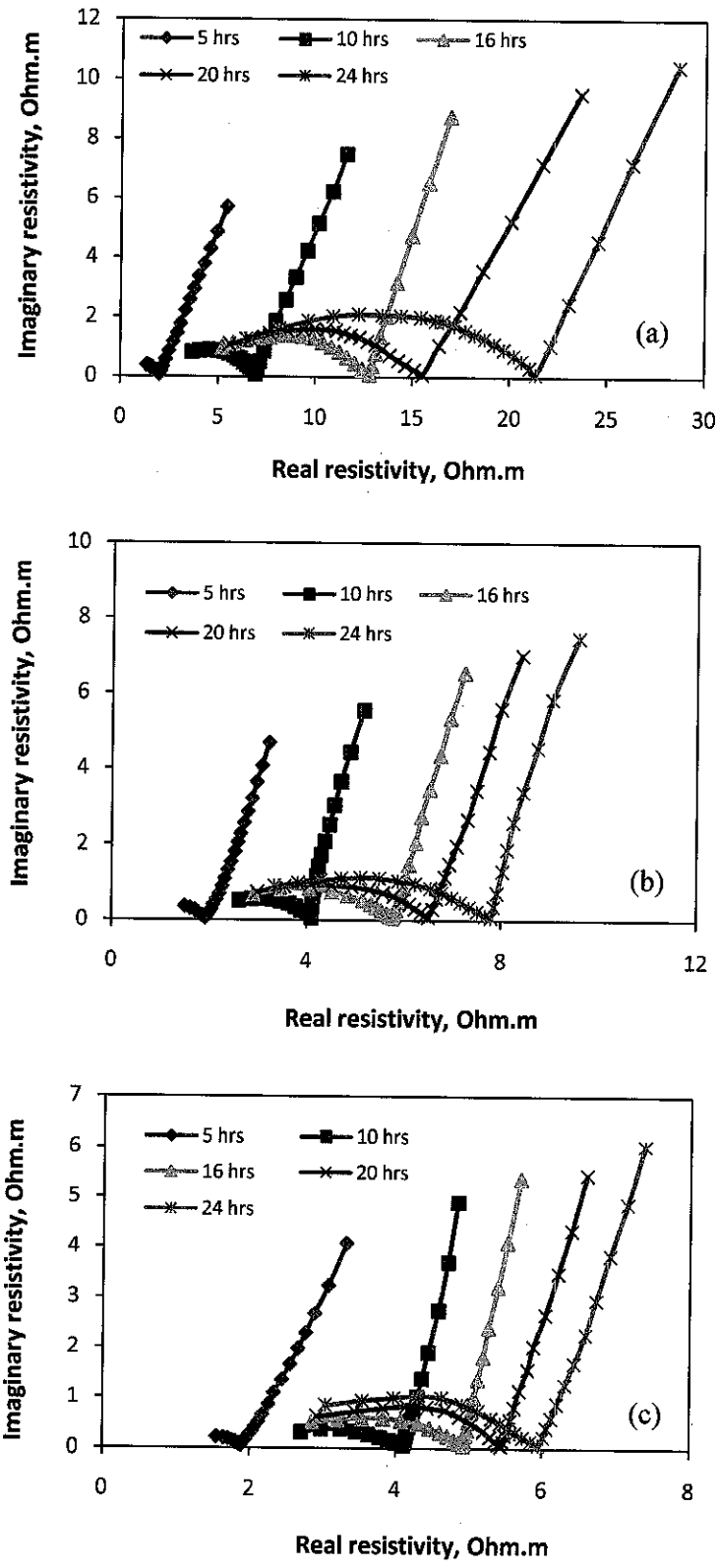

Figure B.3 Plot of real and imaginary resistivity at 65°C & 3000 psi for w/c at (a) 0.3, (b) 0.4 and (c) 0.5

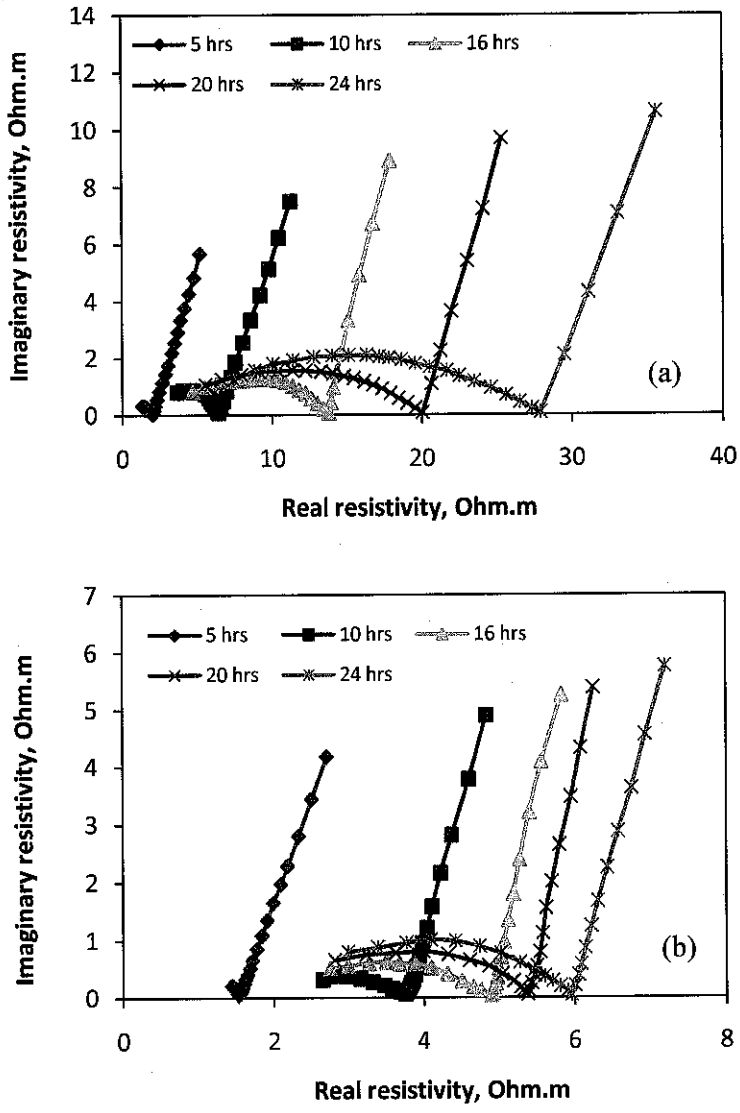

Figure B.4 Plot of real and imaginary resistivity at 70°C & 3000 psi for w/c at (a) 0.25 and (b) 0.55

APPENDIX C

METHOD FOR PORE SOLUTION CONDUCTIVITY PREDICTION

Electrical properties commonly consist of bulk and pore solution conductivities. The latter is experimentally difficult to obtain especially at the latter stages of hydration. It is necessary to squeeze with high pressure for solution to be released from the cement system. Both of these conductivities will produce normalized conductivity. Alternative method for determining pore solution conductivity is by predicting its values based on the concentrations of species ions variety in the pore solution of the well cement as a function of time. In general well cement system, the pore solution is mainly composed on Na^+ and K^+. The concentration of these values can be predicted using numerical cement hydration model that was developed at the National Institute of Standards and Technology (NIST) named Virtual Cement and Concrete Testing Laboratory (VCCTL) and is described in detail by Bentz [89].

The followings are the requirements for pore solution to be analyzed which are the water cement ratio and the content of Na_2O and K_2O in the cement powder. These are input parameters for VCCTL model to estimate the concentration of the three major components (Na^+, OH^- and K^+). The calculation of these parameters is made as a function of hydration time. Given the concentration values, the pore solution conductivity can be calculated using the equation below:

$$\sigma_o = e\Sigma n_i \mu_i$$

where σ_o is pore solution conductivity (S/m), e is electron charge (1.61×10^{-19} C), n_i is density number of ions component i (m^{-3}) (usually taken in the molar concentration and normalized using Avogadro constant), and μ_i is mobility of ions component i ($m^2/V{\cdot}s$).

Table C.1 lists the most ions that are responsible for the charge transport through the cement's pore solution. Table C.2 presents the calculated molar concentration of

Class G oilwell cement using VCCTL model up to 24 hrs of hydration. Table C.2 gives the calculated molar concentration of standard OPC cement up to 400 hrs of hydration.

A comparison of measured pore solution conductivity and those predicted using the above equation is shown in Figures C.1 for sample tested up to 24 hrs of hydration and C.2 for sample up to 400 hrs of hydration. For cement hydration up to 400 hrs, the measured data is taken form literature [4]. It can be seen that a good agreement between experimental observations and model predictions is observed for ages up to 24 hrs and to 400 hrs. In Figure C.2, the deviation between model and experiment for cement at later stages (above 24 hrs) is likely due to the neglect of other mobile ions, and reducing the saturation of the specimen and hence significantly increasing the ionic concentrations.

Table C.1 Major ions mobility in the pore solution of cement paste

Ions component	**Mobility (10^{-7} $m^2/V{\cdot}s$)**
K^+	7.62
Ca^{2+}	6.16
Na^+	5.2
SO_4^{2-}	8.27
Mg^{2+}	5.5
H^+	36.2
OH^-	20.5

Table C.2 Calculated pore water concentration of Class G cement at w/c 0.4 using VCCTL model

Time (hrs)	**Calculated (mol/m^3)**		
	Na^+	**K^+**	**OH^-**
2	31	153	176
4	43	177	255
8	68	194	326
15	82	215	403
24	93	287	479

Table C.3 Calculated pore water concentration of OPC cement at w/c 0.35 using VCCTL model (cement data taken from [4])

Time (hrs)	Calculated (mol/m^3)		
	Na^+	K^+	OH^-
1	25	140	160
6	37	174	250
20	55	219	378
80	68	236	488
400	77	265	584

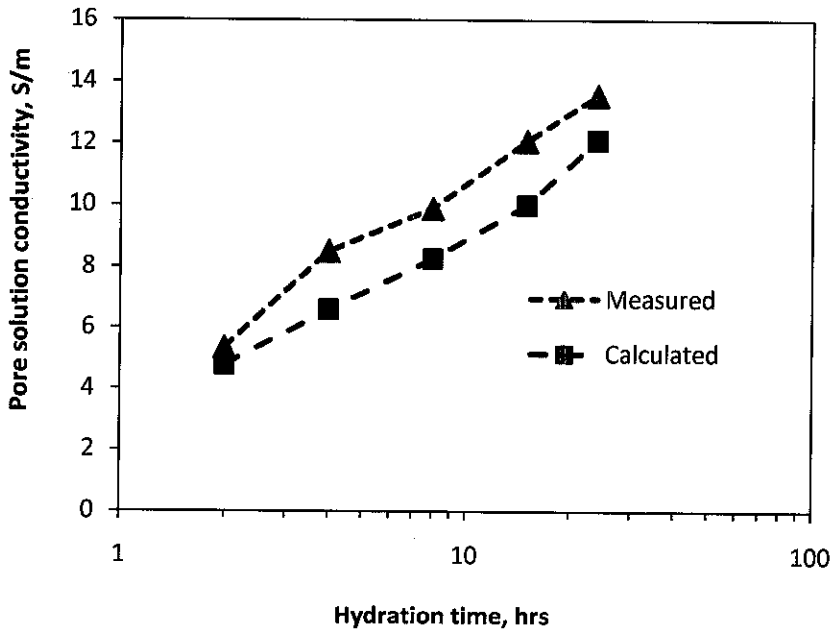

Figure C.1 Pore solution conductivity of Class G cement at w/c 0.4 up to 24 hrs of hydration as obtained by experiment and by prediction based on the alkali content of the cement powder (VCCTL model).

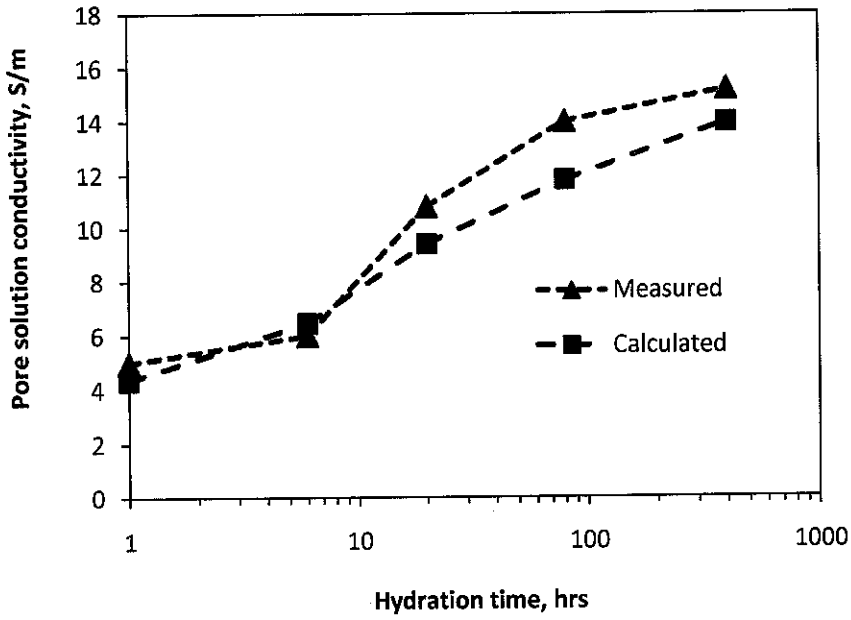

Figure C.2 Pore solution conductivity of OPC cement at w/c 0.35 up to 400 hrs of hydration as experimentally obtained by Christensen [49] and by prediction based on the alkali content of the cement powder (VCCTL model).

APPENDIX D

PLOT OF BULK CONDUCTIVITY AT DIFFERENT W/C AND CURING CONDITIONS

Appendix D details the results of bulk conductivity measurement as a function of hydration time at different curing conditions and water cement ratios. From Figures D.1 to D.4, as expected, a slight increase of bulk conductivity is observed up to about 3 hrs of hydration due to dissolution process of cement ions into mixing water. It then decreases accordingly as cement system proceeds to hardened. The values of bulk conductivity depend on w/c and elevated pressure and temperature. Bulk conductivity decreased as temperature and pressure increased mainly due to the acceleration of hydration process. By that, the connected pore networks start to quickly diminish that barriers the conduction process through the pore solution. Similar to that, high w/c contributes to the increase of bulk conductivity especially at later stages during 24 hrs of hydration.

Due to these influence on bulk conductivity, it suggests that different conductivity responses may be generated at similar hydration periods for sample cured at different w/c and curing temperature and pressure. So, it is important to take into account the effect of these parameters in obtaining representative electrical conductivity data which is, in this case, used to relate to the permeability and strength of Class G oilwell cement.

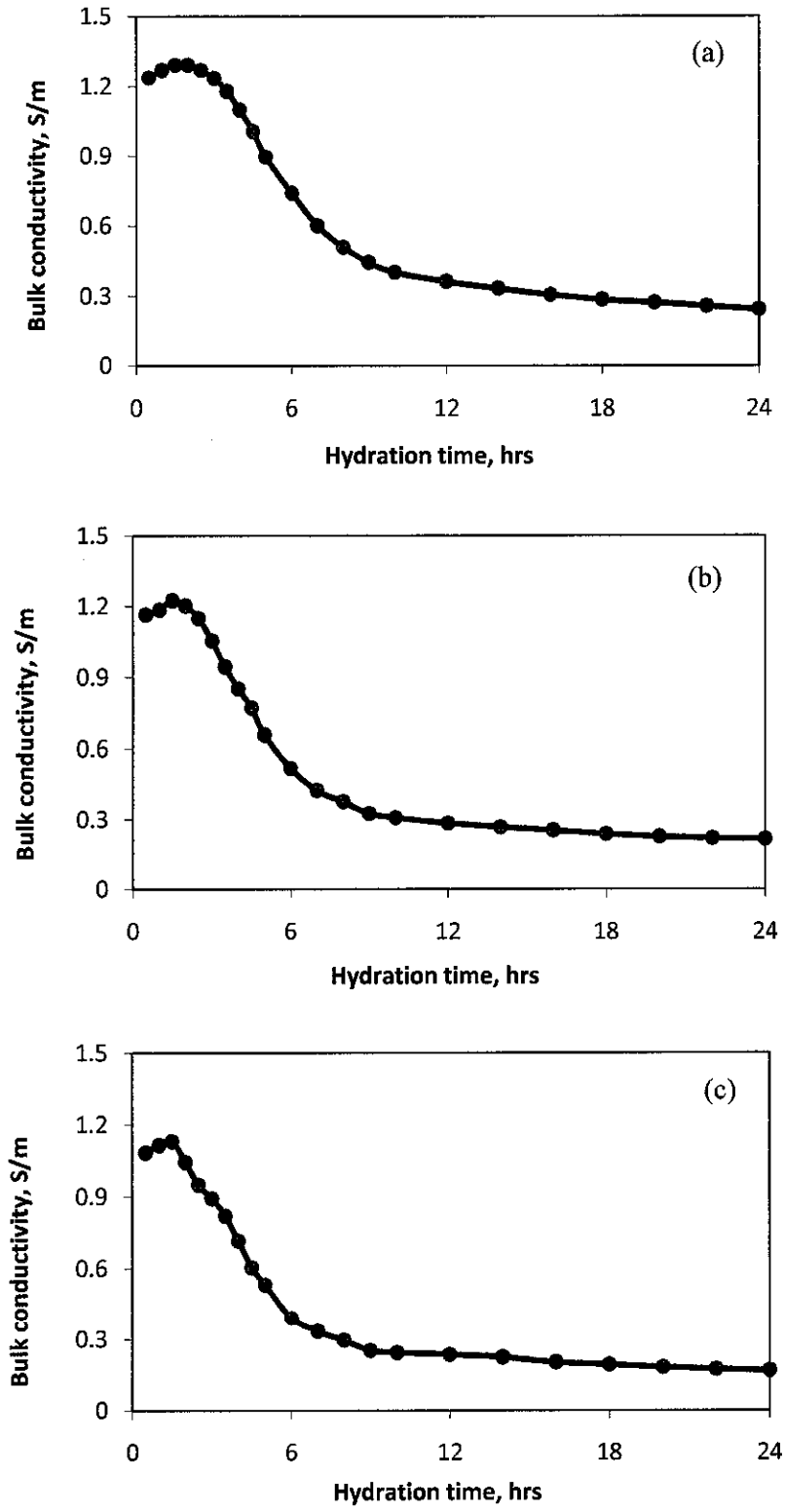

Figure D.1 Plot of bulk conductivity as a function of hydration time of w/c 0.5 at (a) 25°C & 14.7 psi, (b) 40°C & 1500 psi and (c) 65°C & 3000 psi

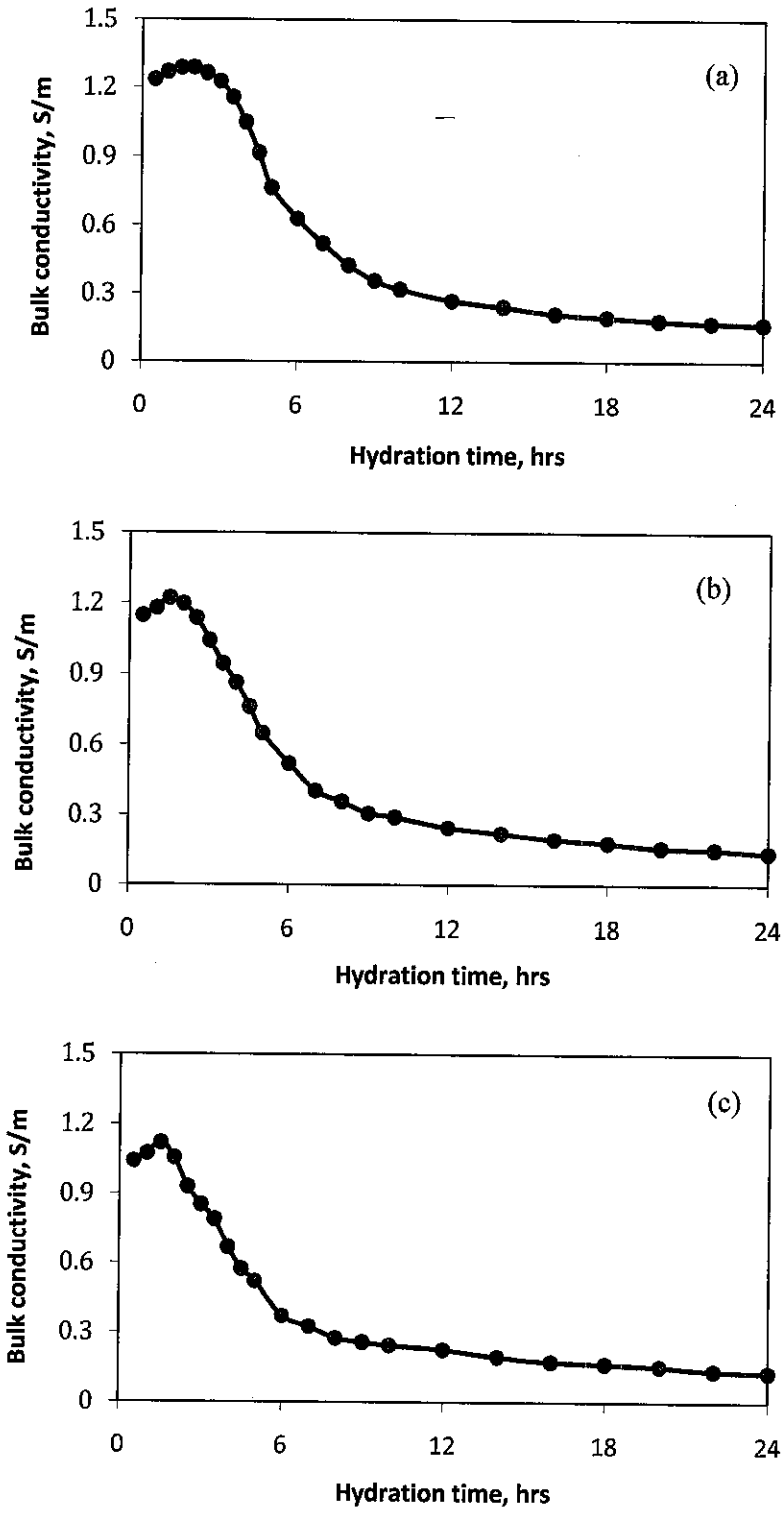

Figure D.2 Plot of bulk conductivity as a function of hydration time of w/c 0.4 at (a) 25°C & 14.7 psi, (b) 40°C & 1500 psi and (c) 65°C & 3000 psi

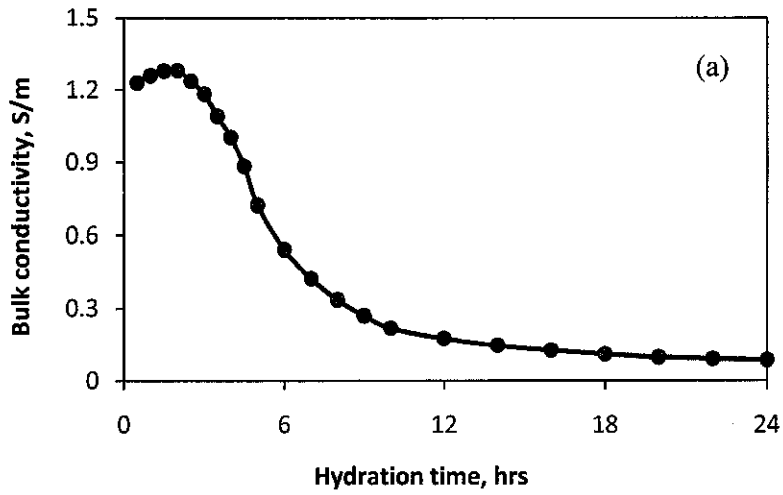

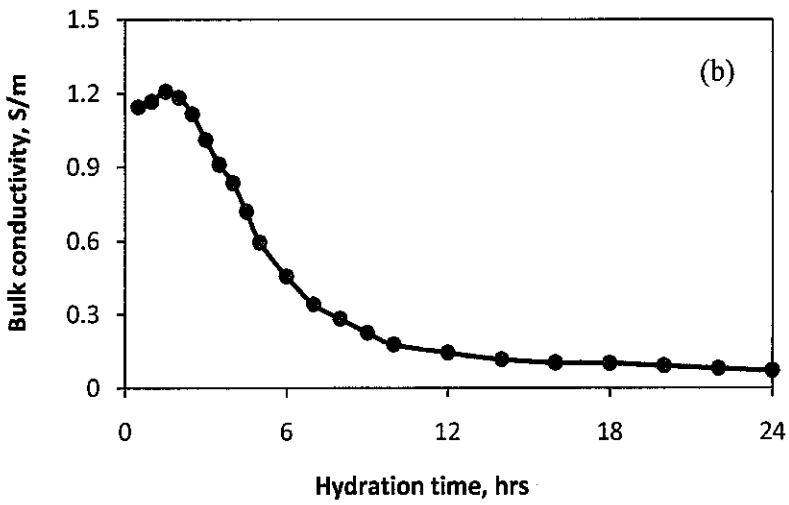

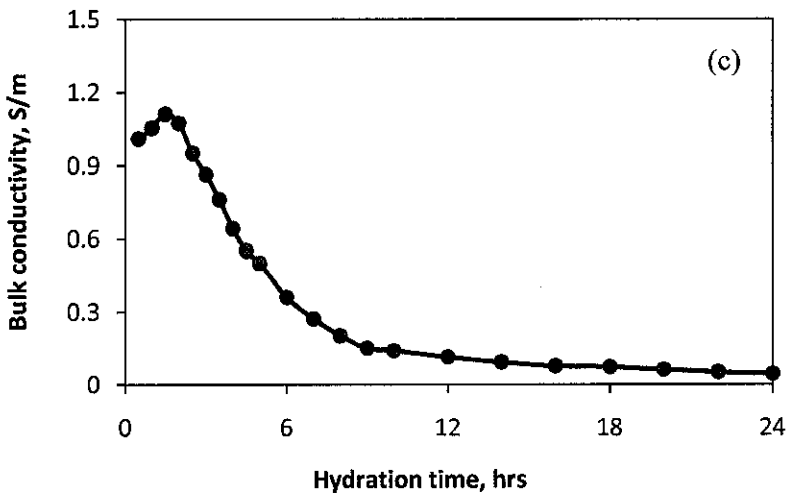

Figure D.3 Plot of bulk conductivity as a function of hydration time of w/c 0.3 at (a) 25°C & 14.7 psi, (b) 40°C & 1500 psi and (c) 65°C & 3000 psi

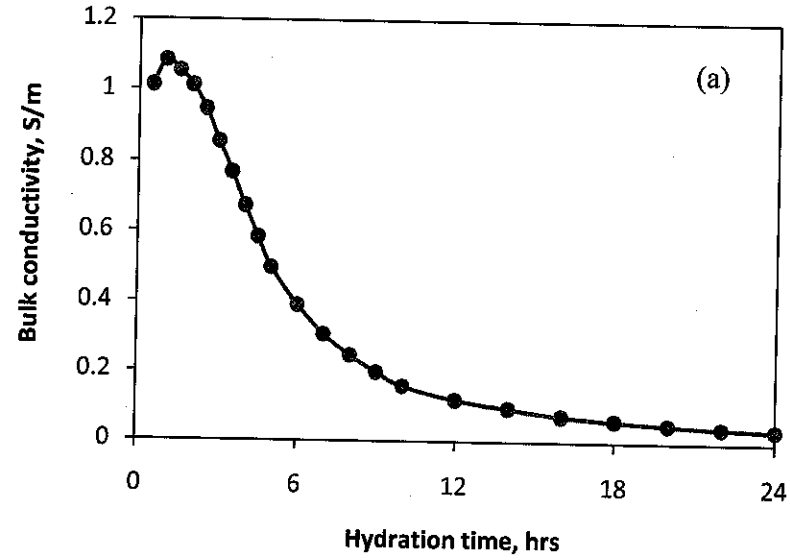

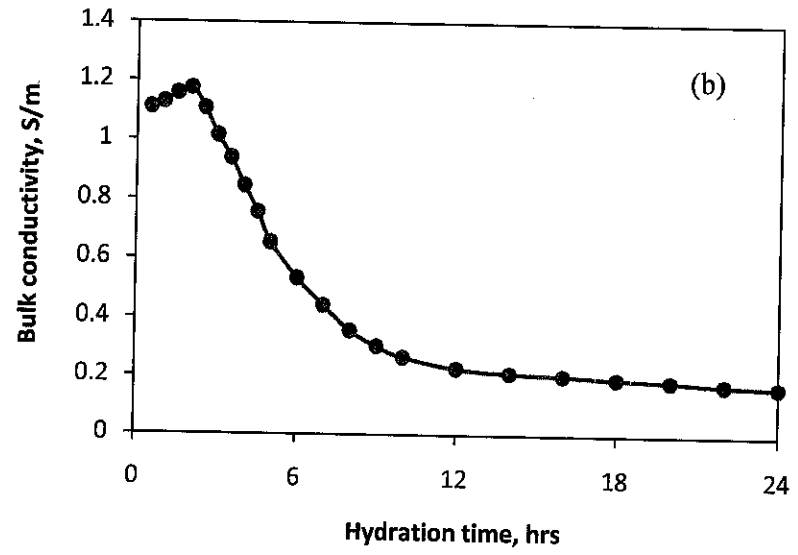

Figure D.4 Plot of bulk conductivity as a function of hydration time at 70°C & 3000 psi for (a) w/c 0.25, and (b) w/c 0.55

APPENDIX E

PLOT OF INDIVIDUAL CONTRIBUTION OF ELEVATED PRESSURE AND TEMPERATURE ON BULK CONDUCTIVITY MEASUREMENT

Appendix E provides the plot of bulk conductivity measurement with constant pressure and varying temperature, and constant temperature and varying pressure. It can be seen from Figures E.1 to E.6 that the contribution of varying temperature on bulk conductivity values at each hydration time is dominant compared to that of varying pressure. In another sentence, the effect of elevated pressure on electrical conductivity was less significant compared to that of elevated temperature.

For a given 10 hrs of hydration of w/c 0.5, the bulk conductivity from 14.7 to 3000 psi is shifted about 0.0375 S/m compared to that of about 0.1357 S/m for conductivity from 25 to 65°C. For w/c 0.4, the shift of bulk conductivity is about 0.059 S/m from 25 to 65°C at 10 hrs of hydration compared to that of about 0.0064 S/m from 14.7 to 3000 psi. Similar appearance also exhibits for w/c 0.3 at which the shift is about 0.061 S/m from 25 to 65°C and about 0.0116 S/m from 14.7 to 3000 psi. These occurrences are due to the pressure has small contribution for cement to accelerate the hydration process compared to that of elevated temperature.

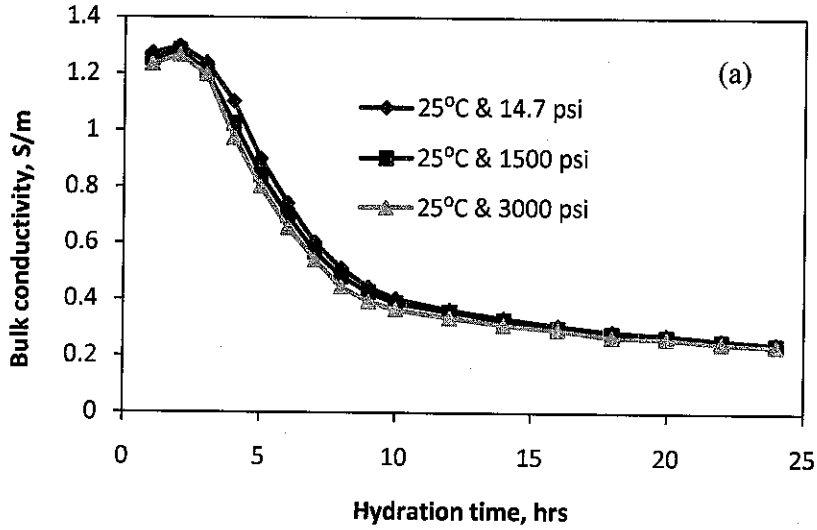

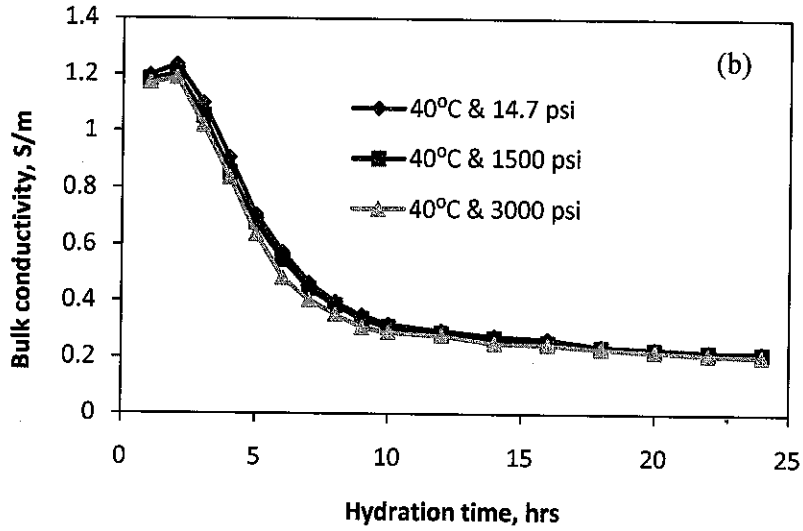

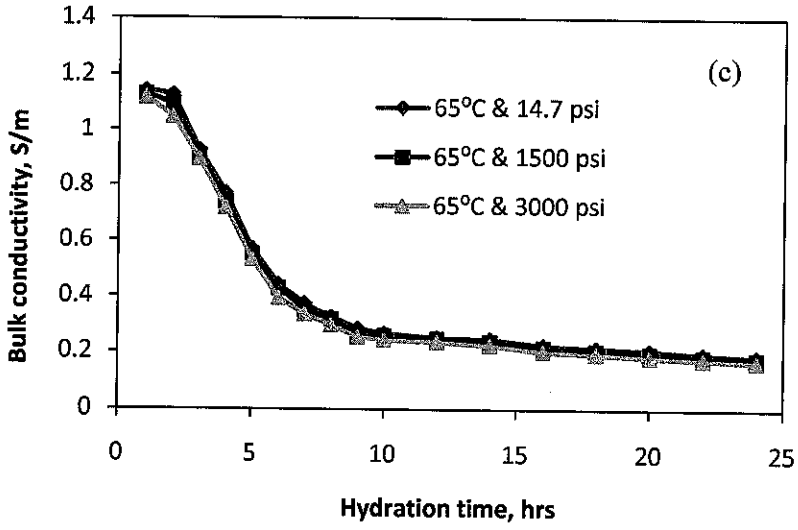

Figure E.1 Effect of varying pressure and constant temperature on bulk conductivity measurement of oilwell cement for w/c 0.5 at (a) 25°C, (b) 40°C, and (c) 65°C

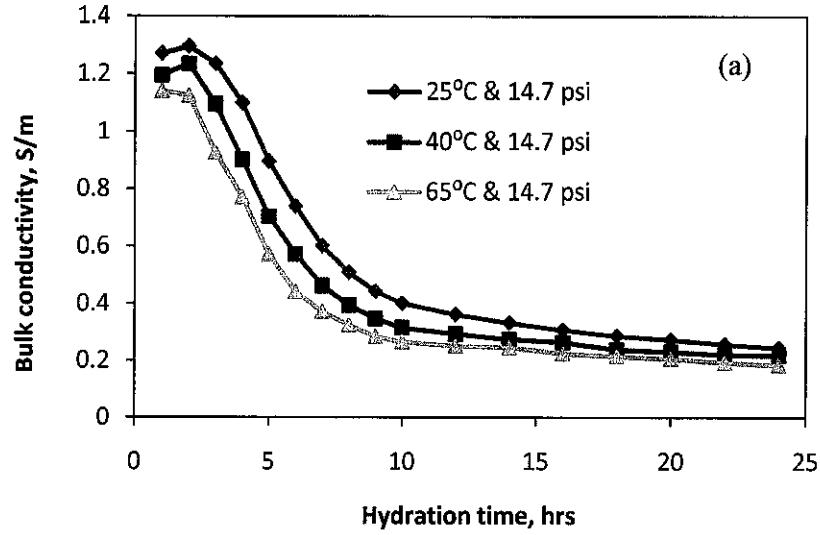

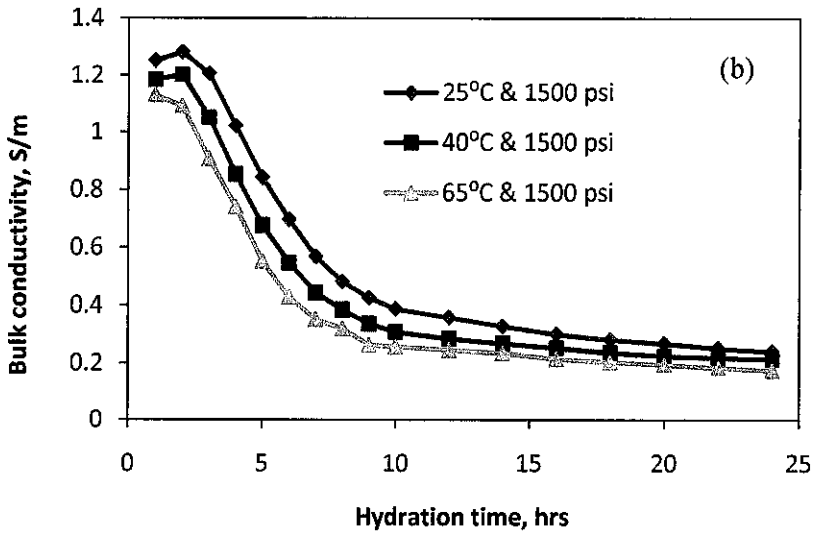

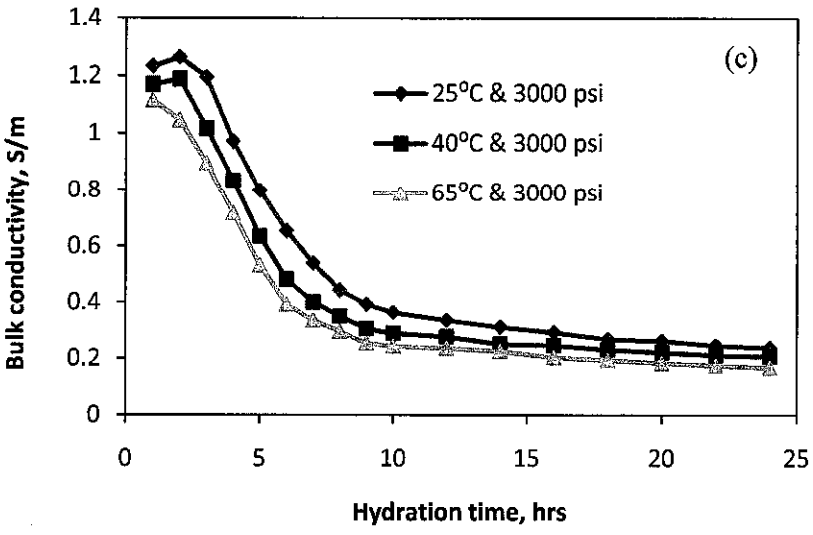

Figure E.2 Effect of varying temperature and constant pressure on bulk conductivity measurement of oilwell cement for w/c 0.5 at (a) 14.7 psi, (b) 1500 psi, and (c) 3000 psi

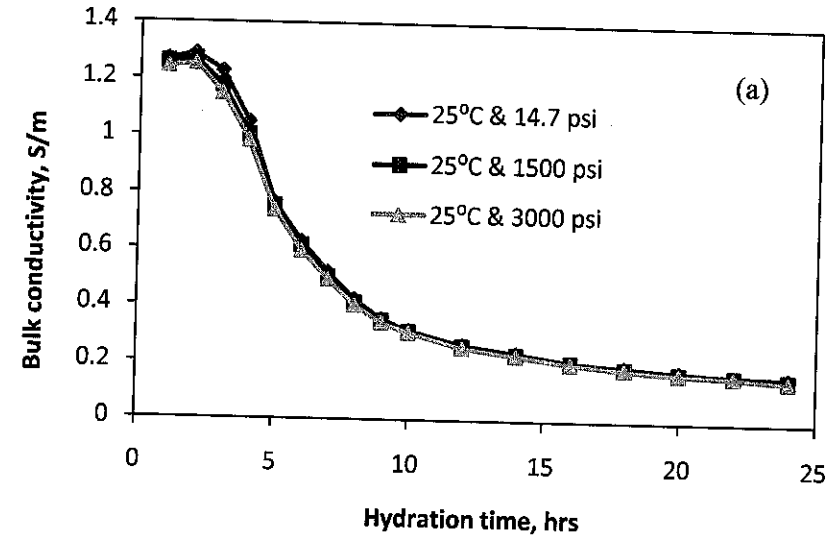

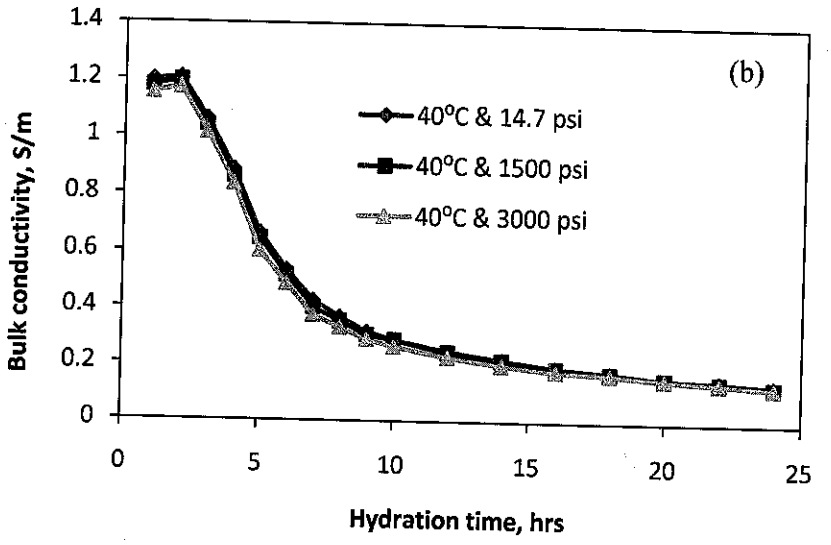

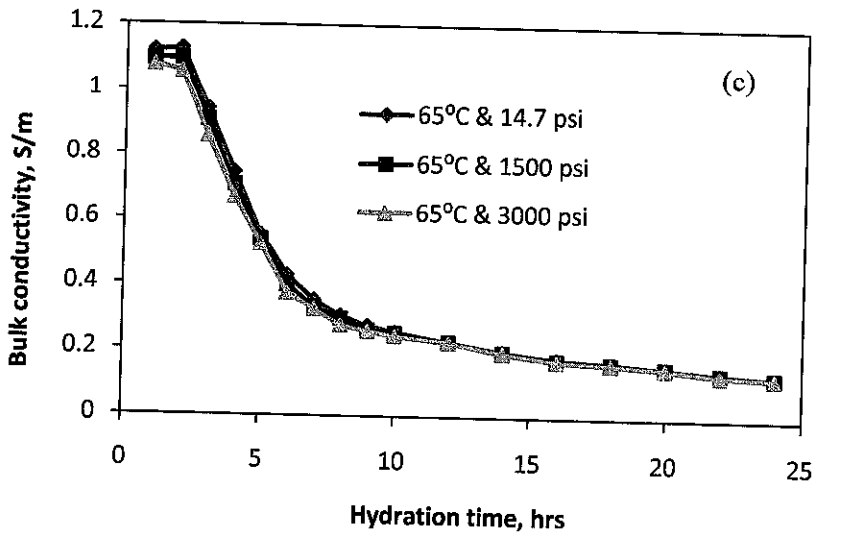

Figure E.3 Effect of varying pressure and constant temperature on bulk conductivity measurement of oilwell cement for w/c 0.4 at (a) 25°C, (b) 40°C, and (c) 65°C

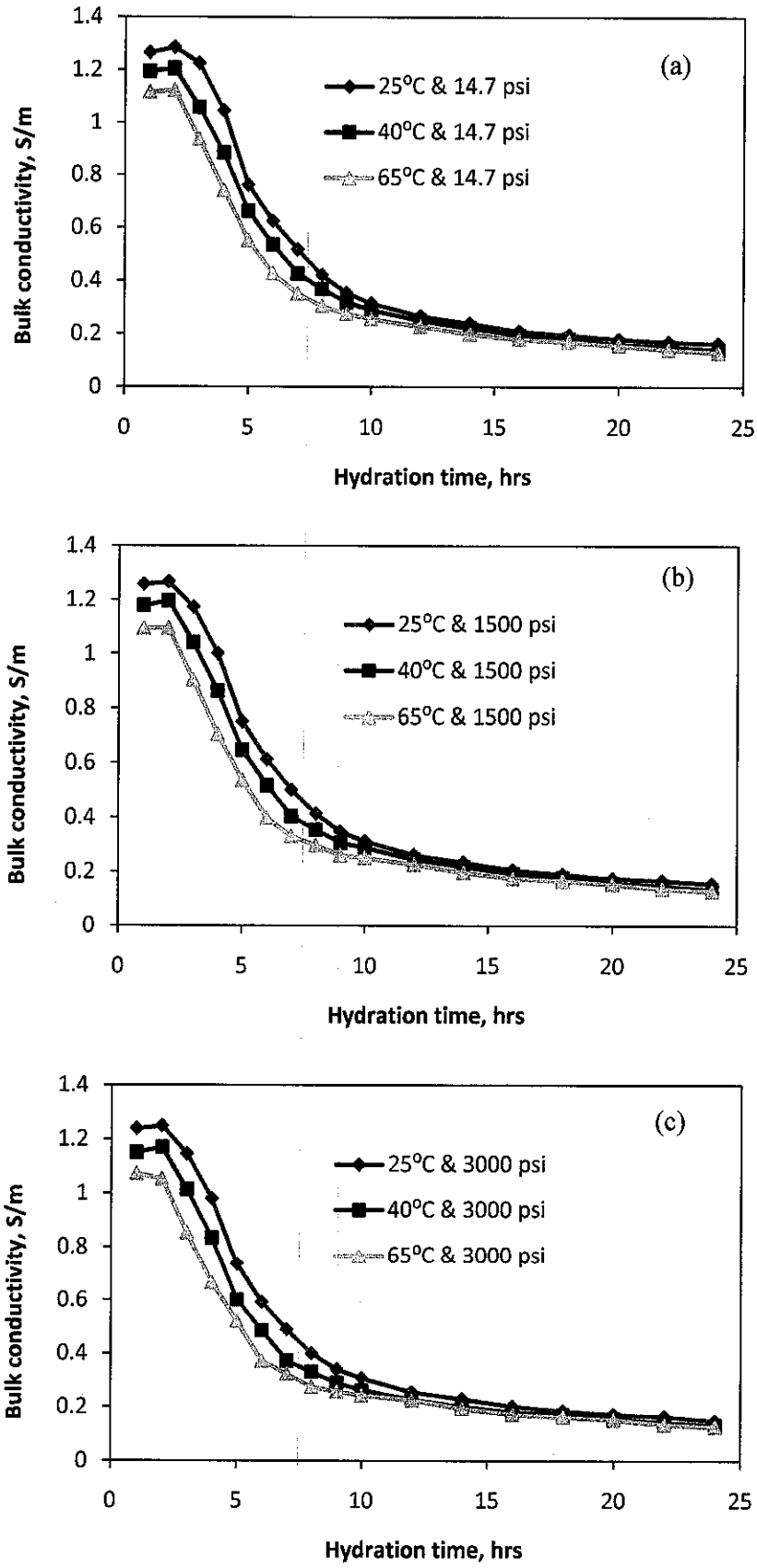

Figure E.4 Effect of varying temperature and constant pressure on bulk conductivity measurement of oilwell cement for w/c 0.4 at (a) 14.7 psi, (b) 1500 psi, and (c) 3000 psi

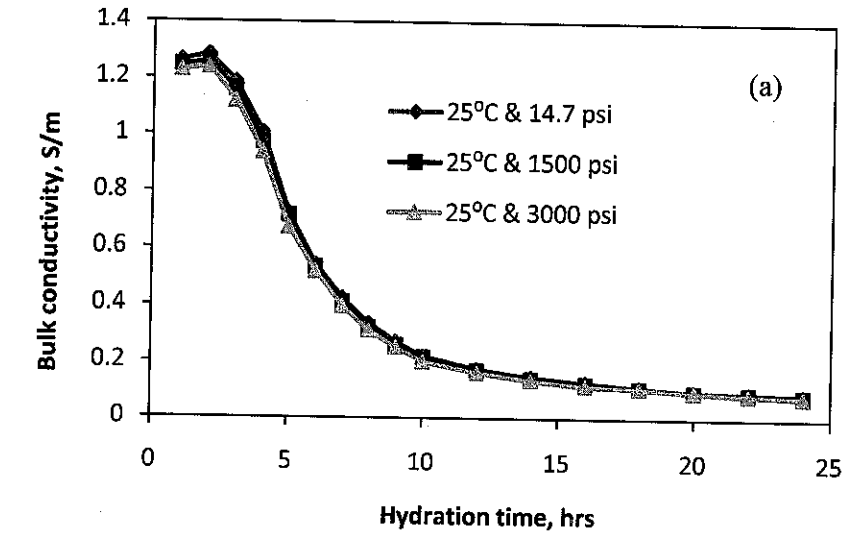

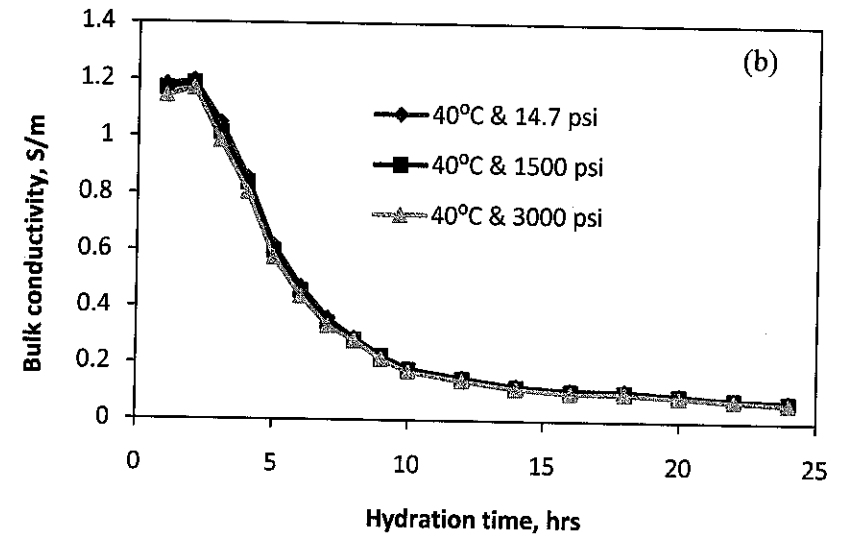

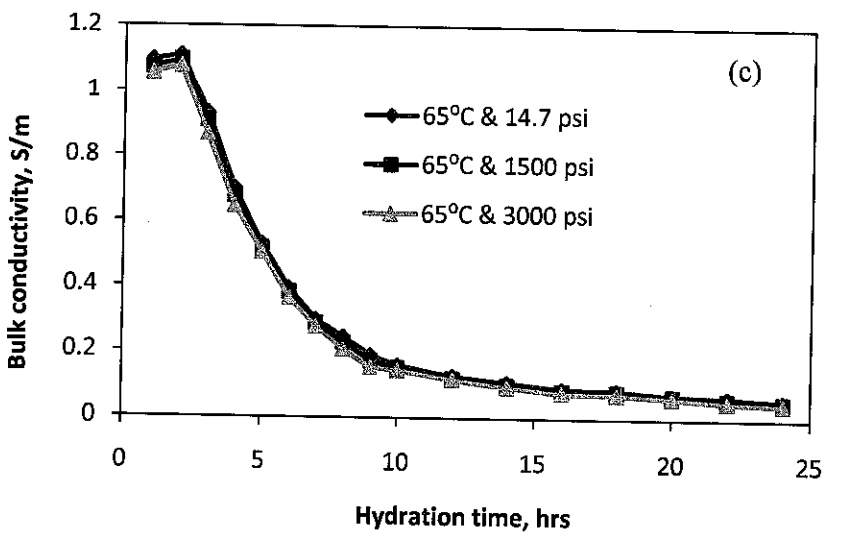

Figure E.5 Effect of varying pressure and constant temperature on bulk conductivity measurement of oilwell cement for w/c 0.3 at (a) 25°C, (b) 40°C, and (c) 65°C

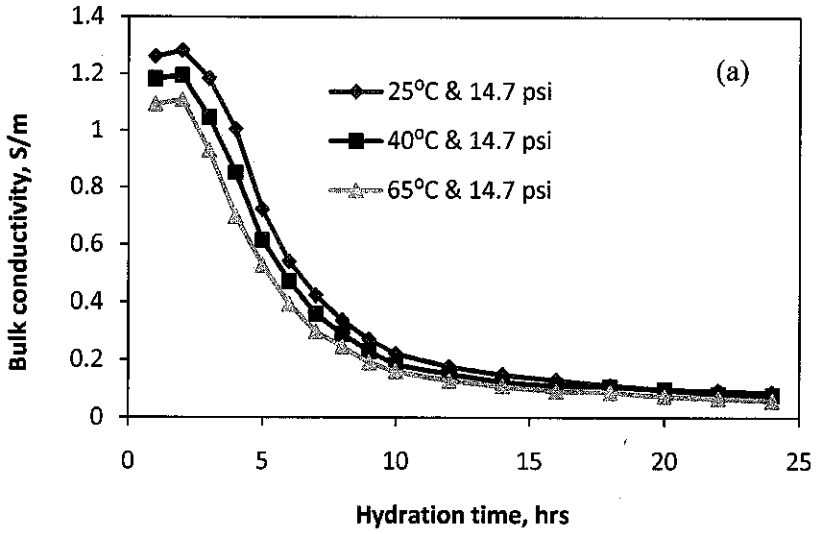

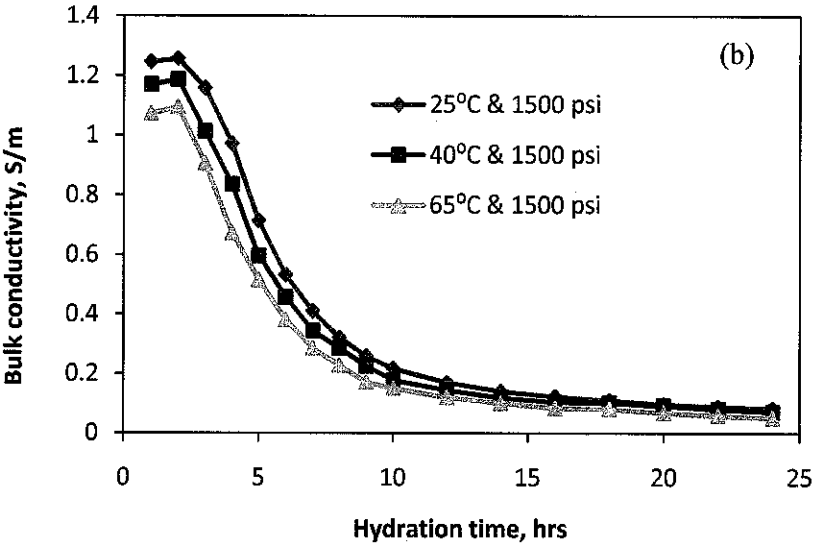

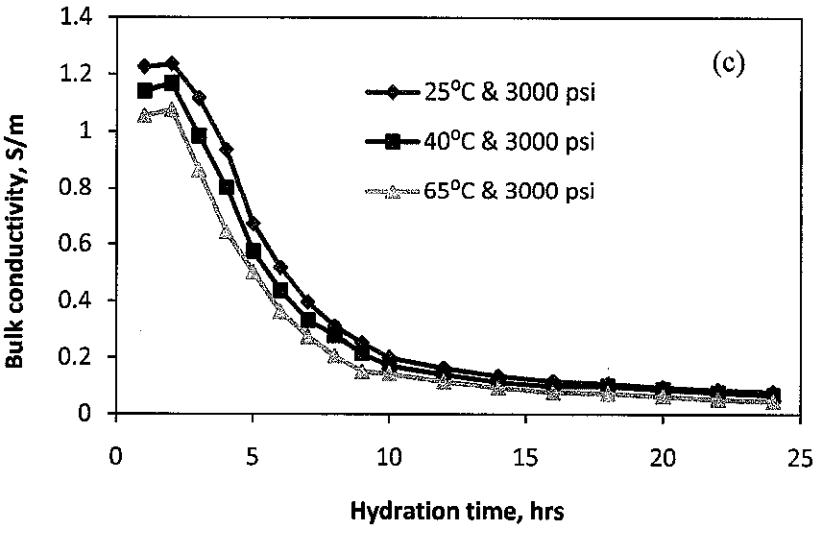

Figure E.6 Effect of varying temperature and constant pressure on bulk conductivity measurement of oilwell cement for w/c 0.3 at (a) 14.7 psi, (b) 1500 psi, and (c) 3000 psi

APPENDIX F

PLOT OF CONDUCTIVITY MODELS AT DIFFERENT W/C AND CURING CONDITIONS

Appendix F presents the plots between normalized conductivity and porosity at different curing conditions and w/c. The measure porosity and normalized conductivity data is then compared to some of conductivity models for composite materials. The porosity increases with normalized conductivity as shown in Figures F.1 to F.3. The profiles of conductivity models to the measured data are relatively similar at different w/c and curing conditions. The values of porosity and normalized conductivity are slightly lower at small w/c and elevated temperature and pressure.

According to Figures F.1 to F.3, most of the conductivity models tend to excessively predict the normalized conductivity especially for parallel, Maxwell, differential effective medium, and Hashin-Shtrikman models which are seemed to have a poor prediction result. The first two models did not consider the contribution of microstructural parameter and only relied on porosity numbers. Furthermore, HS_{ub} model has been developed for the macroscopically isotropic materials and was not directly applicable for a layered composites material. Although DEM and Maxwell model included *d* parameter, but their use was not appropriate for materials in which the inclusions formed large clusters as suggested by Torquato [39].

Among the models, Archie, modified parallel and self-consistency model give an intersectional profile to the experimental measurement at higher porosity. These models provide a qualitative prediction of electrical conductivity behavior. Furthermore, the microstructural parameters of each model should representing the monotonically increasing or decreasing as a function of hydration time.

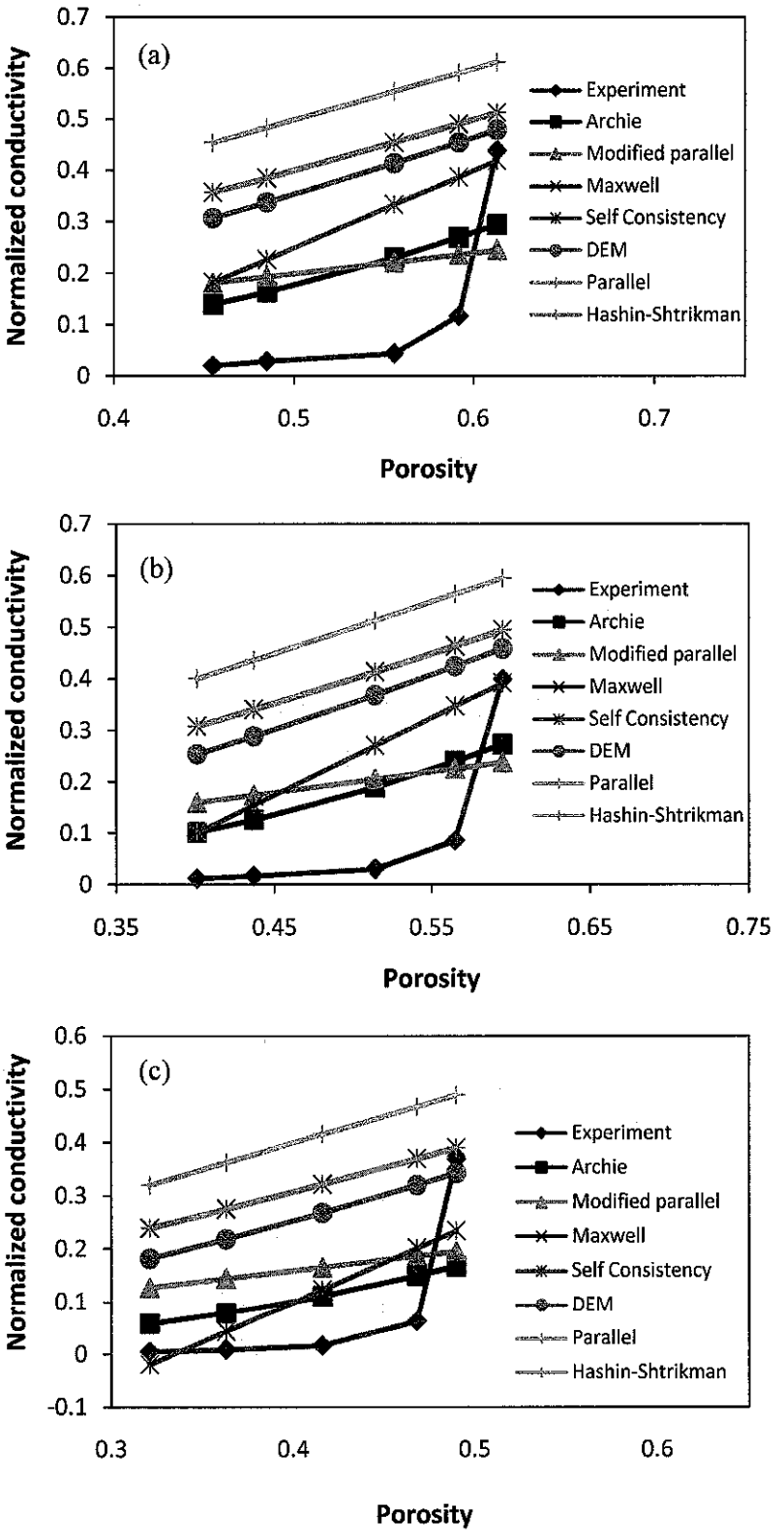

Figure F.1 Plot of conductivity models to experimental data of Class G oilwell cement at 25°C & 14.7 psi for w/c at (a) 0.5, (b) 0.4 and (c) 0.3

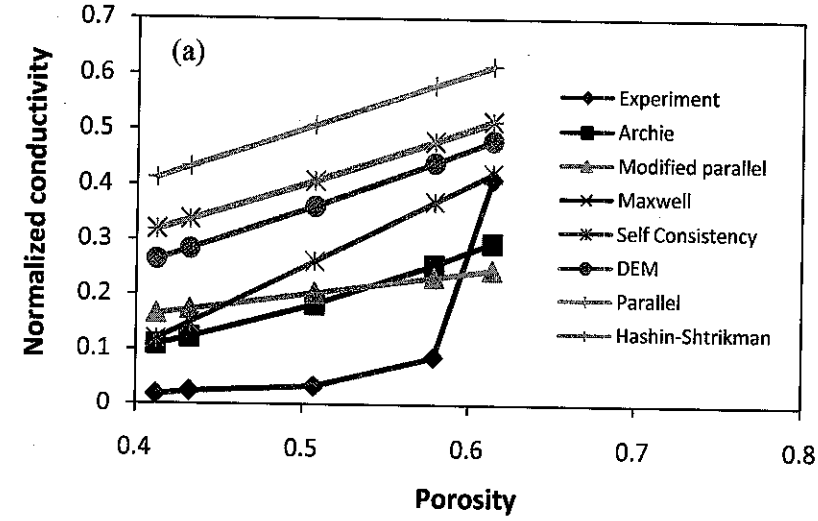

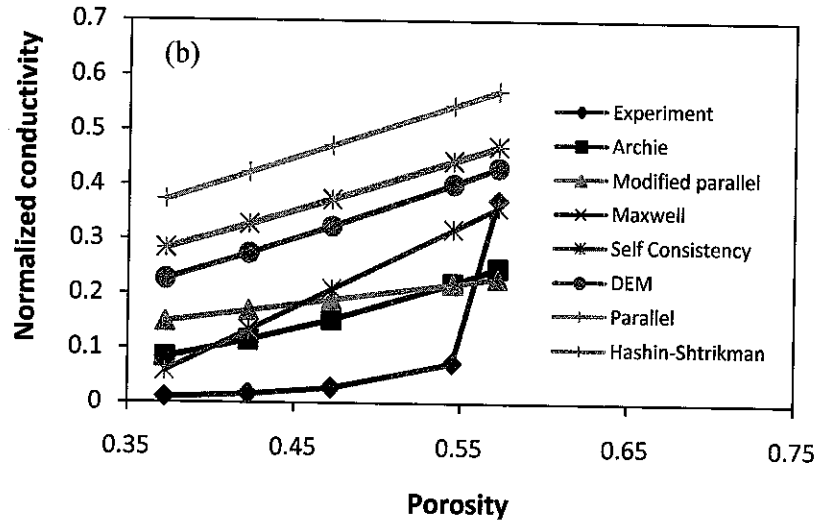

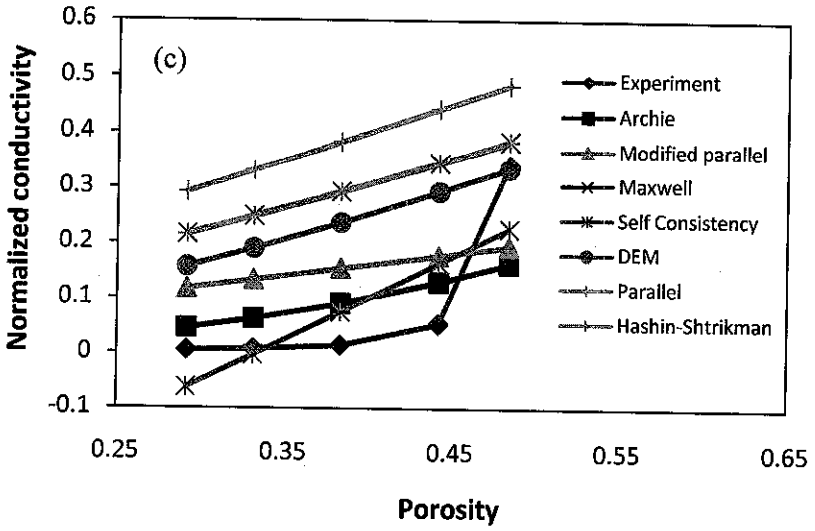

Figure F.2 Plot of conductivity models to experimental data of Class G oilwell cement at 40°C & 1500 psi for w/c at (a) 0.5, (b) 0.4 and (c) 0.3

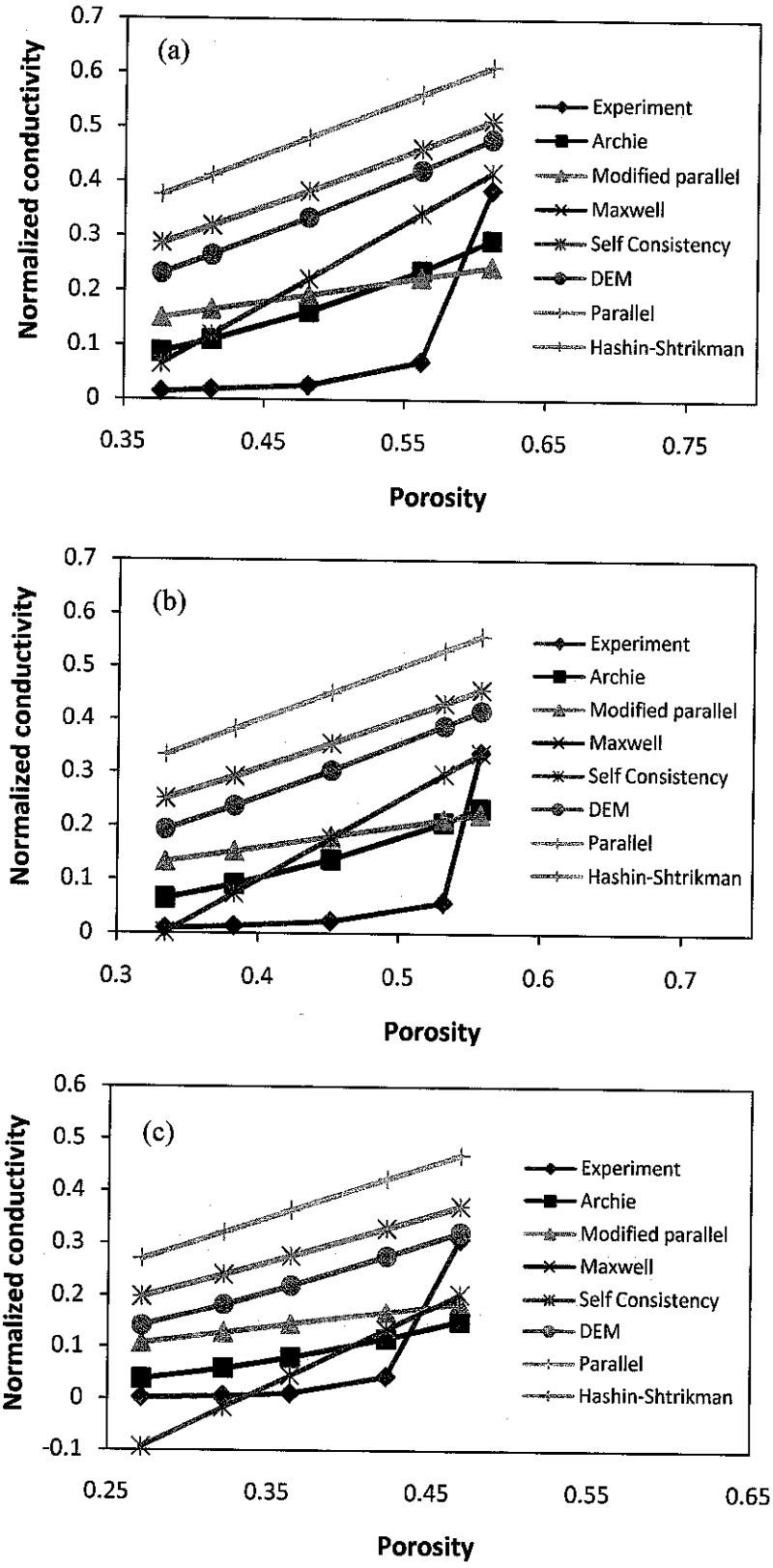

Figure F.3 Plot of conductivity models to experimental data of Class G oilwell cement at 65°C & 3000 psi for w/c at (a) 0.5, (b) 0.4 and (c) 0.3

APPENDIX G

PLOT OF MEASURED PERMEABILITY, KATZ-THOMPSON MODEL, JOHNSON MODEL AND PROPOSED EQUATION

This appendix provides a comparison of measured permeability to that of the Katz-Thompson, Johnson and proposed equations (Equation 4.17). These plots are set as a function of w/c and curing temperature and pressure. As expected, the permeability decreases with hydration time proceed. It can be seen from Figures G.1 to G.3 that the proposed equation has better values closed to the measured data compared with other models. The average level of errors for the proposed equation is about less than 30%, while for the Katz-Thompson and Johnson models are about more that 110% and 80%, respectively.

In these Figures, the effect of elevated temperature and pressure on permeability is pronounce by which it decreases the permeability values. Decreasing values of permeability is also occurred at small w/c. These factors affecting the acceleration of cement hydration process compared to that at ambient conditions.

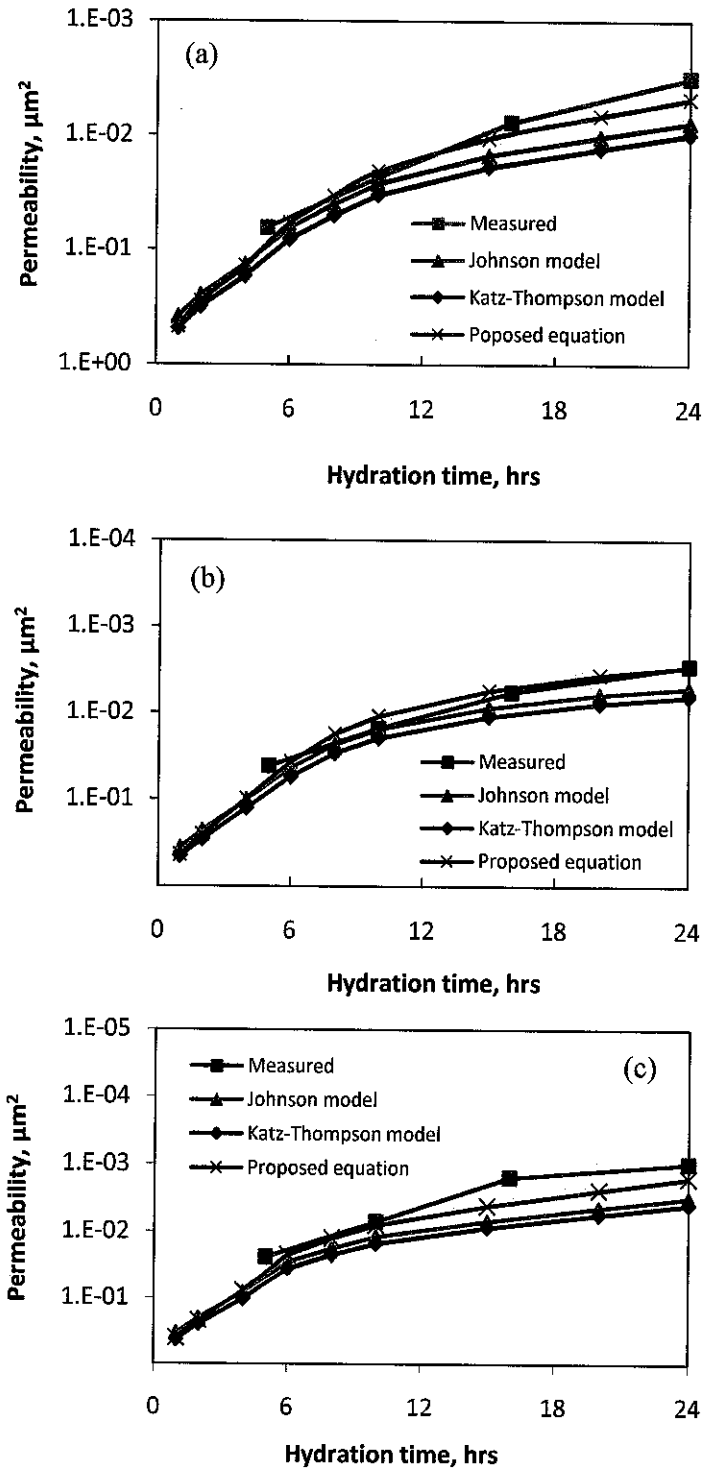

Figure G.1 Plot of measured permeability, Katz-Thompson model, Johnson model and proposed equation of oilwell cement at w/c 0.5 for (a) 25°C & 14.7 psi, (b) 40°C & 1500 psi and (c) 65°C & 3000 psi

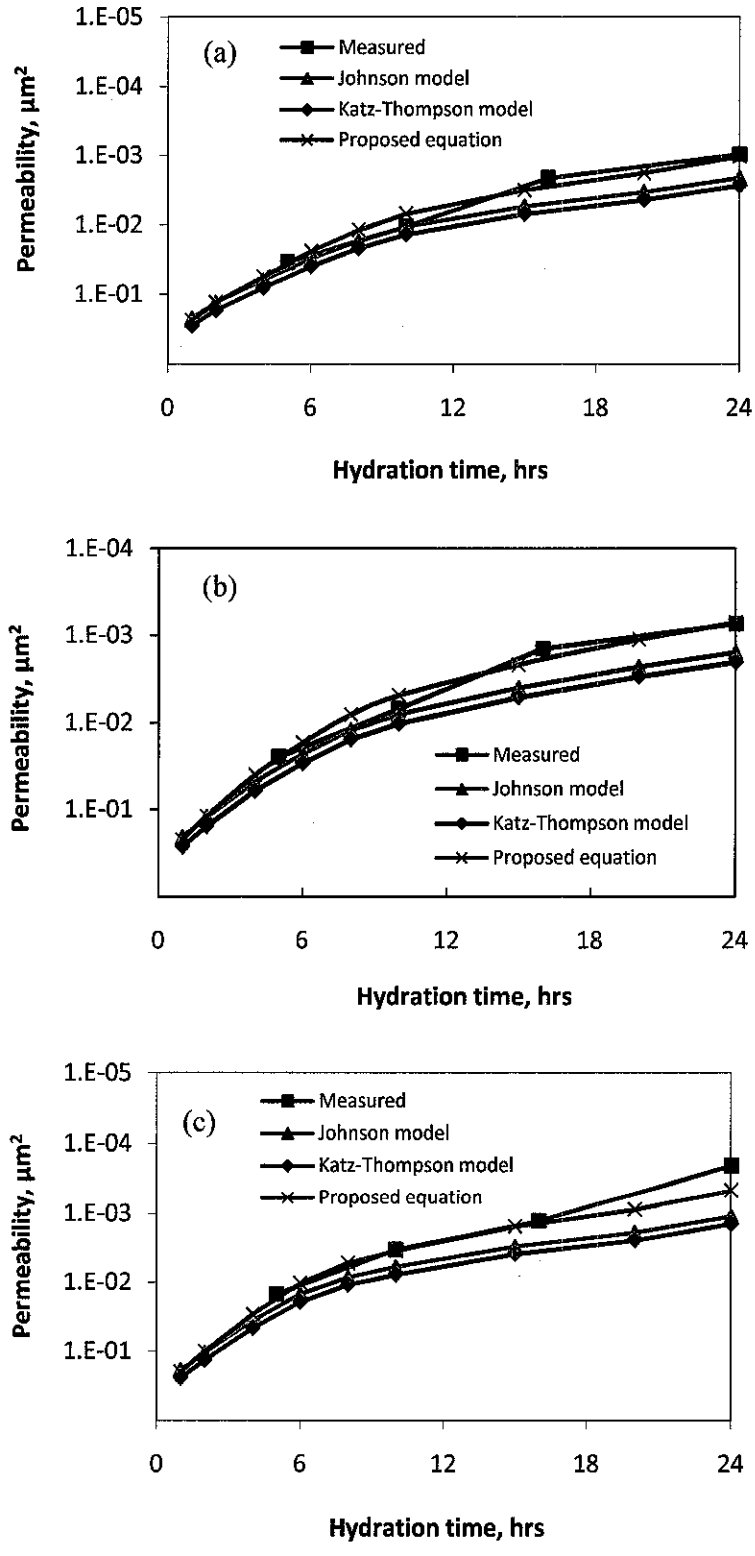

Figure G.2 Plot of measured permeability, Katz-Thompson model, Johnson model and proposed equation of oilwell cement at w/c 0.4 for (a) 25°C & 14.7 psi, (b) 40°C & 1500 psi and (c) 65°C & 3000 psi

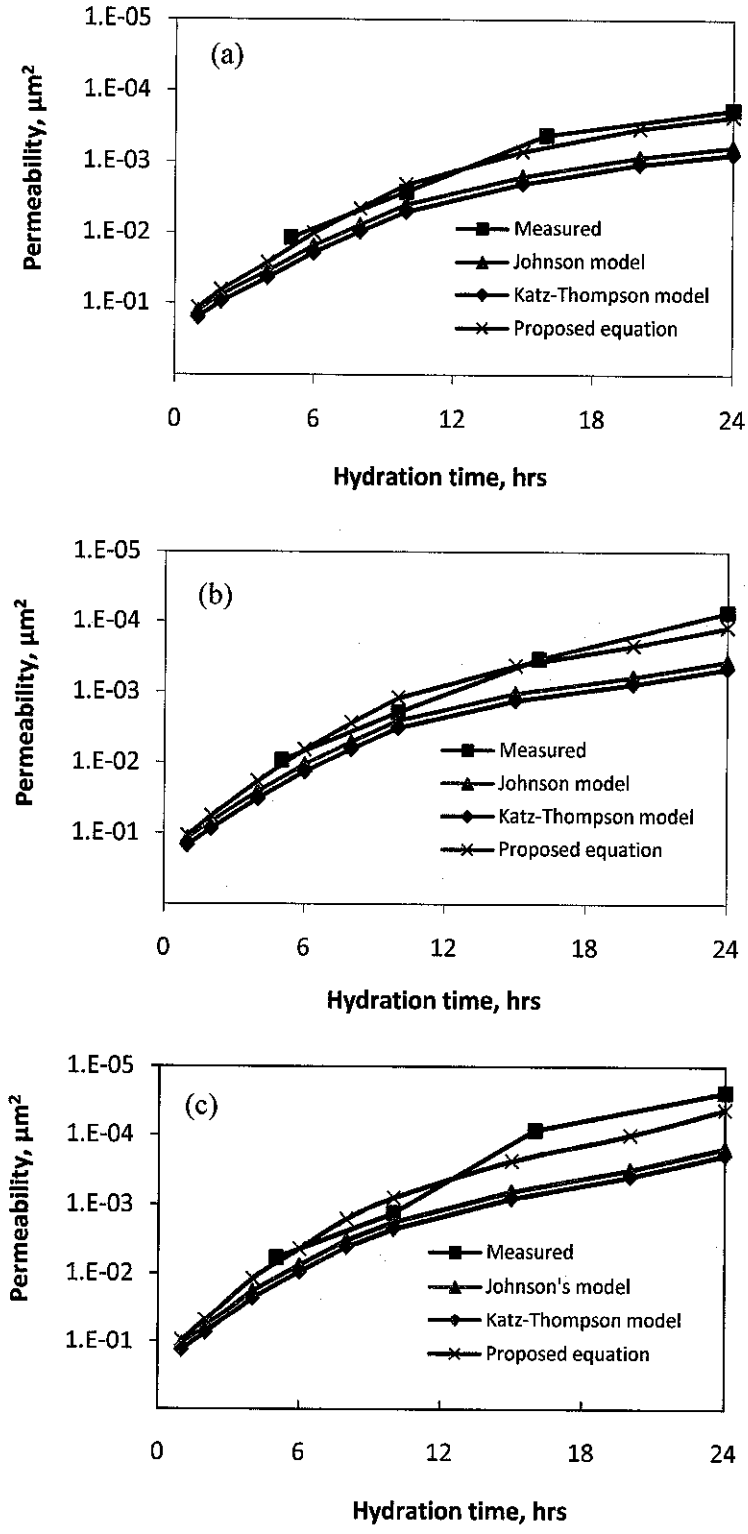

Figure G.3 Plot of measured permeability, Katz-Thompson model, Johnson model and proposed equation of oilwell cement at w/c 0.3 for (a) 25°C & 14.7 psi, (b) 40°C & 1500 psi and (c) 65°C & 3000 psi

APPENDIX H

PLOT OF ULTRASONIC CEMENT ANALYZER FOR CLASS G OILWELL CEMENT AT DIFFERENT W/C AND CURING CONDITIONS

Figures H.1 to H.13 present the measurement results of compressive strength measurement of oilwell cement using Ultrasonic Cement Analyzer (UCA) as a function of hydration time with respect to different w/c and curing conditions. Compressive strength increases as w/c decrease, and temperature and pressure increase.

For w/c 0.5, the increasing strength at 24 hrs of hydration from 25°C and 14.7 psi to 65°C and 3000 psi is about 1000 psi. Comparing to an increasing strength of about 500 psi is observed at 24 hrs of hydration from w/c 0.5 to 0.3 at ambient condition. This implied that elevated temperature and pressure effectively increase the strength of oilwell cement compared to that of decreasing w/c at similar hydration period.

Figures H.12 and H.13 show that the strength development after 50 hrs of hydration is slightly increased with w/c 0.25 has higher strength value compared to that of w/c 0.55 at curing condition of 70°C & 3000 psi up to 1200 hrs of hydration periods.

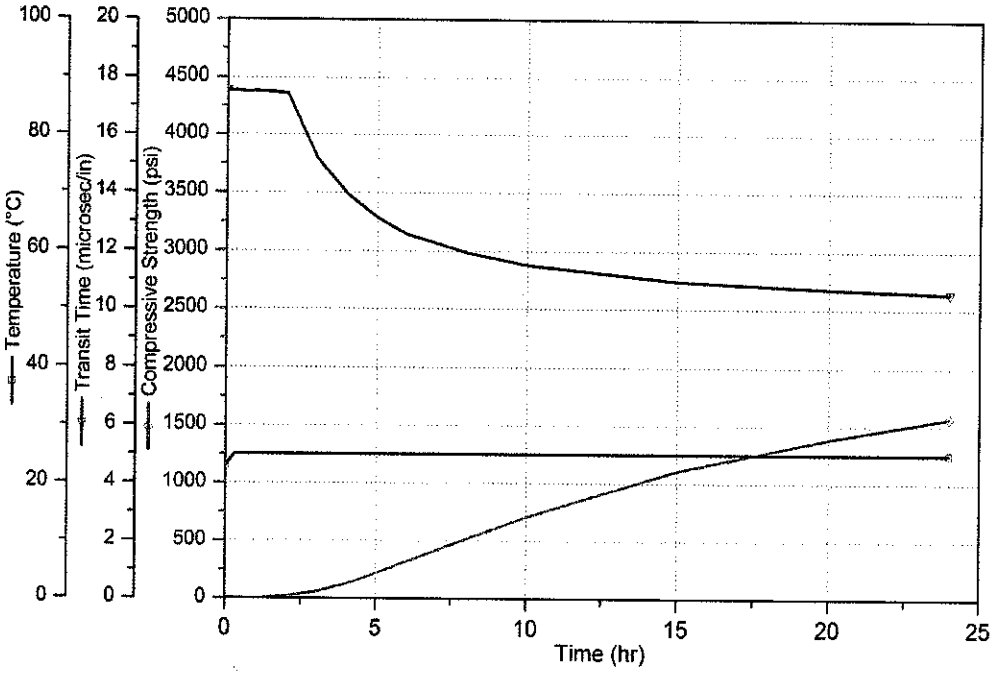

Figure H.1 Measured compressive strength of w/c 0.5 at 25°C & 14.7 psi

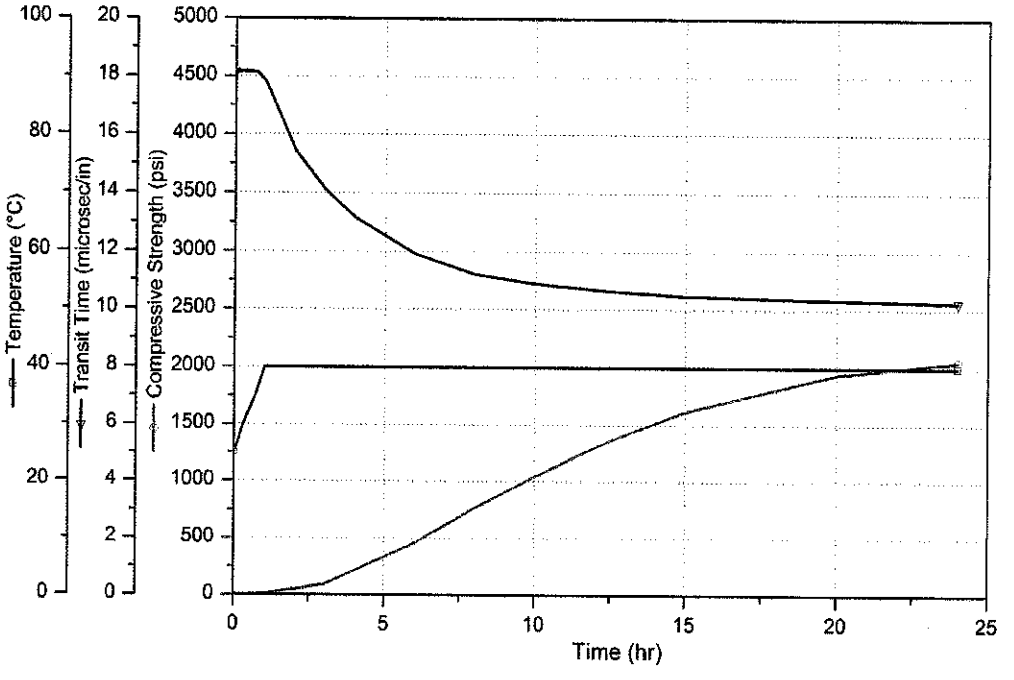

Figure H.2 Measured compressive strength of w/c 0.5 at 40°C & 1500 psi

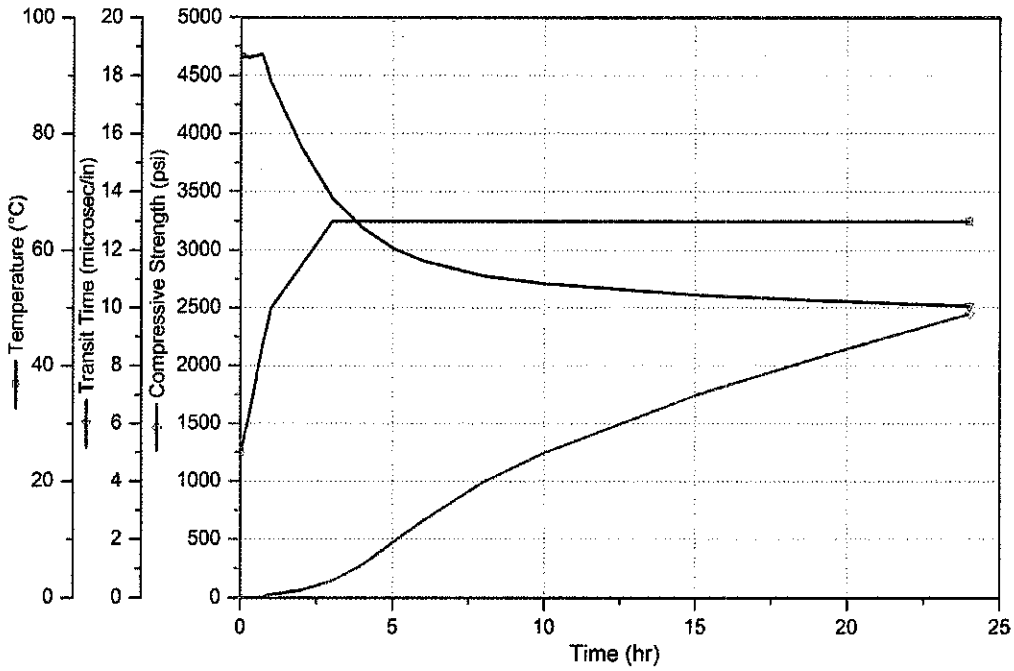

Figure H.3 Measured compressive strength of w/c 0.5 at 65°C & 3000 psi

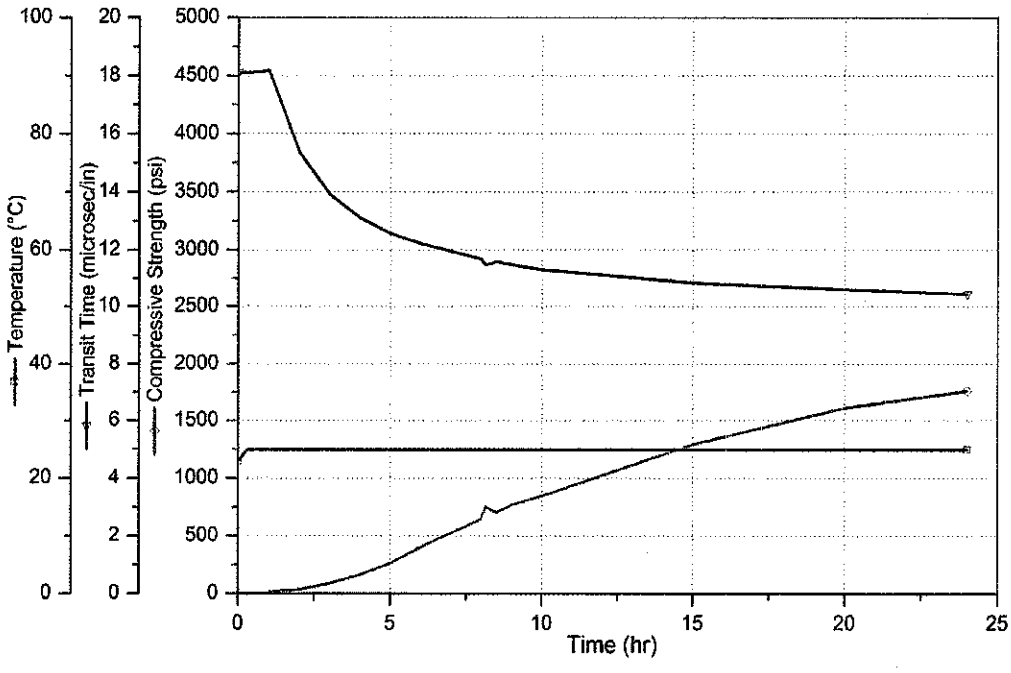

Figure H.4 Measured compressive strength of w/c 0.4 at 25°C & 14.7 psi

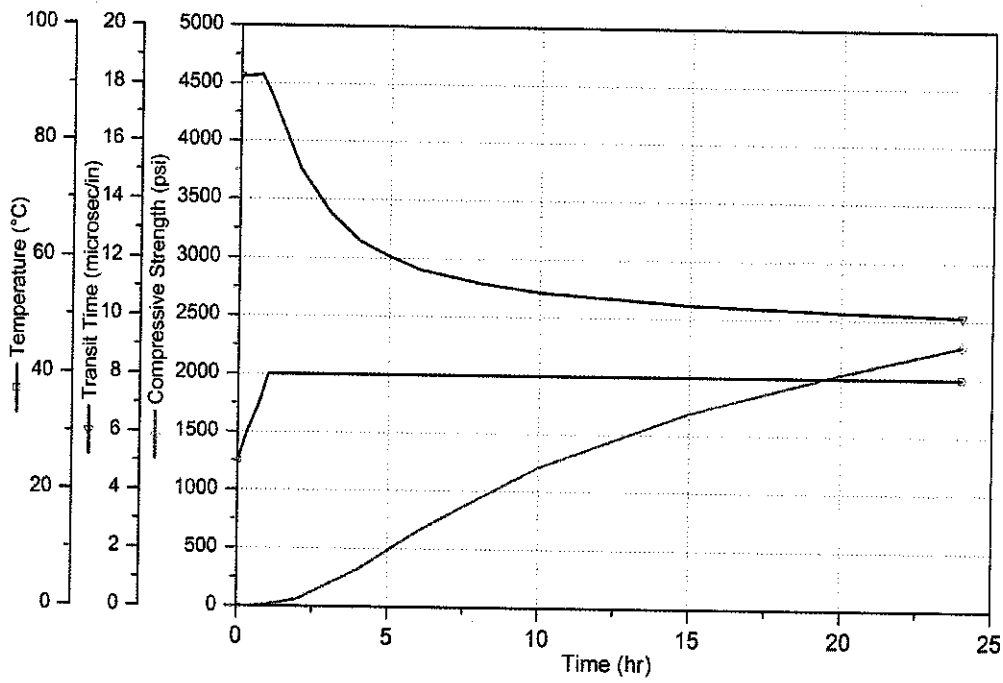

Figure H.5 Measured compressive strength of w/c 0.4 at 40°C & 1500 psi

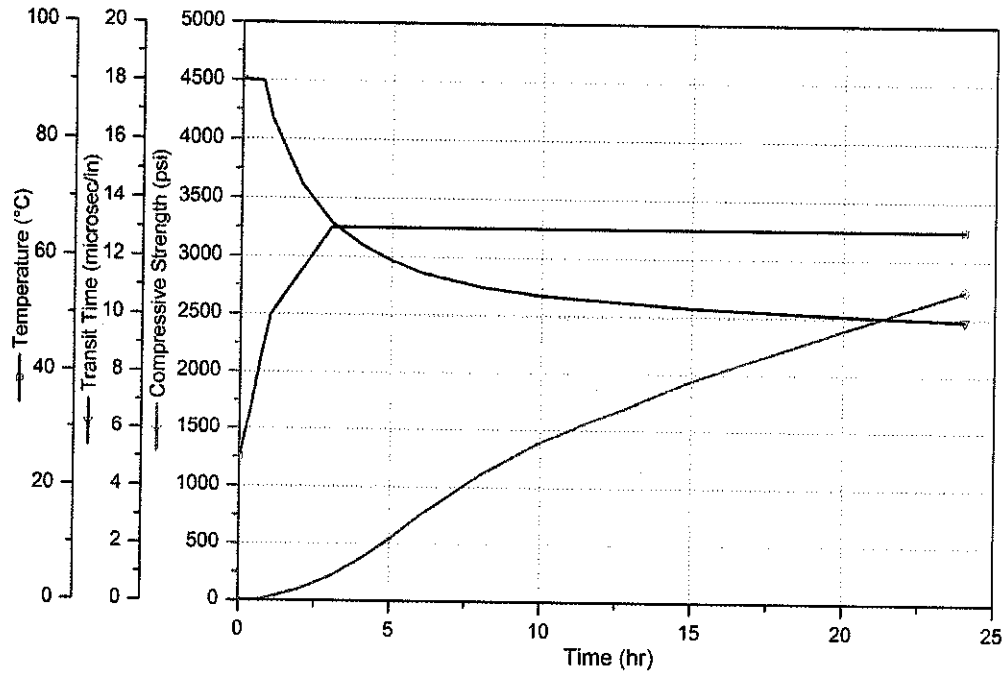

Figure H.6 Measured compressive strength of w/c 0.4 at 65°C & 3000 psi

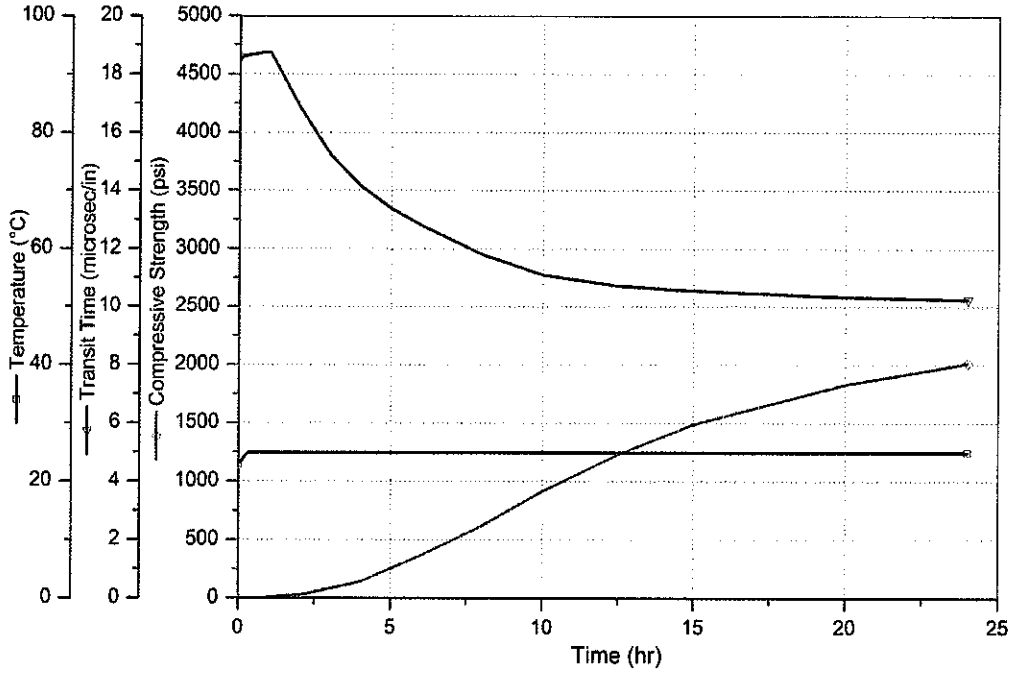

Figure H.7 Measured compressive strength of w/c 0.3 at 25°C & 14.7 psi

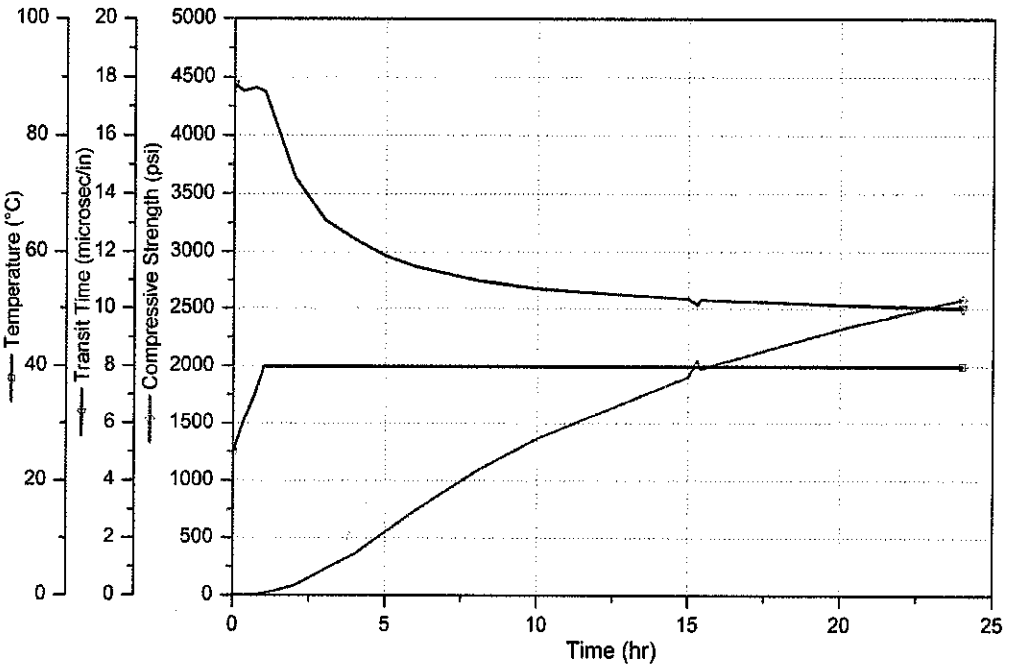

Figure H.8 Measured compressive strength of w/c 0.3 at 40°C & 1500 psi

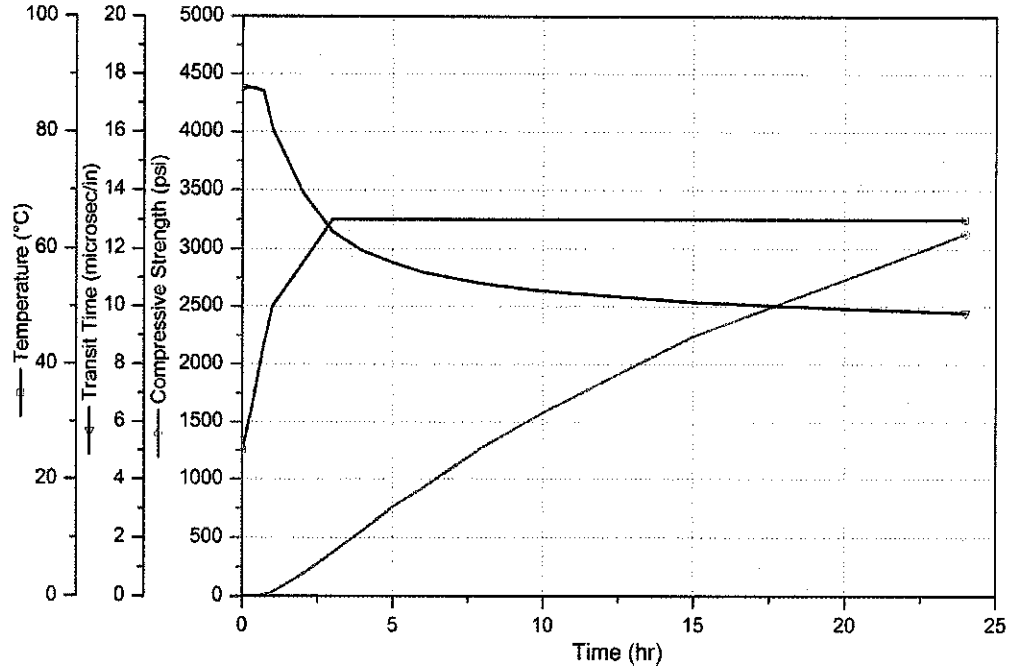

Figure H.9 Measured compressive strength of w/c 0.3 at 65°C & 3000 psi

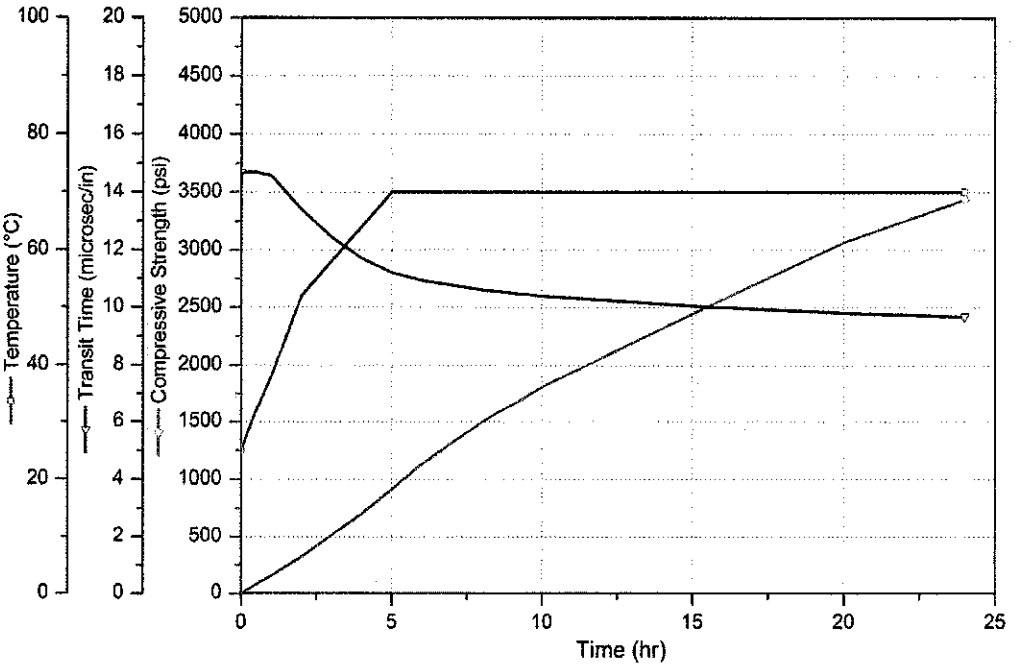

Figure H.10 Measured compressive strength of w/c 0.25 at 70°C & 3000 psi

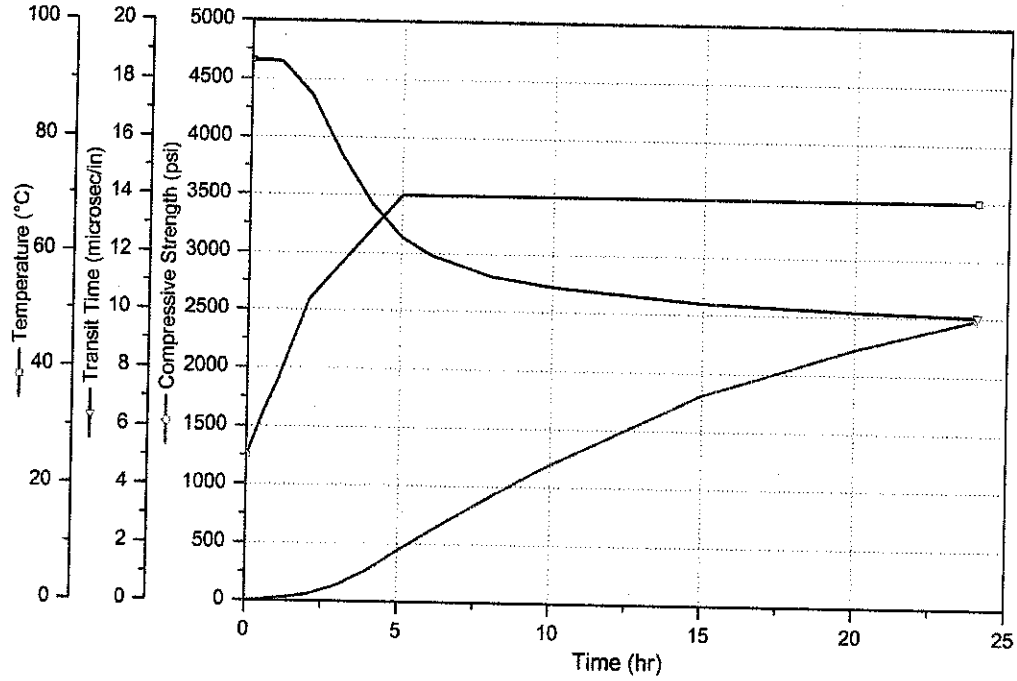

Figure H.11 Measured compressive strength of w/c 0.55 at 70°C & 3000 psi

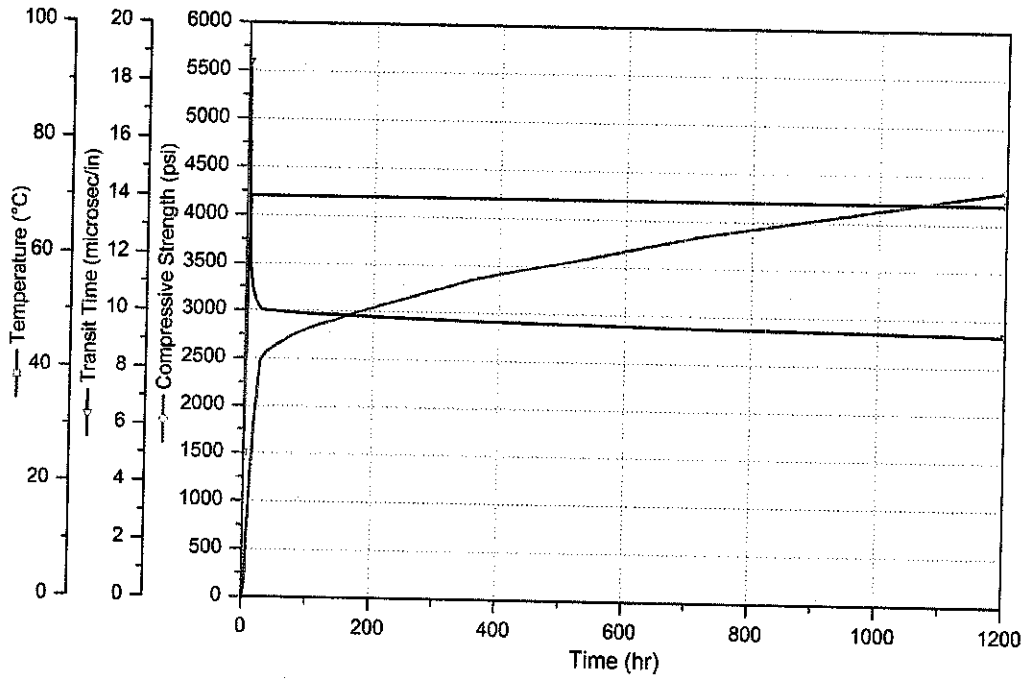

Figure H.12 Measured compressive strength of w/c 0.55 at 70°C & 3000 psi up to 1200 hrs of hydration time

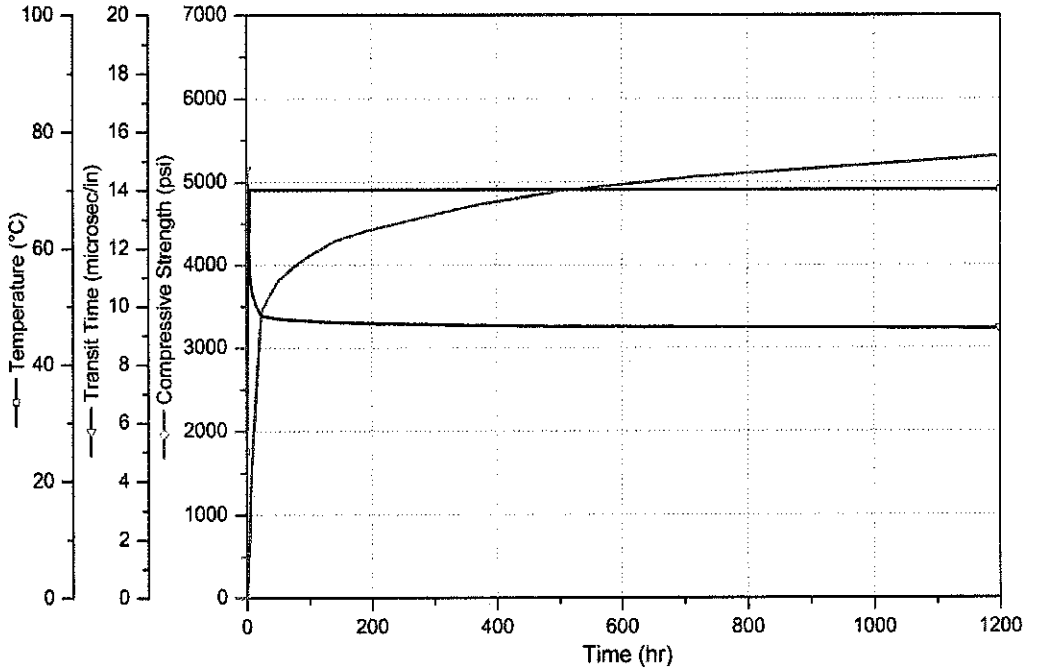

Figure H.13 Measured compressive strength of w/c 0.25 at 70°C & 3000 psi up to 1200 hrs of hydration time